



Modeling and control of Shape Memory Alloy Actuator.

Somasundar Kannan

► To cite this version:

Somasundar Kannan. Modeling and control of Shape Memory Alloy Actuator.. Automatic Control Engineering. Ecole nationale supérieure d'arts et métiers - ENSAM, 2011. English. NNT: 06O9KF013P3 . pastel-00724901

HAL Id: pastel-00724901

<https://pastel.hal.science/pastel-00724901>

Submitted on 23 Aug 2012

HAL is a multi-disciplinary open access archive for the deposit and dissemination of scientific research documents, whether they are published or not. The documents may come from teaching and research institutions in France or abroad, or from public or private research centers.

L'archive ouverte pluridisciplinaire **HAL**, est destinée au dépôt et à la diffusion de documents scientifiques de niveau recherche, publiés ou non, émanant des établissements d'enseignement et de recherche français ou étrangers, des laboratoires publics ou privés.

École doctorale n° 432 : SMI- Sciences des Métiers de l'Ingénieur

Doctorat ParisTech

THÈSE

pour obtenir le grade de docteur délivré par

l'École Nationale Supérieure d'Arts et Métiers

Spécialité “ Automatique ”

présentée et soutenue publiquement par

Somasundar KANNAN

le 21 Décembre 2011

Modélisation et Commande d'Actionneurs

à Alliage à Mémoire de Forme

Directeur de thèse : **Etienne PATOOR**

Co-encadrement de la thèse : **Christophe GIRAUD-AUDINE**

Jury

M. Stefan SEELECKE, Univ –Professeur. Dr. Ing, Saarland University

M. Arnaud HUBERT, Maître de Conférences -HDR, FEMTO-ST, Université de Franche- Comté

Mme Shabnam ARBAB CHIRANI, Professeur, LBMS, Ecole National d'Ingénieur de Brest

M. Manfred KOHL, Dr, IMT, Karlsruhe Institute of Technology

M. Christophe GIRAUD-AUDINE, Maître de Conférences, L2EP, Arts et Métiers ParisTech -Lille

M. Etienne PATOOR, Professeur, LEM3, Arts et Métiers ParisTech –Metz

Rapporteur

Rapporteur

Examinateur

Examinateur

Examinateur

Examinateur

T
H
È
S
E

Dedicated to my family

Acknowledgements

First of all I would like to thank the members of the jury for their consideration to be on my thesis committee. I would like to thank Professor Stefan SEELECKE , Professor Arnaud HUBERT and Dr. Manfred KOHL for accepting to be the referees, and for providing valuable critique of my thesis. I would like to thank Professor Shabnam ARBAB CHIRANI for presiding over the jury committee and her comments on my research work.

I am thankful to my PhD advisors Professor Etienne PATOOR and Dr. Christophe GIRAUD-AUDINE for giving me an opportunity to work on an interesting subject and for all the help they had provided during the period of my research as a PhD student. A special thanks to all the colleagues and staff of the LEM3 (formerly LPMM), CIRAM and Arts et Métiers ParisTech-Metz for providing a conducive environment to work during the period of my research.

I would like to thank friends at Arts et Métiers-Metz campus- Amir, Armaghan, Jawad, Marius, Ly, Sajid and friends off-campus- Indrava, Saumya, Muneeb, Saba.

I am grateful to my parents Kannan and Kannammal for the support and encouragement they had provided throughout my life, to Suresh and Kalaimathi I am thankful for being supportive and good fellow colleagues.

Special thanks also to my old mentors Professor Hyochoong BANG, Professor Joël BORDENEUVE GUIBE and Mr. Banu Gopal for instilling in me the desire to be a researcher.

Finally I owe my deepest gratitude to my wife Praveena for her patience, support and strength, without whom this PhD was not realizable.

I also gratefully acknowledge the financial support provided by Agence National de la Recherche (ANR), Centre National de la Recherche Scientifique (CNRS) and Arts et Métiers ParisTech-Metz .

Table des matières

| | |
|--|-----------|
| I Résumé étendu | 1 |
| 1 Introduction | 3 |
| 1.1 Introduction générale | 3 |
| 1.2 Alliage à Mémoire de Forme (AMF) | 4 |
| 1.3 Actionneurs à Alliage à Mémoire de Forme | 5 |
| 1.4 Modélisations et commandes | 6 |
| 1.4.1 Commandes avec modèles constitutifs | 7 |
| 1.4.2 Commande à partir de modèles phénoménologiques | 8 |
| 1.4.3 Méthodes classiques sans modèles explicites | 11 |
| 1.5 Contribution de la thèse | 11 |
| 2 Modélisation | 15 |
| 2.1 Introduction | 15 |
| 2.2 Modélisation des systèmes linéaires invariants | 15 |
| 2.2.1 Modèle discrets en environnement déterministe | 15 |
| 2.2.2 Environnement stochastique | 16 |
| 2.3 Identification | 17 |

Table des matières

| | | |
|----------|---|-----------|
| 2.3.1 | Moindres carrés | 17 |
| 2.3.2 | Moindres carrés récursifs | 18 |
| 2.4 | Base des fonctions de Laguerre | 18 |
| 2.4.1 | Intérêt | 18 |
| 2.4.2 | Base orthonormale des fonctions de Laguerre discrètes | 19 |
| 2.4.3 | Propriétés | 19 |
| 2.4.4 | Modèle de Volterra-Laguerre | 20 |
| 2.5 | Etude expérimentale | 21 |
| 2.5.1 | Critères d'évaluation | 21 |
| 2.5.2 | Actionneur simple | 22 |
| 2.5.3 | Actionneur antagoniste | 23 |
| 2.6 | conclusion | 24 |
| 3 | Commande | 27 |
| 3.1 | Commande adaptative prédictive | 27 |
| 3.1.1 | Principe de la commande prédictive | 27 |
| 3.1.2 | Commande prédictive avec modèle de Laguerre | 28 |
| 3.1.3 | Stabilité et robustesse | 29 |
| 3.1.4 | Validation expérimentale | 35 |
| 3.2 | Commande modifiée | 36 |
| 3.2.1 | Principe | 36 |
| 3.2.2 | Stabilité | 37 |
| 3.2.3 | Validation expérimentale | 38 |

Table des matières

| | |
|--|-----------|
| 3.3 conclusions | 39 |
| 4 Conclusion | 41 |
| 4.1 Résumé du travail | 41 |
| 4.1.1 Identification | 42 |
| 4.1.2 Commande | 42 |
| 4.2 Perspectives | 43 |
| 4.2.1 Améliorations à apporter | 43 |
| 4.2.2 Limites de l'approche "boite noire" | 43 |
| II Version Anglaise | 45 |
| 5 Introduction | 47 |
| 5.1 Introduction to Actuators | 47 |
| 5.2 Shape Memory Alloys (SMA) | 48 |
| 5.3 Shape Memory Alloy (SMA) Actuators | 51 |
| 5.3.1 General Performance and Thermal Control of SMA element . . | 51 |
| 5.3.2 Different Types of SMA Actuator | 53 |
| 5.4 Modelling methods and Control | 55 |
| 5.4.1 Physical Modeling and Nonlinear Control | 56 |
| 5.4.2 Phenomenological Model and Inverse Control | 63 |
| 5.4.3 Control without using Explicit Model: Linear Control | 70 |
| 5.5 Summary of modelling and control methods and their interaction . . | 71 |
| 5.6 Contribution of this Thesis | 76 |

Table des matières

| | | |
|----------|---|------------|
| 5.7 | Outline of the Thesis | 77 |
| 6 | Modelling | 79 |
| 6.1 | Introduction | 79 |
| 6.2 | Models of linear time invariant processes | 80 |
| 6.2.1 | Discrete model in deterministic environment | 80 |
| 6.2.2 | Modelling the disturbances | 81 |
| 6.3 | Identification | 82 |
| 6.3.1 | Least squares | 82 |
| 6.3.2 | Recursive least squares | 85 |
| 6.3.3 | Adaptive recursive least squares | 86 |
| 6.4 | Laguerre function basis | 88 |
| 6.4.1 | Motivation | 88 |
| 6.4.2 | Discrete Laguerre orthonormal basis | 90 |
| 6.4.3 | Some properties of the Laguerre function basis | 91 |
| 6.5 | Experimental Study | 94 |
| 6.5.1 | Validation of Model in Prediction Error Method | 95 |
| 6.5.2 | Single Wire Actuator | 96 |
| 6.5.3 | Open loop Identification of the single actuator | 99 |
| 6.5.4 | Experimental Setup: Antagonistic Actuator | 113 |
| 6.6 | Conclusion | 116 |
| 7 | Adaptive Predictive Control | 119 |
| 7.1 | Introduction | 119 |

Table des matières

| | | |
|-------|---|-----|
| 7.2 | Closed Loop Identification (Offline/Non-Adaptive) | 120 |
| 7.3 | Introduction to Predictive control | 121 |
| 7.3.1 | Closed loop Identification (Non-Adaptive) for MPC | 122 |
| 7.4 | Predictive control as Receding Horizon Problem | 122 |
| 7.5 | Stability and Robustness | 130 |
| 7.6 | Control of SMA using Classical Laguerre Predictive (CLaP) Control: Experimental Results | 136 |
| 7.6.1 | Position Control using 2 nd order linear Laguerre model with CLaP method | 137 |
| 7.6.2 | Position Control using 5 th order linear Laguerre model with CLaP method | 139 |
| 7.7 | CLaP method using RLS estimation with Directional Forgetting factor | 142 |
| 7.7.1 | Directionnal Forgetting Factor Recursive Least Squares | 142 |
| 7.7.2 | Methodology | 143 |
| 7.7.3 | Position Control using 5 th order linear Laguerre model with CLaP- DFRLS method | 144 |
| 7.7.4 | Influence of Prediction Horizon (H_p) and Control weights (Q, R) | 144 |
| 7.7.5 | Clap-DFRLS using 2 nd order | 148 |
| 7.7.6 | Influence of Thermal Disturbance and Ambient Temperature . . | 149 |
| 7.8 | Conclusion and Perspective on CLaP-DFRLS | 151 |
| 7.9 | Modified Adaptive Predictive Control | 153 |
| 7.9.1 | Main Results | 154 |
| 7.9.2 | Stability analysis | 154 |
| 7.10 | Control of SMA using Modified Laguerre Predictive (MLaP) Control: Experimental Results | 156 |

Table des matières

| | |
|--|------------|
| 7.10.1 Position Control using 5 th order linear Laguerre model with MLaP method | 156 |
| 7.10.2 Position Control using 2 nd order linear Laguerre model with MLaP method | 159 |
| 7.11 Discussions | 161 |
| 7.11.1 Influence of prediction horizon | 161 |
| 7.11.2 Perturbation Rejection | 161 |
| 7.12 Antagonistic Actuator control | 161 |
| 7.12.1 Open loop characteristics | 164 |
| 7.13 Experimental results and discussion | 164 |
| 7.13.1 Position Control | 164 |
| 7.13.2 Influence of Prediction Horizon | 167 |
| 7.14 Antagonistic setup: Discussion | 171 |
| 7.15 Conclusion | 173 |
| 8 Conclusion | 175 |
| 8.1 Summary of this work | 175 |
| 8.2 Contributions | 176 |
| 8.2.1 Modeling for Control | 176 |
| 8.2.2 Adaptive control of SMA actuator | 177 |
| 8.3 Unsolved problems and Future Directions | 178 |
| 8.3.1 Optimal Actuator design | 178 |
| 8.3.2 Modeling Problem | 181 |
| 8.3.3 Control Problem | 182 |

Table des matières

| | |
|---|-----|
| 8.4 Future Applications of the contribution | 182 |
|---|-----|

Table des matières

Liste des tableaux

| | | |
|------|---|-----|
| 2.1 | Algorithme des moindres carrés récursifs | 18 |
| 5.1 | Heating and cooling techniques for SMA actuators | 53 |
| 6.1 | Black-Box Model Structures | 82 |
| 6.2 | Recursive least square algorithm | 86 |
| 6.3 | Recursive least square algorithm | 88 |
| 6.4 | Usual choices of parameters values for adaptive RLS | 88 |
| 6.5 | 2 nd Order Linear Laguerre Filter with Input SNR=45 dB and different Forgetting factor λ | 101 |
| 6.6 | 2 nd Order Linear Laguerre Filter with Input SNR= ∞ dB and different Forgetting factor λ | 102 |
| 6.7 | 2 nd Order Volterra Laguerre Filter with Input $SNR = 45$ dB and different Forgetting factor λ | 104 |
| 6.8 | 2 nd Order Volterra Laguerre Filter with Input $SNR = \infty$ dB and different Forgetting factor λ | 104 |
| 6.9 | 5 th Order linear Laguerre Filter with Input $SNR = \infty$ dB and different Forgetting factor λ | 107 |
| 6.10 | 5 th Order linear Laguerre Filter with Input $SNR = 45$ dB and different Forgetting factor λ | 107 |
| 6.11 | 2 nd Order linear Laguerre Filter with Input $SNR = 45$ dB and different sampling rate T_s | 110 |

Liste des tableaux

| | |
|--|-----|
| 6.12 2 nd Order linear Laguerre Filter with Input $SNR = \infty$ dB and different sampling rate T_s . | 110 |
| 6.13 2 nd Order Volterra Laguerre Filter with Input $SNR = 45$ dB and different sampling rate T_s . | 110 |
| 6.14 2 nd Order Volterra Laguerre Filter with Input $SNR = \infty$ dB and different sampling rate T_s . | 112 |
| 6.15 5 th Order linear Laguerre Filter with Input $SNR = 45$ dB and different sampling rate T_s . | 112 |
| 6.16 5 th Order linear Laguerre Filter with Input $SNR = \infty$ dB and different sampling rate T_s . | 113 |
| 6.17 Antagonistic:2 nd Order linear Laguerre Filter with Input $SNR = \infty$ dB and different Forgetting factor λ . | 118 |
| 6.18 Antagonistic:2 nd Order linear Laguerre Filter with Input $SNR = \infty$ dB and different sampling rate T_s . | 118 |
| 7.1 Evaluation criteria for the adaptive predictive control. The entries resulting in instability are signaled by the “n.a” abbreviation | 147 |
| 7.2 MLaP: 5 th order model performance indexes. | 157 |
| 7.3 MLaP 2 nd order model. | 159 |

Table des figures

| | | |
|------|---|----|
| 1.1 | Schéma bloc du principe de l'asservissement d'un système mono-entrée, mono-sortie | 6 |
| 1.2 | Schéma bloc de la commande avec linéarisation par retour d'état | 7 |
| 1.3 | Exemple d'évolution du modèle de Preisach dans le plan de Preisach | 9 |
| 5.1 | Actuator comparison based on weight and output power-to-weight | 48 |
| 5.2 | Material Crystalline arrangement during the Shape Memory Effect | 49 |
| 5.3 | Stress-Strain relationship of Shape Memory Alloy | 50 |
| 5.4 | Hysteresis loops in Shape Memory Alloy | 50 |
| 5.5 | Different forms of SMA actuators | 54 |
| 5.6 | Block diagram of a SMA actuator using physical modelling | 56 |
| 5.7 | Schematic diagram of Extended Kalman Filter (EKF) | 62 |
| 5.8 | Nonlinear control using Extended Kalman Filter | 62 |
| 5.9 | Preisach Hysteron | 64 |
| 5.10 | Discretized Preisach operator. | 65 |
| 5.11 | Memory curves on Preisach plane. | 66 |
| 5.12 | KP Hysteresis operator | 67 |
| 5.13 | PI linear stop operator. | 69 |

Table des figures

| | |
|--|-----|
| 5.14 Schematic of Adaptive inverse control | 69 |
| 5.15 Implementation of PWM | 71 |
| 5.16 Summary of methods | 73 |
| | |
| 6.1 Block diagram representing the relationship (6.30) | 87 |
| 6.2 Block diagram of the adaptive recursive least squares algorithm | 87 |
| 6.3 Transversal Tap filter | 90 |
| 6.4 Bode diagram of the transfer functions of the (continuous) Laguerre functions $L_0(s)$, $L_1(s)$, $L_2(s)$ ($\alpha = 10$ is a continuous pole chosen) | 92 |
| 6.5 Practical realization of a Laguerre filter. | 94 |
| 6.6 Schematic of the experimental setup using a single wire under constant stress | 96 |
| 6.7 Experimental Setup. | 98 |
| 6.8 Drift in SMA wire. | 99 |
| 6.9 2 nd order linear Laguerre filter with input SNR=45 dB and $\lambda = 1$. Left: Hysteresis measured and Predicted,Right:(a)Identification Error (b) Filter Weights. | 102 |
| 6.10 2 nd order linear Laguerre filter with input SNR=45 dB and $\lambda = 0.5$. Left: Hysteresis measured and Predicted,Right:(a)Identification Error (b) Filter Weights(c)Filter weights zoomed. | 102 |
| 6.11 2 nd order linear Laguerre filter with input SNR= ∞ dB and $\lambda = 1$. Left: Hysteresis measured and Predicted,Right:(a)Identification Error (b) Filter Weights. | 103 |
| 6.12 2 nd order linear Laguerre filter with input $SNR = \infty$ dB and $\lambda = 0.5$. Left: Hysteresis measured and Predicted,Right:(a)Identification Error (b) Filter Weights. | 103 |
| 6.13 2 nd order Volterra Laguerre filter with input $SNR = 45$ dB and $\lambda = 1$. Left: Hysteresis measured and Predicted,Right:(a)Identification Error (b) Filter Weights. | 105 |

| | |
|--|-----|
| 6.14 2 nd order Volterra Laguerre filter with input $SNR = 45$ dB and $\lambda = 0.9$. Left: Hysteresis measured and Predicted, Right:(a)Identification Error (b) Filter Weights. | 105 |
| 6.15 2 nd order Volterra Laguerre filter with input $SNR = \infty$ dB and $\lambda = 1$. Left: Hysteresis measured and Predicted, Right:(a)Identification Error (b) Filter Weights. | 106 |
| 6.16 2 nd order Volterra Laguerre filter with input $SNR = \infty$ dB and $\lambda = 0.99$. Left: Hysteresis measured and Predicted, Right:(a)Identification Error (b) Filter Weights. | 106 |
| 6.17 5 th order linear Laguerre filter with input $SNR = 45$ dB and $\lambda = 1$. Left: Hysteresis measured and Predicted, Right:(a)Identification Error (b) Filter Weights. | 108 |
| 6.18 5 th order linear Laguerre filter with input $SNR = 45$ dB and $\lambda = 0.9$. Left: Hysteresis measured and Predicted, Right:(a)Identification Error (b) Filter Weights. | 108 |
| 6.19 5 th order linear Laguerre filter with input $SNR = \infty$ dB and $\lambda = 1$. Left: Hysteresis measured and Predicted, Right:(a)Identification Error (b) Filter Weights. | 108 |
| 6.20 2 nd order linear Laguerre filter with input $SNR = 45$ dB, $\lambda = 0.9$ and $T_s = 1$ sec.. Left: Hysteresis measured and Predicted, Right:(a)Identification Error (b) Filter Weights. | 111 |
| 6.21 2 nd Order linear Laguerre filter with input $SNR = \infty$ dB, $\lambda = 0.9$ and $T_s = 1$ sec.. Left: Hysteresis measured and Predicted, Right:(a)Identification Error (b) Filter Weights. | 111 |
| 6.22 2 nd Order Volterra Laguerre filter with input $SNR = 45$ dB, $\lambda = 0.9$ and $T_s = 1$ sec.. Left: Hysteresis measured and Predicted, Right:(a)Identification Error (b) Filter Weights. | 112 |
| 6.23 2 nd Order Volterra Laguerre filter with input $SNR = 0$ dB, $\lambda = 0.9$ and $T_s = 1$ sec.. Left: Hysteresis measured and Predicted, Right:(a)Identification Error (b) Filter Weights. | 113 |
| 6.24 5 th order linear Laguerre filter with input $SNR = 45$ dB, $\lambda = 0.9$ and $T_s =$ 1 sec.. Left: Hysteresis measured and Predicted, Right:(a)Identification Error (b) Filter Weights. | 114 |

Table des figures

| | |
|---|-----|
| 6.25 5 th order linear Laguerre filter with input $SNR = \infty$ dB, $\lambda = 0.9$ and $T_s = 1$ sec.. Left: Hysteresis measured and Predicted,Right:(a)Identification Error (b) Filter Weights. | 114 |
| 6.26 Antagonistic actuator Experimental setup | 115 |
| 6.27 Antagonistic actuator: Identification with $\lambda = 1$ | 117 |
| 6.28 Antagonistic actuator: Identification with $\lambda = 0.9$ | 117 |
| | |
| 7.1 Left: Hysteresis measured in the single wire SMA actuator,Right: Input reference and the output displacement. | 120 |
| 7.2 Closed loop system. | 121 |
| 7.3 Predictive control: basic idea | 124 |
| 7.4 Classical Laguerre Predictive control | 130 |
| 7.5 Tracking using CLaP method with 2 nd order model,($a = 0.9, H_p = 30, \lambda = 0.8, R/Q = 10^{-3}$). | 138 |
| 7.6 (i)Tracking error and (ii) Control signal using CLaP method with 2 nd order model,($a = 0.9, H_p = 30, \lambda = 0.8, R/Q = 10^{-3}$). | 138 |
| 7.7 (i)Identification error and (ii) Laguerre filter weights using CLaP method with 2 nd order model,($a = 0.9, H_p = 30, \lambda = 0.8, R/Q = 10^{-3}$). | 139 |
| 7.8 Tracking using CLaP method with 5 th order model,($a = 0.9, H_p = 30, \lambda = 0.99, R/Q = 10^{-3}$). | 140 |
| 7.9 (i)Tracking error and (ii) Control signal using CLaP method with 5 th order model,($a = 0.9, H_p = 30, \lambda = 0.99, R/Q = 10^{-3}$). | 140 |
| 7.10 (i)Identification error and (ii) Laguerre filter weights using CLaP method with 5 th order model,($a = 0.9, H_p = 30, \lambda = 0.99, R/Q = 10^{-3}$). | 141 |
| 7.11 Tracking using CLaP-DFRLS method with 5 th order model,($a = 0.9, H_p = 3, \lambda = 0.5, \epsilon = 10^{-3}, Q = 1, R = 0$). | 145 |
| 7.12 (i)Tracking error and (ii) Control signal using CLaP-DFRLS method with 5 th order model,($a = 0.9, H_p = 3, \lambda = 0.5, \epsilon = 10^{-3}, Q = 1, R = 0$). | 145 |

| | |
|---|-----|
| 7.13 (i)Identification error and (ii) Laguerre filter weights using CLaP-DFRLS method with 5 th order model,($a = 0.9, H_p = 3, \lambda = 0.5, \epsilon = 10^{-3}, Q = 1, R = 0$). | 146 |
| 7.14 Tracking using CLaP-DFRLS method with 5 th order model,($a = 0.9, H_p = 3, 30, \lambda = 0.5, \epsilon = 10^{-3}, Q = 1, R = 0$). | 146 |
| 7.15 (i)Tracking error and (ii) Control signal using CLaP-DFRLS method with 5 th order model,($a = 0.9, H_p = 3, 30, \lambda = 0.5, \epsilon = 10^{-3}, Q = 1, R = 0$). | 148 |
| 7.16 Tracking using CLaP-DFRLS method with 2 nd order model,($a = 0.9, H_p = 3, \lambda = 0.5, \epsilon = 10^{-3}, Q = 1, R = 0$). | 149 |
| 7.17 (i)Tracking error and (ii) Control signal using CLaP-DFRLS method with 2 nd order model,($a = 0.9, H_p = 3, \lambda = 0.5, \epsilon = 10^{-3}, Q = 1, R = 0$). | 150 |
| 7.18 (i)Identification error and (ii) Laguerre filter weights using CLaP-DFRLS method with 2 nd order model,($a = 0.9, H_p = 3, \lambda = 0.5, \epsilon = 10^{-3}, Q = 1, R = 0$). | 150 |
| 7.19 Perturbation Rejection:Tracking using CLaP-DFRLS method with 5 th order model,($a = 0.9, H_p = 3, \lambda = 0.5, \epsilon = 10^{-3}, Q = 1, R = 0$). | 151 |
| 7.20 Perturbation Rejection:Control signal using CLaP-DFRLS method with 5 th order model,($a = 0.9, H_p = 3, \lambda = 0.5, \epsilon = 10^{-3}, Q = 1, R = 0$). | 152 |
| 7.21 Perturbation Rejection:Tracking using CLaP-DFRLS method with 5 th order model,($a = 0.9, H_p = 3, \lambda = 0.5, \epsilon = 10^{-3}, Q = 1, R = 10^{-4}$). | 152 |
| 7.22 Perturbation Rejection:Control signal using CLaP-DFRLS method with 5 th order model,($a = 0.9, H_p = 3, \lambda = 0.5, \epsilon = 10^{-3}, Q = 1, R = 10^{-4}$). | 153 |
| 7.23 Modified Laguerre Predictive (MLaP) Control scheme. | 155 |
| 7.24 Tracking using MLaP method with 5 th order model,($a = 0.9, H_p = 3, \lambda = 1$). | 157 |
| 7.25 (i)Tracking error and (ii) Control signal using MLaP method with 5 th order model,($a = 0.9, H_p = 3, \lambda = 1$). | 158 |
| 7.26 (i)Identification error and (ii) Laguerre filter weights using MLaP method with 5 th order model,($a = 0.9, H_p = 3, \lambda = 1$). | 158 |
| 7.27 Tracking using MLaP method with 2 nd order model,($a = 0.9, H_p = 3, \lambda = 1$). | 159 |

Table des figures

| | |
|--|-----|
| 7.28 (i)Tracking error and (ii) Control signal using MLaP method with 2 nd order model,($a = 0.9, H_p = 3, \lambda = 1$) | 160 |
| 7.29 (i)Identification error and (ii) Laguerre filter weights using MLaP method with 2 nd order model,($a = 0.9, H_p = 3, \lambda = 1$) | 160 |
| 7.30 Tracking using MLaP method with 5 th order model,($a = 0.9, H_p = 3, 30, \lambda = 1$) | 162 |
| 7.31 (i)Tracking error and (ii) Control signal using MLaP method with 5 th order model,($a = 0.9, H_p = 3, 30, \lambda = 1$) | 162 |
| 7.32 Perturbation Rejection: Tracking using MLaP method with 5 th order model,($a = 0.9, H_p = 3, \lambda = 1$) | 163 |
| 7.33 Perturbation Rejection:Control signal using MLaP method with 5 th order model,($a = 0.9, H_p = 3, \lambda = 1$) | 163 |
| 7.34 Displacement vs normalized time for different frequencies for a sinusoidal voltage | 164 |
| 7.35 For different frequencies semilog plot of gain (mm/V) for a sinusoidal voltage | 165 |
| 7.36 Hysteresis for input frequencies $\omega=0.12 \text{ rad.s}^{-1}$ | 165 |
| 7.37 Hysteresis for input frequencies $\omega=1.2 \text{ rad.s}^{-1}$ | 166 |
| 7.38 Antagonistic setup: Displacement response for tracking a mixed square wave. | 167 |
| 7.39 Antagonistic setup: Control signal for tracking a mixed square wave. | 168 |
| 7.40 Antagonistic setup: Identified Laguerre weights for tracking a mixed square wave. | 168 |
| 7.41 Antagonistic setup: Closed loop Identification Error for tracking a mixed square wave. | 169 |
| 7.42 Antagonistic setup: Hysteresis in open loop antagonistic system. | 169 |
| 7.43 Antagonistic setup: Hysteresis in closed loop controlled system. | 170 |
| 7.44 Antagonistic setup: Output of the actuator under a thermal perturbation. | 170 |

Table des figures

| | |
|---|---------|
| 7.45 Antagonistic setup: Applied voltage under a thermal perturbation. | 171 |
| 7.46 Antagonistic setup: Actuator output for prediction horizons $H_p = 3$ and $H_p = 30$ | 172 |
| 7.47 Antagonistic setup: tracking error for prediction horizons $H_p = 3$ and $H_p = 30$ | 172 |
| 7.48 Antagonistic setup: control signals for prediction horizons $H_p = 3$ and $H_p = 30$ | 173 |
| 8.1 Effects of thermomechanical treatment on the achievable strain of the actuators | 180 |
| 8.2 Schematic illustration of the building up of stress and temperature during actuation. | 181 |

Première partie

Résumé étendu

Chapitre 1

Introduction

1.1 Introduction générale

Les domaines d'application des actionneurs se sont grandement étendus durant ces dernières années avec l'"explosion de la mécatronique. Généralement, les actionneurs mis en œuvre restent des actionneurs électriques pour des applications courantes de petites à moyennes puissances. Il reste que le domaine de fonctionnement de ces moteurs restent autour de vitesses relativement élevées (typ. 1500 à 8000 tr/min) ce qui nécessite l'utilisation de réducteurs encombrants, bruyants et si les rapports de réduction sont importants source de pertes. Par ailleurs dans la logique de l'approche mécatronique, l'intégration des fonctions est recherchée. Dans le cas de l'actionnement, on essaie d'associer les mesures associées (vitesse, force, ou couple). A côté des techniques matures (moteurs électriques, pneumatiques ou hydrauliques), la recherche est active autour des perspectives ouvertes par l'emploi des matériaux et systèmes adaptatifs.

Depuis les années 1990, la notion de matériaux adaptatifs a émergée comme étant une voie prometteuse pour le développement de systèmes intégrés. Cette idée repose sur les propriétés de ces matériaux qui présentent de couplages réversibles forts entre différents domaines physiques et permettent ainsi de cumuler des fonctions actionneurs/capteurs. L'exemple des piézoélectriques est le plus abouti avec des applications telles que les injecteurs ou des actionneurs utilisés dans les microscopes à force atomique. Le panel de ces nouveaux matériaux est vaste : electro ou magnétostrictifs, électro ou magnéto rhéologiques, polymère électroactifs.

Cependant, les applications développées se limitent encore trop souvent à la seule exploitation du domaine linéaire de leur comportement, comme dans les piézoélectriques, ou à des applications de type tout ou rien, comme dans les alliages à mémoire de forme. Le comportement fortement non linéaire (hystérésis) de ces matériaux explique la difficulté de développer des outils de commande performants adaptés aux particularités de cette classe de matériau. La réalisation de tels outils constitue un domaine de recherche très actif ces dernières années. L'objectif de ce travail consiste à démontrer que l'utilisation d'une stratégie de commande adaptative prédictive constitue une réponse pertinente dans le cas des actionneurs en alliage à mémoire de forme. Le principal avantage de

cette démarche est de s'affranchir au maximum de la contrainte d'une connaissance a priori du système et donc de la lourdeur et de l'imprécision d'une phase d'identification hors ligne des paramètres du matériau.

1.2 Alliage à Mémoire de Forme (AMF)

Les alliages à mémoire de forme sont depuis longtemps présentés comme étant particulièrement performants pour les applications de type actionneurs car ils peuvent développer des efforts et des déplacements importants et ils disposent d'une énergie massique élevée. Nous présentons ici les principales caractéristiques de leur fonctionnement en insistant sur les principales propriétés qui concernent leur utilisation en tant qu'actionneurs. Les AMF les plus courants sont les nickel-titane, les bases cuivre (CuAlNi , CuAlBe) et les NiMnGa . Quelqu'en soit la composition, ce type de matériau présente deux phases :

- austénite : c'est la phase à haute température. Sa maille est cubique à face centrée. En refroidissant elle donne naissance à la martensite par une transformation displacive sans diffusion.
- martensite : cette phase est présente à basse température. La transformation de l'austénite en martensite s'accompagne d'une très faible variation de volume et d'une déformation par cisaillement très importante, typiquement de l'ordre de 20%. La nécessité d'accommorder ce cisaillement conduit à la formation de domaines martensitiques dont les cisaillements se compensent mutuellement. Ce phénomène est à l'origine de la structure en chevron caractéristique de la martensite. On parle alors de martensite auto-accommodante. La grande mobilité des interfaces interdomaines ainsi créées confère à la martensite une ductilité apparente très importante par réorientation des domaines martensitiques. Sous l'effet d'une contrainte induite par un chargement externe, la martensite se développe ou se réoriente selon une direction particulière donnant naissance à une déformation importante. La martensite est alors orientée.

L'utilisation des AMF en tant qu'actionneurs consiste à exploiter la transition entre la phase austénitique et la phase martensitique orientée par l'utilisation d'une précontrainte externe. Cela suppose donc d'agir sur la température afin de déclencher la transition. Une difficulté est introduite par le fait que les températures à partir desquelles la transformation s'opère sont variables selon :

- la valeur de précontrainte
- le sens de la variation de température

ceci introduit donc une hystérésis schématisée sur la Fig .5.4 où on peut voir sur la sous figure (b) que le racourcissement d'un échantillon intervient entre les température A_s (austenite start) et A_f (austenite finish), alors que l'allongement se produit entre M_s et M_f (martensite start et finish resp.). Il apparaît donc des zones "mortes" entre A_f et M_s et A_s et M_f , tandis que les zones effectives se situent sur des plages relativement étroites. Pour appréhender complètement la problématique que cela induit pour la commande, il convient d'insister sur le fait que ces températures évoluent en fonction de la précontrainte, or la charge qui devra être actionnée participe à ce chargement. En bref, l'hystérésis est modifiée par la force produite par le mécanisme devant être actionné et

qui n'est pas nécessairement connu.

1.3 Actionneurs à Alliage à Mémoire de Forme

L'utilisation des alliages à mémoire de forme pour la réalisation d'actionneur selon le principe énoncé précédemment se base sur deux principales configurations :

- un fil (ou une plaque) prédeformée en traction (sous l'effet d'une précontrainte) : par chauffage la déformation est récupérée. Dans ce fonctionnement la totalité du matériau est exploitée car le champs de déformation est homogène. La déplacement est directement proportionnel à la déformation initiale et à la dimension du dispositif (dans la direction où la déformation est appliquée)
- un ressort est prédeformée et la déformation récupérée par chauffage qui déclenche la transformation martensite → austénite. Le matériau travaille en torsion, et la déformation n'étant plus homogène (mais proportionnelle au rayon) le matériau est moins bien utilisé. En revanche grâce aux effets géométrique, la course obtenue est importante pour des niveaux de déformations acceptables.

Dans les deux cas le mouvement obtenu est linéaire, il peut être ensuite transformé en mouvement de rotation par l'utilisation de leviers par exemple. La Fig. 5.5 présente certaines solutions pour différentes fonctions.

Du point de vue dynamique, la transformation de phase étant extrêmement rapide, le temps de réponse d'un système actionné par des AMF est imposé par les échanges thermiques qui sont par nature beaucoup plus lents. Pour les températures qui nous intéresseront, un modèle convectif est suffisant. L'équation d'évolution de la différence de température par rapport à la température ambiante $\theta = T - T_{amb}$ est alors donnée par :

$$mc \frac{d\theta}{dt} + hA\theta = P_t + P_{ex} \quad (1.1)$$

avec m la masse de l'échantillon, c la chaleur spécifique, h le coefficient de convection, A est l'aire de la surface d'échange, P_t la puissance échangée, et P_{ex} est la puissance dégagée par la transition de phase. En introduisant la chaleur spécifique équivalente qui inclut la puissance P_{ex} , Reynaerts & Van Brussel (1998) expriment le temps d'actionnement pour le refroidissement t_c (qui n'est en général pas contrôlé par l'utilisateur et constitue donc la phase la plus lente lors de l'actionnement) :

$$t_c = -mc'/hA \ln(M_f/M_s) \quad (1.2)$$

Il découle de cette expression que le choix du matériau est important pour les performances dynamiques. Il est difficile d'agir sur le refroidissement artificiellement. Ceci nécessite des équipements permettant la convection forcée ou des dispositifs utilisant le couplage électro-calorique (effet Peltier) ou magnéto-calorique. Mais dans ces derniers cas, la complexité du dispositif augmente fortement. Certaines architectures peuvent également être envisagées telles que l'association en parallèle de plusieurs fils fins ce qui a pour effet d'augmenter la surface d'échange, tout en conservant des efforts importants puisqu'ils résultent de la section cumulées des différents fils (voir Fig. 5.5-(d)). Les architectures (b) et (c) de la même figure, dites antagonistes permettent une action dans

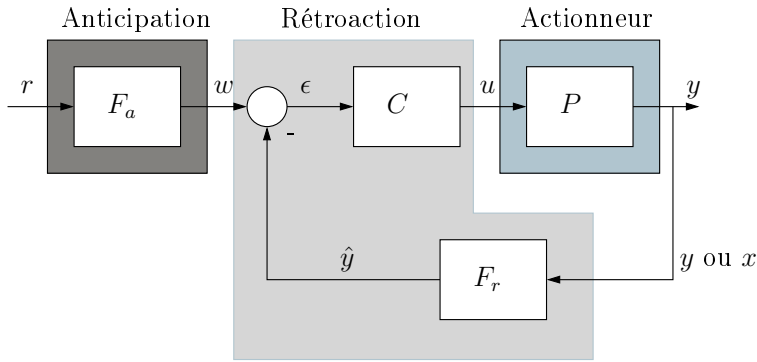


FIGURE 1.1 – Schéma bloc du principe de l’asservissement d’un système mono-entrée, mono-sortie. Ici par simplification, on a supposé que la sortie été captée, mais on peut en réalité capter x l’état du système

les deux sens, et un certain gain de temps car dans ce cas l’actionnement est uniquement produit par le chauffage de l’un des deux éléments.

Après ce rapide examen des propriétés des SMA, en adoptant un point de vue orienté vers la commande, les points importants sont d’une part la non-linéarité de l’hystérésis, et la dynamique imposée par les échanges thermiques.

1.4 Modélisations et commandes

Les difficultés posées par la commande des actionneurs en AMF ont suscitées de nombreuses recherches soit pour effectivement adresser le problème, soit comme démonstrateurs pour des modèles de commandes. Dans tous les cas le problème de la modélisation est central. Les approches sont différentes suivant les stratégies de commande adoptées par les auteurs. La Fig. 1.1 représente une configuration classique pour un système mono-entrée mono-sortie. L’objectif est de réaliser en sortie y de l’actionneur P la référence r . Pour cela, on dispose de plusieurs possibilités, celle représentée sur la figure regroupant l’ensemble des actions pouvant être utilisés :

1. une action d’anticipation : si on dispose de la connaissance a priori d’une perturbation ou d’une non-linéarité statique, celle-ci peut être prise en compte pour traiter la référence et générer un signal de référence w grâce à un opérateur F_a qui compense en partie l’effet de la perturbation. Elle intervient en boucle ouverte, c’est à dire que les incertitudes peuvent se retrouver en sortie ;
2. une action sur la mesure due à l’opérateur F_r : celle ci peut être un simple filtrage destiné à la suppression du bruit, mais elle peut être plus complexe comme dans le cas de la linéarisation par retour d’état, le signal \hat{y} est alors utilisé pour définir l’erreur d’asservissement $\epsilon = w - \hat{y}$;
3. une action de correction C qui en fonction de l’erreur d’asservissement calcule l’entrée u à appliquer au système pour minimiser cette erreur.

Trois approches de modélisation radicalement différentes sont utilisées pour la commande des actionneurs AMF. La première consiste à adapter au problème de la commande les modèles de comportement des AMF proposés par les mécaniciens des maté-

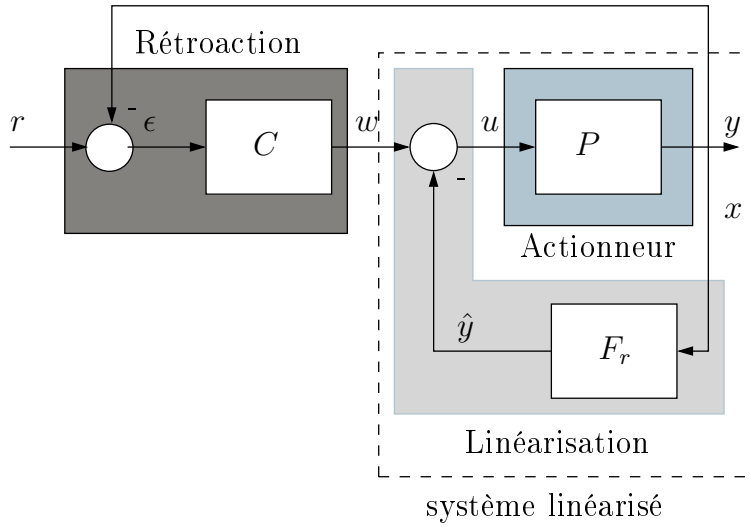


FIGURE 1.2 – Schéma bloc de la commande avec linéarisation par retour d'état (Benzaoui *et al.*, 1999)

riaux. Les travaux réalisés à FEMTO-ST et dans l'équipe du Pr. Elahina relèvent de cette approche. La seconde met en oeuvre les modèles phénoménologiques développés par les physiciens pour décrire les phénomènes d'hystéresis. Le modèle de Preisach est le plus utilisé de ces modèles. La dernière approche, radicalement différente, s'affranchie de toute description du comportement des AMF en adaptant à la commande d'un système fortement non linéaire l'utilisation des PID classiques.

1.4.1 Commandes avec modèles constitutifs

La compréhension des phénomènes thermodynamiques sous jacent à la transformation de martensitique permet d'élaborer des modèles macroscopiques décrivant le comportement non linéaire avec hystéresis. Ainsi, le modèle proposé par Leclercq & Lexcellent (1996) permet, après identification adéquate des paramètres matériau du modèle, de prévoir le comportement dans des cas de chargement mécanique analogues à ceux rencontrés dans les actionneurs AMF, c'est à dire lors de trajets de refroidissement et de chauffage sous contrainte appliquée. En apportant un certains nombres de simplification visant à linéariser par morceau l'hystéresis, Benzaoui *et al.* (1999) a pu appliquer des technique de linéarisation par retour d'état. En effet, le système peut alors se mettre sous la forme standard d'un système non-linéaire affine :

$$\begin{aligned}\dot{x} &= f(x) + g(x)u \\ y &= h(x).\end{aligned}\tag{1.3}$$

En se basant sur les notation de la Fig. 1.2, le signal $\hat{y} = \frac{L_f^n h(x)}{L_g L_f^{n-1} h(x)}$ où $L_f h(x)$ et $L_g h(x)$ sont les dérivées de Lie de la fonction $h(x)$ selon les fonctions $f(x)$ et $g(x)$ permettent de substituer au système initial un système linéarisé constitué par une chaîne de n intégrateurs (n étant le degré relatif lié aux propriétés différentielles du système non linéaire).

Un correcteur est alors utilisé pour générer le signal w . Dans le cas du modèle proposé, le système est suffisamment simple pour se ramener à un unique intégrateur, et un simple correcteur proportionnel s'avère alors suffisant. La principale difficulté de cette approche reste lié à l'identification du modèle qui doit être faite hors ligne. Cela pose la question de la robustesse de la commande avec les variations des paramètres matériau de la loi de comportement au cours du temps (vieillissement) et au cours du cyclage (fatigue). Des phénomènes auxquels les AMF sont tout particulièrement sensibles.

Une autre approche faisant intervenir un modèle de comportement issu de la mécanique des matériaux a été proposée par Elahinia ([Elahinia & Ashrafiou, 2002](#); [Elahinia & Ahmedian, 2006](#); [Williams et al., 2010](#)). Son approche n'est pas à proprement parler fondée sur un modèle constitutif pour la commande. En effet dans les applications présentées, une régulation par modes glissants est proposée. Cependant, l'utilisation d'un modèle constitutif permet d'estimer l'état interne de l'actionneur par le biais d'un estimateur de Kalman, ce qui permet d'améliorer le fonctionnement de la commande ([Elahinia & Ahmedian, 2006](#)). Son principe est résumé sur la Fig. 5.8 : à partir des mesures de la tension appliquée et du déplacement le filtre de Kalman reconstruit la contrainte et la température dans le fil. Ceci permet d'améliorer la proposition initiale qui reposait uniquement sur un correcteur proportionnel dérivé ([Elahinia & Ashrafiou, 2002](#)).

Dans ces études, le problème que soulève l'utilisation de modèle constitutif est la complexité des modèles proposés qui nécessite la connaissance de nombreux paramètres : 19 dans le cas de [Benzaoui et al. \(1999\)](#) et 17 dans le cas de [Elahinia & Ashrafiou \(2002\)](#).

Ceci présente deux inconvénients : il faut mettre en place des protocoles d'essais qui soient applicables dans un contexte industriel, et surtout il faut que les paramètres du modèle constitutif restent stables pendant la durée de vie de l'actionneur pour conserver l'efficacité de la commande. Dans la section suivante, les techniques proposées prennent de la distance avec la réalité physique pour ne décrire que le comportement entrée-sortie du système et diminuer le nombre de paramètres nécessaires.

1.4.2 Commande à partir de modèles phénoménologiques

La modélisation des hystérosis a été très étudiée dans le contexte du magnétisme (voir par exemple l'article de Mayergoyz de la ref. [Bossavit et al. \(1991\)](#)). Il existe plusieurs variations de cette approche, nous présentons ici rapidement la plus ancienne, le modèle de Preisach. Ces méthodes reposent sur l'utilisation :

- d'opérateurs élémentaires non linéaires
- d'une fonction de pondération

Dans le cas du modèle de Preisach, un opérateur élémentaire (hystéron) est défini par :

$$\Gamma_{(\alpha,\beta)}(\bullet, \gamma_{-1}) : u \in [u_{min}, u_{max}] \mapsto \{-1, 1\}$$

$$\Gamma_{(\alpha,\beta)}(u, \gamma_{-1}) = \begin{cases} +1 & \text{si } u > \alpha \\ -1 & \text{si } u < \beta \\ \gamma_{-1} & \text{si } \beta \leq u \leq \alpha \end{cases} \quad (1.4)$$

où γ_{-1} est le précédent état de l'hystéron. Par ailleurs, les seuils α et β doivent vérifier $\alpha \geq \beta$ pour que l'opérateur soit correctement défini, ainsi les hystérons admissibles sont

définis dans le demi plan $\mathbb{P} := \{(\alpha, \beta) \in \mathbb{R}^2 : \alpha \geq \beta\}$. En pratique l'entrée u est bornée, elle appartient donc à l'intervalle $\mathcal{D} = [u_{min}, u_{max}]$. Finalement, cela définit une portion du plan, appelée communément plan de Preisach : $\mathbb{P} := \{(\alpha, \beta) \in \mathcal{D}^2 : \alpha \geq \beta\}$. La sortie de l'hystérésis est égale à la somme pondérée par la fonction de pondération $\mu(\alpha, \beta)$ de la sortie des différents hystérésis soit :

$$P_\mu(u, \gamma_{-1}) = \iint_{\mathbb{P}} \Gamma_{(\alpha, \beta)}(u, \gamma_{-1}) \mu(\alpha, \beta) d\alpha d\beta \quad (1.5)$$

Si $\mu(\alpha, \beta) \geq 0 \quad \forall (\alpha, \beta) \in \mathbb{P}$ alors l'hysteresis préserve l'ordre c'est à dire que pour une suite ordonnée d'entrée $u(t_1) < u(t_2) < \dots < u(t_n)$ la sortie est également une suite ordonnée vérifiant la relation $P(u(t_1), \gamma_0) < P(u(t_2), \gamma_0) < \dots < P(u(t_n), \gamma_0)$. Ainsi pour une entrée monotone, la sortie est monotone et il est possible d'inverser la relation entrée sortie pour ce chemin particulier.

Une interprétation géométrique simple est possible, illustrée par la Fig. 1.3. Une entrée

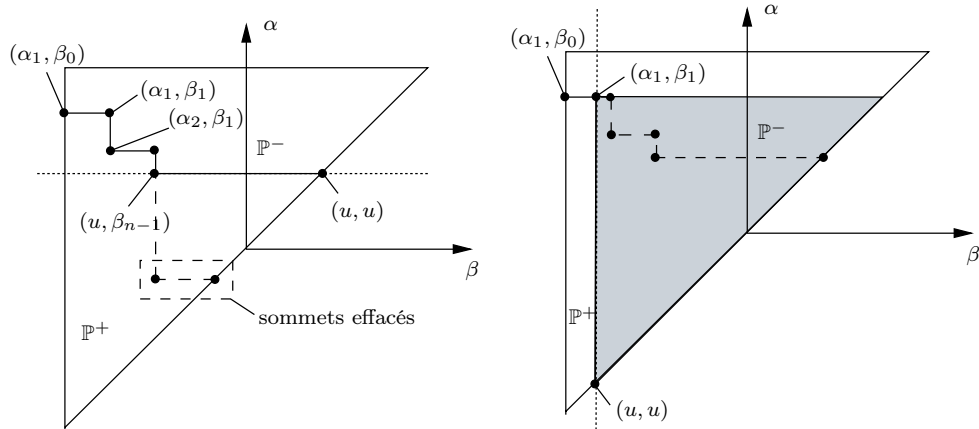


FIGURE 1.3 – Exemple d'évolution du modèle de Preisach dans le plan de Preisach : (a) pour une entrée croissante u , (b) pour une entrée décroissante. Dans les deux cas illustrés, il y a effacement des coins qui représente une inversion de l'entrée. Le triangle coloré présente un intérêt pratique particulier car il permet l'identification de la fonction de pondération μ .

croissante provoque le changement d'état à 1 des hystérons tel que $\alpha < u$ ce qui se traduit par une frontière horizontale se déplaçant vers le haut et laissant tout les hystérons au dessous à l'état "haut" (Fig.1.3-a). (Fig.1.3-b). Une entrée décroissante se traduit par un déplacement de la frontière vers la gauche en laissant tout les hystérons à sa droite à l'état "bas". On note que durant cette évolution des sommets représentant des extrema locaux de l'entrée sont effacés (cas de la Fig. 1.3) ce qui illustre qu'une partie de l'historique des entrées est effacée. A l'extrême, l'hystérésis peut être réinitialisé à sa valeur de saturation supérieure ou inférieure selon que l'entrée atteint l'une ou l'autre des bornes du domaine \mathcal{D} . L'hystérésis est alors saturée.

Dans des cas intermédiaires le plan de Preisach est divisé en deux régions (\mathbb{P}^+ and \mathbb{P}^-) qui ne contiennent que des hystérons dans des états semblables. Les sommet de cette

Chapitre 1. Introduction

frontière en escalier représente des extrema locaux de l'entrée comme il l'a déjà été mentionné. Sans entrer dans les détails qui peuvent être trouvés dans [Bossavit et al. \(1991\)](#), deux suites d'entrées peuvent produire la même sortie pour l'hystérésis, elles ont alors la même frontière dans le plan de Preisach. Cette unicité de la frontière permet donc une inversion de l'hystérésis qui peut être mise à profit pour compenser l'influence de l'hystérésis dans la réponse de l'actionneur ([Iyer et al., 2005](#)).

Des applications de cette stratégie ont été proposées pour la commande de dispositifs utilisant des matériaux magnétostrictifs ([Tan & Baras, 2004, 2005; Tan et al., 2005](#)). Dans ces travaux, le modèle de Preisach est identifié en ligne c'est à dire que la fonction de pondération est déterminée à partir de mesures effectuées au cours de l'évolution de l'actionneur. Pour des raisons pratiques, cette fonction est discrétisée et des poids sont affectés aux différentes zones du plan de Preisach. Le principe proposé est alors d'utiliser le modèle pour compenser *a priori* la non linéarité de l'hystérésis en modifiant la consigne. Il s'agit donc d'une anticipation. Les incertitudes liés à cette identification doivent être ensuite compensées par l'utilisation d'une rétroaction, dans le cas d'espèce soit une commande robuste, soit une commande adaptative.

Des variantes de ce principe sont définies en changeant de modèle de l'hystérésis. Citons les travaux de [Janocha & Kuhnen \(2000\)](#) qui utilisent un modèle de Prandtl-Ishlinskii pour lequel l'existence d'un inverse exact est présentée. [Chen et al. \(2009\)](#) propose également l'utilisation d'un tel modèle combiné avec une commande adaptative.

Enfin, de façon analogue, [Webb et al. \(1998\)](#) a adressé le problème de la commande d'actionneur AMF en utilisant une autre classe de modèle de l'hystérésis, le modèle de Krasnosel'skii et Pokovskii. Dans ce dernier cas, le modèle n'est pas utilisé pour une anticipation, mais exploité pour définir une commande adaptative.

Il ressort de l'analyse des différentes approches basées sur les modèles phénoménologiques que ces derniers ont pour avantage de substituer aux modèles non linéaires obtenus à partir des raisonnements physiques, un modèle linéaire, au sens où la sortie est la combinaison linéaire des contributions d'opérateurs non linéaires présentant une mémoire locale. Cela offre la possibilité d'utiliser des méthodes d'identification en ligne, et d'éviter ainsi la lourdeur et l'imprécision d'une phase d'identification hors ligne de paramètres. Il reste néanmoins un certain nombre de points délicats :

- pour calculer la sortie il est nécessaire de mémoriser l'état des hystérons ;
- la présence de bruit risque d'introduire une estimation erronée de l'état de ces hystérons qui peut introduire une instabilité dans l'identification ;
- l'utilisation d'un modèle inverse en anticipation dérivant d'un modèle d'hystérésis ne peut pas prendre en compte la dynamique du système car le modèle de Preisach est statique ;
- le modèle de Preisach ne peut pas prendre en compte des hystérésis assymétrique ;
- la discrétisation de l'hystérésis introduit nécessairement une erreur ;
- l'ensemble des modèles présentés suppose qu'une seule entrée est appliquée au système, or dans les cas des AMF l'hystérésis dépend à la fois de la température et de la contrainte.

pour l'ensemble de ces raisons, une rétroaction est systématiquement employée. L'approche phénoménologique n'a qu'une relation lointaine avec les phénomènes physiques, il reflète cependant le fait que dans le matériau un phénomène de commutation (la tran-

sition de phase) prend place, et qu'il est "moyenné" du fait de la répartition aléatoire des domaines. En s'éloignant encore de la réalité physique, on retrouve des approches plus spécifiques à l'automatique que nous évoquons à présent.

1.4.3 Méthodes classiques sans modèles explicites

En premier lieu, l'utilisation de PID a été étudiée par Jayendran *et al.* (2008) qui a montré que si elle était possible, elle nécessitait une mise au point expérimentale et que si certains paramètres devaient trop s'éloigner de conditions expérimentales, les performances s'en trouvaient dégradées.

Shameli *et al.* (2005) propose une amélioration au PID classique en introduisant une correction supplémentaire proportionnelle au cube de l'erreur, soit :

$$u(t) = K_p \cdot e(t) + K_i \cdot \int_0^t e(\tau) d\tau + K_d \dot{e}(t) + K_t e(t)^3 \quad (1.6)$$

La stabilité est prouvée en démontrant la passivité du système, et l'auteur montre que les transitoires sont améliorés au sens où les temps de réponse et les dépassements sont réduits. Cependant, le choix de K_t n'est pas explicité.

Ma & Song (2003) utilisent une commande par régime glissant élaborée en combinant un correcteur proportionnel dérivé et une modulation de largeur d'impulsion. Par la suite il propose une approche consistant à estimer la position à partir de la mesure de la résistance électrique de l'actionneur (Ma *et al.*, 2004). Pour cela un réseau de neurone est mis en œuvre. Le contrôleur implémenté est un proportionnel intégral agissant sur l'erreur entre la position de référence et la position estimée par le réseau de neurone. Cette technique impose de passer par une phase d'apprentissage du réseau de neurone ce qui est fait hors ligne en préliminaire. Cette approche est néanmoins intéressante parce qu'elle permet de supprimer le capteur de position une fois le réseau de neurone entraîné. Cependant il se pose encore une fois le problème de la sensibilité à la variation des paramètres avec le vieillissement et la fatigue du matériau. On note également un certain nombre de variation autour des modèles de type phénoménologiques associés au le problème de l'identification de la fonction de pondération. Ces variations proposent de résoudre le problème de l'identification de la fonction de pondération par l'utilisation de méthodes typiquement utilisées en intelligence artificielle (Song, 2003; Kumagai *et al.*, 2006; Ahn & Kha, 2007; Nguyen & Ahn, 2009) tel que les réseaux de neurones ou la logique floue. Dans l'ensemble des études citées, on remarque que l'identification est faite hors ligne ce qui enlève de l'intérêt à l'utilisation d'un modèle phénoménologique, dont le principal avantage, comme cela a été signalé, est d'offrir la possibilité d'une identification en ligne.

1.5 Contribution de la thèse

La motivation première de cette thèse est liée au constat suivant : bien que les AMF soient présentés comme une solution prometteuse, force est de constater que leur utilisation reste limitée. En effet, les propriétés de ces matériaux sont liées à une transition de phase : en passant d'une structure austénitique à une structure martensitique de grandes déformations sont possibles. Cependant, cette transition présente deux incon-

Chapitre 1. Introduction

vénients car d'une part elle est hystérotique et d'autre part elle est déclenchée à la fois par la température et par les conditions de chargement mécaniques. Ceci rend leur comportement sensible aux conditions d'échange thermique et aux interactions mécanique avec l'environnement. Ainsi, la plupart des applications rencontrées à l'heure actuelle se limitent à des utilisations de type "tout ou rien" où il est possible de fonctionner sur les parties "saturées" de l'hystérésis. Ce sont donc essentiellement des mécanismes offrant deux positions d'équilibre qui constituent l'essentiel des applications jusqu'à aujourd'hui.

Paradoxalement, une recherche active autour de la commande des actionneurs en alliages à mémoire de forme démontre sans conteste la possibilité d'utiliser ce type de solution pour du positionnement. Toutefois, la présence d'une hystérésis a donné lieu à plusieurs études cherchant à définir des lois structurelles ou phénoménologiques traduisant cette particularité, puis de s'appuyer sur ces modèles pour construire un contrôleur. Compte tenu de la complexité du phénomène physique, les stratégies résultantes présentent un fort degré de sophistication ce qui peut détourner le praticien de ces solutions. Un obstacle de taille reste la nécessité dans la majorité des cas d'introduire une phase d'identification hors ligne alors qu'il est connu que les paramètres caractérisant le comportement du matériau évoluent au cours du temps. De ce point de vue, les méthodes adaptatives présentent un intérêt indéniable. D'un autre côté, elles sont relativement délicates à mettre en œuvre dès lors que la stabilité rentre en compte, et ce même pour des systèmes linéaires. En ce qui concerne les applications non-linéaires la difficulté est naturellement accrue.

Un angle d'approche différent consistant à considérer l'effet de l'hystérésis sur la dynamique du système est adopté dans le cadre de cette thèse, l'objectif étant de simplifier au maximum la technique de commande. En effet, étymologiquement, l'hystérésis est un retard, même si dans le cas présent il soit variable, et qu'il y ait également une influence sur le gain. L'idée est donc de considérer le système comme étant linéaire à paramètres variant dans le temps étant entendu que cette dépendance temporelle est induite par la variation des variables d'état de l'hystérésis. L'étude de tels systèmes est à l'heure actuelle un sujet de recherche en plein développement ([Tóth, 2010](#)) mais d'un point de vue pratique se posent encore des problèmes quant à la lourdeur du formalisme et des algorithmes qui en découlent. Dans un souci de simplification, il sera supposé dans ce travail que le système est échantillonné suffisamment rapidement comparé à sa constante de temps dominante. Si une méthode d'identification suffisamment précise est mise en œuvre, et que la classe du modèle inclut le système, on peut alors supposer que le modèle identifié est une représentation linéaire du comportement réelle du système autour du point de fonctionnement considéré. Dès lors, il est possible d'adapter un contrôleur linéaire à partir des paramètres du modèle dans le cadre d'une commande adaptive prédictive.

L'intérêt de cette démarche est :

- de substituer au système non-linéaire réel un système linéaire approchant le comportement dans un voisinage ;
- de capturer le comportement dynamique ;
- de s'affranchir au maximum d'une connaissance a priori, et ainsi d'éviter une identification hors ligne de paramètres.

Il est alors possible en se replaçant dans le cadre des systèmes linéaires invariant d'exploiter des outils bien établis. La principale difficulté est que tout repose sur la capacité à identifier un modèle linéaire. Or l'une des conditions préliminaire pour y parvenir est que le modèle linéaire inclue la dynamique du système. Cela suppose en pratique que l'ordre du système réel soit connu. Pour lever cet obstacle, la proposition de la thèse est d'utiliser une famille de fonction orthogonale de l'espace des fonctions rationnelles pour le modèle paramétré : les fonctions de Laguerre. En effet, ces fonctions constituent une base orthogonale sur laquelle les fonctions rationnelles peuvent être projetées. Dès lors, le problème du choix de l'ordre est contourné puisque le choix de l'ordre de troncation de l'approximation par une combinaison linéaire ne se pose plus en terme d'existence d'un jeu de paramètres qui permettent de décrire le système réel : dans tous les cas, l'approximation linéaire du système réel admettant une projection sur une base de fonction de Laguerre, c'est la précision du modèle qui est en cause, mais pas son existence. De plus, la convergence du modèle de Laguerre¹ est assuré et son taux de convergence est lié, comme il sera expliqué plus tard au choix du pole du filtre de Laguerre. Ce choix est simple, dans la mesure où il doit être proche de la constante de temps dominante du système.

Le mémoire s'articule ainsi de la façon suivante :

- Dans le chapitre 2, les techniques de modélisation en vue de l'identification sont présentées. Les fonctions de Laguerre sont introduites. L'algorithme des moindre carré récursifs est introduit et son extension au cas des modèles de Laguerre présentée. De plus, une série de Volterra utilisant les fonctions de Laguerre pour noyaux est introduite. L'intérêt est leur capacité à modéliser des systèmes non-linéaire de façon simple, en se basant sur les fonctions déjà introduites. Une validation expérimentale est ensuite présentée. Elle consiste à identifier deux actionneurs linéaire à AMF, l'un fonctionnant à contrainte constante, le second est un actionneur antagoniste qui fonctionne par définition à contrainte variable. Dans les deux cas des indicateurs sont proposés et l'influence des différents paramètres de l'algorithme et du modèle évalué.
- Le chapitre 3 aborde le problème de la commande prédictive adaptative. Après un rappel des principes de la commande prédictive, une loi de commande simple basée sur un prédicteur exploitant le modèle de Laguerre est présentée. Cette méthode n'est pas nouvelle puisqu'elle a été présenté par Dumont *et al.* (1990) mais nous apportons une preuve de la stabilité conditionnelle de l'algorithme. L'introduction d'une norme matricielle particulière permet en effet de démontrer la dépendance de la stabilité vis à vis de l'horizon de prédiction, évoquée par Dumont et al. mais à notre connaissance jamais démontré. Il résulte de nos développements une borne qui reste conservative compte tenu de l'outil proposé pour la démonstration. Une étude expérimentale suit qui met en évidence la nécessité d'améliorer l'algorithme d'identification mis en défaut par la pauvreté du signal d'excitation. Un algorithme avec facteur d'oubli directionnel amène une amélioration notable. La validation est basé sur des critères qui permettent d'examiner

1. par souci de concision, le terme "modèle de Laguerre" désigne la décomposition en une combinaison linéaire de fonction de Laguerre à un ordre N dans la suite.

Chapitre 1. Introduction

l'influence des différents paramètres de l'algorithme sur les mêmes actionneurs que précédemment. Finalement une modification de la structure du contrôleur est proposée inspirée de la commande adaptative avec modèle de référence. La preuve de la stabilité est présentée et une validation expérimentale est présentée qui montre une nette amélioration comparé avec l'algorithme de Dumont.

- Enfin la conclusion résume nos résultats et présente les améliorations possibles.

Chapitre 2

Modélisation

2.1 Introduction

L'objectif du chapitre est de mettre en place et d'évaluer un outil de modélisation et d'identification capable de prendre en compte l'effet de l'hystérésis sur la dynamique du système. Ainsi, il s'agit d'un nouveau paradigme par rapport aux approches qui ont été utilisées jusqu'à présent pour la commande des AMF. Plutôt que de comprendre les mécanisme physique, il s'agit de capturer le comportement dynamique à court terme, c'est à dire de disposer d'un modèle capable de prédire la sortie à échéance donnée en ne se basant que sur les états actuels et passés de la sortie et de l'entrée, ce qui est communément appelé une approche boîte noire. En ce qui concerne le cas des systèmes à paramètres variables, les outils classiques sont à la marge de leur domaine d'application, et ce qu'ils représentent doit être compris comme le modèle linéarisé du système réel autour de l'instant considéré. L'algorithme doit remplir deux objectifs contradictoires :

- permettre l'identification rapide des paramètres ;
- être stable vis à vis du bruit.

Nous introduisons à présent les techniques usuelles de modélisation et d'identification des systèmes linéaires invariants, et leur extension dans le cas où le modèle est un modèle de Laguerre.

2.2 Modélisation des systèmes linéaires invariants

2.2.1 Modèle discrets en environnement déterministe

Dans ces hypothèses, un modèle général de système à entrée et sortie unique ne dépendant que des états et des entrées passés peut s'exprimer par :

$$y(t+1) = -A^*(q^{-1})y(t) + q^{-d}B^*(q^{-1})u(t) \quad (2.1)$$

où q est l'opérateur de décalage temporel :

$$q^{-1}y(t) = y(t-1) \quad (2.2)$$

signifie la valeur prise par y à l'instant d'échantillonnage précédent. $A^*(q^{-1})$ et $B^*(q^{-1})$ sont des polynômes :

$$A(q^{-1}) = 1 + A^*(q^{-1}) = 1 + a_1 q^{-1} + \cdots + a_n q^{-n_a} \quad (2.3)$$

$$B(q^{-1}) = b_1 q^{-1} + \cdots + b_n q^{-n_b} = q^{-1} B^*(q^{-1}) \quad (2.4)$$

La relation (2.1) est utile pour construire un prédicteur à un pas. En supposant qu'à un instant t on dispose d'une évaluation des coefficients des différents polynômes a_i ($i \in 1 \dots n_a$), b_i ($i \in 1 \dots n_b$) et des mesures des entrées et sorties (respectivement $\{u(t - n_b) \dots u(t)\}$ et $\{y(t - n_a) \dots y(t)\}$) :

$$\hat{y}(t+1|t) = -A^*(q^{-1})y(t) + q^{-d}B^*(q^{-1})u(t) \quad (2.5)$$

où $\hat{y}(t+1|t)$ est la prédiction pour le pas $t+1$ compte tenu des connaissances disponibles à l'instant t . Par récurrence, il est possible de construire un prédicteur à j pas.

2.2.2 Environnement stochastique

La modélisation précédentes ne prend pas en compte les perturbations. Une approche consiste à les considérer comme étant la sortie filtrée $v(t)$ d'un processus stochastique $e(t)$ supposé être un bruit blanc de valeur moyenne nulle :

$$v(t) = \frac{C(q^{-1})}{D(q^{-1})}e(t) \quad (2.6)$$

où $C(q^{-1})$, et $D(q^{-1})$ sont des polynômes, le degré de $C(q^{-1})$ étant inférieur ou égal à celui de $D(q^{-1})$.

Le modèle à erreur de sortie couramment utilisé consiste à prendre ces polynômes égaux à l'unité (pas de structure particulière de la perturbation) :

$$y(t+1) = \frac{q^{-d}B^*(q^{-1})}{A(q^{-1})}u(t) + v(t+1) \quad (2.7)$$

En présence de la perturbation, le meilleur estimateur minimisera la variance de l'erreur, condition écrite comme suit :

$$E \left\{ [y(t+1) - \hat{y}(t+1)]^2 \right\} = E \left\{ \left[\frac{q^{-d}B^*(q^{-1})}{A^*(q^{-1})}u(t) + v(t+1) - \hat{y}(t+1) \right]^2 \right\} \quad (2.8)$$

laquelle devient après développement :

$$\begin{aligned} E \left\{ [y(t+1) - \hat{y}(t+1)]^2 \right\} &= E \left\{ \left[\frac{q^{-d}B^*(q^{-1})}{A^*(q^{-1})}u(t) - \hat{y}(t+1) \right]^2 \right\} + E \left\{ [v(t+1)]^2 \right\} \\ &\quad + 2E \left\{ v(t+1) \left[\frac{q^{-d}B^*(q^{-1})}{A^*(q^{-1})}u(t) - \hat{y}(t+1) \right] \right\} \end{aligned} \quad (2.9)$$

dans l'hypothèse où la perturbation est indépendante de l'entrée (et donc de la sortie), le dernier terme de l'équation précédente tend vers 0. La variance de la perturbation

$v(t)$ étant bornée, il faut minimiser le premier terme en choisissant pour prédicteur :

$$\hat{y}(t+1) = \frac{q^{-d}B^*(q^{-1})}{A^*(q^{-1})}u(t)$$

ce qui en multipliant par $A^*(q^{-1})$ des deux côtés donne :

$$\hat{y}(t+1) = -A^*(q^{-1})\hat{y}(t) + q^{-d}B^*(q^{-1})u(t) \quad (2.10)$$

ce qui montre que le prédicteur optimal dépend des entrées et de *ses prédictions* passées.

2.3 Identification

2.3.1 Moindres carrés

En définissant le vecteur des mesures :

$$\varphi(t)^T = [\hat{y}(t) \ \dots \ \hat{y}(t-n_a) \ u(t) \ \dots \ u(t-n_b)] \quad (2.11)$$

et le vecteur des paramètres :

$$\theta^T = [a_1 \ \dots \ a_{n_a} \ b_0 \ \dots \ b_{n_b}] \quad (2.12)$$

L'Eq. (6.14) est réécrite comme une régression linéaire :

$$\hat{y}(t+1) = \varphi(t)^T \cdot \theta \quad (2.13)$$

On peut écrire les relations auxquelles doit satisfaire le modèle pour N_m mesures sous forme matricielle :

$$\underbrace{\begin{bmatrix} y(1) \\ y(2) \\ \vdots \\ y(N_m) \end{bmatrix}}_Y = \underbrace{\begin{bmatrix} \varphi(1)^T \\ \varphi(2)^T \\ \vdots \\ \varphi(N_m)^T \end{bmatrix}}_\Phi \theta \quad (2.14)$$

En soustrayant des deux côtés de l'égalité par $\Phi\theta$ on obtient l'erreur. Pour minimiser la distance entre le modèle et le système, on cherche le vecteur de paramètre $\hat{\theta}$ qui minimise ce critère :

$$J(\theta) = \{(Y - \Phi\theta)^T(Y - \Phi\theta)\} \quad (2.15)$$

On peut montrer que ceci revient à résoudre :

$$\hat{\theta} = (\Phi^T\Phi)^{-1}\Phi Y \quad (2.16)$$

A condition que la matrice $\Phi^T\Phi$ (de dimension $N_m \times N_m$) soit inversible. Elle est nécessairement semi-définie positive. Pour qu'elle soit strictement positive, il faut que le signal $u(t)$ comporte un nombre de fréquences au moins égal au nombre de paramètres à identifier $n_A + n_B$. Ceci constitue la condition d'excitation permanente et joue un rôle très important dans le domaine de l'identification (Ljung, 1999). Il est du ressort de

l'utilisateur de définir correctement le signal $u(t)$ pour vérifier cette condition.

2.3.2 Moindres carrés récursifs

Les moindres carrés peuvent s'exprimer de façon récursive, contrairement à l'expression donnée par l'Eq. (2.16) qui nécessite un traitement par lot (toutes les mesures doivent être disponibles au moment de l'évaluation). On définit la matrice dite de corrélation $R(t) = \Phi(t)^T \Phi(t)$. La mise à jour de cette matrice étant définie par un algorithme de type gradient :

$$R(t) = \mu R(t-1) + \lambda \varphi^T \varphi \quad (2.17)$$

où μ et λ sont deux coefficients qui pour des raisons de stabilité doivent vérifier : $0 < \lambda \leq 1$, et $0 < \mu \leq 1$. Par le lemme d'inversion, on peut établir l'algorithme résumé sur la Tab. (2.1) Le choix du doublet $\{\lambda, \mu\}$ confère à l'identification des comportements

| Initialisation |
|---|
| $R(0) = \delta^{-1} I_{N \times N}$ avec $\delta \in \mathbb{R}^+ \setminus \{0\}$ |
| $\hat{\theta}(0) = 0$ |
| $0 < \lambda \leq 1$ et $0 < \mu \leq 1$ |
| Pour $t \in 1..t_f$ calculer : |
| $k(t) = \frac{R^{-1}(t-1)\varphi(t)^T}{\frac{\lambda}{\mu} + \varphi(t)R^{-1}(t-1)\varphi(t)^T}$ $\varepsilon(t) = Y(t) - \varphi^T(t)\hat{\theta}(t-1)$ $\hat{\theta}(t) = \hat{\theta}(t-1) + k(t)\varepsilon(t)$ $R^{-1}(t) = \frac{1}{\lambda} (R^{-1}(t-1) - k(t)\varphi(t)^T R^{-1}(t-1))$ |

TABLE 2.1 – Algorithme des moindres carrés récursifs

différents. Pour l'application qui nous intéresse, il s'agit de donner à l'identification une certaine adaptabilité. Il faut progressivement effacer les données obsolètes en faveur de celles plus récentes, qui traduisent le comportement du système autour de l'instant considéré. Cela est obtenu par l'utilisation d'une fenêtre glissante à pondération exponentielle. Ceci correspond à des valeurs constantes $0 < \lambda < 1$ et $\mu = 1$.

2.4 Base des fonctions de Laguerre

2.4.1 Intérêt

L'utilisation de modèles tels que ceux donnés par l'Eq. (2.1) est lié au fait que leur réponse impulsionnelle est finie. De ce fait, la modélisation de systèmes dont la réponse impulsionnelle est longue comparée à la période d'échantillonage suppose des degrés élevés des polynômes $A(q^{-1})$ et $B(q^{-1})$. Des problèmes se posent alors :

- instabilité de l'algorithme d'identification liée aux erreurs d'arrondis (oscillations des coefficients d'ordre élevés) ;
- instabilité du modèle identifié par compensation de pôles et zéros instables.

Il est naturel dans ce cas d'utiliser des filtres à réponse impulsionale infinie (RII). L'utilisation de ce type de filtre pose cependant des problèmes de stabilité. Il est donc intéressant de considérer des classes particulières de filtres RIF qui soient stables et forment des bases orthogonales. Dans une telle base, le modèle d'un système s'écrit comme la combinaison linéaire des filtres $F_i(q^{-1})$:

$$y(t+1) = \sum_{i=0}^{N_f} c_i F_i(q^{-1}) u(t) \quad (2.18)$$

On peut alors réécrire le modèle sous la forme de l'Eq. (6.14) où le vecteur des régresseurs est à présent donné par :

$$\begin{cases} f_i(t) &= F_i(q^{-1}) u(t) \quad \text{pour } i \in \{1 \dots N_f\} \\ \phi^T(t) &= [f_0(t) \ f_1(t) \ \dots \ f_{N_f}(t)] \end{cases} \quad (2.19)$$

dès lors toute la démarche de l'algorithme des moindres carrés et sa forme récursive sont applicables.

2.4.2 Base orthonormale des fonctions de Laguerre discrètes

Elle est obtenue soit à partir de la forme continue des polynômes de Laguerre laquelle admet une transformée de Laplace, soit par la forme discrète des polynômes de Meixner pour une paramétrisation particulière (Belt, 1997). Ces derniers admettent une transformée en z et forment une base orthogonale sur l'espace de Hardy des fonctions causales de carrés sommables.

La transformée en z d'une fonction de Laguerre est donnée par :

$$L_m(a, z) = \frac{\sqrt{1-a^2}z}{z-a} \left(\frac{1-az}{z-a} \right)^{m-1} \quad (2.20)$$

où a est le pôle de Laguerre.

2.4.3 Propriétés

En utilisant la transformation conforme :

$$w^{-1} = \frac{1-az}{z-a} \Leftrightarrow z = \frac{1+w^{-1}a}{w^{-1}+a} \quad (2.21)$$

on montre facilement que tout système admettant une transformée en z admet une représentation donnée par :

$$G(z) = \sum_{m=0}^{\infty} g_m L_m(a, z) \quad (2.22)$$

Une propriété intéressante pour l'identification de cette représentation est que la matrice de covariance $R(t)$ introduite dans la présentation de l'algorithme des moindres carrés récursifs conserve sa structure, c'est à dire qu'elle reste Toepliz.

Chapitre 2. Modélisation

Soit la transformée en z d'un système du premier ordre :

$$H(z) = \frac{K}{z - z_0} \quad (2.23)$$

sa décomposition sous la forme d'une décomposition sur la base de Laguerre est donnée par Richard (2001) :

$$H(z) = \sum_{i=1}^{\infty} \frac{K\sqrt{1-a^2}}{1-az_0} \left(\frac{z_0-a}{1-az_0} \right)^{i-1} L_i(a, z) \quad (2.24)$$

On voit donc que les coefficients de la décomposition décroîtront d'autant plus rapidement que le pôle de Laguerre est proche du pôle du système, ce qui rejoint la recommandation usuelle de choisir le pôle de Laguerre proche de la constante dominante du système. En pratique, les fonctions de Laguerre peuvent être mises sous forme récursive :

$$\begin{cases} L_0(a, z^{-1}) = \frac{\sqrt{1-a^2}}{(1-az^{-1})} \\ L_k(a, z^{-1}) = L(a, z^{-1})L_{k-1}(a, z^{-1}) \end{cases} \quad \text{où} \quad L(a, z^{-1}) = \frac{z^{-1}-a}{1-az^{-1}} \quad (2.25)$$

ce qui permet de les implémenter simplement sous la forme d'un filtre transversal classique, d'où la dénomination filtre de Laguerre. Un modèle de Laguerre peut être très simplement mis sous forme de représentation ce qui sera mis en application pour la définition de la commande :

$$\begin{aligned} \begin{bmatrix} l_0(t+1) \\ l_1(t+1) \\ \vdots \\ l_n(t+1) \end{bmatrix} &= \underbrace{\begin{bmatrix} a & 0 & \dots & \dots & 0 \\ \beta & a & 0 & & 0 \\ -a\beta & \beta & a & 0 & 0 \\ \vdots & \ddots & \ddots & & \\ (-a)^{n-2}\beta & & & \beta & a \end{bmatrix}}_A \underbrace{\begin{bmatrix} l_0(t) \\ l_1(t) \\ \vdots \\ l_n(t) \end{bmatrix}}_1 + \underbrace{\sqrt{\beta} \begin{bmatrix} 1 \\ -a \\ a^2 \\ \vdots \\ (-a)^{n-1} \end{bmatrix}}_B u(t) \\ y(t) &= \underbrace{\begin{bmatrix} c_0 & c_1 & \dots & c_n \end{bmatrix}}_{C^T} \begin{bmatrix} l_0(t) \\ l_1(t) \\ \vdots \\ l_n(t) \end{bmatrix} \end{aligned} \quad (2.26)$$

où les l_i sont les sorties du filtre de Laguerre (voir la Fig. (6.5)).

2.4.4 Modèle de Volterra-Laguerre

La réponse d'un système non-linéaire sans discontinuité peut être calculée par la généralisation du produit de convolution à m noyaux (Campello et al., 2006) :

$$y(k) = \sum_{m=1}^{\infty} \sum_{k_1=1}^{\infty} \sum_{k_2=1}^{\infty} \dots \sum_{k_m=1}^{\infty} h_m(k_1, k_2, \dots, k_m) \prod_{j=1}^m u(k - kj) \quad (2.27)$$

où u , y et h_m sont l'entrée, la sortie et le noyau m respectivement. Ceci peut être vu comme le développement de Taylor d'un opérateur non linéaire analytique.

En pratique, les ordres supérieurs peuvent être négligés et il en résulte une troncation à l'ordre M i.e. $m \in \{1, \dots, M\}$. Le problème de l'utilisation de ce type de modèle est lié à la nécessité de générer des excitations permettant d'isoler la contribution de chaque noyau. L'idée pour simplifier le problème consiste à considérer des noyaux eux même décomposés sur une base de Laguerre. Dans ce cas, on obtient le modèle de Volterra-Laguerre (Dumont & Fu, 1993a) :

$$y(k) = \sum_{k_1=0}^M c_{k_1} L_i(k) + \sum_{k_1=0}^M \sum_{k_2=0}^M c_{k_1, k_2} L_i(k) L_j(k) + \dots + \sum_{k_1=0}^{\infty} \dots \sum_{k_M=0}^{\infty} c_{k_1, \dots, k_M} L_{k_1}(k) L_{k_2}(k) \dots L_{k_M}(k) \quad (2.28)$$

Ce modèle sera également évalué par la suite.

2.5 Etude expérimentale

Dans ce qui précéde, les outils nécessaires à une modélisation et sa mise en œuvre par l'utilisation d'un algorithme récursif ont été introduits. Il reste que tout a été élaboré dans l'hypothèse que l'échantillonage était assez rapide pour permettre de considérer que le système non linéaire restait proche d'un point de fonctionnement dans l'intervalle où la convergence de l'identification s'opérait. Devant l'incertitude liée à cette hypothèse et compte tenu du manque d'outil mathématique pour évaluer un domaine de validité, il a été décidé de mener une évaluation expérimentale sur deux types d'actionneurs comme évoqué en introduction.

2.5.1 Critères d'évaluation

Les critères retenus sont les suivants :

- **La moyenne de l'erreur au carré :**

$$MSE := \mathbf{E}\{(y - \hat{y})^2\}. \quad (2.29)$$

elle représente la distance entre le modèle et le système et doit donc être minimisée.

- **Le "best fit percentage"** (Ljung, 2006) : il permet de discriminer entre modèles utiles, il est généralement admis qu'un taux de 90% indique un "bon" modèle.

$$BFT = 100\% \cdot \max \left(1 - \frac{\|y - \bar{y}\|_2}{\|y - \hat{y}\|_2}, 0 \right), \quad (2.30)$$

où \bar{y} est la moyenne de y .

- **La variance prise en compte** : elle mesure la fraction de la variance de sortie

expliquée par le modèle (Verdult & Verhaegen, 2002).

$$VAF = 100\% \cdot \max \left(1 - \frac{\text{var}\{y - \hat{y}\}}{\text{var}\{y\}}, 0 \right) \quad (2.31)$$

Tous les calculs sont effectués en utilisant la sortie de l'hystérésis prédictive.

2.5.2 Actionneur simple

Le schéma du montage est représenté sur la Fig. (6.6). L'actionneur est un fil de Nitinol fixé à une extrémité au bâti, l'autre déplaçant la charge mécanique. Des guiderages (poulie, roulement linéaire) réduisent les frottements et évitent le balancement de la charge. La mesure du déplacement est assuré par un laser (résolution 5µm, période d'échantillonage 1 ms). L'alimentation est réalisée par un montage à amplificateur opérationnel (L165H) qui permet de délivrer des courants jusqu'à 3 A dans de bonnes conditions de refroidissement. Ce montage n'est pas contrôlé en courant, en pratique des limites ont été mises sur les tensions de sortie pour éviter la détérioration du fil AMF. Les traitements et acquisitions sont réalisés en utilisant une carte dSPACE 1104 qui permet de tester des codes en temps réel, avec un développement simplifié sur Matlab/Simulink.

Le fil a pour dimensions 200 µm de diamètre et 21 cm de longueur. Il est précontraint à 87 MPa. Les températures de transformation sont $A_s=65$ °C, et $A_f= 93$ °C. Il a été noté que les caractéristiques dérivaient de façon notable au cours du fonctionnement et un protocole de prétraitement a dû être mis en place pour stabiliser le comportement des échantillons.

Dans l'étude qui suit, trois modèles sont considérés : deux modèles de Laguerre respectivement d'ordre deux et cinq et un modèle de Volterra-Laguerre comportant deux filtres ce qui correspond à un ordre six. Dans tous les cas, les coefficients sont initialisés à zéro et la matrice de covariance est initialisée avec $\delta = 0,01$, ce qui confère une vitesse de convergence relativement faible, mais réduit la sensibilité de l'identification au bruit. Deux signaux ont été utilisés :

- Un signal constitué par la somme de deux sinusoïdes : ne comportant que deux fréquences, il ne remplit pas la condition d'excitation persistente pour le filtre du cinquième ordre;
- Un signal, consistant à additionner au précédent un bruit de façon à avoir un rapport signal bruit de 45 dB, dans ce cas la persistance de l'excitation est assurée pour chaque filtre étudié.

Les influences du facteur d'oubli λ et de la période d'échantillonage T_s sont successivement étudiées.

Facteur d'oubli

Les valeurs $\lambda = 0,5; 0,9; 0,99; 1$ ont été testées pour les 3 modèles soumis aux deux excitations décrites précédemment. Les résultats correspondent aux Fig. (6.9) à Fig. (6.19). Les différents critères d'évaluations sont résumés pour chaque expérience dans les Tab. (6.6) à Tab. (6.10).

Globalement les résultats sont très encourageants et surtout ont des comportements

conformes à la théorie. En résumé :

- Pour tous les modèles, un facteur d'oubli inférieur à 1 est nécessaire pour restituer et prédire l'hystérésis de façon satisfaisante ;
- Pour le premier signal on retrouve les comportements attendus au sens où le modèle du cinquième ordre est instable, alors que ceux basés sur deux filtres sont stables. On vérifie donc que la condition de persistance de l'excitation n'est pas modifiée par la non-linéarité ;
- Hormis pour le filtre du second ordre, le choix d'un facteur d'oubli trop petit mène à une instabilité ;
- L'utilisation d'un facteur d'oubli $\lambda = 0,99$ donne d'excellents résultats dans tous les cas. Dans tous les cas le BFT est supérieur à 95 %. Une légère supériorité du cinquième ordre peut être notée. Le modèle de Volterra-Laguerre donne aussi de très bons résultats proche de ceux du cinquième ordre.
- Si on considère la variation des coefficients des différents modèles, on peut noter qu'elle est plus prononcée avec l'ordre du filtre.

Il ressort de cette première étude que l'utilisation d'un modèle de Laguerre et de l'algorithme des moindres carré récursifs permet d'atteindre l'objectif de modéliser la dynamique non-linéaire de l'hystérésis si les règles de l'art sont respectées, et valide donc l'hypothèse la plus délicate de l'approche proposée.

Période d'échantillonnage

L'hypothèse d'adaptation rapide comparée à la période d'échantillonnage est testée plus avant en faisant varier cette dernière. On choisit les valeurs $T_s = 1e - 2, 1e - 1, 1$ s. La valeur d'échantillonnage 1 s correspond à un rapport dix entre T_s et la constante de temps approximative du fil. Les résultats sont représentés sur les Fig. (6.20) à Fig. (6.25), et les critères regroupés pour chaque expérience dans les Tab. (6.11) à Tab. (6.16). Un facteur d'oubli $\lambda = 0.9$ a été utilisé pour tous les tests.

On retrouve des résultats similaires à l'étude précédente pour ce qui concerne la stabilité relative des différents modèles. Il est à noter que la stabilité s'améliore lorsque la période d'échantillonnage diminue. Ceci peut être compris dans une certaine mesure car à mesure que la période d'échantillonnage les variations en sortie du système sont de moins en moins affectées par la variabilité du bruit superposé au signal d'entrée, et surtout entre deux instants éloignés il y a plus de probabilité d'avoir des informations sur la dynamique du système dans la matrice de corrélation. Ceci a pour effet d'améliorer le conditionnement numérique. Le modèle de Laguerre-Volterra et le modèle de Laguerre du 5^{ème} ordre sont très performants pour un échantillonnage lent. En considérant les coefficients identifiés, il apparaît une forte variance dans le cas du dernier modèle, tandis que ceux du modèle de Volterra-Laguerre varient plus lentement et dans une bien moindre mesure. Ceci semble conforter l'intérêt de cette structure pour prendre en compte des non-linéarité douce dans un système.

2.5.3 Actionneur antagoniste

Ce type d'actionneur a été proposé comme solution au problème de bande passante des AMF. En effet, il n'est plus nécessaire dans cette structure d'attendre le refroidissement du fil. On résout également le problème du sous-actionnement et de la dissymétrie

du fonctionnement. Il reste cependant que la contrainte dans les fils est variable ce qui pose un problème supplémentaire car l'hystéresis se trouve très modifiée.

Un schéma du montage est présentée sur la Fig. (6.26). L'instrumentation est la même que pour l'étude précédente. L'alimentation a été modifiée en répliquant le montage autour du L165H, et en intégrant au niveau logiciel un "aiguillage" de la consigne vers l'une ou l'autre des alimentations en fonction du signe du déplacement souhaité. Ainsi, le problème reste mono-entrée mono-sortie.

Un problème spécifique à cette architecture a été constaté : probablement en raison du chargement combiné en contrainte et température, et à l'augmentation du niveau de contrainte subit par les fils AMF. La tendance à accumuler une déformation plastique est plus prononcée que dans le cas de l'actionneur précédent. Il s'ensuit une plus forte variation de la course au cours du temps et également une annulation progressive de la précontrainte initiale. Ce dernier phénomène induit une "zone morte". Ces points ont d'ailleurs été constatés dans d'autres études [Sofla et al. \(2008b,a\)](#) où des solutions ont été proposées. Le signal d'identification à consisté en une sinusoïde, ce qui donne uniquement une identification selon un cycle d'hystéresis, cependant, l'expérimentation en commande a montré que les observations restent valables même si des cycles internes sont parcourus. Compte tenu de la pauvreté du signal, seul le premier modèle a été expérimenté. Les Fig. (6.27) et Fig. (6.28) présentent ces résultats et les différents critères sont résumés dans les Tab. (6.17) et Tab. (6.18). Il ressort que la solution reste capable de prendre en compte l'hystéresis même pour des fonctionnements où l'hystéresis est influencée par la contrainte. Les tendances des différents critères sont également retrouvés et démontrent la validité de l'approche proposée.

2.6 conclusion

Ce chapitre a été consacré à la faisabilité d'un modèle dynamique entrée-sortie pour la modélisation d'un actionneur à AMF. L'hypothèse principale est de supposer qu'un modèle linéaire suffisamment rapidement adapté permet de prédire la sortie du système non-linéaire constitué par un actionneur AMF. Il faut souligner que cette idée est effectivement recevable dans ce cas parce que les temps de réponse sont relativement lents dans ce cas, ce n'est en général pas le cas et pour des systèmes plus complexes et rapides il faut recourir à des théories plus élaborées. L'approche classique consiste à se donner un modèle linéairement paramétré et utiliser les moindres carré pour identifier le jeu de coefficients qui minimise l'erreur entre prédiction et mesure. Si la base canonique classique est utilisée il peut résulter des modèles d'ordre élevés ce qui suppose une bonne connaissance du système et peut entraîner des instabilités. L'utilisation de fonctions particulières comme les bases de Laguerre permettent de relaxer la connaissance préalable de l'ordre du système, car l'ordre du modèle est alors lié à la précision de l'approximation. La seule connaissance préalable souhaitable est celle de la constante dominante du système car si le pôle de Laguerre est proche de celle ci, la convergence de la troncation se trouve améliorée.

La démarche a été validée expérimentalement, et il s'est avéré que l'hypothèse de base de cette proposition a été validée puisque les tendances classiques de l'identification appliquée au système linéaire ont été retrouvées. Il s'est également avéré que les mo-

dèles sont très performants y compris pour des ordres relativement bas. Le modèle de Volterra-Laguerre est également très intéressant mais en raison de sa non-linéarité, il n'est pas dans l'objectif de départ qui était de se limiter à un modèle linéaire et ne sera par conséquent pas retenu dans l'étude de la commande qui suit.

Chapitre 2. Modélisation

Chapitre 3

Commande

Les modèles présentés précédemment permettent de prédire la sortie du système et une technique naturelle tirant partie de cette information est celle de la commande prédictive. Pour des raisons pratiques, il a été décidé de se limiter aux modèles linéaires qui permettent aisément définir des correcteurs. Cette technique suppose donc que le modèle du système soit identifié en ligne, c'est à dire que le signal d'excitation est fourni par le correcteur. Une difficulté supplémentaire qui apparaît dans cette configuration car il est impossible de garantir que l'excitation soit effectivement persistance ce qui entraîne donc des instabilités.

Dans ce chapitre, nous présentons donc rapidement la commande prédictive qui a été utilisée pour la commande des deux actionneurs déjà évoqués. La technique a été proposée par [Zervos et al. \(1988\)](#). Dans cette communication, les auteurs évoquent la stabilité de façon assez vague et nous apportons ici une justification de ce qui a été conjecturé. Un première validation expérimentale démontre la nécessité d'améliorer la technique d'identification, et cette modification est validée.

Afin de répondre au problème latent de la persistance de l'excitation, une modification de la structure du contrôleur est proposée et sa stabilité démontrée. Finalement, une validation expérimentale est apportée.

3.1 Commande adaptative prédictive

3.1.1 Principe de la commande prédictive

L'approche classique de la commande prédictive (on suppose ici le système mono-entrée, mono-sortie) est de trouver une suite de commande $u(k)$, $k \in 1 \dots H_p$ qui amène le système vers une référence w (y étant la sortie du système), selon une trajectoire pré-définie (représentant en fait le comportement souhaité du système). Pour ce faire, on utilise un prédicteur, c'est à dire une modélisation de la dynamique du système utilisable pour prédire la sortie à $t + H_p$. Dans le cas linéaire, on se ramène ainsi à problème de programmation linéaire, avec ou sans contraintes suivant les limitations des actionneurs. Seule la première valeur de la suite de commande est appliquée, puis la procédure est réitérée à partir des nouvelles mesures. L'horizon est donc glissant. La solution n'est pas

nécessairement unique, et une façon de simplifier le problème est d'imposer un profil de commande qui soit constant passé un certain temps.

3.1.2 Commande prédictive avec modèle de Laguerre

Le modèle de Laguerre est mis sous la forme de l'Eq. (6.59). Par récurrence, on montre que le prédicteur peut s'écrire :

$$\hat{y}(t + H_p) = \hat{C}^T A^{H_p} l(t) + \hat{C}^T \sum_{k=1}^{H_p} A^{H_p-k} B u(t+k-1) \quad (3.1)$$

Dans cette équation, la sortie prédictée $\hat{y}(t + H_p)$ est la somme de la réponse libre et du régime forcé respectivement. La notation \hat{C} rappelle que les coefficients du prédicteur sont identifiés. Ce prédicteur est en boucle ouverte, pour prendre en compte les imperfections du modèle et les perturbations extérieures, on introduit la mesure réelle par l'introduction d'une correction entre la sortie mesurée et la sortie estimée à l'instant t $\hat{y}(t + H_p) = \hat{C}^T l(t + H_p) + y(t) - \hat{C}^T l(t)$. Afin de simplifier le problème, on considère le cas où la commande est maintenue constante durant l'horizon de prédiction, soit $u(t+k) = u(t+1) \quad k \in \{1 \dots H_p\}$. Ainsi, l'Eq. (3.1) se réécrit sous la forme :

$$\hat{y}(t + H_p) = y(t) + C^T (A^{H_p} - \mathbb{I}) l(t) + \hat{C}^T \left(\sum_{k=1}^{H_p} A^{H_p-k} B \right) u(t) \quad (3.2)$$

où \mathbb{I} est la matrice unité de dimension compatible. Comme, il l'a été dit, la sortie $y(t + H_p)$ doit atteindre la référence (qui peut être une trajectoire de référence), il suffit donc de remplacer $y(t + H_p) = y_{ref}$ et de résoudre pour $u(t)$ pour obtenir l'équation du correcteur :

$$u(t) = \frac{w - y(t) - \hat{\Psi}^T(t) l(t)}{\hat{\Phi}(t)} \quad (3.3)$$

avec les définitions suivantes :

$$\hat{\Phi}(t) = \hat{C}_l^T(t) \sum_{j=1}^{H_p} A_l^{H_p-j} B_l \quad (3.4)$$

qui est un gain scalaire et :

$$\hat{\Psi}^T(t) = \hat{C}_l^T(t) (A_l^{H_p} - I) \quad (3.5)$$

qui est un vecteur de gains de dimension $N \times 1$ (N étant l'ordre du modèle de Laguerre). On peut donc voir ce correcteur comme la superposition d'un correcteur proportionnel, et d'un retour de l'état du modèle.

Il peut être montré que ce correcteur minimise le carré de l'erreur en sortie. En partant d'un critère mixte faisant intervenir l'erreur en sortie et l'effort de commande, on peut

construire l'index de performance :

$$J = \sum_{j=1}^{H_p} q(j) (y_r(t+j) - \hat{y}(t+j))^2 + r(j) u(t+j-1)^2 \quad (3.6)$$

En considérant des coefficients de pondération constants $q(j) = Q$ $r(j) = R$ le contrôleur prend la forme :

$$u(t) = \frac{[w - y(t) - \hat{\Psi}^T(t)l(t)] Q \hat{\Phi}(t)}{\hat{Q} \hat{\Phi}^2(t) + R} \quad (3.7)$$

Ces paramètres supplémentaires peuvent être exploités pour affiner le réglage.

3.1.3 Stabilité et robustesse

On s'intéresse à la forme première du correcteur donnée par l'Eq. (3.3) qui a été proposée par Zervos *et al.* (1988). A partir des équations Eq. (3.3), Eq. (3.4) et Eq. (3.5) du correcteur, et de l'équation dynamique du système dans la base de Laguerre pour un ordre de troncation donné (qui correspond à la représentation d'état de l'Eq. (2.25)), on exprime le système en boucle fermée¹ :

$$l(t+1) = [A - BC^T A^{H_p} \hat{\Phi}^{-1}(t)] l(t) + B \hat{\Phi}^{-1}(t) [w + \hat{y}(t) - y(t)] \quad (3.8)$$

Stabilité

Pour démontrer la stabilité nous utilisons le lemme proposé par Landau *et al.* (1998) :

Lemme 1. Soit le système :

$$\mathbf{l}(t+1) = \mathcal{A}(t)\mathbf{l}(t) + \mathbf{v}(t) \quad (3.9)$$

vérifiant :

1. les coefficients de la matrice $\mathcal{A}(t)$ sont finis pour tout t
2. les valeurs propres de $\mathcal{A}(t)$ sont comprises dans le cercle unité pour tout t
3. $\|\mathcal{A}(t) - \mathcal{A}(t-1)\| \rightarrow 0$ lorsque $t \rightarrow \infty$

Alors il existe t tel que :

$$\|\mathbf{l}(t+1)\|^2 \leq C_1 + C_2 \max_{0 \leq \tau \leq t} \|\mathbf{v}(\tau)\|^2; \quad 0 \leq C_1, C_2 < \infty \quad (3.10)$$

En comparant les Eq. (3.8) et Eq. (7.31), on a :

$$[A - BC^T A^{H_p} \hat{\Phi}^{-1}(t)] = \mathcal{A}(t) \quad (3.11)$$

1. Le modèle et le système étant projetés sur la même base, les matrices d'état A et de commande B sont identiques.

Chapitre 3. Commande

et :

$$B\hat{\Phi}^{-1}(t) [w + \hat{y}(t) - y(t)] = \mathbf{v}(t). \quad (3.12)$$

Proposition 1. Si le vecteur des paramètres \hat{C}^T n'est pas orthogonal au vecteur d'entrée B , et si la persistance de l'excitation est vérifiée, alors le gain $\hat{\Phi}(t)$ défini par l'Eq. (3.4) est borné et on a la propriété :

$$0 < |\hat{\Phi}(t)| < \gamma \quad 0 < \gamma < \infty \quad (3.13)$$

Démonstration 1. Pour les besoins de la démonstration on introduit une norme induite spécifique (Tao, 2003). La matrice A admet pour valeur propre a (avec un ordre de multiplicité N), il existe donc une matrice de passage P telle que $P^{-1}AP = J_a$ avec J_a le bloc de Jordan de dimension $N \times N$ ayant a sur la diagonale principale. Soit D la matrice diagonale telle que $D = \text{diag}\{1, \epsilon, \dots, \epsilon^{N-1}\}$ et soit la matrice $Q = PD$, alors on a l'identité :

$$J_\epsilon = Q^{-1}AQ = \begin{bmatrix} a & \epsilon & 0 & \dots & 0 \\ 0 & \ddots & \ddots & \ddots & \\ & \ddots & \ddots & \ddots & 0 \\ 0 & \dots & 0 & a & \epsilon \\ 0 & \dots & & 0 & a \end{bmatrix} \quad (3.14)$$

On définit alors la norme matricielle induite :

$$\|M\|_2 = \max_{\|\bar{x}\|=1} \|MQ\bar{x}\|_2 \quad (3.15)$$

En appliquant cette norme à A il vient :

$$\|A\|_2^2 = \left[\begin{array}{ccc} \lambda\bar{x}_1 + \epsilon\bar{x}_2 & \dots & \lambda\bar{x}_{n-1} + \epsilon\bar{x}_n & \bar{x}_n \end{array} \right] \begin{bmatrix} \lambda\bar{x}_1 + \epsilon\bar{x}_2 \\ \vdots \\ \lambda\bar{x}_{n-1} + \epsilon\bar{x}_n \\ \lambda\bar{x}_n \end{bmatrix} \quad (3.16)$$

on en déduit alors :

$$\|A\|_2^2 \leq (\lambda + \epsilon)^2 \|\bar{x}\|_2^2 \quad (3.17)$$

De façon similaire, puisque :

$$A^n = P^{-1} \begin{bmatrix} \lambda^n & \binom{n}{1} \lambda^{n-1} & \binom{n}{2} \lambda^{n-2} & \dots \\ 0 & \lambda^n & \binom{n}{1} \lambda^{n-1} & \ddots \\ & \ddots & \ddots & \\ & & 0 & \lambda^n \end{bmatrix} P \quad (3.18)$$

il découle en appliquant la procédure précédente que :

$$\|A^n\|_2 \leq |\lambda + \epsilon|^n \quad (3.19)$$

Nous pouvons maintenant démontrer que si $\hat{C}^T(t)$ est borné alors le gain $\hat{\Phi}(t)$ est borné. En examinant l'Eq. (3.4), on peut considérer $\Phi(\hat{H}_p, t)$ une suite dépendant de H_p pour le vecteur de coefficients $\hat{C}^T(t)$ à l'instant considéré. En utilisant la norme induite précédemment définie, la valeur absolue de l'incrément de gain (qui est une suite dépendant de H_p) est majorée comme suit :

$$\|\hat{\Phi}(H_p + 1, t) - \hat{\Phi}(H_p, t)\| \leq \|\hat{C}^T(t)\| \|B\| |a + \epsilon|^{H_p} \quad (3.20)$$

en choisissant ϵ tel que $|\epsilon| < 1 - |a|$, on obtient donc la limite :

$$\lim_{H_p \rightarrow \infty} \|\hat{\Phi}(H_p + 1, t) - \hat{\Phi}(H_p, t)\| = 0 \quad (3.21)$$

En conclusion le module du gain croît de façon monotone vers une limite dont la valeur peut être majorée. En effet, on a la propriété :

$$\lambda[\mathcal{P}(A)] = \mathcal{P}(\lambda[A]) \quad (3.22)$$

où la notation $\lambda[A]$ signifie "les valeurs propres de A ", et \mathcal{P} est un polynôme. Compte tenu de ce que A a pour valeur propre a (valeur multiple d'ordre N), il découle que $\sum_{i=0}^{H_p} A^{H_p-i}$ a pour valeur propre d'ordre de multiplicité N :

$$\lambda \left[\sum_{i=0}^{H_p} A^{H_p-i} \right] = \sum_{i=0}^{H_p} a^{H_p-i} = \frac{a^{H_p} - 1}{a - 1} \quad (3.23)$$

d'où la limite :

$$\lim_{H_p \rightarrow \infty} \|\hat{\Phi}(H_p + 1, t)\| \leq \lim_{H_p \rightarrow \infty} \frac{(a + \epsilon)^{H_p} - 1}{(a + \epsilon) - 1} \|\hat{C}^T(t)\| \|B\| \quad (3.24)$$

pour un choix de ϵ vérifiant $|a + \epsilon| < 1$, on obtient :

$$\lim_{H_p \rightarrow \infty} \|\hat{\Phi}(H_p + 1, t)\| \leq \frac{1}{1 - (a + \epsilon)} \|\hat{C}^T(t)\| \|B\| \quad (3.25)$$

Il en découle donc que :

$$\|\hat{C}^T(t)B\| \leq \Phi(H_p, t) \leq \frac{1}{1 - (a + \epsilon)} \|\hat{C}^T(t)\| \|B\|$$

En vertu de la persistance de l'excitation, le vecteur $\hat{C}(t)$ est borné, il s'ensuit que $\|\hat{C}(t)\|^2 < \kappa^2$ avec $0 < \kappa^2 < \infty$, ce qui a pour conséquence avec l'hypothèse introduite

$\hat{C}^T(t)B \neq 0$ que :

$$\|\hat{C}^T(t)B\| \leq \|\hat{\Phi}(t)\| \leq \frac{(a+\epsilon)^{H_p}-1}{(a+\epsilon)-1} \|\hat{C}^T(t)\| \|B\| \leq \frac{1}{(a+\epsilon)-1} \kappa \|B\| = \gamma$$

ce qui démontre le résultat annoncé.

Proposition 2. Si la condition de persistance de l'excitation est vérifiée alors $\hat{\Phi}(t+1) - \hat{\Phi}(t)$ appartient à \mathcal{L}_2 .

Démonstration 2. On a :

$$\|\hat{\Phi}(H_p, t+1) - \hat{\Phi}(H_p, t)\| \leq \|\hat{C}^T(t+1) - \hat{C}^T(t)\| \|B\| \frac{(a+\epsilon)^{H_p}-1}{(a+\epsilon)-1} \quad (3.26)$$

en raison de la persistence de l'excitation, $\|\hat{C}^T(t+1) - \hat{C}^T(t)\|$ appartient à \mathcal{L}_2 , il découle donc que $\|\hat{\Phi}(H_p, t+1) - \hat{\Phi}(H_p, t)\|$ appartient également à \mathcal{L}_2 .

Pour appliquer le lemme 1, il faut vérifier $\mathcal{A}(t)$ a ses valeurs propres dans le cercle unité.

Proposition 3. Dans le cas d'une excitation persistente, il existe un horizon de prédition H_p tel que $\mathcal{A}(t)$ définie par (3.11) est stable i.e. toute ses valeurs propres sont contenues dans le cercle unité.

Démonstration 3. On a l'inégalité :

$$\begin{aligned} \|\mathcal{A}\|^2 &\leq \|\mathbf{A}\|^2 + |\Phi(t)|^{-2} \|\mathbf{B}\hat{\mathbf{C}}^T(t)\|^2 \|\mathbf{A}^{H_p}\|^2 \\ &\leq \|\mathbf{A}\|^2 + |\hat{\mathbf{C}}(t)^T \mathbf{B}|^{-2} \|\mathbf{B}\hat{\mathbf{C}}^T(t)\|^2 \|\mathbf{A}^{H_p}\|^2 \end{aligned} \quad (3.27)$$

où la norme utilisée est celle définie précédemment. La matrice $\mathbf{B}\hat{\mathbf{C}}^T$ est de rang 1, son image est la droite vectorielle supportée par \mathbf{B} qui est aussi le vecteur propre correspondant à la seule valeur propre non nulle $\hat{\mathbf{C}}^T(t)\mathbf{B}$. On suppose que $\hat{\mathbf{C}}^T(t)\mathbf{B} \neq 0$. Dans ce cas, il existe une matrice de passage $\mathbf{M}(t) = [\mathbf{B} | \mathbf{C}_1(t)^\perp | \dots | \mathbf{C}_{N-1}(t)^\perp]$ ($\mathbf{C}_i(t)^\perp$ sont des vecteurs colonnes formant une base pour le sous espace orthogonal à $\hat{\mathbf{C}}$). $\mathbf{M}(t)$ est par construction de rang plein, donc inversible. $\mathbf{B}\hat{\mathbf{C}}(t)^T = \mathbf{M}(t)\mathbf{Z}(t)\mathbf{M}^{-1}(t)$. $\mathbf{Z}(t)$ est une matrice nulle à l'exception de $\mathbf{Z}(1, 1) = \hat{\mathbf{C}}^T(t)\mathbf{B}$. Par conséquent, $\mathbf{z} = \frac{1}{\hat{\mathbf{C}}^T(t)\mathbf{B}}\mathbf{Z}(t)$ est une matrice constante nulle à l'exception de $\mathbf{z}(1, 1) = 1$. On déduit alors une borne supérieure pour $\|\mathcal{A}(t)\|^2$:

$$\|\mathcal{A}(t)\| \leq |a + \xi| + \|\mathbf{M}(t)\mathbf{z}\mathbf{M}(t)^{-1}\| |a + \xi|^{H_p} \quad (3.28)$$

Puisque $\|\mathbf{M}(t)\mathbf{z}\mathbf{M}(t)^{-1}\|$ est borné et choisissant $|\xi| < 1 - |a|$, on peut conclure à l'existence d'une valeur de H_p telle que le terme à la droite de l'inégalité soit inférieur à 1. Ceci signifie que le rayon spectral est inférieur à 1 c.q.f.d.

En conclusion sous réserve que la persistence de l'excitation soit vérifiée et que $\hat{C}(t)B \neq 0$:

1. Les coefficients de $\mathcal{A}(t)$ sont bornés, ce qui découle du fait que la norme calculée précédemment est bornée (cette propriété est indépendante de H_p mais nécessite la condition $\hat{C}(t)B \neq 0$);
2. Les valeurs propres peuvent être confinées dans le cercle unité pour un choix de H_p approprié;
3. En raison de la propriété de l'algorithme d'identification dans des conditions de persistence de l'excitation $\lim_{t \rightarrow \infty} \|\hat{C}(t) - \hat{C}(t-1)\| = 0$ il existe une matrice M_∞ telle que $\lim_{t \rightarrow \infty} = M_\infty$. Nous avons pu démontrer par ailleurs que $\hat{\Phi}(t)$ a une limite $\hat{\Phi}_\infty$ par conséquent $\lim_{t \rightarrow \infty} \|\mathcal{A}(t)\| = |a + \epsilon| - \hat{\Phi}_\infty \|\mathbf{M}_\infty \mathbf{z} \mathbf{M}_\infty^{-1}\| |a + \epsilon|^{H_p}$

les conditions du lemme sont donc vérifiées.

Puisque $\mathcal{A}(t+1)$ a des coefficients bornés $\mathbf{l}(t)$ ne peut devenir non borné uniquement si $\mathbf{v}(t)$ est lui-même non borné. Toutefois, puisque w est supposé borné et compte tenu de ce que l'algorithme d'identification dans des conditions d'excitation persistante garantit que $\lim_{t \rightarrow \infty} |\hat{y}(t) - y(t)| < \infty$, on a $\mathbf{v}(t) < \infty$. Il découle donc du lemme que $\mathbf{l}(t)$ est borné. Le système est donc stable au sens une entrée bornée donne une sortie bornée. Soit l'erreur sur l'état :

$$\varsigma(t) = \mathbf{l}_s(t) - \mathbf{l}(t) \quad (3.29)$$

où $\mathbf{l}_s(t)$ est l'état du système et $\mathbf{l}(t)$ l'état du modèle. Le système et le modèle étant régit par les équations d'état :

$$\mathbf{l}_s(t+1) = \mathbf{A}\mathbf{l}_s(t) + \mathbf{B}u(t) \quad \mathbf{l}(t+1) = \mathbf{A}\mathbf{l}(t) + \mathbf{B}u(t) \quad (3.30)$$

En soustrayant ces deux équations, on obtient :

$$\varsigma(t+1) = \mathbf{A}\varsigma(t) \quad (3.31)$$

ce qui montre que l'erreur sur l'état converge exponentiellement vers 0.

Robustesse vis à vis de la non-linéarité

On définit le graphe d'une application :

Définition 3.1.1 (Graphe). (*Safonov, 1980*) Soit \mathbf{G} une application des points $x \in \mathcal{X}$ sur $\mathbf{G}x \in \mathcal{Y}$, alors le graphe \mathbf{G} est :

$$Graph(\mathbf{G}) \triangleq \{(x, y) \in \mathcal{X} \times \mathcal{Y} \mid x \in \mathcal{X} \text{ et } y = \mathbf{G}x\}. \quad (3.32)$$

Elshhafei et al. (1994) a proposé l'approche suivante pour justifier la robustesse vis à vis des non-linéarités en se basant sur un résultat de *Safonov (1980)*. supposons que le système réel soit donné par

$$l(t+1) = Al(t) + bu(t) \quad (3.33)$$

$$y(t) = cl(t) \quad (3.34)$$

Chapitre 3. Commande

où A, b and c sont des opérateurs non linéaires, et considérons le modèle linéarisé de ce même système :

$$l(t+1) = \hat{A}l(t) + \hat{B}u(t) \quad (3.35)$$

$$y(t) = \hat{C}l(t) \quad (3.36)$$

et considérons la commande par retour d'état :

$$u = -Kl(t) \quad (3.37)$$

Lemme 2. Soit les matrices constantes symétriques et positives $P \in \mathbb{R}^{n \times n}$ et $S \in \mathbb{R}^{n \times n}$ solution de l'équation de Lyapunov :

$$P = (A - \hat{B}K^T)P(A - \hat{B}K^T) + S \quad (3.38)$$

et si uniformément pour tous les points $(l(t), u(t))$ le graphe :

$$\text{Graph}\left(P^{1/2} \left[A - \hat{B}K^T + \Delta A + \Delta B(-K^T)\right]\right) \quad (3.39)$$

avec $\Delta A = A - \hat{A}$ et $\Delta B = b - \hat{B}$ strictement compris dans $(0, P^{1/2})$ alors le système donné par l'Eq. (3.33) avec le retour d'état de l'Eq. (3.37) est stable en boucle fermée.

Remarquons que la commande de l'Eq. (3.3) peut s'écrire en considérant une consigne nulle et en supposant que les états du modèle et du système ont convergé :

$$\begin{aligned} u &= \frac{-y(t) - \hat{\Psi}^T(t)l(t)}{\hat{\Phi}(t)} \\ &= \frac{-\hat{C}l(t) - \hat{\Psi}^T(t)l(t)}{\hat{\Phi}(t)} \\ &= -K^Tl(t) \end{aligned} \quad (3.40)$$

ce qui montre que nous sommes dans les conditions du lemme.

Or, ce lemme se base pour montrer la stabilité non sur le système réel, mais sur son approximation linéaire et nécessite que le gain K^T stabilise cette dernière, *et non le système réel*. Puisqu'il a été démontré qu'il existe un horizon de prédiction H_p qui soit effectivement stabilisant, l'équation de Lyapunov (3.38) admet dans ce cas une solution. Le lemme est vérifié si l'erreur de modélisation $(\Delta A, \Delta B)$ est suffisamment petite. Les fonctions de Laguerre étant une base orthonormale, l'ordre du modèle peut être augmenté pour rendre l'erreur entre le modèle et le système linéarisé qui est équivalent au système réel autour d'un point de fonctionnement, il est par conséquent théoriquement toujours possible de stabiliser le système non-linéaire par cette approche autour d'un point de fonctionnement.

3.1.4 Validation expérimentale

La stratégie de commande a été testée sur le premier actionneur. Les paramètres choisis étant :

- filtre du deuxième ordre $\lambda = 0.8$
- filtre du cinquième ordre $\lambda = 0.99$
- période d'échantillonage $T_s = 10 \text{ ms}$
- $\frac{R}{Q} = 1.10^{-3}$
- $H_p = 30$
- initialisation de la matrice de covariance $\delta = 1.10^{-2}$

Certains résultats sont représentés sur les Fig. (7.5) à Fig. (7.10). Dans le cas du modèle du deuxième ordre, les dépassements sont très importants et l'erreur en régime permanent également. La commande est aussi extrêmement active. En revanche l'identification est relativement performante. En utilisant cinq filtres, les dépassements sont éliminés, mais on note que l'actionneur n'atteint pas réellement de régime permanent, même si il a tendance à rester autour de la consigne. Parallèlement, l'activité de la commande se trouve réduite. L'identification reste satisfaisante, avec notamment une variance réduite. L'examen des poids montre qu'un phénomène parasite prend place. En effet, bien que la prédiction soit correcte, on note l'apparition de "bouffée" d'activité durant lesquelles les coefficients varient brutalement. Ce phénomène a été identifié par [Anderson \(1985\)](#) et provient du manque d'excitation persistante. On note effectivement qu'elle se manifeste particulièrement autour des paliers de la consigne, où l'information recueillie par les MCR est pauvre. Or il est clair que dans ces phases l'adaptation n'a pas lieu d'être, et compte tenu du facteur d'oubli, les informations stockées durant les transitoires sont peu à peu éliminées au profit d'informations redondantes. Une solution est de modifier ce comportement en sélectionnant les données à éliminer de la matrice de corrélation. Un algorithme de moindre carrés récursif à facteur d'oubli directionnel, résumé à la section 7.7.1 p. 142, a été alors implémenté, ce qui a permis de résoudre le problème efficacement.

Afin d'étudier les performances de l'asservissement, le signal de consigne consiste en une suite d'échelons d'amplitude variable ce qui entraîne un fonctionnement selon des cycles internes de l'hystérésis. Les réponses ont été analysées sur l'ensemble du signal en considérant les valeurs moyennes :

- dépassement (MO) %
- temps de réponse (MST) s
- erreur en régime permanent %
- variation autour de la valeur de régime permanent (MOS) %

L'étude a porté sur l'influence de la pondération $r = \frac{Q}{R}$, et l'horizon de prédiction H_p . Le modèle consiste en un filtre du cinquième et du deuxième ordre avec le pôle $a = 0.9$ (correspondant respectivement aux Fig. (7.11) à Fig. (7.15) et Fig. (7.16) à Fig. (7.18)). L'identification est initialisée avec $\delta = 1.10^{-5}$ et un facteur d'oubli $\lambda = 0.5$ correspondant à une fenêtre longue. La zone morte est fixée par $\varepsilon = 1.10^{-3}$. L'ensemble des résultats concernant le modèle du cinquième ordre est résumé par la Tab. (7.1). Il ressort de cette étude que :

- pour $r = 0$ (pas de pénalisation sur l'effort de commande), la stabilité est assurée

conformément à la théorie, et dans ce cas un horizon de prédiction petit donne les meilleurs résultats selon tous les critères ;

- pour r faible la stabilité demeure, la tendance est similaire avec une dégradation des performances ;
- si r est trop important, le système est déstabilisé.

Lorsqu'un modèle d'ordre moins élevé est utilisé, l'asservissement fonctionne également avec des performances inférieures en ce qui concerne le temps de réponse. La qualité de l'identification est également un peu dégradée avec une augmentation de la variance. La sensibilité aux perturbations a été testée également sur le modèle du cinquième ordre en imposant une modification des échanges thermiques. Ceci est obtenu en soufflant de l'air en direction du fil passant d'un régime de convection naturelle à un régime de convection forcée. On constate alors que la perturbation est rejetée dans la mesure du possible. En effet, des limitations ont été imposées à l'alimentation. Il s'avère néanmoins que bien que cela n'ait pas été pris en compte dans la modélisation, le système reste stable et retrouve un fonctionnement normal dès que la perturbation cesse. Dans le cas où $r = 0$ on constate un phénomène transitoire avec l'apparition d'oscillations peu après le retour à la normale. Ce phénomène provient de la limitation. Une solution consiste alors à augmenter légèrement la pénalisation $r = 1.10^{-4}$ ce qui a pour effet de les supprimer au détriment de la précision puisqu'une légère erreur statique apparaît alors.

L'utilisation d'un facteur d'oubli directionnel a dans tous les cas été décisive, on constate en effet sur l'ensemble des relevés la disparition des variations brusques des coefficients identifiés, on peut y voir une complexité accrue puisque des relations de récurrences supplémentaires sont nécessaires. Pour éviter ce problème, le schéma de commande a été modifié afin d'éviter le problème de l'absence d'excitation suffisante et de la corrélation entre la sortie et le signal de commande qui peuvent être source de biais dans l'estimation.

3.2 Commande modifiée

3.2.1 Principe

L'idée est de choisir une entrée différente pour le modèle qui soit décorrélée de la sortie. Un choix simple consiste à utiliser la consigne qui influe la sortie, mais n'est pas corrélée avec le bruit. Elle peut donc être vue comme une variable instrumentale pour le problème d'identification. Le schéma est celui de la Fig. (7.23) p. 155. La différence notable est que c'est à présent le système en boucle fermé qui sera identifié. Une étude est donc nécessaire.

Le modèle est donné par :

$$\begin{aligned} l(t+1) &= \hat{A}l(t) + \hat{B}w \\ \hat{y}(t) &= \hat{C}_l^T(t)l(t) \end{aligned} \tag{3.41}$$

et le système en boucle fermée par :

$$\begin{aligned} x(t+1) &= Ax(t) + Bu(t) \\ y(t) &= C^T x(t) \end{aligned} \tag{3.42}$$

notons que du moment que les deux sont projetés dans la même base, la distinction entre \hat{A} et A , \hat{B} et B respectivement n'est pas nécessaire. La commande appliquée est inchangée :

$$u(t) = \frac{w - y(t) - \hat{\Psi}^T l(t)}{\hat{\Phi}} \quad (3.43)$$

3.2.2 Stabilité

En regroupant les états des deux systèmes, et après quelques réarrangements des équations, il vient :

$$\begin{bmatrix} x(t+1) \\ l(t+1) \end{bmatrix} = \left[\begin{array}{c|c} A & -\hat{C}_l^T B \hat{A}_l^{H_p} \hat{\Phi}^{-1} \\ \hline 0 & \hat{A}_l \end{array} \right] \begin{bmatrix} x(t) \\ l(t) \end{bmatrix} + \begin{bmatrix} B \hat{\Phi}^{-1} \\ \hat{B}_l \end{bmatrix} w + \begin{bmatrix} B \hat{\Phi}^{-1} \\ 0 \end{bmatrix} (\hat{y}(t) - y(t)) \quad (3.44)$$

Proposition 4. Soit le contrôleur prédictif donné par l'Eq. (3.43) qui utilise le signal de référence $w(t)$ et la sortie du système en boucle fermée $y(t)$ pour calculer les gains selon les Eq. (3.4) et Eq. (3.5). Ce système est stable au sens où une entrée bornée donne une sortie bornée si :

- le signal $w(t)$ respecte la condition de persistance de l'excitation ;
- la condition $\hat{C}^T(t)B \neq 0$ est vraie.

Démonstration 4. On remarque que le système est de la forme :

$$\mathbf{x}(t+1) = \mathbf{F}(t)\mathbf{x}(t) + \mathbf{v}(t) \quad (3.45)$$

où $\mathbf{F}(t)$ est la matrice d'état de l'Eq. (3.44) et la suite $\mathbf{v}(t)$ est donnée par :

$$\mathbf{v}(t) \doteq \begin{bmatrix} v_1(t) \\ v_2(t) \end{bmatrix} = \begin{bmatrix} B \hat{\Phi}^{-1} \\ \hat{B}_l \end{bmatrix} w + \begin{bmatrix} B \hat{\Phi}^{-1} \\ 0 \end{bmatrix} (\hat{y}(t) - y(t)) \quad (3.46)$$

1. Il a été déjà établi que $\hat{\Phi}(t)$ est borné (voir la proposition 1), et \hat{C}^T est borné compte tenu de la persistance de l'excitation donc les éléments de la matrice $\mathbf{F}(t)$ sont bornés ;
2. $\mathbf{F}(t)$ est triangulaire par blocs donc $\lambda\{\mathbf{F}(t)\} = \lambda\{A\} \cup \lambda\{\hat{A}_l\}$. Le pôle du filtre de Laguerre est choisi tel que $a < 1$ donc $\lambda\{\hat{A}_l\} < 1$, puisque le système est stable en boucle ouverte pour admettre une projection sur la base de Laguerre, $\lambda\{A\} < 1$, par conséquent $\lambda\{\mathbf{F}(t)\} < 1$.
3. avec l'hypothèse de persistance de l'excitation, il existe une valeur bornée pour le vecteur des paramètres $\lim_{t \rightarrow \infty} \hat{C}(t) = \hat{C}_\infty$ et le gain $\lim_{t \rightarrow \infty} \hat{\Phi}(t) = \hat{\Phi}_\infty$ ainsi $\lim_{t \rightarrow \infty} F(t+1) - F(t) = 0$

Le système ne peut donc être instable que si $\{\mathbf{v}(t)\}$ n'admet pas de borne. Or elle dépend :

- du gain $\hat{\Phi}(t)$ qui est borné ;
- de w qui est borné ;

– de l’erreur d’identification $\{\hat{y}(t) - y(t)\}$ qui est bornée si l’identification converge. Clairement $v_2(t)$ est bornée. Par ailleurs, puisque $|v_1(t)| \leq \|B\hat{\Phi}^{-1}\|(|w(t)| + |y(t) - \hat{y}(t)|)$ on conclut que $|v_1(t)|$ est bornée, donc naturellement $\|\mathbf{v}(t)\| \leq |v_1(t)| + |v_2(t)|$ est bornée. Les conditions du lemme sont donc vérifiées et il s’en suit le résultat annoncé.

Notons que $l(t+1) = A_l l(t) + B_l w(t)$ est stable, et en raison des propriétés de l’algorithme d’identification on sait que dans de bonnes conditions $|C^T - \hat{C}^T|$ est borné et admet une limite de même que $|\hat{y}(t) - y(t)|$. On peut aisément en conclure que cette propriété est aussi vérifiée par $|x(t)|$, mais on n’a plus $\lim_{t \rightarrow \infty} |x(t) - l(t)| = 0$.

3.2.3 Validation expérimentale

Pour la partie expérimentale, l’algorithme d’identification est de nouveau les moindres carrés récursifs, avec pour paramètres $\lambda = 1$ et une initialisation de la matrice de covariance $\delta = 1.10^{-2}$. L’algorithme est volontairement peu réactif pour permettre de différencier les dynamiques de l’actionneur en boucle fermé et de l’identification.

Les tests ont été effectués sur les deux actionneurs simple et antagoniste. Les modèles sont du second et du cinquième ordre (pôle $a = 0.9$). On s’est intéressé à l’horizon de prédiction en choisissant les valeurs $H_p = 3$ et $H_p = 30$ dans le cas du cinquième ordre. Les essais sont évalués à partir des mêmes critères que précédemment.

Les résultats pour le modèle du second ordre appliqués à l’actionneur simple sont présentés sur les Fig. (7.27) à Fig. (7.29) et la Tab. (7.3). Les résultats sont globalement bons avec la suppression des variations en régime statique. Les temps de réponse sont comparables à ceux obtenus avec la technique précédente. On note cependant la présence d’une erreur statique qui bien que faible est inévitable puisque dans ce cas le gain statique n’est pas celui de l’actionneur, mais celui du système en boucle fermé.

On remarque un comportement très particulier des coefficients du modèle qui si on tient compte de la relation (2.24) indique que l’asservissement linéarise le système et le rapproche du comportement d’un premier ordre ce qui semblerait indiquer qu’il y a une connexion entre ce contrôleur et les approches adaptatives avec modèle de référence.

L’étude du cinquième ordre (Fig. (7.24) à Fig. (7.25) et Tab. (7.2)) amène aux mêmes conclusions. L’influence de l’horizon de prédiction est notable en terme d’erreur statique. Un grand horizon de prédiction l’augmente mais avec $H_p = 30$ elle reste en dessous de 10% en moyenne. Il induit également des dépassemens qui sont absents pour $H_p = 3$. Soumis à des perturbations comme précédemment, la commande reste stable malgré les limitations.

L’application du contrôleur à un actionneur antagoniste était a priori plus problématique en particulier compte tenu des nombreuses imperfections liées à la réalisation et la mauvaise maîtrise de l’état de précontrainte dans les fils AMF. De plus le comportement en boucle ouverte montre des changements radicaux de l’hystérosis comme le montre les Fig. (7.36) et Fig. (7.37). Sur les Fig. (7.38) à Fig. (7.41) on peut voir que la commande fonctionne néanmoins très bien, et la sortie de l’actionneur est correctement linéarisée comme en témoigne les Fig. (7.42) et Fig. (7.43).

En ce qui concerne la réjection de perturbation, on observe un meilleur comportement qui peut aussi être attribué à la rigidité du montage antagoniste (Fig. (7.45)) et au fait

que les limitations ne sont pas activées dans cet essai. Enfin, la sensibilité à l'horizon de prédiction est similaire à ce qui a été observé avec l'actionneur simple : un plus grand horizon de prédiction entraîne des erreurs statiques plus importantes Fig. (7.46) à Fig. (7.48).

3.3 conclusions

Dans ce chapitre, deux commandes ont été appliquées à la commande d'actionneurs AMF. La première est relativement classique, mais ce travail a apporté des éclaircissements :

- cette commande adresse une classe de système où la condition $\hat{C}^T B$ est non nul, ce qui en fait correspond aux systèmes dont la sortie dépend de l'entrée précédente (pas de retard) ;
- les conditions de stabilité ont été clairement établies et démontrent qu'il existe effectivement un horizon de prédiction qui garantit la stabilité ;
- que la clé de voûte de la stabilité reste l'algorithme d'identification
- L'étude expérimentale a en effet clairement montré la sensibilité de la commande au manque d'excitation malheureusement inévitable en boucle fermée et une amélioration de l'algorithme d'identification consistant à implémenter un facteur d'oubli directionnel a été appliquée avec succès
- les principaux paramètres de réglage ont été examinés et ont amené à la conclusion que la pondération de l'effort de commande n'avait pas un intérêt décisif, et que l'horizon de prédiction petit donnait les meilleures performances ;
- une modification de la commande a été proposée, et sa stabilité prouvée. Elle permet de se passer d'un algorithme d'identification trop élaboré ;
- elle a été validée expérimentalement avec succès sur deux actionneurs très différents avec des performances équivalentes ;
- l'étude expérimentale a révélé la nature de cette commande qui peut être considérée comme une commande adaptative avec modèle de référence ;
- l'utilité de l'identification demeure car il n'y a pas de nécessité d'ajuster a priori le modèle pour exiger des performances compatibles avec les limitations de l'actionneur.

Chapitre 3. Commande

Chapitre 4

Conclusion

4.1 Résumé du travail

L'objectif de cette étude était de réaliser la commande d'actionneur à AMF. Pour y parvenir deux points essentiels ont dû être adressés : la modélisation et la commande. Concernant le premier point, après une étude bibliographique sur le sujet, deux tendances ont été dégagées la première cherche à comprendre et modéliser les mécanismes physiques, la seconde s'attache à restituer macroscopiquement le comportement hystérotique. Dans le premier cas, les modèles sont complexes et exigent une connaissance a priori sous la forme de paramètres devant être identifiés hors ligne compte tenu de la complexité des relations qui les lient. La seconde mettant en œuvre des approches telle que le modèle de Preisach faisant abstraction de la nature non linéaire en substituant au problème initial un problème paramétré linéairement n'est pas moins difficile à mettre en application. En effet, si elle permet une identification en ligne, elle introduit un certain nombre d'approximations dues notamment à la nécessité de discréteriser le plan de Preisach et de plus ne prend pas en compte la dynamique. Utilisée en anticipation, elle ne permet pas de résoudre à elle seule le problème de la commande. Dans les deux cas, une commande en boucle fermée est nécessaire.

L'approche proposée dans ce travail de thèse consiste à prendre encore du recul par rapport à la physique sous jacente en ne considérant que la dynamique par une relation entrée-sortie, connue sous le nom de boite noire. Pour pouvoir mettre en application ce paradigme, tout en conservant une mise en œuvre simplifié, il a été proposé de se baser sur l'hypothèse que l'identification était suffisamment rapide et la fréquence d'échantillonnage grande comparée à la constante de temps naturelle d'un actionneur à AMF. Dans le cadre de cette hypothèse, on peut supposer qu'un modèle linéaire identifié autour d'un point de fonctionnement est la dynamique linéarisée du système. Partant de ce modèle il a été proposé d'appliquer une commande adaptative prédictive.

Compte tenu de l'hypothèse forte sous-jacente, les résultats ont systématiquement été validés expérimentalement.

4.1.1 Identification

L'originalité du modèle repose sur l'utilisation de fonctions de Laguerre qui permettent de modéliser des systèmes ayant de longue réponse impulsionnelle avec des ordres réduits. En l'occurrence, le problème était précisément que la réponse du système est plus grande que la fréquence d'échantillonnage. Les fonctions de Laguerre formant une base orthogonale, la décomposition d'un système est parcimonieuse et les propriétés de convergence sont uniquement liées au choix d'un paramètre le pôle de Laguerre qui doit être choisi proche de la constante de temps dominante du système. De plus des méthodes d'identification classiques tels que les moindres carrés récursifs sont encore applicables. En outre, il existe une extension simple au cas non linéaire par le biais des modèles de Volterra. On aboutit alors aux modèles de Volterra-Laguerre, l'utilisation de fonctions orthogonales simplifiant considérablement les modèles de Volterra, ce qui permet encore d'utiliser des méthodes d'identification classiques.

Dans ce mémoire deux modèles linéaires l'un du second ordre et l'autre du cinquième ordre ont été utilisés ainsi qu'un modèle de Volterra-Laguerre équivalent à un sixième ordre mais ne nécessitant en réalité qu'un filtre du second ordre. Les tests se sont révélés positifs dans tous les cas de figure ce qui a démontré la validité de l'hypothèse initiale. Il a été en outre démontré que le comportement des algorithmes d'identification n'étaient pas perturbé par la nature non-linéaire du système réel, et que des propriétés telles que la nécessité d'une excitation persistence restaient vraies. Il a pu être mis en évidence également que la stabilité des modèles était bonne même pour des périodes d'échantillonage faibles. Cette étape a donc permis de disposer d'un outil de modélisation suffisamment simple pour construire des prédicteurs nécessaires à la mise en œuvre de la commande.

4.1.2 Commande

La première étape dans cette partie a été d'utiliser une stratégie simple proposée par [Zervos et al. \(1988\)](#). Dans cette communication certains éléments étaient restés un peu dans le vague, en particulier les questions de stabilité. Nous avons donc proposé une justification argumentée qui a mis en évidence que la stabilité était conditionnelle, et pas aussi générale que les auteurs le pensaient. Cela a aussi permis de mettre en évidence la sensibilité de cette stratégie à la stabilité de l'identification. Cette conclusion a été effectivement constatée expérimentalement et les résultats relativement médiocres initialement obtenus ont été beaucoup améliorés par l'utilisation d'un second algorithme d'identification. Ce dernier plus robuste vis à vis d'une excitation faible qui est plus la règle que l'exception dans le cas de l'identification en boucle fermée, consiste à ne mettre à jour dans la matrice de corrélation uniquement les données apportant une innovation suffisante. Cette performance se paie par une complexité accrue et par conséquent une puissance de calcul plus importante.

Pour remédier à cela, une nouvelle structure a été proposée. Elle consiste à contourner le problème en pratiquant l'identification directement à partir de la consigne du système en boucle fermée qui constitue une variable instrumentale qui évite les corrélations existantes lorsque l'entrée utilisée pour l'identification est la sortie du correcteur. Compte tenu de la modification, il a été nécessairement de démontrer la stabilité qui s'avère

encore dépendante du résultat de l'identification, mais plus de l'horizon de prédiction. En outre, il est plus facile de maîtriser le signal de référence et garantir ainsi sa nature persistante. Cette proposition a été validée expérimentalement, et le parallèle avec les méthodes de commande de référence avec modèle de référence a été ainsi mis en évidence. Les résultats obtenus sur deux actionneurs différents, avec des caractéristiques très éloignées permettent de conclure à la validité de cette proposition.

4.2 Perspectives

4.2.1 Améliorations à apporter

Les limites de la technique de commande initiale ont été démontrées. La proposition d'une autre structure a donné des résultats comparables avec une technique d'identification plus simple. Il reste que le calcul des gains est resté similaire et n'exploite pas le potentiel de cette solution. En particulier, une propriété intéressante est l'effet de linéarisation obtenu. Comme cette dernière est perceptible au travers de l'évolution des coefficients du modèle, il semble intéressant d'envisager un réglage implicite du contrôleur qui soit soumis à un objectif exprimé à partir des gains. En effet il est simple de traduire une dynamique d'un modèle de référence par projection dans la base de Laguerre et il reste à déterminer un algorithme permettant d'approcher autant que possible cette répartition des coefficients. Compte tenu de l'orthogonalité des fonctions de Laguerre, si le système réel et le modèle ont la même projection, il découle qu'ils sont équivalents aux ordres supérieurs de la troncation près.

Une seconde voie qui n'a pas été poursuivie est l'utilisation des modèles de Laguerre-Volterra qui ont donnés d'excellents résultats. Cependant étant non-linéaires, la commande a paru moins immédiate, toutefois pour des ordres restreints qui se sont révélés suffisant dans le cas d'espèce, la structure est assez simple. Il est donc permis d'imaginer des techniques non-linéaires relativement simples. Pour les actionneurs actuels, ceci peut être superflu, mais on peut s'interroger sur la validité de l'hypothèse d'un échantillonage suffisamment rapide dans le cas d'actionneurs miniaturisés où les temps de réponse seront nécessairement plus courts.

4.2.2 Limites de l'approche "boîte noire"

Dans cette étude pionnière au sein du LPMM, il a été décidé de faire abstraction autant que possible du matériau. Si elle est justifiée dans une phase d'exploration, elle n'est pas très réaliste et il a été à plusieurs reprises constaté qu'elle pouvait être problématique particulièrement dans le cas d'une structure antagoniste.

Un point important concerne les limites du matériau qui ont été initialement rencontrées : le premier actionneur utilisé a rapidement cessé de fonctionner en raison des courants trop élevés qui ont entraînés la formation de martensite stabilisée. Aussi il a été décidé, relativement heuristiquement de limiter le courant (indirectement en imposant une limite sur les tensions appliquées). Si cette solution a permis d'épargner le matériau dans le cas d'un actionneur simple où la contrainte est constante, ce n'est pas le cas pour l'actionneur antagoniste où la contrainte est fortement variable. Ces chargements combinés ont eu les mêmes conséquences. Un autre exemple est que dans le cas de l'actionneur simple avec le vieillissement, la résistance du matériau a varié et

Chapitre 4. Conclusion

la plage d'utilisation réduite en raison des limitations fixes de la tension. Il ressort donc que cette question des limites du matériau est centrale. Si la démarche proposée n'est pas réellement mise en question dans la mesure où elle adresse le court terme (réaliser la consigne à un instant donné), il semble nécessaire qu'à un niveau supérieur la connaissance de l'état du matériau soit intégrée dans la commande. Cela pourrait s'obtenir à l'aide d'une approche hiérarchisée se composant d'un étage de commande pour lesquels les temps de commande sont brefs et d'un étage de supervision à même de prendre en compte et de diagnostiquer les évolutions du comportement du matériau pendant la durée de vie de l'actionneur. Cette seconde approche peut s'inspirer de l'utilisation de filtre de Kalman étendu tel que celui utilisé par [Elahinia & Ahmadian \(2006\)](#).

Part II

Version Anglaise

Chapter 5

Introduction

5.1 Introduction to Actuators

Actuators are used in automated mechanical systems to generate motion or apply forces and torques. Majority of the actuators are hydraulic, pneumatic and electric actuators, so called as conventional actuators. Recently, advances in material technology have introduced various light weight materials with interesting properties, making it possible to design efficient actuation mechanisms that are compact and weightless. Examples of such “smart” materials that can be used to develop novel actuators are shape memory alloys (SMA), electro-rheological fluids (ERF), electrostrictive and magnetostrictive materials including piezoelectric and electroactive polymers. Actuators made out of these materials are called “unconventional” actuators. In [Mavroidis \(2002\)](#) an interesting account and comparison of these actuators has been made. There is an ever increasing demand for advanced actuators in various fields requiring lightweight devices able to apply large forces, develop high speeds, achieve large displacements and be energy efficient. In many applications, efforts have been made to reduce mass, dimension, power and cost. Improvements in actuator robustness and reliability related to power efficiency and compact size can lead to better devices that are significantly more capable and reliable at lower cost. Conventional actuators, such as electric motors, hydraulic and pneumatic cylinders prevent miniaturization necessary for various applications. Electric motors for example run at high speeds and produce low torque, therefore they require a reduction gear system to produce the exact torque necessary for a given mechanical application. This increases the weight and complexity and has the disadvantage of higher noise and friction, leading to wear and finally reducing the life time. Hydraulic and pneumatic actuators are much lighter than electric motors with the same power capability. However they require a complex system of pumps, pressurized chambers, pipes, and valves to hold the working fluid. The hydraulic actuators are often noisy and prone to leaks. They also have lower operation speed. Actuators based on smart materials can eliminate these disadvantages of conventional actuators. To emphasize differences in performance of various actuators refer to Figure 5.1 which compares the power density to weight of conventional DC motor, hydraulic and pneu-

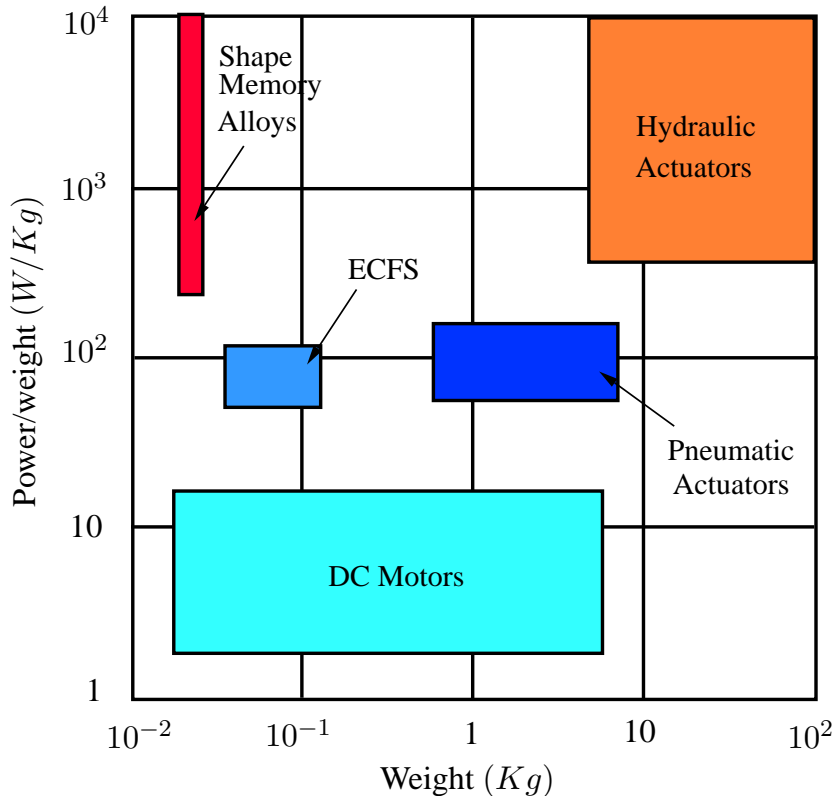


Figure 5.1: Actuator comparison based on weight and output power-to-weight.(Mavroidis, 2002)

matic actuators to the corresponding properties of shape memory alloy actuators (SMA) and electro-rheological fluid (ERF) based motors which are called as electrically controlled force and stiffness (ECFS) actuators. From the Figure 5.1 it can be seen that hydraulic actuators can apply very large forces, but are heavy. DC motors have the lowest power density of the four types of actuators considered here. Their weight varies from low to moderate. SMAs have very high power density which is comparable to hydraulic actuators and are very light in weight. Pneumatic and ECFS actuators can apply moderate forces, with ECFS being smaller in size. From the Figure 5.1 it can be clearly seen that the smart material based actuators can reduce the size of the actuators by at least two or three times of magnitude while having the same force-to-weight output.

5.2 Shape Memory Alloys (SMA)

Shape memory alloy consists of a group of materials that have the capability to return to a predefined shape or size when subjected to appropriate thermal input. Some examples of these alloys are *NiTi*, *NiTiCu*, *CuAlNi*, *CuAlBe*, *NiMnGa*, *AuCd* and *Fe-Mn-Si*. A shape memory alloy is able to remember its original configuration after it has been deformed by heating the alloy above characteristic transition temperature. This unique effect of returning to its original geometry after a large inelastic deformation

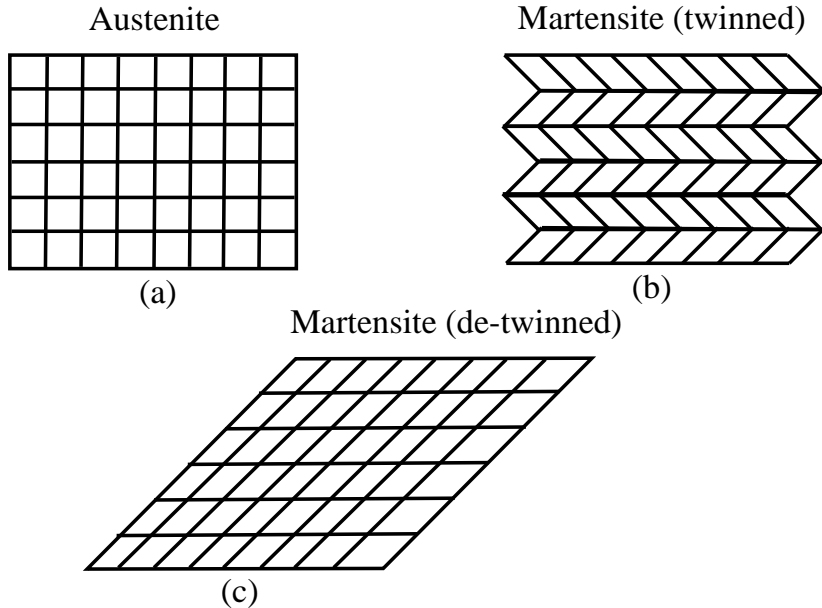


Figure 5.2: Material Crystalline arrangement during the Shape Memory Effect.(Mavroidis, 2002)

is known as shape memory effect(SME)(Mosley & Mavroidis, 2001; Van Humbeeck, 2001). The SME behavior is due to a temperature and stress dependent transition in the material's crystalline structure between two different phases ; a high temperature parent phase called austenite, and a low temperature product phase called martensite. Let us consider the example of a straight SMA rod (Mavroidis, 2002). If the straight rod of SMA in its austenite i.e., high temperature phase is allowed to cool below the phase transition temperature, the crystalline structure will change to martensite. If the bar is then plastically deformed, for example by bending and then reheated above the phase transition temperature, it will return to its original straight configuration. This phenomenon can be explained in a simplified manner using the material's crystalline arrangement as shown in Figure 5.2. At high temperature, the material is in a cubic austenite structure (Fig. 5.2-a). When cooling below the phase transition temperature, the crystalline structure changes to martensite having a lower crystal symmetry and a very typical twinned pattern (Fig. 5.2-b). Now, if sufficient stress is applied, the martensite structure is detwinned producing a large deformation at the crystal length scale (Fig. 5.2-c). This behaviour can be illustrated by studying the stress-strain curve for the martensite phase (Figure 5.3). For small stresses, the martensite- twinned structure in Figure 5.2-b behaves elastically from stage-0 to stage-1. At stage 1, the material yields and de-twinning occurs between stage-1 and stage-2. At stage-2 the martensitic structure is completely de-twinned as represented by Figure 5.2-c. Now a second elastic region starts from stage-2 and ends at stage-3. At stage 3, permanent plastic deformation begins that is not recoverable by the Shape Memory Effect. During the phase transition there is energy dissipation due to internal friction. As a result a thermal hysteresis occurs which can be seen in Figure 5.4-a. Starting at stage 1 the

Chapter 5. Introduction

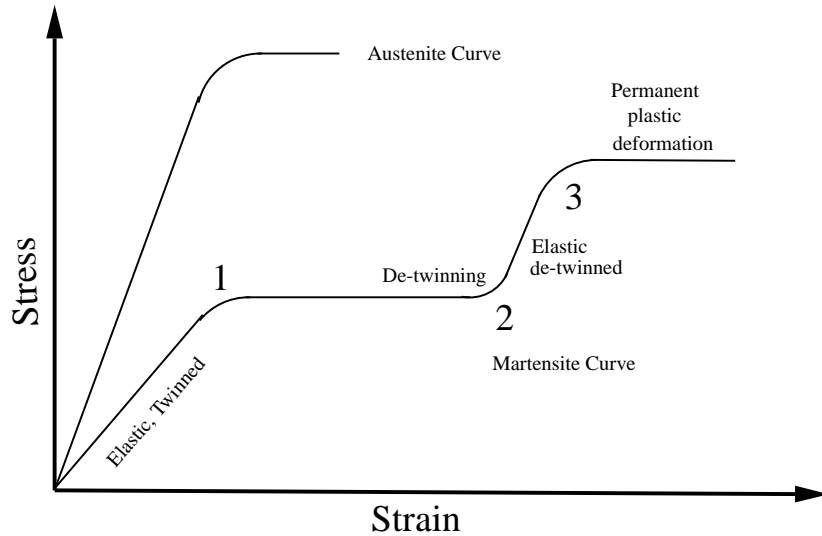


Figure 5.3: Stress-Strain relationship of Shape Memory Alloy.(Mavroidis, 2002)

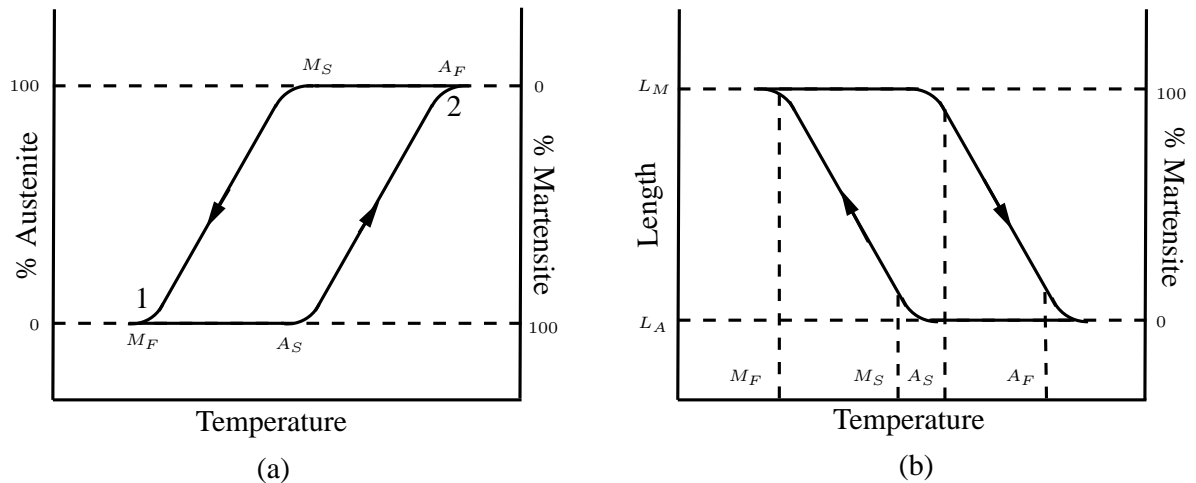


Figure 5.4: Hysteresis loops in Shape Memory Alloy.(Mavroidis, 2002)

material is 100 % martensite. During heating the material composition follows the lower curve. When the temperature reaches A_s the austenite begins and continues until A_F is reached and the material is 100 % austenite. If cooling occurs from stage 2 the material composition follows the upper curve. When the temperature drops to M_S , martensite phase begins and continues until M_F which is the original phase 100 % martensite. This thermal hysteresis can be seen in the strain/temperature relationship (Figure 5.4-b).

5.3 Shape Memory Alloy (SMA) Actuators

5.3.1 General Performance and Thermal Control of SMA element

The general design guidelines of SMA actuators in terms of performance is briefly discussed here. Performance of SMA actuators is to be understood in terms of dynamic performance (input-output time response) and positioning accuracy which are considered to be typical requirements for certain applications such as robotic or any precision displacement actuator. The performance requirements of SMA actuators also rely heavily on aspects like energy efficiency or the stroke of the actuator element. For SMA actuators, the efficiency of the conversion of heat into mechanical work is very low. Theoretical Carnot value is itself very low for SMAs because the difference between high and low temperature is only a few tens of degrees. When considering friction and losses, this efficiency go down to about 1%. According to [Reynaerts & Van Brussel \(1998\)](#), a SMA actuator will never compete with conventional drive types, as it has been compared in [Mavroidis et al. \(2000\)](#) that the efficiency of an electrical actuator is 90% (for large systems). For hydraulic and pneumatic it is rare although possible to achieve efficiency above 60% and 30%, which is still higher compared to SMA actuators. But there are interesting applications where the disadvantages of SMA actuators can be ignored, and considering the performance point of view the design of SMA actuators has more prominent takers in applications such as robotic actuators, to name one of the many fields of applications.

Commercially the two main groups of SMA alloys available are copper based alloys such as *CuAlBe*, *CuAlNi* alloys and *NiTi* alloys. Depending on the type of applications and price of the final product the two major types of SMA alloys are utilized. *NiTi* SMAs are more expensive than copper based alloys but fatigue resistance and functional properties are better. For applications such as “clamps” copper based alloys are preferred. In robotic applications *NiTi* based SMAs are preferred. *NiTi* has a considerably larger resistance than cooper-based alloys, so smaller current is sufficient in case of electrical resistive heating. The functional properties of *NiTi* are far better reproducible and has higher mechanical strength and allows a higher working stress. *NiTi* alloys have also appeared to have shown a higher work density (delivered work per unit volume) and have good corrosion resistive properties.

As the martensitic transformation is at the origin of the unique SMA properties, thermal control of SMA element is of first importance. In this subsection the thermal control is discussed. First cooling of the SMA element is addressed. It can be achieved in three ways: radiation, conduction and convection. Because the conventional operational temperature of the SMA actuators are usually below 100°C(excluding high temperature SMA), the radiation effects can be ignored. When using a fluid for cooling, the heat transfer is due to conduction when the fluid is static and convection if the fluid used is non-stationary. Generally the heat transmission under ideal laboratory condition could be considered as convection or forced convective. Heat transfer between the SMA

Chapter 5. Introduction

element and ambient can be given by

$$P_t = hA\Delta T \quad (5.1)$$

where the variables

| | |
|------------|---|
| P_t | transmitted power (W) |
| h | heat transmission coefficient (W/m^2K) |
| A | cooling surface (m^2) |
| ΔT | temperature difference between actuator and ambient (K) |

In the above equation the transmitted heat is mainly influenced by changing the parameters h or A . The cooling time t necessary to cool from M_s to M_f can be approximated by (Reynaerts & Van Brussel, 1998)

$$t = -mc' / hA \ln(M_f/M_s) \quad (5.2)$$

| | |
|------|---------------------------------------|
| t | cooling time (s) |
| m | mass of active element (kg) |
| c' | equivalent specific heat ($J/kg.K$) |

In the Eq. (5.2) the equivalent specific heat c' is the sum of the specific heat of the SMA and the transformation enthalpy divided by the transformation temperature interval. It is supposed that the transformation enthalpy is freed uniformly during cooling.

The cooling of the SMA element can also be obtained using Peltier elements or heat sinks. But in this case due to elongation and contraction of the SMA component, it is difficult to maintain a good physical contact between the active element and the cooling device which in-turn could reduce the heat transfer. The maximal heat transfer coefficient can be obtained in the case of moving liquid due to good physical contact between active element and cooling device. Hence liquid convection cooling is preferable for designing high performance SMA actuators. In Reynaerts & Van Brussel (1998) a comparison was made between heat transmission coefficients for air and oil cooling. The analysis show that small air circulation around wire is sufficient to obtain an improvement compared to natural convection case although further increasing the rate of air flow only showed minor improvements. In the case of air cooling using higher flow rates several drawbacks could be noted such as consumption of more air which has to be implemented with a powered ventilator. For oil cooling a higher cooling rate could be obtained by increasing the flow rate as compared to air cooling with higher flow rate. In general cooling liquids offer a much better cooling performance than air, except water which introduces electrical isolation problem. Among all the liquid cooling methods, oil cooling seems the best solution but requires leakage proof designs which could pose more problems in the actual design of the SMA actuator.

| Heating Techniques | Cooling Techniques |
|--------------------------------|--------------------|
| Resistive(I^2R) | Still air |
| Capacitance assisted(I^2R) | Water Immersion |
| Conductive | Heat sinking |
| Convective | Forced air/liquid |
| Radiative | Peltier effect |

Table 5.1: Heating and cooling techniques for SMA actuators(Sreekumar *et al.*, 2007)

Experiments (Reynaerts & Van Brussel, 1998) have shown that cooling time decreases by increasing the load (stress). Since the transformation temperatures increases with increasing stress, the parent austenite (A_S) as well as the full martensite (M_F) state will be at a higher temperature so that a better transfer is obtained. This results in a shorter cooling time. The contact surface A is another important issue in the cooling of the SMA element. When using wires as active element, the contact surface A can be increased by using rectangular cross-section (Reynaerts & Van Brussel, 1998).

The heating of the SMA element can be obtained by several methods

- electrical current fed through the element.
- a separate heating device.
- heating with external fluid.

Heating with fluids is very complicated and has a negative influence on the total bandwidth of the system. External heating elements are bulky and not very efficient so only resistive or inductive heating could be alternatives. Inductive heating induces non homogeneous temperature distribution over the cross-section of the SMA element which causes internal stress. So resistive heating by Joule effect is an attractive solution. Since resistive heating requires a higher resistivity of the SMA material, $NiTi$ are the preferred materials compared to copper based alloys.

Another method for achieving active heating and cooling capability are the Peltier elements (Abadie *et al.*, 2002; Bhattacharyya *et al.*, 1995; Romano & Tannuri, 2009). These elements can either heat or cool the SMA element by changing the polarity of the voltage applied to the Peltier element. The drawbacks of using Peltier elements is that they require space and create additional weight to the actuator itself. The various heating and cooling methods discussed here are summarized in Table 5.1.

5.3.2 Different Types of SMA Actuator

For macro level applications, the actuator is mostly in single/multiple wire form or in the coil form. The important advantage of spring is that it generates a large macroscopic displacement from a relatively small strain, but the stress distribution over the cross-section is not constant (Reynaerts & Van Brussel, 1998). Hence in a SMA spring a greater material volume is required for generating a given force. This has a negative effect on the efficiency and bandwidth of the spring based actuator as for a given output displacement, a larger material volume has to be heated and cooled. Thus

comparatively wires optimize the material used with respect to the amount of thermal energy put in the SMA device. For the micro level applications such as micro robotic devices, the foil/diaphragm/strip form has found more applications ([Sreekumar et al., 2007](#)). Thin film of Nitinol is another form of SMA actuator mostly used in MEMS devices. To summarize the selection of particular form of SMA actuator for a specific task is based on strain, bias force, actuation force/torque, and frequency of operation.

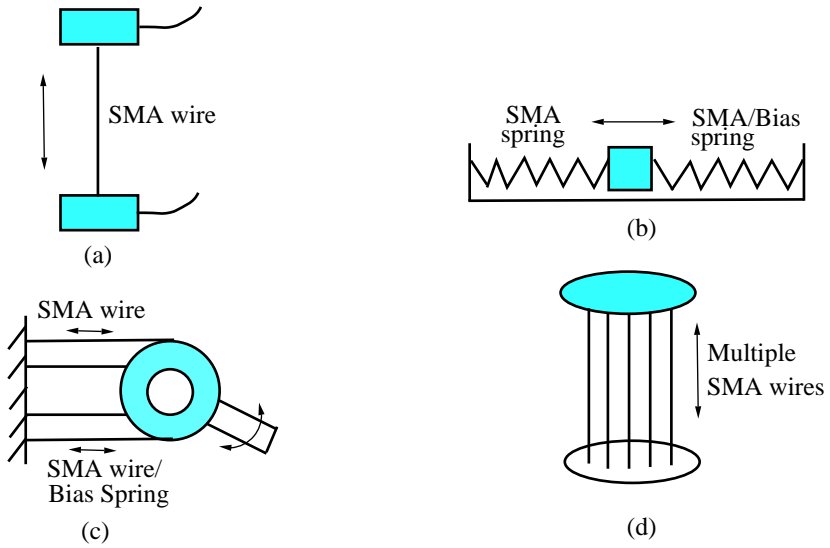


Figure 5.5: Different forms of SMA actuators: (a)Linear (b)Spring (c)Rotary (d)Bundle. ([Sreekumar et al., 2007](#))

Linear Displacement actuator: The linear displacement using SMA element can be achieved in two different ways as shown in Figure 5.5-a and 5.5-b. In the schematic in Figure 5.5-a, a SMA wire is used as active element along with a mass at the other end to provide bias using gravity. In a similar fashion a SMA spring can also replace the SMA wire to provide a linear displacement operation. For both the SMA spring and SMA wire setup the bias could also be provided using a spring. The schematic in Figure 5.5-b shows a possible setup for SMA spring arrangement provided with bias spring. The bias spring could be replaced by another SMA spring and would then function as an antagonistic actuator. In the similar setup the SMA springs could also be replaced by SMA wires. In the two actuators mentioned here the linear displacement is usually measured on the mass.

Angular Displacement actuator: The angular displacement actuators are generally combination of a SMA wire with a pulley system or a SMA strip in coil form or just a SMA spring in a pulley setup. The SMA actuator is used in a pulley setup in order to mimic a joint used in robotic applications ([Elahinia & Ashrafiun, 2002](#)). A simplified schematic of an angular displacement SMA actuator can be seen in Figure 5.5-c.

This type of setup uses a bias arrangement with the help of spring bias or mass bias. Certain types of actuators also use an antagonistic two SMA wire setup, with each SMA wire exerting restoring force on the other in the opposite direction. The angular displacement is normally measured on the pulley.

Bundle SMA actuator (Large Force actuator) (Mavroidis, 2002): In SMA actuators large forces can be achieved by increasing the overall cross-sectional area of the SMA material normal to the direction of the actuation. This can be achieved by using thicker wires or connecting many wires mechanically in parallel. Though both these methods can increase the force of the SMA actuator, there are other problems with the first method. The actuator bandwidth and power supply requirements are drastically changed by changes in cross-sectional area. One of the factors that greatly affects the bandwidth of the SMA wire actuator is the diameter. This change is due to the change in surface to volume ratio and thus change in the heat transfer characteristics of the SMA element. Larger the surface to volume ratio, higher the heat transfer, and larger the bandwidth. In order to improve the force capabilities of a SMA actuator while not decreasing the bandwidth, it is necessary to use many thin wires connected in parallel rather than a single thick wire. A schematic can be seen in Figure 5.5-d. The individual SMA wires used in the setup has to be separated from each other in order to allow free flow of air between them to increase the heat transfer rate by increasing the contact surface area.

5.4 Modelling methods and Control

There is considerable interest in development of SMA actuators due to interesting advantages such as high power-to-weight ratio, low driving voltages and ability to produce large strains. These advantages have found them interesting applications in biomedical field (Sars *et al.*, 2010), robotics (Cocaud *et al.*, 2006) and space applications (Peng *et al.*, 2008). However application to precise engineering systems are difficult due to the highly nonlinear relationship between output strain and input current. SMA actuators have hard nonlinearities such as backlash like hysteresis and saturation due to SME. The efficiency of an SMA actuator depends on the accuracy of its control, which in turn depends on good reliable model which can be efficiently used to compensate the hysteretic nonlinearity and perform the control task. This section is entirely dedicated to study the various modelling and control methods popular among SMA actuators.

Many models for SMA control have been proposed in literature, which can be coarsely classified into physical and phenomenological models. For specific problems, models describe the given hysteretic SMA system based on physical laws. Normally this is a difficult task and the resulting models are too complex to be used for practical purposes. In general, engineering applications require alternative models which although not giving enough description about the physical behaviour of the system, do describe the Input-Output features. Such input-output models are useful for identification design and control purposes of systems involving such behaviours. These models

are referred to as phenomenological models. This section briefly introduces the physical and phenomenological models. Although a large number of models could be classified in the physical and phenomenological category for studying the problem of hysteresis, only a few will be discussed here.

Remark 5.4.1. *The choice of models being discussed here pertain closely to the perspective of mechatronics and control problem in developing SMA actuators rather than going into details about the perspective of material science.*

5.4.1 Physical Modeling and Nonlinear Control

Considerable research for modelling the microscopic and macroscopic behaviour of SMAs has been performed. Since the mechanical behaviour of SMAs is closely related to microscopic phase transformation, stress-strain based constitutive relations are not sufficient to describe SMA behaviour ([Elahinia & Ashrafiou, 2002](#)). There are two classes of shape memory alloy models: microscopic and macroscopic. A general macroscopic description for thermomechanical behaviour was given in [Leclercq & Lcellent \(1996\)](#). An improved macroscopic constitutive model based on the work presented by [Liang & Rogers \(1992\)](#) in combination with a heat convection model was used by [Elahinia & Ashrafiou \(2002\)](#). Due to simplicity and as being application oriented the model used in [Elahinia & Ashrafiou \(2002\)](#) is discussed here.

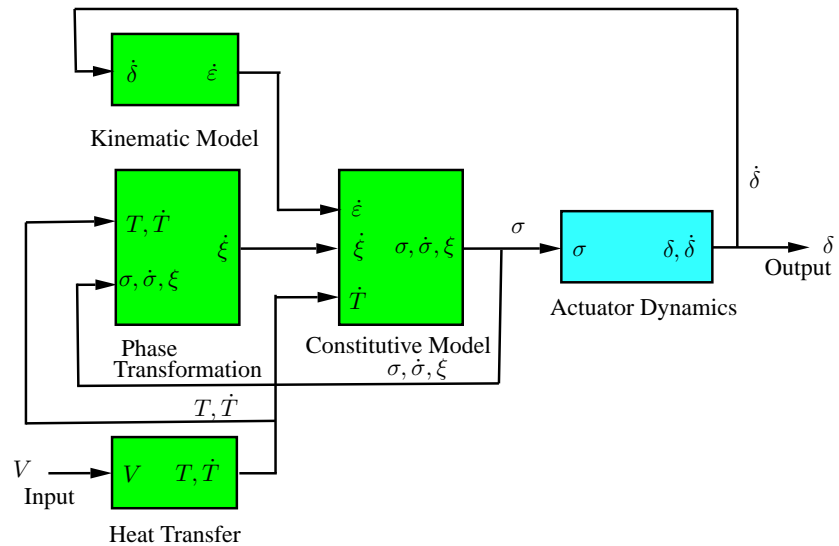


Figure 5.6: Block diagram of a SMA actuator using physical modelling ([Elahinia & Ashrafiou, 2002](#)).

The model used by [Elahinia & Ashrafiou \(2002\)](#) can be subdivided into two major blocks (see Figure 5.6). The first block consists of actuator dynamic model. The second block consists of phase transformation, wire constitutive model, heat transfer model and the kinematic model. The input to the model is voltage (V) and the output of the model

is displacement δ . The displacement could be linear or angular depending on the design of the actuation system. Depending on the design of the actuator setup the model of the actuator dynamics and the kinematic model would differ. The details of the wire constitutive model, phase transformation and heat transfer model are discussed in the following paragraphs.

Wire constitutive model: The wire constitutive model relates stress rate ($\dot{\sigma}$), strain rate and temperature rate (\dot{T}) by using the relationship (see Liang & Rogers (1992) and references in there):

$$\dot{\sigma} = D\dot{\varepsilon} + \theta_T \dot{T} + \Omega \dot{\xi} \quad (5.3)$$

where $0 \leq \xi \leq 1$ is the Martensite fraction coefficient, $D = (D_M + D_A)/2$ is the mean Young modulus or elastic modulus, D_A is Austenite Young modulus, D_M is Martensite Young modulus, θ_T is thermal expansion factor or thermoelastic tensor, $\Omega = -D\varepsilon_0$ is phase transformation contribution factor(phase transformation tensor) and ε_0 is the initial strain.

SMA wire Phase Transformation Model: Due to hysteretic behaviour of SMA wire, the phase transformation equations are different for heating and cooling. Heating results in reverse transformation from Martensite to Austenite ($M \rightarrow A$):

$$\xi = \frac{\xi_M}{2} \{ \cos[a_A(T - A'_s) + b_A \sigma] + 1 \} \quad (5.4)$$

where ξ_M is the maximum Martensite fraction obtained during cooling, T is the SMA wire temperature, A'_s and A'_f are Austenite phase start and final state, and $a_A = \pi/(A'_f - A'_s)$, $b_A = -a_A/C_A$ and C_A are curve fitting parameters.

Cooling results in forward transformation from Austenite to Martensite ($A \rightarrow M$):

$$\xi = \frac{1 - \xi_A}{2} \cos[a_M(T - M'_f) + b_M \sigma] + \frac{1 + \xi_A}{2} \quad (5.5)$$

where ξ_A is the minimum Martensite fraction obtained during heating, M'_s and M'_f are Martensite phase start and final state, and $a_M = \pi/(M'_s - M'_f)$, $b_M = -a_M/C_M$ and C_M are curve fitting parameters.

The derivatives of Eq. (5.4) and Eq. (5.5) yields the state equation during heating:

$$\dot{\xi} = -\frac{\xi_M}{2} \sin[a_A(T - A'_s) + b_A \sigma] [a_A \dot{T} + b_A \dot{\sigma}] \quad (5.6)$$

and during cooling the state equation is given by

$$\dot{\xi} = \frac{1 - \xi_A}{2} \sin[a_M(T - M'_f) + b_M \sigma] [a_M \dot{T} + b_M \dot{\sigma}] \quad (5.7)$$

Heat Transfer Model: The SMA wire heat transfer equation consists of electrical (joule) heating and natural convection:

$$mc_p \frac{dT}{dt} = \frac{V^2}{R} - hA(T - T_\infty) \quad (5.8)$$

where V is voltage, R is resistance per unit length, c_p is the specific heat, $m = \rho\pi d^2/4$ is mass per unit length, ρ is density, d is diameter, and $A = \pi d$ is circumferential area of the SMA wire. T_∞ is the ambient temperature and h is heat convection coefficient. In [Elahinia & Ashrafiuon \(2002\)](#) the value of h was approximated by a second order polynomial of temperature to improve the heat transfer model,

$$h = h_0 + h_2 T^2. \quad (5.9)$$

Kinematic Model: The kinematic model gives the relation between the strain rate $\dot{\varepsilon}$ and the displacement rate $\dot{\delta}$. The displacement rate $\dot{\delta}$ could be angular velocity for a rotary SMA actuator and linear velocity for a linear displacement actuator. For a linear SMA actuator the kinematic model depends on the linear velocity and initial length of the SMA wire. For a rotary SMA actuator the kinematic model depends on the radius of the pulley used, angular velocity and the initial length of the SMA. For further details please refer to [Elahinia & Ashrafiuon \(2002\)](#).

Thermomechanical model by Leclercq & Lcellent (1996): The given model makes use of thermodynamics of irreversible processes. The model is based on assumption that there exists a representative volume where one can define and measure certain internal variables. In their model elastic strain ε^e , temperature T , the volume fraction of self-accommodating matensite z_T and volume fraction of oriented martensite z_σ are taken as internal variables. The Helmholtz free energy for the total range of phase transition is defined. A study of thermodynamic absolute equilibrium during phase transition explains the hysteretic behaviour of the SMA.

In the model by [Leclercq & Lcellent \(1996\)](#) certain parameters have to be determined from experimental data. For simplicity certain parameters are assumed to be known such as :

- isotropic elastic tensor.
- mass density.
- latent heat of phase transition.
- phase transition temperature.
- maximum pseudoelastic strain (γ)

The parameters that have to be determined can be classified into thermodynamic constants and kinetic constants. There are four thermodynamic constants which are determined from the equations explaining the pseudoelastic behaviour of SMA, forward and reverse phase transition equations including the equation for reorientation of self-

accommodating martensite. The kinetic constants are involved in the yield functions and are linked to the z_σ and z_T . These are estimated from experimental results iteratively.

Control with Explicit model Information: Nonlinear Control

The controller methods classified under this category are the methods which use controller with knowledge of the physical model based on thermomechanical behaviour. In this category nonlinear control technique based on feedback linearization ([Sastry, 1999](#); [Benzaoui et al., 1999](#)) is discussed which uses a model based on macroscopic thermomechanical description developed in [Leclercq & Lcellent \(1996\)](#). Also in this category the sliding mode control of SMA using an improved macroscopic model with heat equation as used in [Elahinia & Ashrafiou \(2002\)](#) and [Williams et al. \(2010\)](#) is discussed.

Control using Input-Output Linearization ([Sastry, 1999](#)): Feedback linearization uses a state feedback control with a specific structure that allows change of variables (coordinates) transforming the nonlinear system into an equivalent linear system. Feedback linearization can be classified into full-state linearization where the state equation is completely linearized and input-output linearization where the input-output map is linearized while the state equation may be only partially linearized. The methodology of input-output linearization is discussed further. Consider a single-input single-output system given as below:

$$\dot{x} = f(x) + g(x)u, \quad (5.10)$$

$$y = h(x). \quad (5.11)$$

where $x \in \mathbb{R}^n$, f, g are smooth vector fields on \mathbb{R}^n and h is a smooth nonlinear function. Differentiating y with respect to time, we get

$$\dot{y} = \frac{\partial h}{\partial x}f(x) + \frac{\partial h}{\partial x}g(x)u, \quad (5.12)$$

$$:= L_f h(x) + L_g h(x)u. \quad (5.13)$$

Here $L_f h(x) : \mathbb{R}^n \mapsto \mathbb{R}$ and $L_g h(x) : \mathbb{R}^n \mapsto \mathbb{R}$ are the Lie derivatives of h with respect to f and g respectively. If $L_g h(x)$ is bounded away from zero for all $x \in U$, the state feedback law can be given by

$$u = \frac{1}{L_g h(x)}(-L_f h(x) + v) \quad (5.14)$$

gives the first order linear system from the new input v to y as

$$\dot{y} = v. \quad (5.15)$$

Consider that $L_g h(x) \equiv 0$, meaning that $L_g h(x) = 0 \forall x \in U$, we differentiate Eq. (5.16) to get

$$\ddot{y} = \frac{\partial L_f h}{\partial x} f(x) + \frac{\partial L_f h}{\partial x} g(x) u, \quad (5.16)$$

$$:= L_f^2 h(x) + L_g L_f h(x) u. \quad (5.17)$$

where $L_f^2 h(x)$ stands for $L_f(L_f h)(x)$ and $L_g L_f h(x) = L_g(L_f h(x))$. If $L_g L_f h(x)$ is bounded away from zero for all $x \in U$ the control law given by

$$u = \frac{1}{L_g L_f h(x)} (-L_f^2 h(x) + v) \quad (5.18)$$

gives the linear second order system from input v to output y :

$$\ddot{y} = v. \quad (5.19)$$

Generally if γ is the smallest integer for which $L_g L_f^i h(x) \equiv 0$ on U for $i = 0, \dots, \gamma - 2$ and $L_g L_f^{\gamma-1} h(x) \equiv 0$ is bounded away from zero on U the the control law given by

$$u = \frac{1}{L_g L_f^{\gamma-1} h(x)} (-L_f^\gamma h(x) + v) \quad (5.20)$$

gives the γ – th order linear system from input v to output y :

$$y^\gamma = v. \quad (5.21)$$

From the nonlinear control law of Eq. (5.20) it can be seen that the expression $L_g L_f^{\gamma-1} h(x)$ should be nonzero and the knowledge of the states is essential.

In Benzaoui *et al.* (1999) the feedback lineraization was used to experimentally control SMA actuator using state information. The nonlinear dynamic model of the SMA included measurement of physical quantities such as stress, strain, applied current, applied voltage and temperature. For constant stress condition the the state vector of the nonlinear model used for displacement control was $x = [y \ (T - T_a)]$, where y is the displacement measurement and $T - T_a$ was the difference between temperature of the SMA wire and the ambient temperature. For further details refer to Benzaoui *et al.* (1999) for the modeling and nonlinear control.

Control using Sliding mode (Elahinia & Ashrafiun, 2002): The variable structure control uses a switching control law to drive and maintain the nonlinear systems state trajectory onto a chosen surface in state space. When the state trajectory of the system is above the chosen surface then a given controller structure is used and when the state trajectory is below the chosen surface a different controller structure is used. The controller is robust to model uncertainties and nonlinearities. The model

presented in section 5.4.1 can be used here to be defined by a set of nonlinear state equations as

$$\dot{\mathbf{x}} = \mathbf{A}(\mathbf{x}, t) + \mathbf{B}(\mathbf{x}, \mathbf{u}, t) \quad (5.22)$$

where the state vector \mathbf{x} and the control input \mathbf{u} are given as

$$\mathbf{x} = (\delta \ \dot{\delta} \ T \ \sigma \ \xi) \text{ and } \mathbf{u} = V \quad (5.23)$$

The variable structure control used to control the above nonlinear system equation can be given using the function $s(\mathbf{x})$ as:

$$\mathbf{u}(\mathbf{x}, t) = \begin{cases} \mathbf{u}^+(\mathbf{x}, t) & \text{if } s(\mathbf{x}) > 0 \\ \mathbf{u}^-(\mathbf{x}, t) & \text{if } s(\mathbf{x}) < 0 \end{cases} \quad (5.24)$$

such that the switching surface $s(\mathbf{x}) = 0$ can be reached in finite time. A simple VSC two-stage control using a switch between high voltage and low voltage can be given by

$$\mathbf{u} = \begin{cases} V_{high} & \text{if } s > 0 \\ V_{low} & \text{if } s < 0 \end{cases} \quad (5.25)$$

where the switching surface $s := \tilde{\delta} = \delta - \delta^*$ and δ^* is the displacement reference. A boundary layer was used around the switching surface $s = \tilde{\delta}$ to minimize chattering given by a thickness ϕ and hence the control input can be given by:

$$\mathbf{u} = \begin{cases} V_{high} & \text{if } \frac{s}{\phi} < -1 \\ V_{low} & \text{if } \frac{s}{\phi} > +1 \\ Ks & \text{if } -1 < \frac{s}{\phi} < +1 \end{cases} \quad (5.26)$$

where K is a proportional gain. Another switching layer can also be given as a weighted combination of position and velocity errors,

$$s = \left(\frac{d}{dt} + \lambda \right) \tilde{\delta} = \dot{\tilde{\delta}} + \lambda \tilde{\delta} \quad (5.27)$$

where $-\lambda$ is the slope of the sliding surface in the phase space.

Adaptive Nonlinear control

Generally adaptive controls are considered advantageous for controlling systems with complex nonlinearities and modelling uncertainties. Specially these techniques are helpful in systems hysteresis like SMA where the behaviour of the systems depend on various material states which provided problems in measurement and prediction. Extended Kalman Filter would be an interesting solution to estimate the states required in nonlinear control.

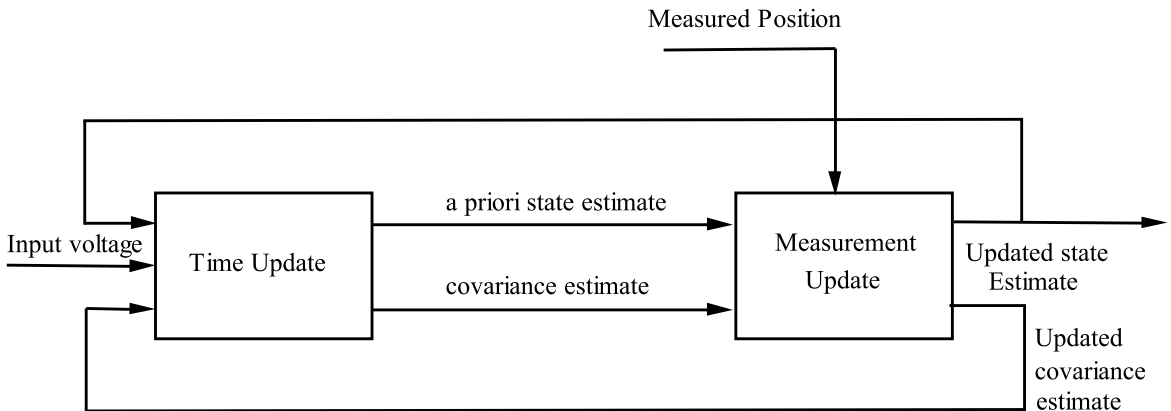


Figure 5.7: Schematic diagram of Extended Kalman Filter (EKF) ([Elahinia & Ahmadian, 2006](#)).

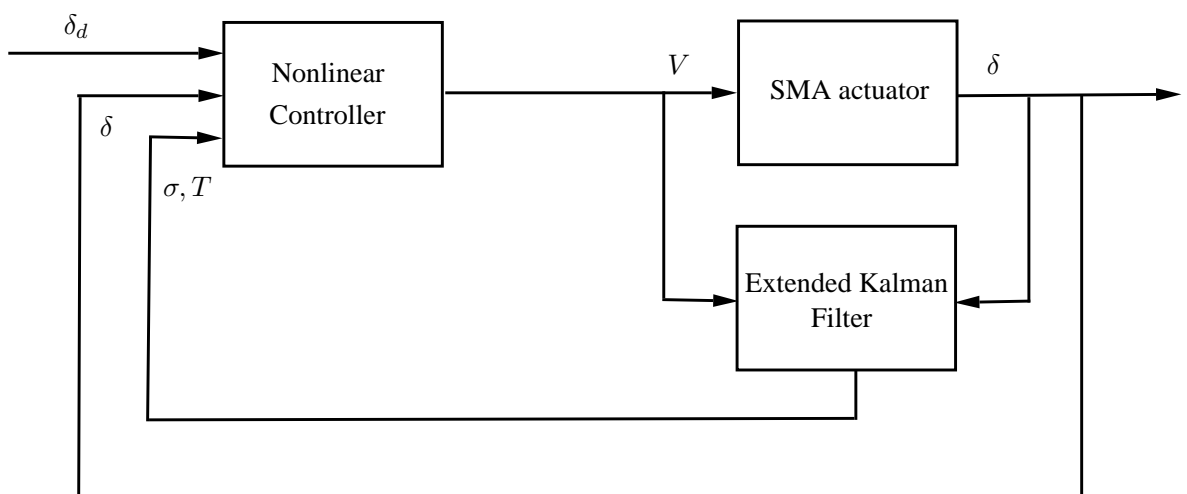


Figure 5.8: Nonlinear control using Extended Kalman Filter ([Elahinia & Ahmadian, 2006](#)).

Adaptive Nonlinear control using Extended Kalman Filter(EKF)([Elahinia & Ahmadian, 2006](#)): Often information of states of the system is essential for developing efficient control algorithms. In systems such as SMA actuator it is often difficult to measure the state variables of the systems such as temperature and stress which would need additional sensors on the actuators system. In order to minimize the usage of sensors an Extended Kalman Filter (EKF) can be used to estimate the states of the SMA actuator. The EKF is often used when the states of the system have a nonlinear dynamic. EKF is based on linearization about the current error mean and covariance.

The schematic diagram of the implementation of EKF can be seen in Figure 5.7. In [Elahinia & Ahmadian \(2006\)](#) a nonlinear control using Variable structure(VSC) method with EKF as used to control a shape memory alloy arm as seen in Figure 5.8, the EKF used the control input and the output displacement to predict the other state variables

such as SMA wire stress and SMA wire temperature. The SMA stress and temperature were further used in the variable structure controller (VSC) to control the SMA system.

Although the EKF was used in the context of VSC control in Elahinia & Ahmadian (2006), the same approach of control by estimation of states could also be employed with other nonlinear control techniques such as feedback linearization(Benzaoui *et al.*, 1999).

5.4.2 Phenomenological Model and Inverse Control

The Preisach model (Ahn & Kha, 2008; Bossavit *et al.*, 1991; Tan & Baras, 2004; Iyer *et al.*, 2005; Tan & Baras, 2005; Tan *et al.*, 2005) is a very popular model which falls in this category of phenomenological model amongst others such as Krasnosel'skii-Pokrovskii (KP)(Visintin, 1994) and Prandtl-Ishlinskii (PI)(Jostrom & Visone, 2006). Preisach and Krasnosel'skii-Pokrovskii (KP) models are parametrized by a pair of threshold variables, where as Prandtl-Ishlinskii (PI) model is a superposition of elementary stop operators which are parametrized by a single threshold variable (Chen *et al.*, 2009).

Preisach Modeling(Tan & Baras, 2005)

The main assumption made in the Preisach model is that the system can be thought of as a parallel summation of a continuum of weighted relay hysteresis (see Figure 5.10). For a pair of threshold values (β, α) with $\beta \leq \alpha$, a simple hysteretic element $\hat{\gamma}_{\beta,\alpha}[\cdot, \cdot]$ can be seen in Figure 5.9. Let $C([0, T])$ be the space of continuous functions on $[0, T]$. For $x \in C([0, T])$ and an initial configuration $\zeta \in \{-1, 1\}$, $y = \hat{\gamma}_{\beta,\alpha}[x, \zeta]$ for $t \in [0, T]$ is defined as,

$$y(t) \triangleq \begin{cases} -1, & \text{if } x(t) < \beta \\ 1, & \text{if } x(t) > \alpha \\ y(t^-), & \text{if } \beta \leq x(t) \leq \alpha \end{cases} \quad (5.28)$$

where $y(0^-) = \zeta$ and $t^- \triangleq \lim_{e>0, e \rightarrow 0} t - e$.

This operator is referred to as elementary Preisach hysteron as it is building block of the Preisach operator. Let us define

$$\mathcal{P}_0 \triangleq \{(\beta, \alpha) \in \mathbb{R}^2 : \beta \leq \alpha\}. \quad (5.29)$$

\mathcal{P}_0 is called the Preisach plane and each $(\beta, \alpha) \in \mathcal{P}_0$ is identified with the hysteron $\hat{\gamma}_{\beta,\alpha}$. For $x \in C([0, T])$ and an initial condition ζ_0 of all hysterons, $\zeta_0 : \mathcal{P}_0 \rightarrow \{-1, 1\}$, the output of the Preisach operator Γ is defined as

$$\Gamma[x, \zeta_0](t) = \int_{\mathcal{P}_0} \mu(\beta, \alpha) \hat{\gamma}_{\beta,\alpha}[x, \zeta_0(\beta, \alpha)](t) d\beta d\alpha \quad (5.30)$$

where the weighting function μ is called as the Preisach function or density function. It is assumed that μ is positive semidefinite ($\mu \geq 0$). Furthermore to simplify, assume $\mu(\beta, \alpha) = 0$ if $\beta < \beta_0$ or $\alpha > \alpha_0$ for some $\{\beta_0, \alpha_0\}$. In this case, a finite triangular area is

considered in the Preisach plane $\mathcal{P} \triangleq \{(\beta, \alpha) \in \mathcal{P}_0 | \beta \geq \beta_0, \alpha \leq \alpha_0\}$ (see Figure 5.11-a). The memory effect of the Preisach operator can be given by the memory curves in \mathcal{P} . At time t , \mathcal{P} can be divided into two regions

$$\mathcal{P}_+(t) \triangleq \{(\beta, \alpha) \in \mathcal{P} | \text{output of } \hat{\gamma}_{\beta, \alpha} \text{ at } t \text{ is } +1\} \quad (5.31)$$

$$\mathcal{P}_-(t) \triangleq \{(\beta, \alpha) \in \mathcal{P} | \text{output of } \hat{\gamma}_{\beta, \alpha} \text{ at } t \text{ is } -1\} \quad (5.32)$$

such that $\mathcal{P}_-(t) \cup \mathcal{P}_+(t) = \mathcal{P}$ at all times. It becomes clear that each set is connected. The time dependence will often be implicit, with \mathcal{P}_- and \mathcal{P}_+ used to denote these regions. Now, assume that at some initial time t_0 , the input $x(t_0) = x_0 < \beta_0$. Then

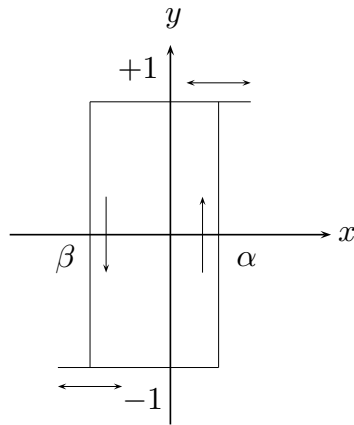


Figure 5.9: Preisach Hysteron (Tan & Baras, 2005).

the output of every hysteron is -1 . Therefore, $\mathcal{P}_-(t_0) = \mathcal{P}, \mathcal{P}_+(t_0) = \emptyset$ which is called as the negative saturation (see Figure 5.11-b). Now if the input $x(t)$ is monotonically increased to a maximum value at t_1 with $x(t_1) = x_1$. The output of $\hat{\gamma}_{\beta, \alpha}$ is switched to $+1$ as the input $x(t)$ is greater than α . Therefore at time t_1 the boundary between $\mathcal{P}_-(t_1)$ and $\mathcal{P}_+(t_1)$ is the horizontal line $\alpha = x_1$ (see Figure 5.11-c). Now if the input $x(t)$ starts to decrease monotonically until t_2 with $x(t_2) = x_2$ then the output of $\hat{\gamma}_{\beta, \alpha}$ is -1 as $x(t)$ sweeps past β and a vertical line segment $\beta = x_2$ is generated as part of the boundary (see Figure 5.11-c). Further input reversals generate additional horizontal or vertical boundaries. From the explanation given here we can see that the output of Γ is determined by the boundary between \mathcal{P}_- and \mathcal{P}_+ which is called as the memory curve as it describes the states of the hysterons.

Krasnosel'skii-Pokrovskii Modeling (Webb et al., 1998)

The parametrized hysteresis model using the Krasnosel'skii-Pokrovskii modelling can be given by an integral operator model defined as follows:

$$[\Gamma_\mu(x, f)](t) = \int_{\mathcal{P}} [y_p(x, \xi_p)](t) d\mu(p). \quad (5.33)$$

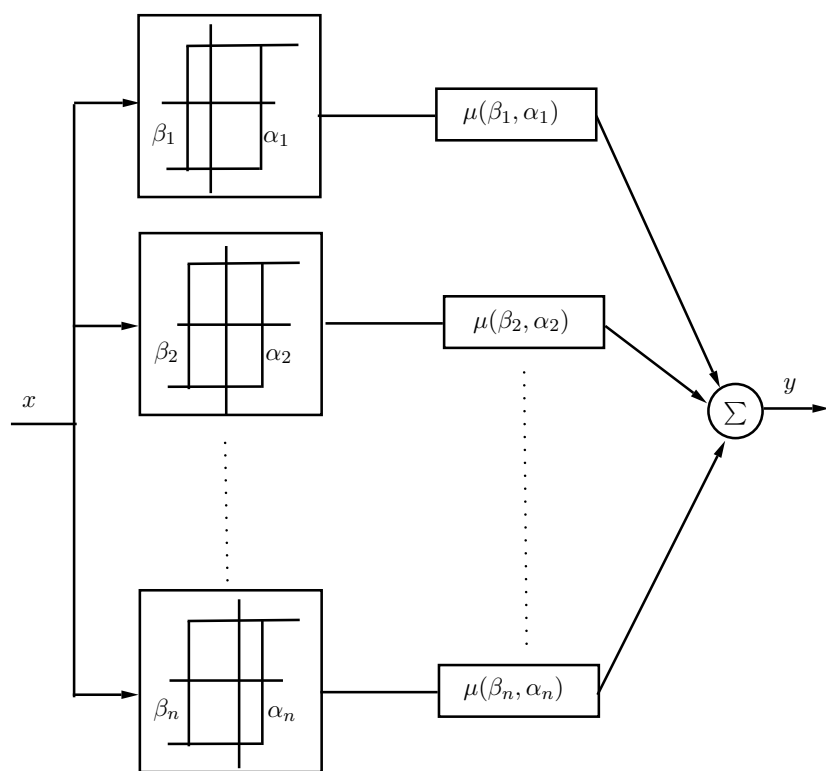


Figure 5.10: Discretized Preisach operator. (Tan *et al.*, 2005).

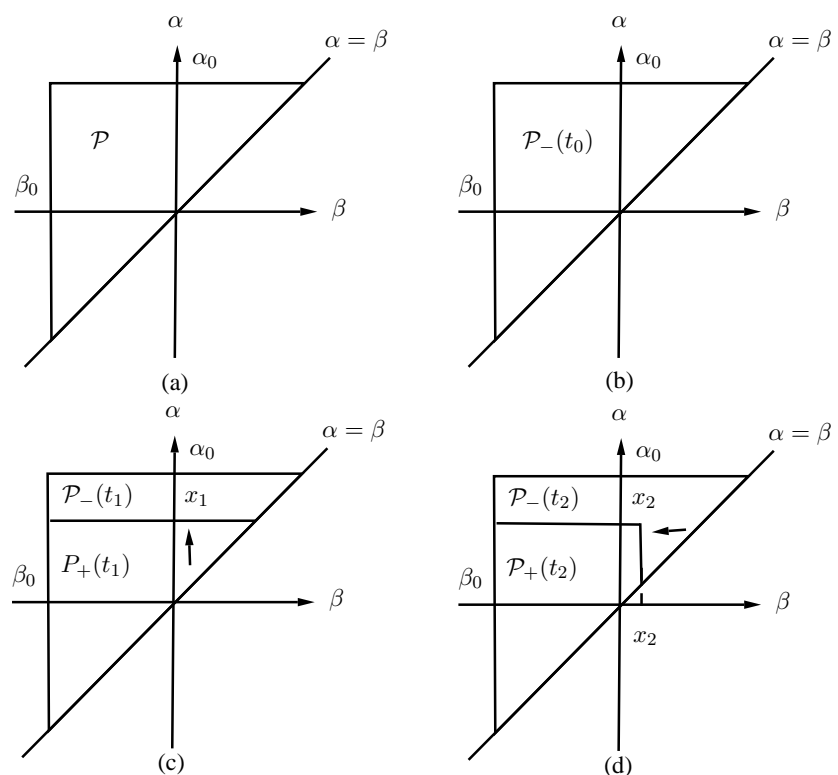


Figure 5.11: Memory curves on Preisach plane ([Tan & Baras, 2005](#)).

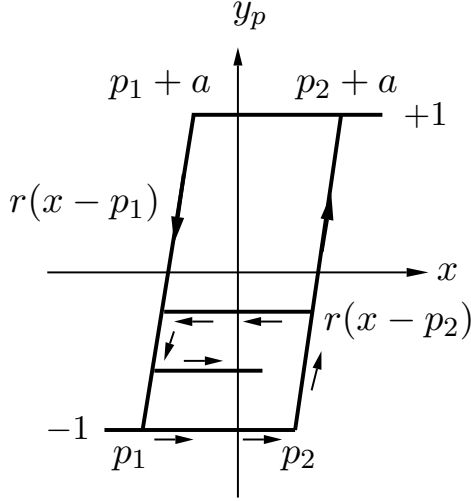


Figure 5.12: KP Hysteresis operator (Webb *et al.*, 1998).

Here $\Gamma_\mu(x, f)$ represents the integral hysteresis operator, where x is the input to the hysteresis. In the above equation (5.33), $y_p(x, \xi_p)$ is the kernel function of an individual element $p \in \mathcal{P}$ in the Preisach plane \mathcal{P} is given below

$$\mathcal{P} = \{p \in \mathbb{R}^2 : p = (p_1, p_2), p_2 \geq p_1\}. \quad (5.34)$$

The variable ξ_p represents the memory of the kernel and μ_p is the weight of the kernel for $p \in \mathcal{P}$. The integral model used here is comparable to the Preisach model and can be interpreted as parallel connection of a weighted kernels. In this given hysteresis the kernel would be the KP kernel. The kernel function for a given $p = (p_1, p_2)$ is given below

$$y_p(x, \xi_p) = \begin{cases} \max\{\xi_p, r(x - p_2)\} & \text{for } \dot{x} \geq 0 \\ \min\{\xi_p, r(x - p_1)\} & \text{for } \dot{x} \leq 0 \end{cases} \quad (5.35)$$

The memory term ξ_p is updated depending on the sign of \dot{x} . From Figure 5.12 we can see the function $r(x - p_1)$, $r(x - p_2)$ forms the hysteresis switching between -1 and $+1$. The width of the hysteresis is determined by the switching values of input, p_1 and p_2 . The slope of the switching between -1 and $+1$ is determined by the rise constant a . The ridge function $r(u)$ is given by

$$r(u) = \begin{cases} -1 & u < 0 \\ -1 + 2\frac{u}{a} & 0 \leq u \leq a \\ 1 & u > a \end{cases} \quad (5.36)$$

For numerical implementation the above discussed KP model has to be discretized by converting the \mathcal{P} -plane into a mesh grid. Let K be the number of horizontal or vertical partitions with an input $x \in X$, and let μ_K be the discretized measure. The number of grid points in the \mathcal{P} -plane can be given by $N = K(K + 1)/2$. There exists a kernel function $y_{p_i}(x, \xi_i)$ for each grid point $p_i = (p_1, p_2)$. The discrete hysteresis model could

then be given by

$$\Gamma_{\mu K}(x, f) = \sum_{i=1}^K \sum_{j=i}^K [y_{p_{ij}}(x, \xi_{ij})](t) \cdot \theta_{ij}. \quad (5.37)$$

where $p_{ij} = (p_{1i}, p_{2j})$, θ_{ij} is the weighting value for the p_{ij} pair and $y_{p_{ij}}$ is the kernel function.

Prandtl-Ishlinskii Model ([Chen et al., 2009](#))

The basic element of the PI model is the so called stop operator $y(t) = S_r[x](t)$ with threshold r seen in Figure [5.13](#). For piece-wise monotone function $x(t)$, define $s_r : \bar{R} \rightarrow \bar{R}$ (where \bar{R} denotes the space of real numbers) as

$$s_r(t) = \min(r, \max(-r, x)). \quad (5.38)$$

suppose the function $x(t)$ is monotone on $t_i \leq t \leq t_{i+1}$ (for $i = 0, 1, \dots$) and $t_0 = 0$. For any initial value $y_{-1} \in R$ and $r \geq 0$, the stop operator $S_r[\cdot; y_{-1}](t)$ is defined as

$$S_r[x; y_{-1}](0) = s_r(x(0) - y_{-1}) \quad (5.39)$$

$$S_r[x; y_{-1}](t) = s_r(x(t) - x(t_i) + S_r[x; y_{-1}](t_i)) \quad (5.40)$$

for $t_i \leq t \leq t_{i+1}$. The stop operator is mainly described by the threshold value $r \geq 0$ which determines the height of the hysteresis region in the (x, y) plane. For simplicity let $S_r[x; y_{-1}](t)$ by $S_r[x](t)$. It can be noted that the stop operator is rate independent. The PI hysteresis model is defined by

$$y(t) = \int_0^\infty q(r) S_r[x](t) dr, \quad (5.41)$$

where $q(r)$ is the unknown density function, such that $q(r) \geq 0$ with $\int_0^\infty r q(r) dr < \infty$. Since the density function $q(r)$ vanishes for large values of r , it is assumed that there exists a constant R such that $q(r) = 0$ for $r > R$. Thus the model [\(5.41\)](#) gives

$$y(t) = \int_0^R q(r) S_r[x](t) dr, \quad (5.42)$$

The parallel connection of elementary hysteresis operator leads to the so called discrete Prandtl-Ishninskii operator of stop type.

Adaptive inverse control using Hysteresis Model:

The adaptive inverse control of SMA actuator involves control of SMA actuator using an inverse model of the hysteresis which is adapted in realtime. The most common model used for modelling hysteresis in this context are Preisach, KP and PI which have been introduced already. [Tan & Baras \(2005\)](#) studied the adaptive inverse control of magnetostrictive actuator using Preisach model. In [Webb et al. \(1998\)](#) adaptive inverse control was studied using KP model. Figure. [\(5.14\)](#) shows a schematic of adaptive inverse control where the inverse hysteresis model $\hat{\Gamma}^{-1}$ represents the inverse of the Preisach operator Γ with piecewise uniform density function. $\hat{\Gamma}$ represents the Preisach

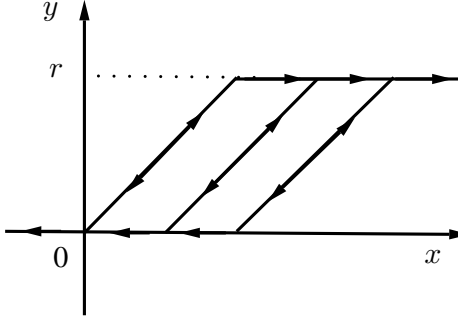


Figure 5.13: PI linear stop operator (Kuhnen, 2003).

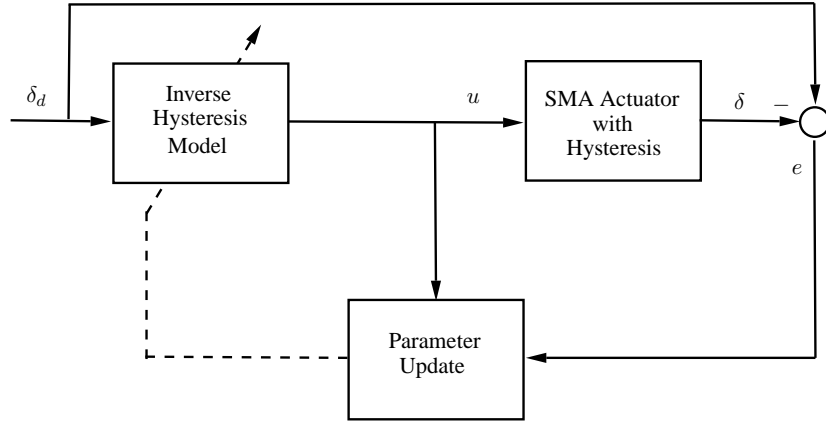


Figure 5.14: Schematic of Adaptive inverse control(Tan & Baras, 2005).

operator with the estimated density function. The error between the reference trajectory $\delta_d(t)$ and the achieved trajectory $\delta(t)$ is then used to update the estimate the density function and thus the inverse model $\hat{\Gamma}^{-1}$. The inverse scheme for $\hat{\Gamma}$ as developed in Tan & Baras (2005) is discussed here. Let $\psi(t-1)$ be the memory curve of $\hat{\Gamma}$ and Γ at time $(t-1)$ and $\hat{\delta}_{sat}(t)$ be the saturation with respect to the current values of the density function. The input $u(t)$ is generated through the following inversion algorithm.

Algorithm (Tan & Baras, 2005):

1. If $\delta_d(t) < -\hat{\delta}_{sat}(t)$, $u(t) = u_{min}$;
2. If $\delta_d(t) > \hat{\delta}_{sat}(t)$, $u(t) = u_{max}$;
3. Otherwise $u(t) = \hat{\Gamma}^{-1}[\delta_{ref}(t), \psi(t-1)]$, where $\hat{\Gamma}^{-1}$ is the (right) inverse of $\hat{\Gamma}$ as constructed as in Tan & Baras (2004).

Let $\hat{y}(t)$ be the predicted output of $\hat{\Gamma}$. When $\delta_d(t) > \hat{\delta}_{sat}(t)$, there exists no $u(t)$ such that $\hat{\Gamma}[u(t), \psi(t-1)] = \delta_d(t)$. Step-1 (step-2 respectively) makes sure that $\hat{\delta}(t)$ equals $-\hat{\delta}_{sat}(t)$ ($\hat{\delta}_{sat}(t)$, respectively) and hence is nearest to $\delta_d(t)$. On the other hand, when $\delta_d(t) \leq \hat{\delta}_{sat}(t)$, $\delta_d(t)$ can be inverted exactly (Tan & Baras, 2004) and, hence $\hat{\delta}(t) = \delta_d(t)$.

5.4.3 Control without using Explicit Model: Linear Control

PID methods and PWM schemes

The simplest of control methods that could be implemented for a SMA control is the proportional controller which does not need an explicit model of the SMA actuator. But generally proportional controllers are not suitable for precision tracking application due to the hysteretic behaviour. So mostly the modified forms such as *PI*, *PD* and *PID* are used for SMA control. Further more PD controller can also be used to generate command signal while using with PWM control method. In the proceeding paragraphs modified PID methods and PWM methods are introduced.

Control using *PID* and *PID*–*P*³ ([Shameli et al., 2005](#)): The *PID* controller is the most common controller used in industrial problems. Since the controller structure is simpler suitable controller gains can be found for most control problems using linear model information. SMA actuators are highly nonlinear systems hence, the nonlinear model cannot be used to compute the controller gains. For calculating optimum gain values, the Ziegler-Nichols stability limit tuning method could be employed. Although many applications for SMA controller have used *PID* controller by tuning their gain through some adhoc methods. The output of a continuous time *PID* controller can be given by

$$u(t) = K_P \cdot e(t) + K_I \cdot \int_0^t e(\tau) d\tau + K_D \cdot \dot{e}(t), \quad \tau \leq t. \quad (5.43)$$

where $u(t)$ is the controller output and $e(t)$ is the tracking error. K_P, K_I, K_D are proportional, integral and differential gains respectively.

[Shameli et al. \(2005\)](#) proposed a modified *PID* controller for SMA actuator known as *PID*–*P*³ controller which can be given as

$$u(t) = K_P \cdot e(t) + K_I \cdot \int_0^t e(\tau) d\tau + K_D \cdot \dot{e}(t) + K_T \cdot [e(t)]^3, \quad \tau \leq t. \quad (5.44)$$

The main difference between this proposed controller and the classical *PID* controller is the cubic term of position error with proportional gain K_T . This term helps in reducing the settling time and overshoot of the SMA actuator. For smaller error values the cubic term tends to zero and *PID*–*P*³ works as a regular *PID* controller.

PWM based SMA control ([Ma & Song, 2003](#)): PWM control methods are popular with controlling SMA actuators. A few advantages that could be accredited to PWM methods are: being robust to disturbances, effective in Energy saving, and easily implemented using microprocessors. A PW modulated design for SMA actuators based on experimental setup of a single wire was studied in [Ma & Song \(2003\)](#). A PW modulator was designed to modulate proportional derivative (PD) controller for

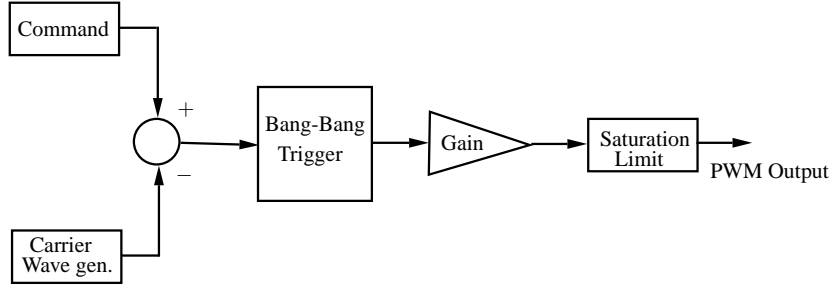


Figure 5.15: Implementation of PWM (Ma & Song, 2003).

position control of SMA actuator. The PW modulator used in Ma & Song (2003) is shown in Figure 5.15. It consists of a carrier wave generator, a bang-bang trigger, a gain and a saturation. The carrier wave generator generates a triangular carrier wave with a constant frequency and amplitude greater than the command signal. If the difference between the carrier wave and command signal is positive and greater threshold of the bang-bang trigger then the output is d which is the on-state, or else it is $d - h$ which is the off-state. The output of the trigger is a pulse sequence and has the frequency of the carrier wave and an amplitude depending on the amplitude of the command signal. In the feedback control implementation the source to the command signal is the output of the PD controller. The output of the PWM is used to control the SMA wire by controlling a programmable power-supply.

5.5 Summary of modelling and control methods and their interaction

In this section the most common modelling and control methods of SMA actuators are discussed. The schematic in Figure 5.16 is helpful in understanding the classification and their interactions. As previously discussed here the modelling methods are classified into physical, phenomenological and Linear or No model types. The control methods are classified into Nonlinear, Inverse Hysteresis control and Linear or Model Free control. Next we will discuss and briefly comment on the different modelling and control methods.

Summary and comments on physics based modelling and control: Two physical models were used for SMA actuators control purpose. The model developed in Leclercq & Lcellent (1996) and used in Benzaoui *et al.* (1999) and the model initially proposed by Liang & Rogers (1992) and latter developed and used by Elahinia & Ashrafiou (2002). Both models required the identification of a large set of material parameters. 19 parameters for Leclecq and Lcellent model and 17 for Elahinia and Ashrafiou model. These parameters have to be identified from specialized thermo-mechanical tests. Elahinia & Ashrafiou (2002) pointed out that the borrowed model parameters had not quantitatively predicted the experimental results. In addition, it is well known that the SMA behaviour is strongly affected by thermomechanical cycling.

Chapter 5. Introduction

After a certain amount of actuation cycles, several material parameters have no longer kept their initial value and the efficiency of the control strategy decreases.

Coming to the nonlinear controller aspect Feedback linearization has been successfully used in Moallem & Jun (2005) and Benzaoui *et al.* (1999). The problem with feedback linearization is that it depends on accurate cancellation of the nonlinear components of the SMA response which depends on the accuracy of the model information and parameters. These problems in feedback linearization method can be overcome by variable structure control which is fairly robust to parameter uncertainties of the model (Grant & Hayward, 1997; Elahinia & Ashrafiou, 2002). The problem with variable structure control is that tracking is possible as long as the tracking error is small (Jayendran *et al.*, 2008). The switching behaviour of the VSC may also introduce steady state oscillations and excite high frequency components in the system which are not desirable. In Williams *et al.* (2010) physical modelling was used along with Sliding Mode Control to position a mirror actuator about two axes. In Romano & Tannuri (2009) the physical model similar to Elahinia & Ashrafiou (2002) and a Sliding Mode control was used to control a SMA rotary actuator with a thermoelectric tablet (Peltier element) for enhanced cooling. It was observed that the performance (settling time 0.92 sec and 0.22 sec respectively for step-down and step-up with cooling) of the SMA actuator was poor during cooling or step-down reference even in the presence of Peltier element, which points out the importance of the cooling systems.

In Kloucka *et al.* (2003) an analytic solution for ON/OFF temperature control of a SMA modelled by thermodynamic constitutive relation (Helmholtz free energy) of Lagoudas *et al.* (1996) was discussed. In Piccirillo *et al.* (1996) simulation studies were also performed using thermodynamic constitutive relation (Helmholtz free energy) and a linear optimal control for displacement was used on a chaotic oscillator with SMA. Asymptotic stability of the closed loop nonlinear system was also guaranteed by Lyapunov methods.

Summary and comments on phenomenological models and control: As discussed in detailed in the previous sections the phenomenological models are formulated by weighted aggregate of all possible elementary hysteresis operators. To sum-up the Preisach and KP models are parameterized by pair of threshold variables where as PI model is a superposition of elementary stop (play) operator which are parameterized by a single threshold variable.

Since the Preisach model is not analytically invertible, numerical methods are used to obtain approximate inversions of the model. Majima *et al.* (2001) applied inverse static Preisach model as a feedforward compensator with PID controller to reduce the hysteresis effects. In Nguyen & Ahn (2009) fuzzy based inverse Preisach model was used in the feedforward along with PID to control the SMA actuator. In Ahn & Kha (2007) an internal model control (IMC) setup was used with fuzzy based inverse Preisach model in the feedforward. The controller loop was stabilized by augmenting the con-

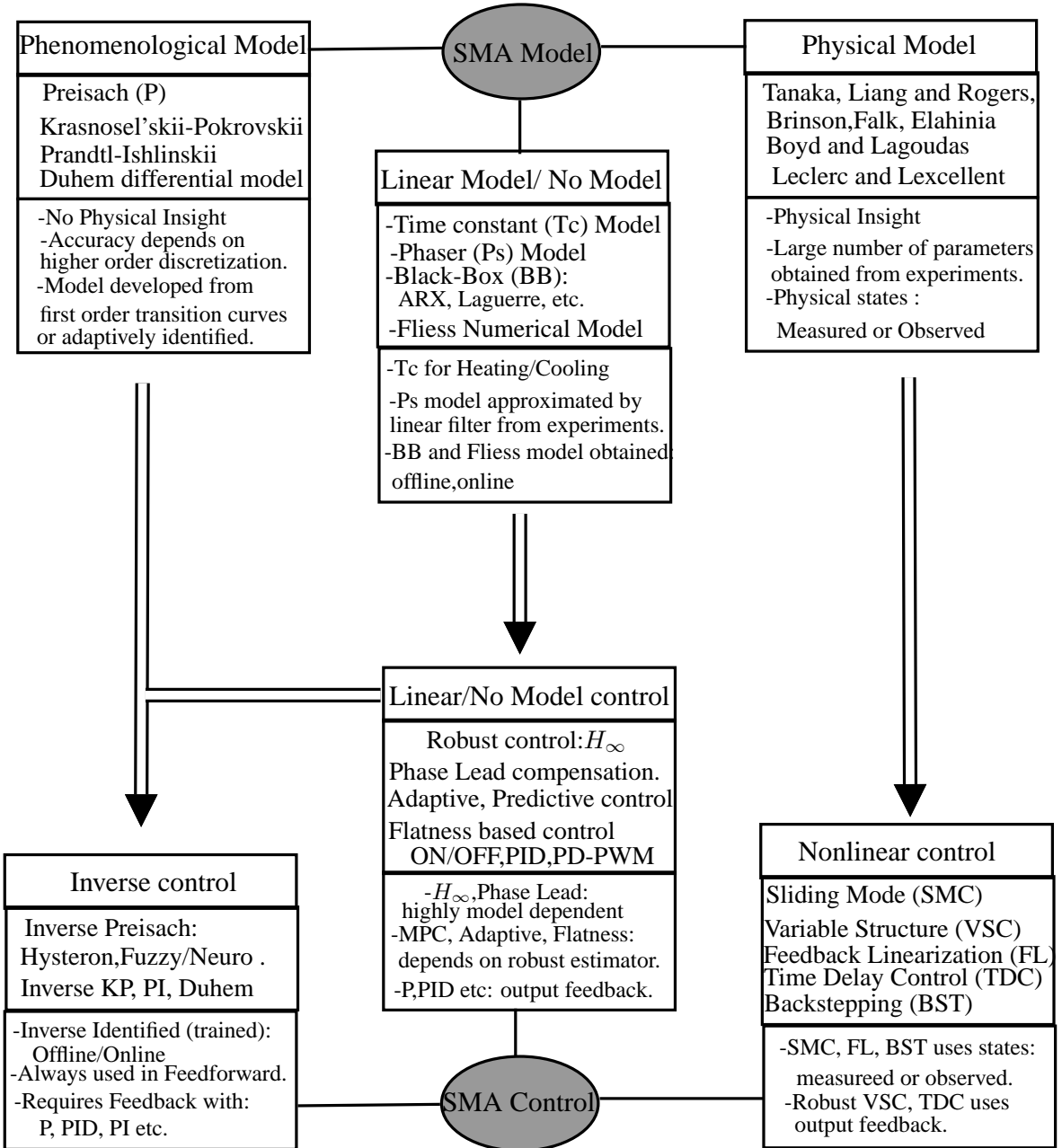


Figure 5.16: Summary of methods.

troller block with a low-pass filter which will help to improve the robustness in case of a plant-model mismatch. In [Asua et al. \(2008\)](#) Proportional-Integral (PI) controller with antiwindup along with hysteresis compensation was tested on linear displacement SMA actuator. Two hysteresis compensation methods were compared, one using linear phase lag model (offline identification from experiments) and another inverse hysteresis model based on Neural-Networks (NN) (trained offline from experimental data). Since NN can provide excellent approximation of input-output nonlinear behaviour the control performance was better in NN inverse compensation as compared to phase compensation.

Chapter 5. Introduction

A neuro-fuzzy feedforward model along with a Proportional-Derivative (PD) feedback was used in [Kumagai *et al.* \(2006\)](#) to control a SMA actuator. Here the MATLAB fuzzy toolbox with ANFIS(Adaptive Neuro Fuzzy Inference System) was used to develop a hysteresis model of the relation between the temperature and displacement. This model was obtained from offline experimental data and formed the feedforwrd element used to calculate the desired feedforwrd input voltage required for tracking a desired displacement.

In [Liu & Yen \(2010\)](#) a tracking control of SMA actuator was discussed based on self-sensing Feedback and PID control with Inverse hysteresis compensation. Here a the inverse hysteresis model was based on Duhem differential model. The self-sensing feedback used here was based on a polynomial model of the nonlinear relation between voltage across the SMA and the displacement. This model was used to retrieve the approximate strain in the actuator which in turn was used for tracking control.

It has been observed that the compensation based merely on numerical inversion of the hysteresis models may yield errors, since a numerical inverse can be considered only as an approximation. Further more a numerical inverse of a hysteresis model cannot be considered unique, and would be considered applicable only in the vicinity of the inputs and limits considered in the numerical algorithm. Hence control using inverse Preisach model often require a secondary control loop.

Unlike the Preisach and KP models the PI is analytically invertible and can be conveniently implemented as a feedforward compensator for annulling the hysteresis nonlinearity. But the classical inverse PI model, derived analytically or numerically cannot compensate for saturated asymmetric hysteresis properties that have been widely observed in magnetostrictive and SMA actuators.

In [Janaideh *et al.* \(2010\)](#) a generalized PI model was modified to ensure continuity and hence invertibility was rendered and verified experimentally for smart actuators including SMA.

The references discussed previously in this section pertain to offline Preisach models which require extensive experimental data to formulate a phenomenological model. For example the Preisach densities in a fixed Preisach model are identified from a large set of First Order transitional curve data. Under such conditions Preisach models cannot guarantee robust performance and stability under different operating conditions. Although inverse Preisach control using robust adaptive Preisach model could be helpful to cope-up with different environmental and operating condition, it has been observed that the quality of the identified model improves by choosing a higher order of discretization of the Preisach plane. For example in [Tan & Baras \(2005\)](#) a discretization order of 10 was used to identify an inverse model for control of magnetostrictive actuator.

Summary and comments on control based on Linear model (or)No-Model (Model free): This method was first introduced in Suleman & Crawford (2008) to control a biomimetic tuna. An array of SMA actuators has been embedded in this structure to induce propulsion. This system was too complex to implement a physical or phenomenological model. Here more effort was made to design the actual array of SMA wire actuators to develop the motion of tail fin of the Tuna fish. No model of the integrated structure was considered or developed rather a constant value of current necessary to drive a set of SMA wires was identified experimentally and then used for developing the movement of the tail made of integrated SMA wire structure. The aforementioned control methods could also be classified under ON/OFF control method. The simple and straightforward ON/OFF control method was also used in Khidir *et al.* (2007); Kim *et al.* (2006); Coaud *et al.* (2006); Peng *et al.* (2008) for control of beam actuation, earthworm-like microrobot, artificial muscle, inflatable SAR antenna respectively. An ON/OFF control was also used in Leary *et al.* (2010) with lagging for enhanced heat transfer and improve the time response.

Other simpler methods of SMA control are different variants of PID control. For example in Da Silva (2007) a proportional controller with feedback error was used to control a beam shape by means of shape memory actuator. In Shamel *et al.* (2005) simulation studies were performed using a modified PID controller known as PID-P³. This controller used an additional cube of the term added to the basic PID controller. This method has been discussed in detail in section 5.4.3.

Another interesting method that can be classified under this category is the basic PI control using the actuating SMA itself as a position sensor. In Furst & Seelecke (2011) a custom made FPGA power controller (Hangekar *et al.*, 2010) was used to measure resistance and regulate the power in a SMA spring to control the deflection of a nozzle. Here a resistance to deflection mapping scheme was developed based on the assumption that the resistance relates approximately linearly and non-hysteretically to the SMA wire strain. A linear curve fit was generated to approximate the relation from resistance to displacement at constant stress. This model was then used to extract the strain displacement value from merely resistance measurement which was then used in feedback controller (PI) to track the reference for displacement.

A fixed gain PID control does not always perform satisfactorily as SMA has highly nonlinear behaviour with strong hysteresis effect. The PID gains are most often calculated by trial and error from experimental tests. The tuned PID gains are fixed and pertain to a given specific experimental condition. Changes in the experimental conditions would adversely affect the performance of the controller (Jayendran *et al.*, 2008). To compensate this problem in Lan & Fan (2010); Ahn & Kha (2008) a fuzzy tuned PID controller was used for SMA control.

Certain authors have considered the hysteresis problem in SMA as phase lag between the periodic input voltage and the output strain for example in Asua *et al.* (2008) a phase shift compensator was used to compensate the hysteresis along with PI control

with antiwindup. In [Choi \(2001\)](#) the SMA actuator based flexible gripper was modelled as transfer function using two different time scales for heating and cooling. Then the force generated by flexible gripper was controlled using H_∞ controller.

In [Gédouin et al. \(2011\)](#) a model free control was introduced for SMA spring actuator. Here a classical PI control and a Flatness-Based controller was implemented. The Flatness based control uses a “Numerical- model” based on derivative estimation. The results demonstrated that the Flatness based controller was better than PI controller even in the presence of thermal disturbance. Further nonlinear Flatness based control and nonlinear PI control were introduced and it was concluded that the Flatness-Based control or Model Free Control (MFC) outperforms the nonlinear Proportional-Integral (PI) control. This Flatness-Based controller is particularly interesting as it is model-free and can be easily confused with Black-Box model. The Numerical-Model or the Derivative estimation model is quite robust for different kinds of systems but is numerically very taxing. For example at the heart of this Numerical-Model is the loop calculating the Integral with T sec as the interval of integration. The calculation is particularly challenging in the case of online computation in the closed loop control. The choice of T is also tricky as it should be chosen small to calculate the derivative estimate within short delay and should be chosen large to have a good quality of the estimate. Practically the integral is often calculated using a Trapezoidal integration method with number of summation steps $M = T/T_s$, where T_s is the sampling rate. In [Zehetner et al. \(2007\)](#) it has been observed that for higher sampling rate (T_s) the integration interval (T) has to be chosen small but reducing the integration interval reduces the quality of the estimate. On the contrary the choice of sampling rate directly affects our ability to make observations of the true system. It should also be noted that the value of T and T_s depends on the noise level in the signal measurements. For a highly noisy measurement the sampling rate has to be faster.

5.6 Contribution of this Thesis

Although the survey discussed in the current chapter is not exhaustive it is representative of the broad classification of model such as physical models and phenomenological models with further extending their usage in control methods which can directly use these models. Controller which do not use any explicitly identified model based on physics or hysteresis phenomenon was also discussed. The contribution and the research performed in this thesis can be coarsely classified as: (i) Modelling for control (ii) Adaptive control of SMA actuator. The work done in these two categories is discussed briefly.

Modelling for control

Compared to the above discussed approaches the strategy of modelling and control used in this thesis is based on black-box approach or Input-Output (I/O) approach using Laguerre functions. As compared to modelling using Preisach operator which is also called as I/O technique but considering the phenomenon of hysteresis behaviour, in the current approach the hysteretic system is studied using an I/O signal model and can be implemented using an I/O filter of a fixed order. A Laguerre filter structure was

used due to its intrinsic stability, convergence properties and ease of implementation in the context of model based control. As compared to the Numerical- Model the Identification of Laguerre model using Recursive Least Square (RLS) Identification algorithm is easier to be implemented and computationally not very cumbersome due to availability of various numerically robust recursive implementation methods. Here the Laguerre model and identification procedure is fairly independent of the choice of sampling rate and noise level in the measurements.

Adaptive control of SMA

The proposed strategy of modelling was first implemented using a model based control such as classical Laguerre Predictive control. The classical Laguerre predictive control was tested on a single wire SMA actuator using a linear 2nd, 5th order and 2nd order Volterra model. Performance of the classical Laguerre predictive control was analysed and modifications on the control strategies were sought. Improvements to the classical Laguerre predictive control was made by using a more robust and stable recursive least square (RLS) estimation method such as directional forgetting RLS (DF-RLS). A modified Laguerre predictive control was proposed for control of SMA actuator. The performance in the sense of minimal tracking error was analysed using linear 2nd and 5th order model. A 2nd order volterra model was also implemented successfully.

The proposed Modified Laguerre predictive control was also implemented on an Antagonistic SMA actuator. The stability properties of the Modified Laguerre Predictive control was studied and analysed in the context of Model Reference Adaptive control.

To sum-up in comparison to the literature review performed in this chapter the contribution of this thesis pertains to the exploitation of robust Black-Box modelling methods and model based control (predictive control) in the context of hysteretic system such as SMA actuator.

5.7 Outline of the Thesis

The outline of the thesis in general can be divided as: literature study of modelling and control, system identification and control.

Chapter-2 briefly studies the black-box modelling method in the context of Laguerre functions. The Recursive Least Square (RLS) algorithm is presented briefly. The recursive identification of single wire SMA actuator is performed using 2nd and 5th order model and the influence of various tuning parameters is analysed. A 2nd order Volterra Laguerre model is also analysed. Similarly a 2nd order Laguerre model is also used to identify recursively the antagonistic SMA actuator.

In Chapter-3 first the classical Laguerre predictive control method is used to control the single wire SMA actuator using the linear 2nd and 5th order model. Problems with classical RLS in closed loop control have been identified and improvements in control performance have been made using a DF-RLS . Next a modified Laguerre predictive control was proposed and tested on the SMA single wire actuator. The controller is

Chapter 5. Introduction

also tested similarly using the two types of models discussed earlier. The performance of the modified method is compared with the classical method. The modified method is also used to control the antagonistic SMA actuator. The stability of the proposed method is also discussed briefly.

In Chapter-4 conclusions have been made for the identification and control methods used in this thesis to solve the problem of SMA control and future perspectives of the problem has been mentioned.

Chapter 6

Modelling

6.1 Introduction

As it was mentioned in the previous chapter, one of the hindrance to the development of an actuator using SMA is their non-linearities. A great deal of researchers try to address this problem using sophisticated models which can describe the inner mechanism of the phase transition.

Those models are generally intended to the understanding and the design. They are often too complex to be useful for the control design, although some examples have shown that they could be used ([Benzaoui et al., 1999](#)). However, the remaining problem is the identification of the parameters which more than often enter non-linearly in the model.

Moreover, it is a known fact that the parameters will depend on the processing of the material and will evolve during the lifetime of the actuator. From a practical point of view, this implies that model parameters would have to be identified for each SMA batch. This, however assumes that the control is robust enough to handle the discrepancies in the parameters during the ageing of material.

Therefore, in this chapter, a new paradigm for modelling is studied. For the control, it is sufficient to have a correct estimate of the future output, given an input and a state value. This means that only the dynamic of the system is to be known, which in the case of linear systems, reduces the problem to the knowledge of recurrence or ordinary differential equations. In this modelling strategy, no real understanding of the physics of the system is necessary, it is only required to have a fair idea of the time response of outputs under given inputs: this is the so-called black-box modelling. On the other hand, the problem of correctly modelling the physics of the system is shifted to the problem of postulating the input-output structure that embraces the dynamic of the system ([Ljung, 1999](#)).

In the case of SMA, due to the hysteresis, the hypothesis of linearity and invariance do not hold, and the Black-Box approach may be questionable. The use of a linear model

should be understood as an approximation of the linearized system in the neighbourhood of the current state. It is thus necessary:

1. to use an on-line identification scheme;
2. to use an adaptation that constantly updates the model as the system evolves;
3. to assess that the adaptation is stable.

These last two requirements require opposite properties, namely the updating should be fast to capture the changes of the system on one hand, but should not diverge under the effect of the measurement noise.

In this chapter, the main models of linear time invariant (LTI) process are recalled. The goal of models is to predict the output and the predictors will thus be explained. Then the principles of systems identification will be explained. The Laguerre functions will then be introduced. The properties of this class of function will be used to approximate the system, and it will be shown that they can be useful in the context of identification. The Laguerre functions will then be applied to the problem of identifying hysteresis of two SMA actuators :

- a constant stress actuator
- an antagonist actuator

The various parameters available to the designer will be studied, in order to assess the possibility to apply linear model identification to a non-linear system such as the one at hand.

6.2 Models of linear time invariant processes

6.2.1 Discrete model in deterministic environment

To introduce the main concept of identification, the system is suppose to be deterministic, that is its dynamic is fully represented by a set of input output equations, and given an initial state and a sequence of inputs, the future state can be determined. In the case of linear time invariant process, such a single input, single output (SISO) system is described by a discrete model as follows:

$$y(t) = - \sum_{i=1}^{n_a} a_i q^{-i} y(t) + \sum_{i=1}^{n_b} b_i q^{-i} u_i(t-d) \quad (6.1)$$

where a_i and b_i are real constant coefficients, $y(t)$ is the process output, $u(t)$ is the input with d as delay, t is the normalized time. Here q is the shift operator:

$$q^{-1}y(t) = y(t-1) \quad (6.2)$$

The preceding expression can be rewritten:

$$y(t+1) = -A^*(q^{-1})y(t) + q^{-d}B^*(q^{-1})u(t) \quad (6.3)$$

with the polynomials defined as follows:

$$A(q^{-1}) = 1 + A^*(q^{-1}) = 1 + a_1 q^{-1} + \cdots + a_n q^{-n_a} \quad (6.4)$$

$$B(q^{-1}) = b_1 q^{-1} + \cdots + b_n q^{-n_b} = q^{-1} B^*(q^{-1}) \quad (6.5)$$

Note that $A(q^{-1})$ is monic. In the case of a LTI, equation (6.3) is used to define the input-output transfer function, given in terms of the shift operator q :

$$G(q) = \frac{q^{-d} B(q^{-1})}{A(q^{-1})} \quad (6.6)$$

The model is supposed to be irreducible, which means that there are no values cancelling $B(q^{-1})$ (the so called zeros) that cancels also $A(q^{-1})$ (poles)¹. However, during identification, this case may happen, implying that there are uncontrollable or unobservable states. If the common zeros and poles are in the unit circle, there exists a stabilizing feedback law, otherwise the system cannot be stabilized.

The equation (6.3) is useful to define a *predictor*. In the context of an on-line adaptation of the model, as it will be discussed later, the coefficients a_i ($i \in 1 \dots n_a$) and b_i ($i \in 1 \dots n_b$) are changing. If the output values $\{y(t - n_a) \dots y(t)\}$ are measured and stored, and the sequence of the input $\{u(t - n_b) \dots u(t)\}$, the one step ahead value can be calculated using the parameters available at instant t :

$$\hat{y}(t + 1|t) = -A^*(q^{-1})y(t) + q^{-d} B^*(q^{-1})u(t) \quad (6.7)$$

Using this equation, one can derive a j -step ahead predictor for the future values of the output, given the information available at t , by successively replacing the $y(t)$ by $y(t) = -A^*(q^{-1})y(t - 1) + q^{-d} B^*(q^{-1})u(t - 1)$ until the term $y(t - j + 1)$ is reached.

6.2.2 Modelling the disturbances

The deterministic model presented previously cannot account for the disturbances encountered in real situations. By nature, disturbances are random and they can be modelled in a stochastic framework. It has been shown that a large class of processes can be modelled by adding to the previous model the output $v(t)$ of system for which input is a zero mean white noise $e(t)$:

$$v(t) = \frac{C(q^{-1})}{D(q^{-1})} e(t) = H(q)e(t) \quad (6.8)$$

with the polynomials:

$$C(q^{-1}) = c_1 q^{-1} + \cdots + c_n q^{-n_c} \quad (6.9)$$

$$D(q^{-1}) = 1 + d_1 q^{-1} + \cdots + d_n q^{-n_d} \quad (6.10)$$

This very general form is the Box-Jenkins model. By choosing special forms for polynomials (A, B, C, D, F) in delay operator q^{-1} some well known models have been defined

1. the numerator and denominator are coprime

| Model Structure | $G(q, \theta)$ | $H(q, \theta)$ |
|-----------------|---|---|
| ARX | $\frac{B(q^{-1}, \theta)}{A(q^{-1}, \theta)}$ | $\frac{1}{A(q^{-1}, \theta)}$ |
| ARMAX | $\frac{B(q^{-1}, \theta)}{A(q^{-1}, \theta)}$ | $\frac{C(q^{-1}, \theta)}{A(q^{-1}, \theta)}$ |
| OE | $\frac{B(q^{-1}, \theta)}{F(q^{-1}, \theta)}$ | 1 |
| FIR | $B(q^{-1}, \theta)$ | 1 |
| BJ | $\frac{B(q^{-1}, \theta)}{F(q^{-1}, \theta)}$ | $\frac{C(q^{-1}, \theta)}{D(q^{-1}, \theta)}$ |

Table 6.1: Black-Box Model Structures

in Tab. 6.1. In most cases, it is enough to consider that $v(t)$ is directly added to the output of the system leading to the *output error model*:

$$y(t+1) = -A^*(q^{-1}) + q^{-d}B^*(q^{-1})u(t) + A(q^{-1})v(t+1) \quad (6.11)$$

In the presence of stochastic disturbances, the model of Eq. (6.7) cannot predict the future outcome of a given sequence of input since $v(t+1)$ is unknown. First, it is necessary to elaborate a different criterion. A natural approach is to consider the variance of the predictor with respect to the actual output, which can be calculated from the expression:

$$E\{[y(t+1) - \hat{y}(t+1)]^2\} = E\left\{\left[\frac{q^{-d}B^*(q^{-1})}{A^*(q^{-1})}u(t) + v(t+1) - \hat{y}(t+1)\right]^2\right\} \quad (6.12)$$

Once developed, the variance writes:

$$\begin{aligned} E\{[y(t+1) - \hat{y}(t+1)]^2\} &= E\left\{\left[\frac{q^{-d}B^*(q^{-1})}{A^*(q^{-1})}u(t) - \hat{y}(t+1)\right]^2\right\} + E\{[v(t+1)]^2\} \\ &\quad + 2E\left\{v(t+1) \left[\frac{q^{-d}B^*(q^{-1})}{A^*(q^{-1})}u(t) - \hat{y}(t+1)\right]\right\} \end{aligned} \quad (6.13)$$

Assuming that $u(t)$ and $v(t)$ are independent, the last term vanishes. If the variance of the noise $v(t)$ is bounded, then the variance will be minimized by the choice of the predictor:

$$\hat{y}(t+1) = -A^*(q^{-1})\hat{y}(t) + q^{-d}B^*(q^{-1})u(t) \quad (6.14)$$

which depends only on the past and current input and the past prediction (and is independent of the actual past output)

6.3 Identification

6.3.1 Least squares

The system modelled by the Eq. (6.3) can be reformulated in a regressor form:

$$y(t+1) = \varphi(t)^T \cdot \theta \quad (6.15)$$

where $\varphi(t)$ is the vector of measurements:

$$\varphi(t)^T = [y(t) \ \dots \ y(t - n_a) \ u(t) \ \dots \ u(t - n_b)] \quad (6.16)$$

and θ are the vector of parameters:

$$\theta^T = [a_1 \ \dots \ a_{n_a} \ b_0 \ \dots \ b_{n_b}] \quad (6.17)$$

Note that the system's model is linear in the parameters. Hence, using a set of N_m measurements, called observations, one can write the relations in matrix form:

$$\underbrace{\begin{bmatrix} y(1) \\ y(2) \\ \vdots \\ y(N_m) \end{bmatrix}}_Y = \underbrace{\begin{bmatrix} \varphi(1)^T \\ \varphi(2)^T \\ \vdots \\ \varphi(N_m)^T \end{bmatrix}}_\Phi \theta \quad (6.18)$$

The goal is to find the parameter vector $\hat{\theta}$ that minimize the error over the set of observations. Again the variance will be used to define an optimization index and the problem is formulated as follow:

$$\hat{\theta} = \operatorname{argmin} J(\theta) = \operatorname{argmin} \left\{ \sum_{t=1}^{N_m} (y(t) - \varphi(t)\theta)^2 \right\} \quad (6.19)$$

The identification index can be rewritten in matrix form, using Eq. (6.18):

$$J(\theta) = \{(Y - \Phi\theta)^T(Y - \Phi\theta)\} \quad (6.20)$$

The parameter vector optimizing $J(\theta)$ is such that:

$$\frac{\partial J(\theta)}{\partial(\theta)}|_{\theta=\hat{\theta}} = 0 \Leftrightarrow -2\Phi^T Y + 2\Phi^T \Phi \hat{\theta} = 0 \quad (6.21)$$

The matrix $\Phi^T \Phi$ plays a special role. Once developed, its particular structure is revealed:

$$\Phi^T \Phi = \begin{bmatrix} \varphi^T(t)\varphi(t) & \varphi^T(t-1)\varphi(t) & \dots & \varphi^T(t-N+1)\varphi(t) \\ \varphi^T(t-1)\varphi(t) & \varphi^T(t-1)\varphi(t-1) & \dots & \vdots \\ \vdots & \ddots & \ddots & \vdots \\ \varphi^T(t-N+1)\varphi(t) & \dots & \dots & \varphi^T(t-N+1)\varphi(t-N+1) \end{bmatrix} \quad (6.22)$$

It is a positive semi definite symmetric matrix with dimension $N \times N$ where N is the total number of parameters i.e $N = n_A + n_B - 1$.

Adopting the point of view of stochastic process, the cross correlation of two sequences obtained by sampling stable stationary ergodic processes $X(t) = \{x(i)\} \quad i \in \mathbb{N}^+$ and

Chapter 6. Modelling

$Y(t) = \{y(i)\} \quad i \in \mathbb{N}^+$ reads:

$$\rho_{XY}(\tau) = \lim_{M \rightarrow \infty} \frac{1}{M} \sum_{i=0}^M x(i)y(i + \tau) \quad (6.23)$$

Similarly, the autocorrelation is:

$$\rho_{XX}(\tau) = \lim_{M \rightarrow \infty} \frac{1}{M} \sum_{i=0}^M x(i)x(i + \tau) \quad (6.24)$$

$$\Phi^T \Phi = E\{\varphi(t), \varphi(t)\} = \begin{bmatrix} \rho_{\varphi\varphi}(0) & \rho_{\varphi\varphi}(1) & \dots & \rho_{\varphi\varphi}(N-1) \\ \rho_{\varphi\varphi}(1) & \rho_{\varphi\varphi}(0) & \dots & \vdots \\ \vdots & \ddots & \ddots & \vdots \\ \rho_{\varphi\varphi}(N-1) & \dots & \dots & \rho_{\varphi\varphi}(0) \end{bmatrix} \quad (6.25)$$

Therefore, under these assumptions, the matrix is also Toeplitz, and is usually called the correlation matrix.

If it is invertible, then the parameters vector is calculated by:

$$\hat{\theta} = (\Phi^T \Phi)^{-1} \Phi Y \quad (6.26)$$

This latest assumption reveals a key problem of the identification of dynamical system. Consider the more familiar problem of fitting of a line given a set of points, a common application of the least squares. It is clear that the set of samples collected from the experiment should be representative of the behaviour studied over the domain of the model. Thus, one should take care of the experimental conditions in order to satisfy this condition.

Back to the identification problem, Φ and Y is the set of regressors values and the successive outputs of the system excited by an input sequence $u(t)$. In this case, the design engineer, whose action is limited to the choice of the input, has only indirect control on the “sampling set”. The invertibility of $R = \Phi^T \Phi(t)$, which is a necessary condition, thus depends on the excitation $u(t)$. It can be shown that the matrix R is full rank if the spectrum of the excitation signal $u(t)$ contains at least N frequencies. Moreover the conditioning of R is better if it spans a frequency range consistent with the bandwidth of the system.

This condition is known as the persistency of excitation in the field of identification ([Ljung, 1999](#)), and it requires some knowledge of the system dynamic in order to:

- estimate the order of the system
- have a fair idea of its bandwidth

The order of persistency of a signal is the number of frequencies of its spectrum. Ideally a white noise should be used since its persistency is of infinite order. In practice, pseudo-random binary sequences are used, their length (i.e. the number of bits) being equal to the persistency order.

6.3.2 Recursive least squares

In order to derive the recursive version of the least squares, the Eq. (6.26) is rewritten as:

$$(\Phi(t)^T \Phi(t)) \hat{\theta}(t) = \Phi(t) Y(t) \quad (6.27)$$

where the argument t is here to recall that the least solution will be re-evaluated at each sampling point, in contrast with the previous section, where the identification was done supposing that all the measurements were available. Let:

$$R(t) = \Phi(t)^T \Phi(t) \quad (6.28)$$

and:

$$p(t) = \Phi(t) Y(t) \quad (6.29)$$

which can be rewritten in a recursive form:

$$R(t) = \sum_{i=0}^{t-1} \varphi(i)^T \varphi(i) + \varphi(t)^T \varphi(t) = R(t-1) + \varphi(t)^T \varphi(t) \quad (6.30)$$

$$p(t) = \sum_{i=0}^{t-1} \varphi(i) Y(i) + \varphi(t) Y(t) = p(t-1) + \varphi(t) Y(t) \quad (6.31)$$

To apply the least squares, a recursive expression for the *inverse* of the matrix is needed. For this purpose, the Woodbury identity is used. Let A and B be two definite positive matrix of dimensions $m \times m$, verifying the relation:

$$A = B^{-1} + C D^{-1} C^T \quad (6.32)$$

where D is an invertible matrix with the same dimension, and C a matrix of dimensions $m \times n$, then A^{-1} is given by:

$$A^{-1} = B - B C (D + C B C^T)^{-1} C^T B \quad (6.33)$$

With the following correspondence:

$$\begin{aligned} A &= R(t) \\ B^{-1} &= R(t-1) \\ C &= \varphi^T(t) \\ D &= 1 \end{aligned} \quad (6.34)$$

one can recognize that Eq. (6.30) is similar to Eq. (6.32), and thus the following recursion holds:

$$R^{-1}(t) = R^{-1}(t-1) - \frac{R^{-1}(t-1) \varphi(t) \varphi(t)^T R^{-1}(t-1)}{1 + \varphi(t)^T R^{-1}(t-1) \varphi(t)} \quad (6.35)$$

Introducing the gain vector:

$$k(t) = \frac{R^{-1}(t-1)\varphi(t)}{1 + \varphi(t)^T R^{-1}(t-1)\varphi(t)} \quad (6.36)$$

the equation writes:

$$R^{-1}(t) = R^{-1}(t-1) - k(t)\varphi(t)^T R^{-1}(t-1) \quad (6.37)$$

The optimal parameter vector is calculated by:

$$\hat{\theta}(t) = R^{-1}(t)p(t-1) + R^{-1}(t)\varphi(t)Y(t) \quad (6.38)$$

with the help of Eq. (6.37):

$$\begin{aligned} \hat{\theta}(t) &= R^{-1}(t-1)p(t-1) - k(t)\varphi(t)^T R^{-1}(t-1)p(t-1) + R^{-1}(t)\varphi(t)Y(t) \\ \Leftrightarrow \hat{\theta}(t) &= \hat{\theta}(t-1) - k(t)\varphi(t)\hat{\theta}(t-1) + k(t)Y(t) \end{aligned} \quad (6.39)$$

which leads finally to the recursive expression for the updating of the parameters of the filter:

$$\hat{\theta}(t) = \hat{\theta}(t-1) + k(t) \underbrace{\left[Y(t) - \varphi^T(t)\hat{\theta}(t-1) \right]}_{\varepsilon(t)} \quad (6.40)$$

where $\varepsilon(t)$ is the a priori error, that is the difference between the actual output and the predicted output using the previous optimal coefficient for the filter $\hat{\theta}(t-1)$.

The algorithm is summed up below:

| Initialisation |
|--|
| $R(0) = \delta^{-1}I_{N \times N}$ with $\delta \in \mathbb{R}^+ \setminus \{0\}$ |
| $\hat{\theta}(0) = 0$ |
| for $t \in 1..N$ calculate: |
| $k(t) = \frac{R^{-1}(t-1)\varphi(t)^T}{1 + \varphi(t)^T R^{-1}(t-1)\varphi(t)}$ $\varepsilon(t) = Y(t) - \varphi^T(t)\hat{\theta}(t-1)$ $\hat{\theta}(t) = \hat{\theta}(t-1) + k(t)\varepsilon(t)$ $R^{-1}(t) = R^{-1}(t-1) - k(t)\varphi(t)^T R^{-1}(t-1)$ |

Table 6.2: Recursive least square algorithm

6.3.3 Adaptive recursive least squares

The recursive least squares algorithm is storing the regressors values into the matrix $R(t)$ (see Eq. (6.30)). As a matter of fact, using the shift operator, the relation between

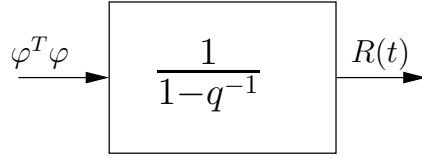


Figure 6.1: Block diagram representing the relationship (6.30). The correlation is the result of integrating the autocorrelation of the regression vector.

this matrix and the regressor is:

$$R(t) = \frac{1}{1 - q^{-1}} \varphi^T \varphi \quad (6.41)$$

This leads to the following remarks:

- in the light of the diagram of Fig. 6.1 the persistency of excitation roughly means that the mean value of $\varphi^T \varphi$ is not nil ;
- thus $R(t)$ being an integrator fed by a signal with non zero mean values will tend to infinity

As a corollary, $\lim_{t \rightarrow \infty} k(t) = 0$ since $\lim_{t \rightarrow \infty} R^{-1}(t) = 0$. The updating rules defined by Eq. (6.40) depending on $k(t)$, indicates that as time advances the algorithm ceases to take into account the information given by the incoming measurement. In other words, the algorithm finds the best fit according to the first measurements, and is unable to adapt the estimate of the optimal of the parameters in the case of a varying filter.

In order to avoid this behaviour, the idea is to replace the integrator of Fig. 6.1 by a first order filter as represented in Fig. 6.2. With this modification, the recursion relation

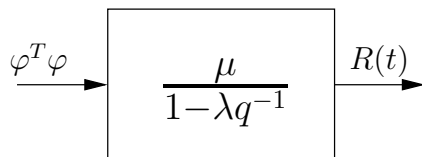


Figure 6.2: Block diagram of the adaptive recursive least squares algorithm. Correlation is calculated by filtering the autocorrelation of the regression vector through a first order.

for the correlation matrix becomes:

$$R(t) = \mu R(t-1) + \lambda \varphi^T \varphi \quad (6.42)$$

where μ and λ are two coefficients verifying the conditions $0 < \lambda \leq 1$, $0 < \mu \leq 1$.

The coefficient λ acts as a forgetting factor which applies an exponential sliding over the set of data. At the same time, the use of the first order filter prevents the asymptotic vanishing of the adaptation gain $k(t)$. Hence the recursive least squares will adapt to parameters changing slowly with respect to the effective window imposed by λ .

The so-called Exponentially forgetting recursive least squares differs from the previous algorithm only slightly (see Tab. 6.3)

| Initialisation |
|--|
| $R(0) = \delta^{-1} I_{N \times N}$ with $\delta \in \mathbb{R}^+ \setminus \{0\}$ |
| $\hat{\theta}(0) = 0$ |
| $0 < \lambda \leq 1$ and $0 < \mu \leq 1$ |
| for $t \in 1..N$ calculate: |
| $k(t) = \frac{R^{-1}(t-1)\varphi(t)^T}{\frac{\lambda}{\mu} + \varphi(t)R^{-1}(t-1)\varphi(t)^T}$ |
| $\varepsilon(t) = Y(t) - \varphi^T(t)\hat{\theta}(t-1)$ |
| $\hat{\theta}(t) = \hat{\theta}(t-1) + k(t)\varepsilon(t)$ |
| $R^{-1}(t) = \frac{1}{\lambda} (R^{-1}(t-1) - k(t)\varphi(t)^T R^{-1}(t-1))$ |

Table 6.3: Recursive least square algorithm

The choice of the parameters λ and μ must be chosen according to the system at hands. The correct combination is a matter of trade-off. For instance, a low value for λ results in a better adaptation of the parameter, on the other hand, too low a value will cause the identification to be too sensitive to measurement noise. An overview of the main combination is summed up in Tab. 6.4, according to [Landau et al. \(1998\)](#).

6.4 Laguerre function basis

6.4.1 Motivation

In the preceding section, the identification is based on models defined by recurrence equations such as Eq. (6.11). The identification task is thus to evaluate the parameters set $\hat{\theta}$ that will minimize the “mean distance” between the model and the process on a given frequency interval. This means that $N = n_A + n_B - 1$ coefficient have to be calculated in the simplest case of an output error model, while up to $N = n_A + n_B + n_C + n_D + 1$ if a Box-Jenkins model is used. In other word, the price to pay when using a general model is that large number of parameters have to be identified, which requires a large storage and computational capability for a practical implementation.

| Name | Algorithm parameters | Purpose of the algorithm |
|----------------------------|---|------------------------------|
| Decreasing Gain | $\lambda = \mu = 1$ | time invariant systems |
| fixed forgetting factor | $0 < \lambda < 1, \mu = 1$ | slowly time varying systems |
| Variable forgetting factor | $\lambda(t) = \lambda_0 \lambda(t-1) + 1 - \lambda_0, \mu = 1$ | Initial conditions treatment |
| Constant adaptation gain | $\lambda(t) = \mu(t)$ such that $\text{tr}(R(t-1)) = \text{tr}(R(t))$ | Time varying systems |
| Constant gain | $\lambda = 0, \mu = 1$ | Slow convergence |

Table 6.4: Usual choices of parameters values for adaptive RLS ([Landau et al., 1998](#))

With the latest progress of Digital Signal Processors (DSP) that made available cheap and computing effective devices, such problem may seem less pregnant than a decade ago. One might think that choosing large polynomials can handle the problem of modelling an unknown process by using brute force. However, this naive approach would fail in most cases for several reasons:

- if the process has a long memory, typically infinite impulse response, the taps in the finite impulse response filter needed are very large ;
- with large $R(t)$ matrices the rounding off errors can cause the loss of symmetry of the problem which annihilate the convergence properties of the RLS ;
- a large number of parameters will induce fluctuation of the parameter estimates in steady state operation.
- to satisfy the persistence of excitation condition, the input signal should be complex which is usually impossible in production situation ;
- with a large number of parameters, the fluctuation of the estimates add a numerical noise to the measurement noise which finally increases the misadjustment of the filter.

The choice of the order of the model is basically a trade-off between accuracy and learning speed. Therefore, the designer should define the smallest structure which meet the accuracy requirements and can be tackled using simple optimization algorithm. This problem of choosing the smallest model set that en-globe the system is difficult, and the designer should use as much a priori knowledge as possible.

To circumvent the problems of the FIR filters, it is possible to use IIR filters. Caution have to be taken though because such filters may become unstable. The solution to this problem consists in using a linear combination of stable IIR filters as represented on Fig. 6.3. The output of such an arrangement reads:

$$y(t+1) = \sum_{i=0}^{N_f} c_i F_i(q^{-1}) u(t) \quad (6.43)$$

Therefore, the least square problem is formally the same as Eq. (6.27) with the following definitions:

$$\left\{ \begin{array}{lcl} \theta^T & = & [c_0 \ c_1 \ \dots \ c_N] \\ f_i(t) & = & F_i(q^{-1})u(t) \quad \text{for } i \in \{1 \dots N_f\} \\ \phi^T(t) & = & [f_0(t) \ f_1(t) \ \dots \ f_{N_f}(t)] \\ \Phi(t) & = & \begin{bmatrix} \phi^T(0) \\ \phi^T(1) \\ \vdots \\ \phi^T(t) \end{bmatrix} \end{array} \right. \quad (6.44)$$

With the transversal classical tap filter of Fig. 6.3, $R(t)$ is a Toeplitz matrix. This, however, is not generally the case when the output of the IIR filters are used, unless they form an orthonormal basis. Such a set of filters will now be discussed.

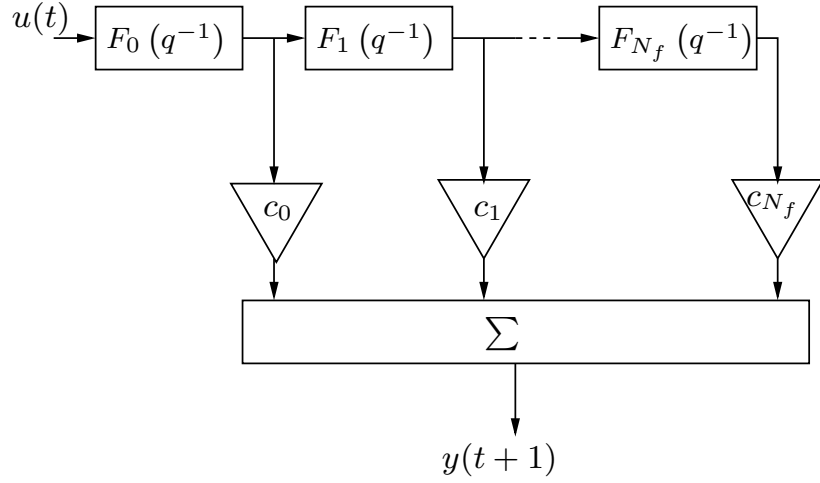


Figure 6.3: Transversal Tap filter

6.4.2 Discrete Laguerre orthonormal basis

Basically, the identification scheme described so far consists in approximating the impulse response $H(z)$ of a system measuring the output $y(t)$ produced by the input $u(t)$. To achieve this, the different models have been expressed using a set of polynomial in the z domain using the canonical basis $\{1, z^{-1}, z^{-2}, \dots\}$ of l^2 . Being very localized in time, it requires large sequences to approximate systems with long impulse response. Although it is theoretically possible to approximate such a system with an arbitrary precision, there are shortcomings already introduced in the previous section. To tackle the problem at its root, an alternative basis can be constructed. One fruitful approach consists in using orthogonal polynomials such as Laguerre, Legendre or Jacobi polynomials.

Discrete orthogonal polynomials on a domain $[A, B]$ are polynomials $q_m(k)$, $q_n(k)$ that they verify the relation:

$$\sum_{k=A}^{k=B} q_m(k) q_n(k) v(k) = \begin{cases} 0 & \text{if } m \neq n \\ h_m^2 & \text{if } m = n \end{cases} \quad (6.45)$$

where h_m^2 is a normalization constant. $v(k)$ is a weighting function. A special family of orthogonal polynomials are the Meixner polynomials which are defined on $[0, \infty]$ and are weighted by the function:

$$v(k) = \theta^k (b)_n \quad \text{with } 0 < \theta < 1 \quad b > 0$$

where $(b)_n$ is the Pochhammer symbol². The special case $b = 1$ corresponds to an exponentially decaying weighting function and defines the set of discrete Laguerre polynomials. These are of particular interest since they are the only ones that admit a z -transform (Belt, 1997):

2. $(b)_n = b(b+1)\dots(b+n-1)$

$$L_m(a, z) = \frac{\sqrt{1-a^2}z}{z-a} \left(\frac{1-az}{z-a} \right)^{m-1} \quad (6.46)$$

called the discrete-time (DT) Laguerre functions. They are orthonormal and form a complete set over $l^2(\mathbb{N}_0)$, the Hilbert space of square-summable causal functions. We will now proceed to some of the most prominent properties of the Laguerre functions for the modelling of LTI systems.

6.4.3 Some properties of the Laguerre function basis

Connexion with the canonical basis of l^2

Consider a sequence $g(t)$ of $l^2(\mathbb{N}_0)$, $g(t)$ is thus the impulse response of a stable process. We shall now suppose that it admits the following decomposition over the set of the DT Laguerre functions:

$$G(z) = \sum_{m=0}^{\infty} g_m L_m(a, z) \quad (6.47)$$

Using the transformation:

$$w^{-1} = \frac{1-az}{z-a} \Leftrightarrow z = \frac{1+w^{-1}a}{w^{-1}+a} \quad (6.48)$$

which maps the unit disk on itself, on $G(z)$, one gets:

$$\begin{aligned} G\left(\frac{1+w^{-1}a}{w^{-1}+a}\right) &= \left[\frac{\sqrt{1-a^2}(1+w^{-1}a)}{1-a^2} \right] \sum_{m=0}^{\infty} g_m w^{-m} \\ &\Rightarrow \frac{\sqrt{1-a^2}}{1+w^{-1}a} G\left(\frac{1+w^{-1}a}{w^{-1}+a}\right) = \sum_{m=1}^{\infty} g_m w^{-m} \end{aligned} \quad (6.49)$$

where one can recognize the expression of $G(w^{-1})$ on the canonical basis $1, w^{-1}, w^{-2}, \dots$. This demonstrate that there exist a decomposition on the Laguerre basis for any function that admits a z -transform. Note that the preceding result gives some insight on how the Laguerre filters resolve the problem of the time selectivity of the canonical basis: The transformation (6.48) has the effect of boosting the higher frequencies and enlarging the bandwidth of the low pass filter as depicted on Fig. 6.4.

Identification

The coefficients of the expansion $G_l(z^{-1}) = \sum_{k=0}^{\infty} g_k L_k(a, z^{-1})$ of the impulse response of a causal, stable process, is theoretically calculated from the projection of its impulse response $g(t)$ on one of the Laguerre impulse response $l_k(a, t)$:

$$c_k = \langle g(t), l_k(a, t) \rangle = \sum_{j=0}^{\infty} g(j) l_k(a, j) \quad (6.50)$$

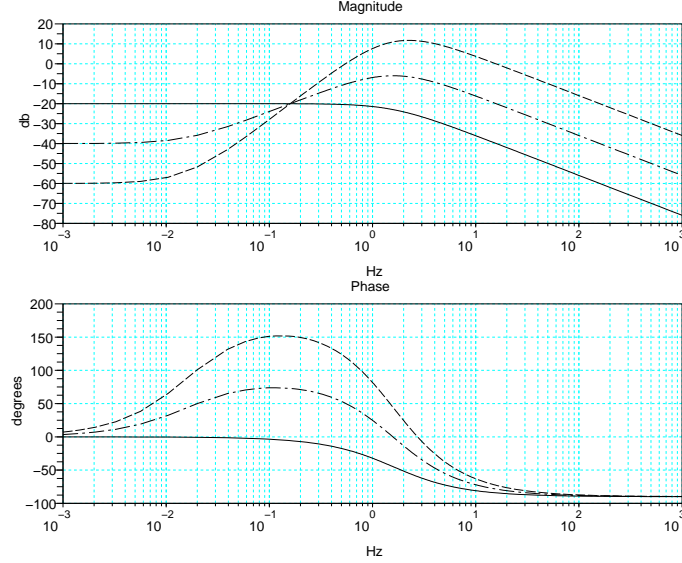


Figure 6.4: Bode diagram of the transfer functions of the (continuous) Laguerre functions $L_0(s)$, $L_1(s)$, $L_2(s)$ ($\alpha = 10$ is a continuous pole chosen)

However, we are more interested in finding the coefficient using the RLS procedure, and the matrix of covariance is of course of particular importance in the efficiency of the algorithm. Therefore, we shall examine the cross-correlation functions of two outputs of the Laguerre filter:

$$R_{mn}(\tau) = E\{l_m(a, k + \tau)l_n(a, k)\} \quad (6.51)$$

This can be calculated using the Fourier transforms of the z-domain expression of the Laguerre filters (Wahlberg, 1991) and of the cross-correlation:

$$r_{mn} = \frac{1}{2\pi} \int_{-\pi}^{\pi} L_m(a, e^{i\omega}) L_n(a, e^{-i\omega}) \Phi_{uu}(e^{i\omega}) d\omega \quad (6.52)$$

changing the integration variable as follows:

$$e^{i\Omega} = \frac{e^{i\omega} - a}{1 - ae^{i\omega}} \Leftrightarrow e^{i\omega} = \frac{e^{i\Omega} + a}{1 + ae^{i\Omega}}, \quad (6.53)$$

$$d\omega = \frac{1 - a^2}{|e^{i\Omega} + a|^2} d\Omega, \quad \frac{1}{e^{i\omega} - a} = \frac{e^{-i\Omega} + a}{1 - a^2}. \quad (6.54)$$

the cross correlation is (Wahlberg, 1991):

$$r_{mn} = \frac{1}{2\pi} \int_{-\pi}^{\pi} e^{i\Omega(n-m)} \Phi_{uu} \left(\frac{e^{i\Omega} + a}{1 + ae^{i\Omega}} \right) d\Omega \quad (6.55)$$

which only depends on m , n and the spectrum of the input $\Phi_{uu}(\Omega)$. Thus, the Toeplitz structure of the covariance matrix is preserved despite that the regressor vector is

constituted by the filter bank output.

Given a first order system described by z-domain transfer function:

$$H(z) = \frac{K}{z - z_0} \quad (6.56)$$

it can be shown that the Laguerre expansion of $H(z)$ is:

$$H(z) = \sum_{i=1}^{\infty} \frac{K\sqrt{1-a^2}}{1-az_0} \left(\frac{z_0-a}{1-az_0} \right)^{i-1} L_i(a, z) \quad (6.57)$$

This result gives an important indication on the rate of convergence of the series, which is directly related to the difference $a - z_0$. If $a = z_0$ the series reduces to one term, and choosing a value of a near z_0 will reduce the number of terms for a given precision. It also shows that in the case of complex z_0 , the rate of convergence will be less rapid. As a matter of fact Laguerre functions are good approximators for system having exponentially decaying impulse responses. In the case of strong oscillatory behaviour, other functions such as Kautz functions should be used. Also, Laguerre filters applied to identify systems with several scattered pole will have slow convergence.

Practical aspects

The Laguerre functions can be defined recursively:

$$\begin{cases} L_0(a, z^{-1}) = \frac{\sqrt{1-a^2}}{(1-az^{-1})} \\ L_k(a, z^{-1}) = L(a, z^{-1})L_{k-1}(a, z^{-1}) \end{cases} \quad \text{where} \quad L(a, z^{-1}) = \frac{z^{-1}-a}{1-az^{-1}} \quad (6.58)$$

This makes them easy to be implemented. This simply consists of a transversal filter where the usual taps are replaced by $L(a, z^{-1})$, the filter is fed by the input filtered through the low pass $L_0(a, z^{-1})$ (see Fig 6.5) The state space representation of a Laguerre filter can be deduced from the Eq. (6.58). It reads:

$$\begin{aligned} \begin{bmatrix} l_0(t+1) \\ l_1(t+1) \\ \vdots \\ l_n(t+1) \end{bmatrix} &= \underbrace{\begin{bmatrix} a & 0 & \dots & \dots & 0 \\ \beta & a & 0 & & 0 \\ -a\beta & \beta & a & 0 & 0 \\ \vdots & \ddots & \ddots & & \\ (-a)^{n-2}\beta & & & \beta & a \end{bmatrix}}_A \underbrace{\begin{bmatrix} l_0(t) \\ l_1(t) \\ \vdots \\ l_n(t) \end{bmatrix}}_1 + \underbrace{\sqrt{\beta} \begin{bmatrix} 1 \\ -a \\ a^2 \\ \vdots \\ (-a)^{n-1} \end{bmatrix}}_B u(t) \\ y(t) &= \underbrace{\begin{bmatrix} c_0 & c_1 & \dots & c_n \end{bmatrix}}_{C^T} \begin{bmatrix} l_0(t) \\ l_1(t) \\ \vdots \\ l_n(t) \end{bmatrix} \end{aligned} \quad (6.59)$$

where $\beta = 1 - a^2$ and it is worth noticing that the state matrix A and the command matrix B are completely defined by the Laguerre pole a . To obtain a nonlinear model

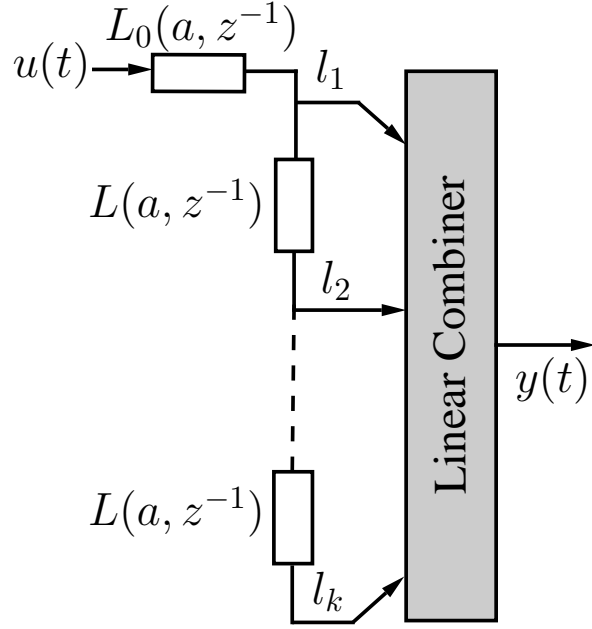


Figure 6.5: Practical realization of a Laguerre filter.

the Volterra series is truncated and the Volterra kernels are expanded using Laguerre functions. Without going into further details the nonlinear output of the Volterra Laguerre model can be given by rewriting $y(t)$ as follows:

$$y(t) = c_0 + C^T \mathbf{l}(t) + \mathbf{l}^T D \mathbf{l}(t) \quad (6.60)$$

where for a second order system we have

$$C = [c_1 \ c_2]^T \quad (6.61)$$

$$\mathbf{l}(t) = [l_1(t) \ l_2(t)]^T \quad (6.62)$$

$$D = \begin{bmatrix} c_{11} & c_{12} \\ c_{21} & c_{22} \end{bmatrix} \quad (6.63)$$

6.5 Experimental Study

The developments presented so far are the tools which are needed for the task of identifying a model of the dynamic of SMA actuators. They are actually meant to deal with LTI systems, a requirement not met by the SMA, which are notably non-linear. Thus the approach proposed relies on the assumption that the process of identification is fast enough compared to the time scales of the actuators, in order to ensure convergence of the identification algorithm. The non linearity is also supposed to be smooth. Therefore, the linear model identified would represent a linearization around the current point, providing the essential information for the controller.

Contrary to some approaches which would consider the system as nonlinear and use

a complicated mathematical understanding to derive a controller structure, this thesis proposes to use a simpler approach. The system is supposed to be “locally” linear and relies on the robustness of the Laguerre functions to use a fast sampling, a setup that would have been cumbersome with usual FIR models due to the high orders required and the consequent numerical stability problems.

Unfortunately, this argument cannot be justified rigorously due to the lack of mathematical tools which could validate the use of linear methods to control nonlinear systems³. The following sections will then be devoted to an experimental assessment of the proposed approach on two actuators presenting rather different behaviour:

- The first is a single SMA wire pulling a weight. Being under constant stress, the hysteresis behaviour is confined to the temperature-strain plane and is thus expected to be less complicated problem.
- The second is an antagonist SMA actuator. This setup is often cited in the literature as a solution to the main drawback of the SMA : the bandwidth is limited by the thermal time constant. Using two wires working in opposite directions would suppress the cooling phase on which no control is possible. Yet, it is not clear whether the cure is not worse than the disease (from a control point of view) since the wires will now work in the whole stress/strain/temperature space, resulting in a very complex hysteresis.

In the process, two types of RLS algorithms, the Exponential Forgetting RLS (EF-RLS) and Directional Forgetting RLS (DF-RLS) will be implemented. As a pre-requisite, some criteria to validate the identified model will be first discussed.

6.5.1 Validation of Model in Prediction Error Method

We will briefly introduce the criteria that have been used to validate the different models tested. The position adopted is based on the prediction error, i.e the error between the measure y and the prediction \hat{y} . The criteria used in the sequel are defined below (Tóth, 2008):

- **the Mean Squared Error:**

$$MSE := \mathbf{E}\{(y - \hat{y})^2\}. \quad (6.64)$$

- **Best fit percentage (Ljung, 2006):**

$$BFT = 100\% \cdot \max \left(1 - \frac{\|y - \hat{y}\|_2}{\|y - \bar{y}\|_2}, 0 \right), \quad (6.65)$$

where \bar{y} is the mean of y .

- **Variance accounted for:**

$$VAF = 100\% \cdot \max \left(1 - \frac{\text{var}\{y - \hat{y}\}}{\text{var}\{y\}}, 0 \right) \quad (6.66)$$

3. This situation is strangely enough the rule rather than the exception. It is usual to consider the linearized model around a set point of a system, and many techniques to design the controller are based on this assumption. The validity bounds of such a controller is yet more difficult to address.

The MSE is representing the mean “distance” between the model and the actual system, or adopting a signal treatment point of view it is the energy of the error. The closer the model is to the system, the smaller will be the value of the MSE.

The BFT is more a threshold value that will discriminate between a “good” or a “bad” model. It is generally admitted that a model should be above the BFT= 90% to be useful.

The VAF measures the amount of the output variation that is explained by the identified model (Verdult & Verhaegen, 2002).

6.5.2 Single Wire Actuator

Experimental setup

The experimental setup studied to validate the identification and the Laguerre model is a wire of Nitinol SMA. It is loaded by a constant mass, so as to work with a constant stress.

Similar setups involving SMA wires have been used in many actuation systems for example SMA actuated flap (Song & Ma, 2007), dexterous robot hand (Price *et al.*, 2007), SMA arm (Elahinia & Ahmadian, 2006) etc. Even though these system were used in different mechanism, the key component of these studies was still the control of SMA wires. Hence the choice of a wire actuation seems an obvious one, first because the simplicity of the setup allows us to concentrate on the problem of identification, second because it is general enough to be extended to different SMA actuation systems.

The Nitinol wire is fixed at one end horizontally while at the other end a payload is

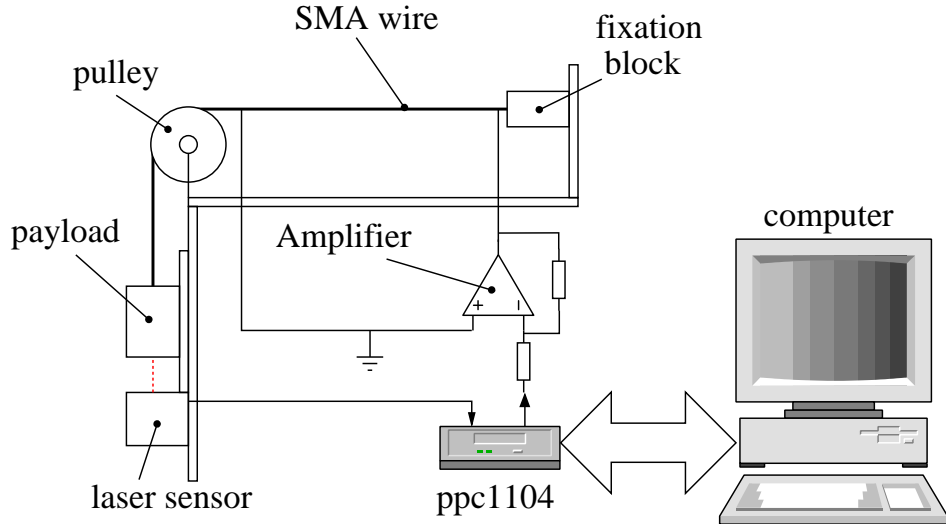


Figure 6.6: Schematic of the experimental setup using a single wire under constant stress (controlled by the payload). Displacement is measured by the laser sensor. Acquired data and identification/control signals are treated in the ppc1104 according to the algorithm developed on the computer.

fixed vertically (see Fig. 6.6 for a schematic and a picture on Fig.6.7). On both sides the wire is isolated by using nylon strings. A pulley is used to reduced the friction.

The payload is fixed on a linear bearing guided carriage to avoid the swinging of the payload and again limit friction.

The displacement is measured thanks to a laser sensor. Initially the measurements were performed using a resistive sensor. The problem of coarse resolution along with the noise on the measurements, became rapidly too tedious to deal with, and it was abandoned in favour of the optical measurement solution. The laser sensor has a resolution of $5 \mu\text{m}$, with a sampling rate of less than 1 ms.

Regarding the power supply, it is realized using an L165H analog operational amplifier having high power capability. Its function is to provide the current to heat the wire. However, it is not current controlled, it only replicates the voltage that the control asks for. This choice is certainly not optimal. Operational amplifiers in A class configuration have low efficiency, and a class D should be preferred if such considerations are in the requirements. Again, simplicity was the main motivation⁴.

Finally, the control design is realized using a MATLAB®/Simulink® -dSPACE® toolchain. Simulink® provides an easy environment to describe the control algorithm in the form of a block diagram. It is then converted into C code by the code generation utility of matlab. The dSPACE® will then insert to this code headers from its own libraries, then cross-compile them and finally load them onto a DS1104 card which runs it in real time. The dSPACE® interface board provides eight analog to digital converters for analog sensors and eight digital to analog converters which can be used for control purposes.

The SMA wire is a Nitinol wire of length 21 cm and diameter $200 \mu\text{m}$. The Austenite start temperature is 65°C and Austenite finish temperature is 93°C . The resistance at ambient temperature was measured initially and is approximately 8Ω . This value is consistent with the theoretical value for the martensitic phase which is around 6Ω (assuming a resistivity of $90 \Omega \cdot \text{m}^{-1}$).

The payload has a weight of 280 g, yielding a stress of 87 MPa. Motion is obtained by heating the wire which will trigger the phase transformation in the material resulting in diminution of the strain.

It should be noted that the current is not directly controlled and not measured and only the voltage across the SMA wire is measured and controlled. The actuation is possible only in the case of heating, which will result in shortening of the wire. In the case where lengthening of the wire is wished, one relies on the cooling dynamic, which is governed by the ambient environment conditions and results in non repeatability of the displacement in openloop. Moreover, it has been observed that the current should be kept in a narrow band of operation (0 to 0.4 A) otherwise a permanent strain rapidly deteriorates the wire. Therefore, a voltage limitation between 0 and 3V was implemented on the control signal entering the voltage control board and a current limit of 0 to 0.4 A was set on the symmetric power supply to the voltage control board. The control was tested using a dSPACE® 1104 that allows to compile in Matlab®/simulink® environment and load it on a PowerPC (PPC) card which runs

4. Not that D class amplifier would have been complicated : a chopper would have been a perfect solution, since it is simple, robust, and a wide choice of readily available product in the market. Here, the main concern was the electromagnetic compatibility.



Figure 6.7: Experimental Setup.

the algorithm in real time. It is equipped with 12 bit analog to digital converters resulting in 4.8 mV precision in the measurement. Thermomechanical treatment of the SMA wire is crucial for the stable behaviour of the material when a given SMA wire is subjected to input current. In order to demonstrate the problem, a test was performed by mounting a Nitinol wire onto the experimental setup with constant stress and applying a sinusoidal voltage of constant amplitude through the SMA wire. The response of the system can be seen in Fig. 6.8.

The deformation and current values in y-axis are plotted against the time samples in x-axis. We can observe that although the voltage's amplitude is constant, the deformation of the SMA wire is drifting as the times passes. This drift in the material behaviour can be attributed to the absence of an adequate thermomechanical treatment of the SMA wire. This can cause serious problems to design controller for the SMA

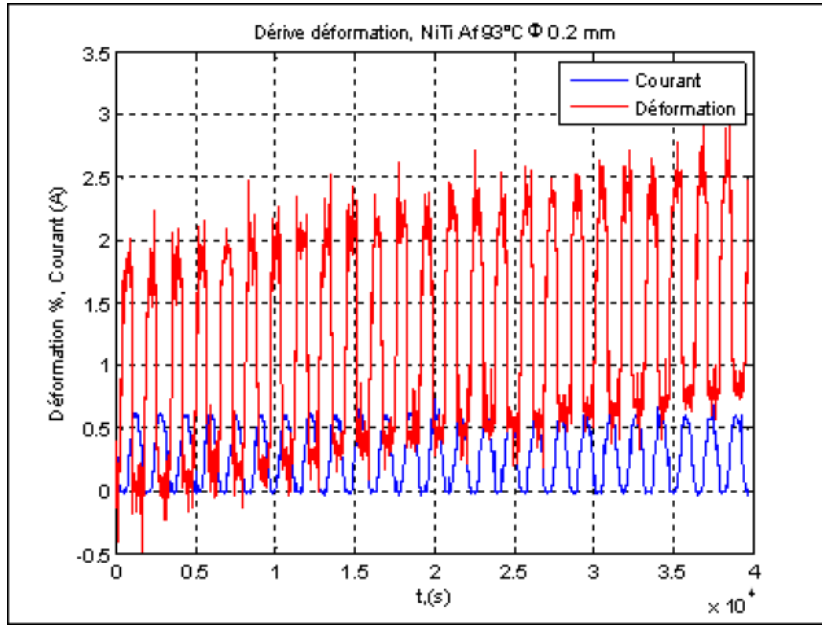


Figure 6.8: Drift in SMA wire.

actuator.

Hence a stabilization treatment was performed through a series of steps which are summarized below:

Step 1 A wire was elongated up to 10% of its original length.

Step 2 The elongated wire was then subjected to an input of 1 A, until the length of the wire is diminished.

Step 3 Next the SMA wire is treated with a cyclic loading of current consisting in square waveforms varying between 0 A and 1 A for a prolonged period of time.

After performing the above steps, the SMA wire subjected to the sinusoidal input on the same experimental setup showed no drift.

6.5.3 Open loop Identification of the single actuator

In this section, open loop identification is performed on the experimental setup of the single wire SMA actuator using the classical Exponential Forgetting RLS (EF-RLS). Three candidates for the model will be tested:

- two linear Laguerre models of second and fifth orders
- a second order non linear Volterra Laguerre. It basically consists in the linear combining of two parallel Laguerre filters which are fed by the inputs and the square of the input. It is claimed that such models can handle smooth nonlinearities.

Their ability to capture the dynamic of the SMA will be evaluated. At the same time, the two tuning parameters of the RLS algorithm will be examined namely the forgetting

factor λ and the sampling rate T_s .

A point that has been left aside so far is the initialization. The initialization parameters of the algorithm are the weights vector $\hat{C}(0)$ and the covariance matrix $P(0) = \delta^{-1}\mathbb{I}$, where δ is a positive scalar value and \mathbb{I} is the identity matrix with dimension $(n \times n)$. Here n is the order of the filter for the linear Laguerre filter, while in the case of the Volterra Laguerre model $n = m^2 + 2$ with m , the order of the Volterra model. From a theoretical point of view, the covariance matrix should be infinite ($\delta = 0$), which of course is practically infeasible, thus usual values for δ lies between 10^{-2} and 10^{-4} .

The smaller the value of δ the larger the gain of the algorithm. It can be shown that the RLS have an exponential convergence towards the values of their non recursive version. However, this is in the case of non-noisy measurements. If the signal to noise ratio is low, the convergence will be slowed down by initial high gain because the algorithm will try to adapt to the noise.

In the following experiments, $\delta^{-1} = 0.01$, this choice is conservative in the sense that convergence might not be optimal, but it should be less sensitive to noise and the results collected through the experiments should be fairly general.

Influence of Forgetting Factor

In RLS with exponential forgetting factor, past data are exponentially weighted according to their obsolescence (Bittanti *et al.*, 1990). The choice of λ as explained earlier influences the adaptability of the identification algorithm so as to be applicable to time varying system (Bittanti *et al.*, 1990; Johnstone *et al.*, 1982).

Its influence will be studied for the three models using two different types of inputs:

- first is the sum of two sinusoids with different frequencies. In this case the spectrum, is limited to two frequencies and does not fulfill the persistence of excitation condition ;
- the second consists in the same signal on which white noise is added, thus resulting in a theoretically constant spectrum.

The two signals will in the sequel be named “SNR ∞ ” dB and “SNR 45” dB signals respectively, referring to their respective signal to noise ratio. These two signals will help to define the practical limits of the various parameters of the RLS (Johnstone *et al.*, 1982). The SNR 45 dB signals being close to the theoretically “good” signal will help to identify the actual limits of the algorithm, with the ∞ dB signal being representative of a “bad” signal in terms of identification. This will allow to select the models that are more robust and the more likely to be used for control purposes. Indeed, as it will be discussed in the next chapter, in this context there is no possibility to control the input signal which depends on the reference signal and the dynamic of the controller. The validation criteria described earlier (MSE, and so on) will help in objectively appreciating the models.

The pole will remain the same for all filters with the value $a = 0.9$, since the system is considered to be slow compared to the sampling period which was fixed to $T_s = 0.01$ s. The forgetting factor takes the values $\lambda \in \{1, 0.99, 0.9, 0.5\}$, thus modifying the identification from non-adapting to extremely adaptive. Note that the usual values remains in the vicinity of 0.98/0.99 in literature.

Second Order Linear Laguerre Filter The test results for this filter are summed up in Tab. 6.5 and Tab. 6.6 for the 45 dB and ∞ dB signals respectively. In the first case, the results are the one expected, with a great improvement of the prediction of the model as λ is reduced which is confirmed by every criteria. With $\lambda = 0.99$, it is clear that the model is already good enough even though the order of the model is very low. This seems to indicate that the projection of the system on the first two vectors of the Laguerre basis already convey most of the necessary information to restitute the dynamic of the system. Further reduction of the forgetting factor is not necessary and even not measurable, most criteria becoming totally meaningless as they are well below the precision of the sensor.

On Fig. 6.9 and Fig. 6.10 one can qualitatively evaluate the impact of the extreme values of forgetting factor on the estimation of the Laguerre filter:

- In the case of $\lambda = 1$, the weights rapidly converge and remain fairly “stable” in the vicinity of some values that keep the error in a band between -2 mm and 2 mm, the slight dissymmetry can probably be attributed to the fact that the system was first identified in the region of the upper part of the hysteresis, which indirectly reflects the strikingly fast convergence of the RLS. The resulting model could be seen as the best linear approximation of the SMA actuator.
- For $\lambda = 0.5$, the RLS are unsurprisingly reactive to the changes of the output dynamic of the SMA actuator. The error reflects this by remaining within a band that actually is the sensor resolution, and it clearly resembles a white noise except for rare burst (e.g around $t = 260$ s). The weights varies extremely rapidly with a large variance which contrast with the previous results. Examining the output, it appears that the RLS also follows the output noise, that is the high frequencies which are certainly not a feature of the system, showing that this value for λ is too low.

From the identification results in Tab. 6.6 we can see that the performance based on MSE of the 2nd order model with ∞ dB is very similar to the one with the input SNR of 45 dB. It is a good result considering that the signal is not respecting the persistence of excitation condition.

This is shown by the time response of the weights vector(see Fig.6.11 and Fig.6.12). For a similar value of MSE, the filter weights magnitude is larger for the no noise case. This is directly related to the poor conditioning of the covariance matrix.

| λ | MSE (mm^2) | BFT (%) | VAF (%) | Mean Error (mm) |
|-----------|------------------------|---------|---------|-------------------------|
| 1 | 1.815 | 45.589 | 70.935 | -0.181 |
| 0.99 | 0.010 | 95.898 | 99.832 | 0.004 |
| 0.9 | 2.532×10^{-5} | 99.798 | 99.999 | -1.445×10^{-5} |
| 0.5 | 4.540×10^{-7} | 99.972 | 100 | 5.358×10^{-6} |

Table 6.5: 2nd Order Linear Laguerre Filter with Input SNR=45 dB and different Forgetting factor λ .

Chapter 6. Modelling

| λ | MSE (mm^2) | BFT (%) | VAF (%) | Mean Error (mm) |
|-----------|------------------------|---------|---------|-------------------------|
| 1 | 1.766 | 46.744 | 72.049 | -0.188 |
| 0.99 | 0.010 | 95.874 | 99.83 | 0.003 |
| 0.9 | 1.807×10^{-5} | 99.828 | 99.999 | 7.486×10^{-6} |
| 0.5 | 1.265×10^{-7} | 99.985 | 100 | -8.260×10^{-8} |

Table 6.6: 2nd Order Linear Laguerre Filter with Input SNR=∞ dB and different Forgetting factor λ .

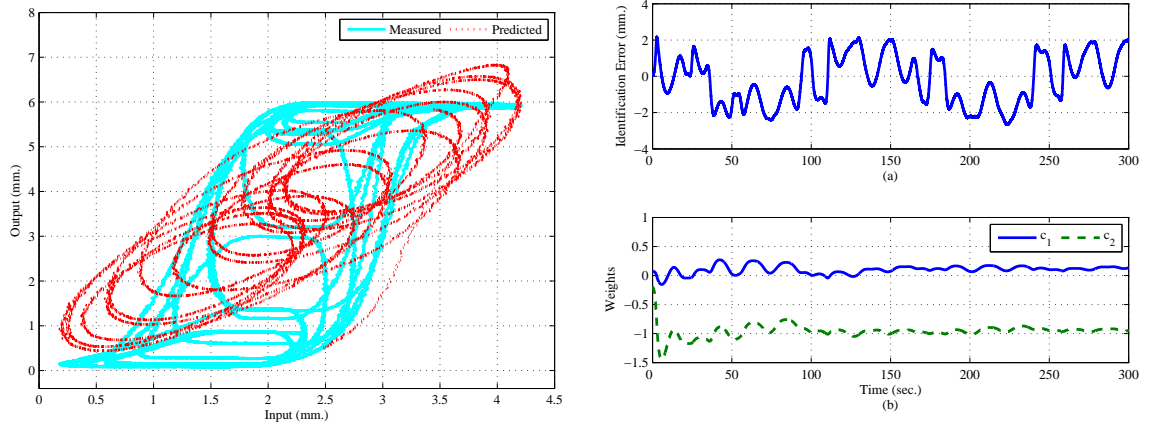


Figure 6.9: 2nd order linear Laguerre filter with input SNR=45 dB and $\lambda = 1$. Left: Hysteresis measured and Predicted, Right:(a)Identification Error (b) Filter Weights.

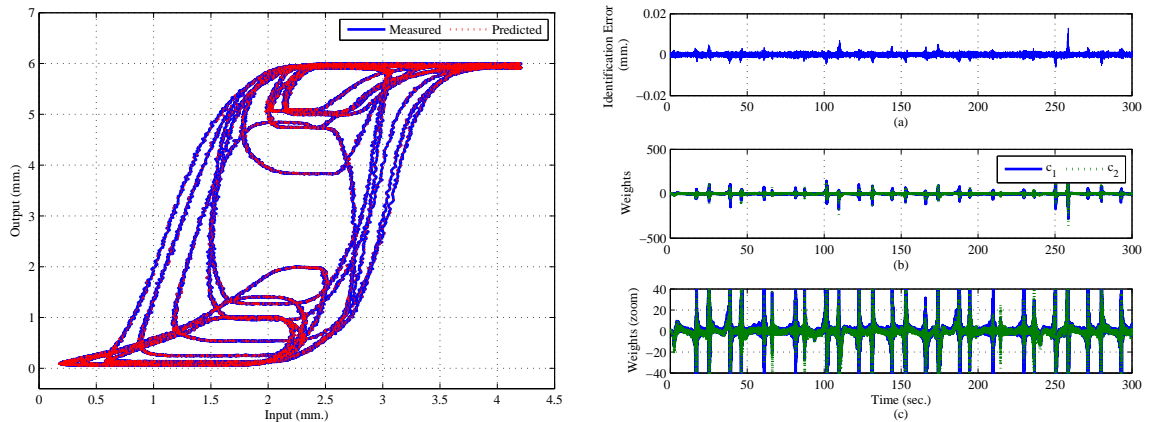


Figure 6.10: 2nd order linear Laguerre filter with input SNR=45 dB and $\lambda = 0.5$. Left: Hysteresis measured and Predicted, Right:(a)Identification Error (b) Filter Weights(c)Filter weights zoomed.

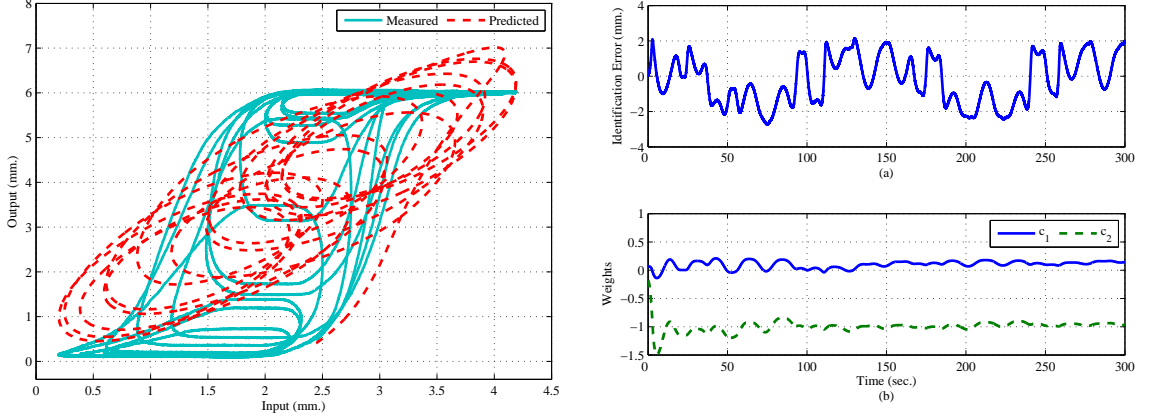


Figure 6.11: 2nd order linear Laguerre filter with input $SNR = \infty$ dB and $\lambda = 1$. Left: Hysteresis measured and Predicted, Right:(a)Identification Error (b) Filter Weights.

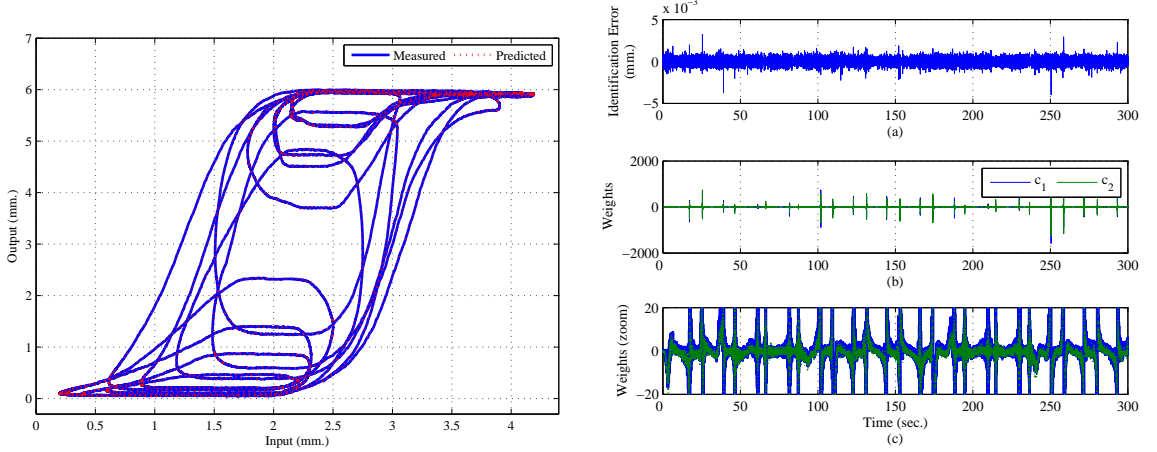


Figure 6.12: 2nd order linear Laguerre filter with input $SNR = \infty$ dB and $\lambda = 0.5$. Left: Hysteresis measured and Predicted, Right:(a)Identification Error (b) Filter Weights.

Second Order Volterra Laguerre Filter The analysis of identification results with input noise is summarized in Tab. 6.7 and the analysis for the identification with no input noise is analyzed in Tab. 6.8.

In order to implement the second order Volterra Laguerre model the model given by Eq. (6.60) is used. In the given equation, it is assumed that the non-linearity passes through the origin (Pajunen, 1992) which is a known practice along with introducing convexity assumption on the true nonlinearity. In Dumont *et al.* (1994) convexity in the nonlinearity of the true system was assumed and constraints were introduced in the estimation of the nonlinear part. In our current problem by making the assumption that the nonlinearity passes through the origin we set $c_0 = 0$ and perform the identification of the rest of the parameters.

Considering the results of Tab. 6.7, it is clear that the identification performances

of the 2nd order Volterra Laguerre filter with input SNR=45 dB gives very good results. Considering for instance the case $\lambda = 0.99$, the Volterra Laguerre outperforms the previous filter. It seems also that this value is optimal, the figures remaining fairly unchanged when decreasing λ , and finally leading to instability for the value 0.5. Their respective plot for hysteresis approximation, identification error and filter weights can be seen in Fig. 6.13 and Fig. 6.14. Considering the case $\lambda = 1$, one can see, when compared to Fig. 6.10 that the filter output is less symmetric, and particularly at the lower values of the hysteresis, it is closer to the actual output. Considering the Tab. 6.8, the performance of the 2nd order Volterra Laguerre with no input noise (in terms of MSE) is similar to the previous one for higher values of the forgetting factor. As anticipated, the filter gets unstable for $\lambda = \{0.9, 0.5\}$. The Volterra models are interesting because they can model non-linear systems using a linear in the parameter model, and combined with the Laguerre filters and their orthogonality, they have also the robustness already observed in the previous filter. However the persistence of excitation condition is more stringent in their case. If n is the number of the filters and m the order of the Volterra series, then the excitation signal should be of order $n \times m$. This is qualitatively what is observed considering the lower “stability” zone of the filter under consideration. Respective figures for the plot of hysteresis identification error and filter weights can be seen on Fig. 6.15 and Fig. 6.16. As explained in the previous section although the MSE for no noise case is similar to the input noise case, the magnitude of weights (Figure 6.16-c) are very high compared to those seen in the noisy case. The large variation of the Laguerre filter can be attributed to numerical problems caused by the calculation of the badly conditioned covariance matrix P .

| λ | MSE (mm^2) | BFT (%) | VAF (%) | Mean Error (mm) |
|-----------|------------------------|---------|---------|-------------------------|
| 1 | 1.536 | 49.670 | 74.756 | -0.072 |
| 0.99 | 2.484×10^{-5} | 99.800 | 99.999 | -4.504×10^{-5} |
| 0.9 | 7.853×10^{-5} | 99.639 | 99.998 | -2.157×10^{-5} |
| 0.5 | - | - | - | - |

Table 6.7: 2nd Order Volterra Laguerre Filter with Input $SNR = 45$ dB and different Forgetting factor λ .

| λ | MSE (mm^2) | BFT (%) | VAF (%) | Mean Error (mm) |
|-----------|------------------------|---------|---------|------------------------|
| 1 | 1.622 | 48.800 | 73.837 | -0.056 |
| 0.99 | 2.300×10^{-5} | 99.807 | 99.999 | 8.433×10^{-6} |
| 0.9 | - | - | - | - |
| 0.5 | - | - | - | - |

Table 6.8: 2nd Order Volterra Laguerre Filter with Input $SNR = \infty$ dB and different Forgetting factor λ .

Fifth Order linear Laguerre filter Finally, the analysis of identification results of the fifth order filter is summarized in Tab. 6.10 and Tab. 6.9 for the noisy and noiseless

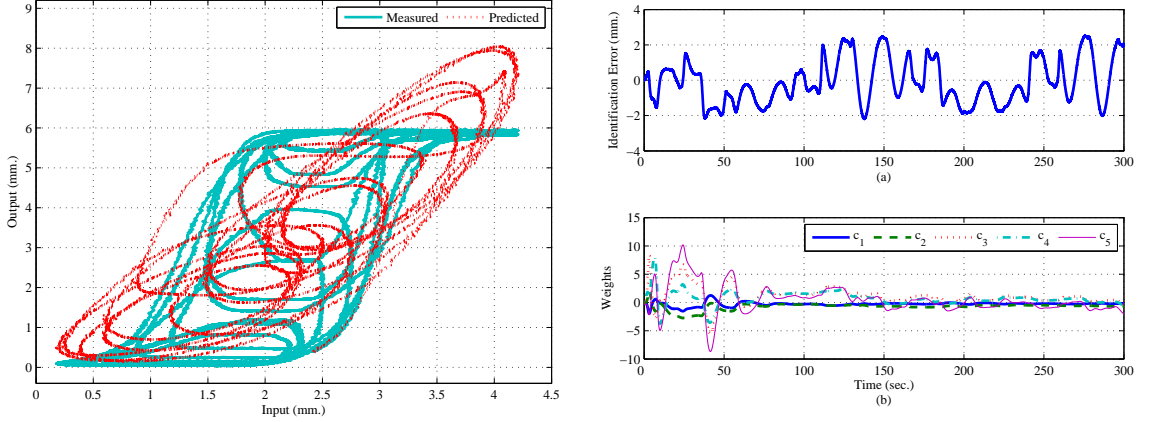


Figure 6.13: 2nd order Volterra Laguerre filter with input $SNR = 45$ dB and $\lambda = 1$. Left: Hysteresis measured and Predicted, Right:(a)Identification Error (b) Filter Weights.

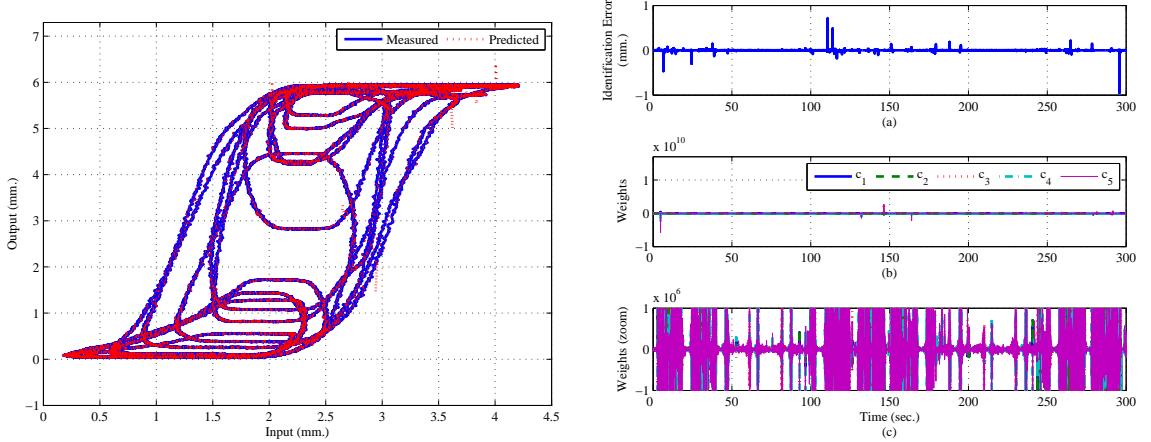


Figure 6.14: 2nd order Volterra Laguerre filter with input $SNR = 45$ dB and $\lambda = 0.9$. Left: Hysteresis measured and Predicted, Right:(a)Identification Error (b) Filter Weights.

input signal. In this case, the persistence of excitation being of order less than 5, the filter is unstable for all forgetting factor beneath 1. For $\lambda = 1$, the identification is similar to the second order, and is useless.

The noise added to the input stabilizes the algorithm, and the results of the identification follow the same trend as the second order Volterra Laguerre filter.

Comparing the results for $\lambda = 1$, there appears no notable difference in the models predictions whatever input signals are used (Fig. 6.19 and Fig. 6.17). The approximation is very poor, since the weights are stabilized and the filter is actually not adapting to the nonlinearities of the hysteresis.

Identification is much better as soon as the forgetting factor is reduced (and the excitation is correct). Although the results seem similar to the second order Volterra Laguerre filter, it can be noticed, that this is done with considerably less variations of the weights (Fig. 6.18). For instance, for $\lambda = 0.99$ (with input SNR 45 dB) the

Chapter 6. Modelling

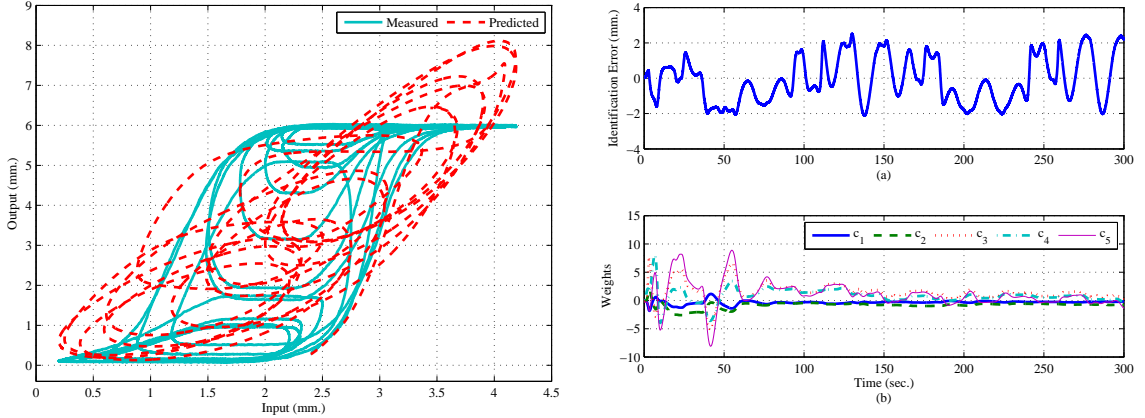


Figure 6.15: 2nd order Volterra Laguerre filter with input $SNR = \infty$ dB and $\lambda = 1$. Left: Hysteresis measured and Predicted, Right:(a)Identification Error (b) Filter Weights.

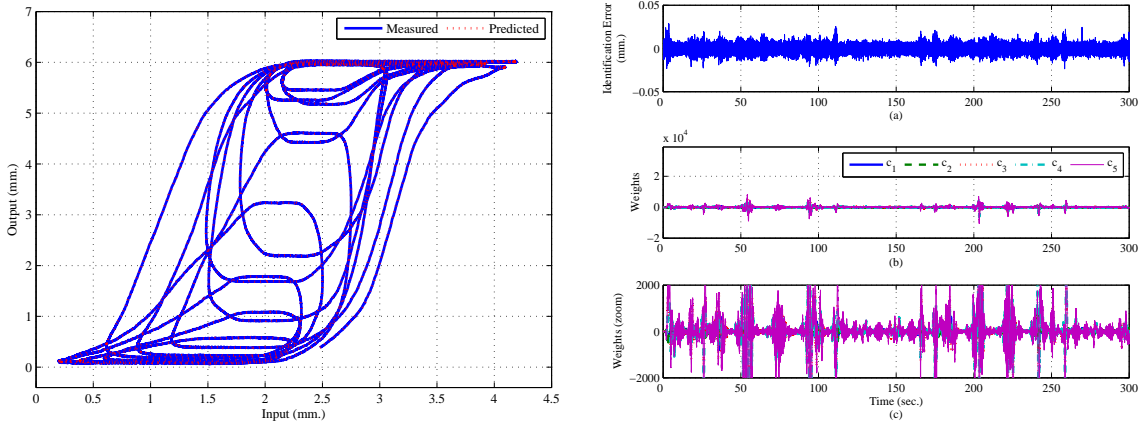


Figure 6.16: 2nd order Volterra Laguerre filter with input $SNR = \infty$ dB and $\lambda = 0.99$. Left: Hysteresis measured and Predicted, Right:(a)Identification Error (b) Filter Weights.

identification error was close to white noise while the magnitude of the filter weight was of order 10^2 compared to the 2nd order Volterra model for which the magnitude of the weights variations were of the order 10^4 (figures not shown).

Summary: Influence of Forgetting Factor on identification

The first goal of this section was to validate the approach of using Laguerre filters combined to an exponential forgetting recursive least square identification. The concept is validated on three different filters:

- a second order linear Laguerre filter for its simplicity (only two weights to identify)
- a second order Volterra Laguerre filter, with a limited number of filters, is supposed to handle better smooth nonlinearities
- finally a fifth order linear Laguerre filter, which theoretically should increase the precision of the second order model.

| λ | MSE (mm^2) | BFT (%) | VAF (%) | Mean Error (mm) |
|-----------|----------------|---------|---------|-----------------|
| 1 | 1.740 | 46.883 | 71.937 | -0.113 |
| 0.99 | - | - | - | - |
| 0.9 | - | - | - | - |
| 0.5 | - | - | - | - |

Table 6.9: 5th Order linear Laguerre Filter with Input $SNR = \infty$ dB and different Forgetting factor λ .

| λ | MSE (mm^2) | BFT (%) | VAF (%) | Mean Error (mm) |
|-----------|------------------------|---------|---------|-------------------------|
| 1 | 1.950 | 44.238 | 69.296 | -0.187 |
| 0.99 | 3.013×10^{-5} | 99.779 | 99.999 | -9.002×10^{-7} |
| 0.9 | 9.091×10^{-7} | 99.961 | 100 | 2.470×10^{-6} |
| 0.5 | - | - | - | - |

Table 6.10: 5th Order linear Laguerre Filter with Input $SNR = 45$ dB and different Forgetting factor λ .

In every configuration, the filters constitute very good models as soon as the forgetting factor is less than one and the excitation is rich enough. This condition is however very broadly varying with the filter structure:

- the second order filter is insensitive to this requirement
- the second order Volterra Laguerre is only unstable in the extreme case where $\lambda = 0.5$
- the fifth order is simply inoperable if noise is not added to the input so as to fulfil the persistence of excitation condition (PEC).

In terms of performances, all the filters provide more than enough precision. A further analysis reveals that the hierarchy presented before is verified in the sense that the second order Volterra Laguerre filter is superior to the linear second order Laguerre, and that the adaptation is less erratic when the order is increased. Similarly, the precision is augmented with the order, although this should not be exaggerated due to the trend of higher order to be more sensitive to the PEC.

The properties of the Laguerre function are however remarkable, and seem appropriate to the problem. To explore further their robustness, the sampling time is varied in the sequel.

Chapter 6. Modelling

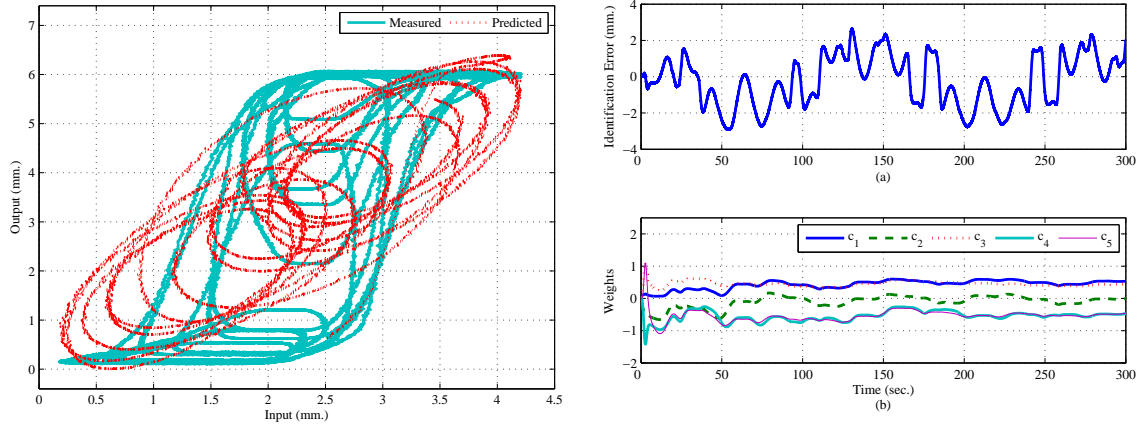


Figure 6.17: 5th order linear Laguerre filter with input $SNR = 45$ dB and $\lambda = 1$. Left: Hysteresis measured and Predicted, Right:(a)Identification Error (b) Filter Weights.

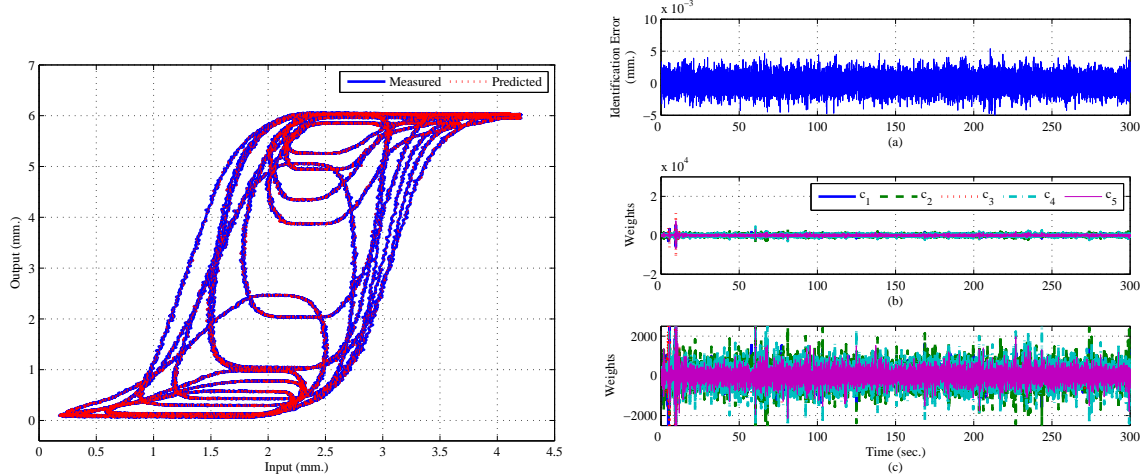


Figure 6.18: 5th order linear Laguerre filter with input $SNR = 45$ dB and $\lambda = 0.9$. Left: Hysteresis measured and Predicted, Right:(a)Identification Error (b) Filter Weights.

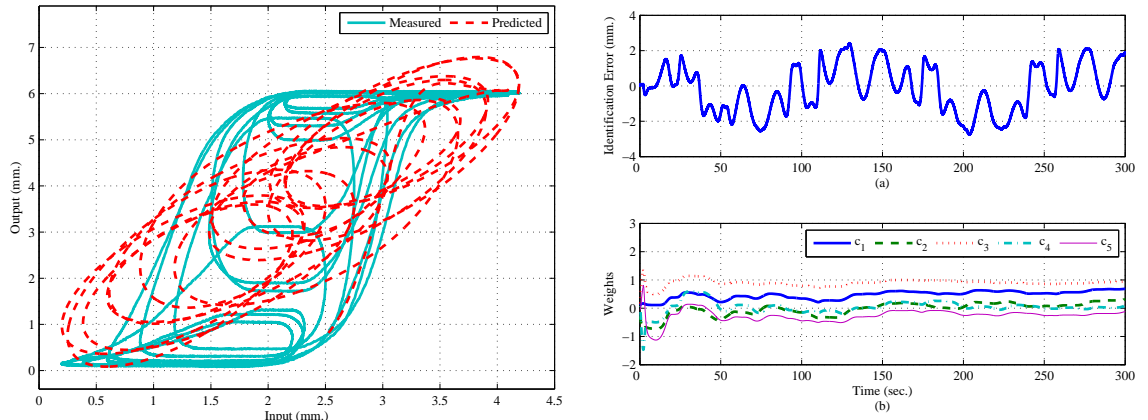


Figure 6.19: 5th order linear Laguerre filter with input $SNR = \infty$ dB and $\lambda = 1$. Left: Hysteresis measured and Predicted, Right:(a)Identification Error (b) Filter Weights.

Influence of Sampling period on the Identification

The sampling time is usually not an issue as long as the signal used fulfils the PEC, and the system's parameters are not changing too rapidly. This condition, however, is difficult to characterize. It supposes to take the non linearity into account and evaluate how it can influence the stability of the identification algorithm. The approach of this study is different : it aims at knowing as little as necessary to predict the output of the system so as to limit the calculation for the controller.

Loosely put, the problem of too slow a sampling is that the information collected might cover a large domain despite the use of sliding window. The identification will then try to adapt the weights over a set of data incompatible with linear nature of the Laguerre filter. This is somewhat comparable to the situation encountered when choosing $\lambda = 1$ in the previous test.

Laguerre filter were chosen partly because they are considered to be robust to the sampling rate (Wahlberg, 1991). In the next test, different sampling rates are used to evaluate how it affects the performance of approximation of a nonlinear system using a linear model updated in realtime. The sampling rate is an important factor because it directly relates to the computational time and capability of the hardware. The greater number of samples per cycle, the faster the approximation error will converge to a minimum (Chase *et al.*, 2005), on the other hand the computation are more limited. In the following, the sampling rate is varied ($T_s \in \{0.01, 0.1, 1\}$ s) and the performances of the filters evaluated in the same way. The pole are set to $a = 0.9$ and forgetting factor is $\lambda = 0.9$.

Second order linear Laguerre filter The analysis of the identification of the model with input noise of $SNR = 45$ dB and with no input noise are summed up in Tab. 6.11 and Tab. 6.12 respectively.

Basically the stabiltiy of the RLS remains unaffected by the sampling time. The condition $T_s = 0.01$ sec has already been treated in Section 6.5.3. We can observe that with the same parameters the sampling rate can be reduced to 0.1sec and 1sec. The approximation progressively deteriorates as reflected by the MSE.

The respective behaviors using $T_s = 1$ sec with input noise can be seen in Fig. 6.20 and for the noiseless case can be seen in Fig. 6.21. From the observation of the experimental results with input SNR 45 dB and $T_s = 0.1$ the hysteresis curve was found to be smooth which could be attributed to the fact that the observation of the physical process using $T_s = 0.1$ sec is ignorant of any noise present in the actual process which obviously can be seen when considering the MSE of the case with $T_s = 0.1$ sec for input noise and no-noise. With $T_s = 1$ sec we can observe that the actual hysteresis in the process has changed considerably from the faster sampling rate. This observation is consistent with the fact that the rate at which the observation is made affects the knowledge of the system itself.

| T_s sec | MSE (mm^2) | BFT (%) | VAF (%) | Mean Error (mm) |
|-----------|------------------------|---------|---------|-------------------------|
| 0.01 | 2.532×10^{-5} | 99.798 | 99.999 | -1.445×10^{-5} |
| 0.1 | 0.006 | 96.706 | 99.891 | -2.272×10^{-5} |
| 1 | 0.368 | 75.485 | 94.020 | -0.044 |

Table 6.11: 2nd Order linear Laguerre Filter with Input $SNR = 45$ dB and different sampling rate T_s .

| T_s sec | MSE (mm^2) | BFT (%) | VAF (%) | Mean Error (mm) |
|-----------|------------------------|---------|---------|------------------------|
| 0.01 | 1.807×10^{-5} | 99.828 | 99.999 | 7.486×10^{-6} |
| 0.1 | 0.007 | 96.641 | 99.887 | 0.002 |
| 1 | 0.382 | 75.020 | 93.789 | -0.043 |

Table 6.12: 2nd Order linear Laguerre Filter with Input $SNR = \infty$ dB and different sampling rate T_s .

Second Order Volterra Laguerre The influence of sampling rate on the identification of the second order Volterra Laguerre filter is analysed in the case of an input noise of $SNR = 45$ dB in Tab. 6.13 and without input noise in Tab. 6.14. The hysteresis approximation plots along with trajectory error and filter weights for $T_s = 1$ sec with input noise and no-noise case be seen in Fig. 6.22 and Fig. 6.23 respectively. From Tab. 6.13 it can be concluded that reducing $T_s = 0.1$ does not affect the MSE as in the case of the 2nd order linear Laguerre model. However the weights reach magnitudes of order 10^4 . Finally, the MSE is deteriorated badly by reducing the sampling rate to $T_s = 1$ sec.

In the no-noise case at $T_s = 0.01$ sec the 2nd order Volterra Laguerre filter is unstable as already discussed earlier in Section 6.5.3. For $T_s = 0.1$ sec the filter is stable and has good approximation properties . The identification error is a white noise at the price of very large magnitude in the variation of the weights which again reaches magnitude of 10^4 .

The MSE of the input noise and no noise case at $T_s = 1$ sec are similar as at a slower sampling rate the filter and observation is ignorant of any noise whatsoever.

| T_s sec | MSE (mm^2) | BFT (%) | VAF (%) | Mean Error (mm) |
|-----------|------------------------|---------|---------|-------------------------|
| 0.01 | 7.853×10^{-5} | 99.639 | 99.998 | -2.157×10^{-5} |
| 0.1 | 1.748×10^{-6} | 99.946 | 100 | -3.640×10^{-5} |
| 1 | 0.001 | 98.526 | 99.978 | -5.630×10^{-4} |

Table 6.13: 2nd Order Volterra Laguerre Filter with Input $SNR = 45$ dB and different sampling rate T_s .

Fifth Order linear Laguerre model The analysis of the identification of the model with input noise of $SNR = 45$ dB can be seen in Tab. 6.15 and with no input noise in

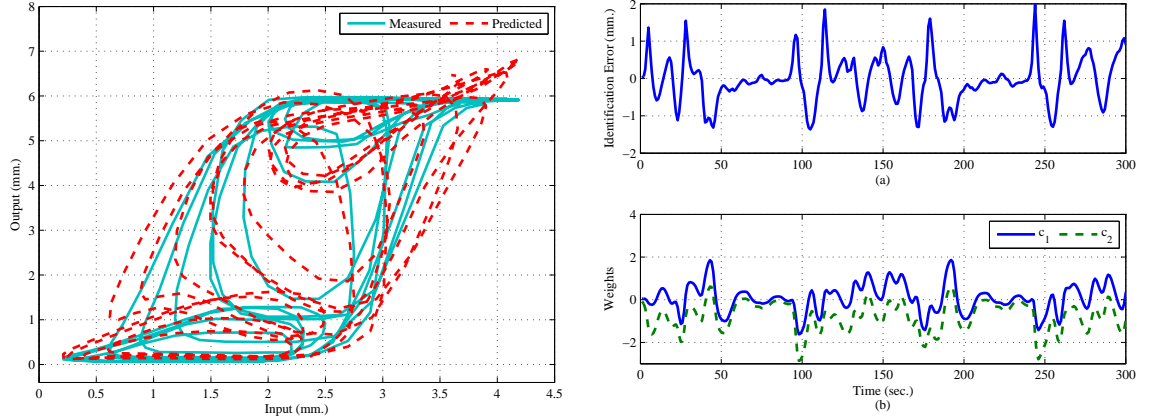


Figure 6.20: 2nd order linear Laguerre filter with input $SNR = 45$ dB, $\lambda = 0.9$ and $T_s = 1$ sec.. Left: Hysteresis measured and Predicted,Right:(a)Identification Error (b) Filter Weights.

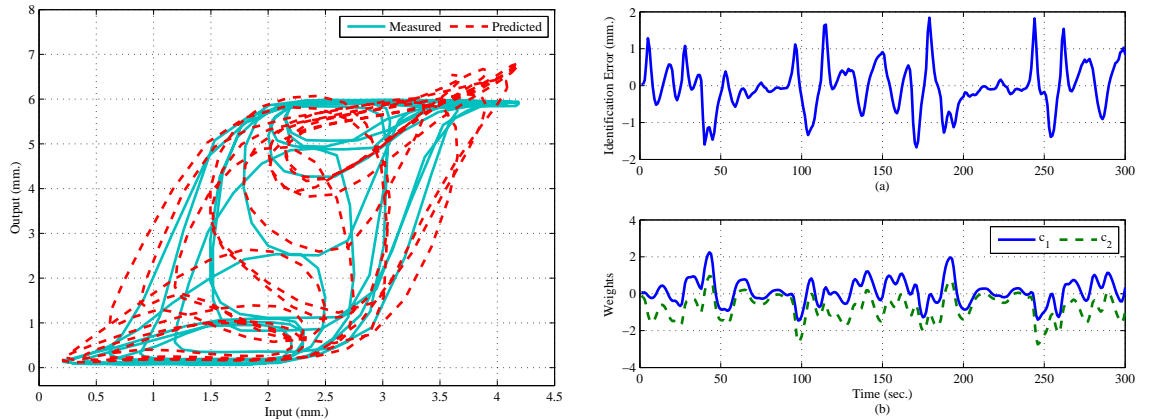


Figure 6.21: 2nd Order linear Laguerre filter with input $SNR = \infty$ dB, $\lambda = 0.9$ and $T_s = 1$ sec.. Left: Hysteresis measured and Predicted,Right:(a)Identification Error (b) Filter Weights.

Tab. 6.16. The plot with respect to response with input noise case for sampling rate $T_s = 1$ sec can be seen in Fig. 6.24. From the Tab. 6.15 for input noise we can see that the approximation is still good at $T_s = 0.1$ sec and the identification error is close to white noise. But the most prominent difference between the identification with input noise at $T_s = 0.01$ sec and $T_s = 0.1$ sec with Laguerre pole $a = 0.9$ is that the weights of the filter in the first case reach 10^4 while in the second case remain within 10^2 . This is due to the fact that at slow sampling rate of $T_s = 0.1$ sec the RLS tend to mitigate the influence of noise. For the no noise case the filter is unstable until the sampling rate is reduced to $T_s = 1$ sec at which the approximation seen in Fig. 6.25 is similar to the approximation with input noise seen in Fig. 6.24.

Summary: Influence of Sampling rate

The influence of sampling rate is summarized in this section. As mentioned earlier the forgetting factor was fixed at $\lambda = 0.9$. For the input SNR 45 dB case the MSE

Chapter 6. Modelling

| T_s sec | MSE (mm) | BFT (%) | VAF (%) | Mean Error (mm) |
|-----------|------------------------|---------|---------|-------------------------|
| 0.01 | - | - | - | - |
| 0.1 | 1.212×10^{-6} | 99.955 | 100 | -3.391×10^{-7} |
| 1 | 0.001 | 98.295 | 99.971 | -4.098×10^{-4} |

Table 6.14: 2nd Order Volterra Laguerre Filter with Input $SNR = \infty$ dB and different sampling rate T_s .

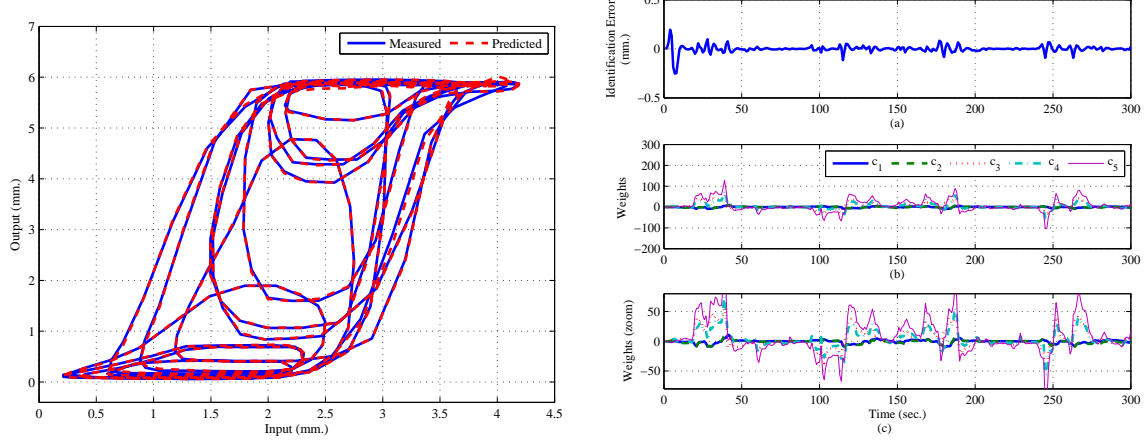


Figure 6.22: 2nd Order Volterra Laguerre filter with input $SNR = 45$ dB, $\lambda = 0.9$ and $T_s = 1$ sec.. Left: Hysteresis measured and Predicted, Right:(a)Identification Error (b) Filter Weights.

was large for $T_s = 1$ for all the three models. The MSE was least for $T_s = 0.01$ for 2nd order linear and Volterra model but was unstable for 5th order model as the forgetting factor $\lambda = 0.9$ is allowing faster update. For input SNR ∞ dB case 2nd order Volterra Laguerre is unstable for $T_s = 0.01$ and the 5th order linear Laguerre is only stable for $T_s = 1$. In general an important aspect that is interesting is that at slower sampling rate the fitting of the model is smoother. This is because noise in the experimental system is ignored by the observation process, identification and ultimately the model, although it must be kept in mind that a proper PE condition is usually provided by a noise in the input. At a faster sampling rate the Laguerre filter picks up noise prevailing in the experimental setup.

| T_s sec | MSE (mm^2) | BFT (%) | VAF (%) | Mean Error (mm) |
|-----------|------------------------|---------|---------|------------------------|
| 0.01 | 9.091×10^{-7} | 99.961 | 100 | 2.470×10^{-6} |
| 0.1 | 2.404×10^{-6} | 99.936 | 100 | 3.759×10^{-5} |
| 1 | 0.002 | 98.040 | 99.961 | -0.001 |

Table 6.15: 5th Order linear Laguerre Filter with Input $SNR = 45$ dB and different sampling rate T_s .

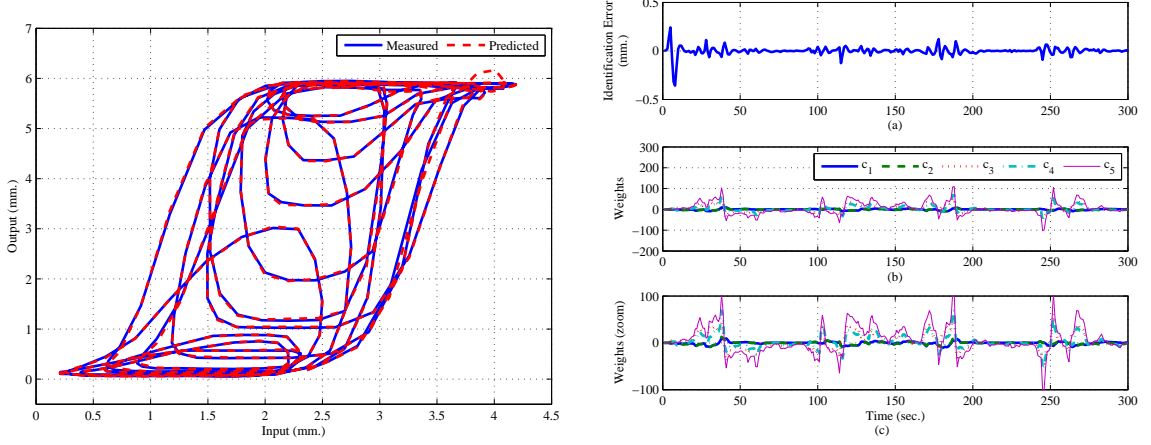


Figure 6.23: 2nd Order Volterra Laguerre filter with input $SNR = 0$ dB, $\lambda = 0.9$ and $T_s = 1$ sec.. Left: Hysteresis measured and Predicted, Right:(a)Identification Error (b) Filter Weights.

| T_s sec | MSE (mm^2) | BFT (%) | VAF (%) | Mean Error (mm) |
|-----------|----------------|---------|---------|-------------------------|
| 0.01 | - | - | - | - |
| 0.1 | - | - | - | - |
| 1 | 0.002 | 98.225 | 99.968 | -2.113×10^{-4} |

Table 6.16: 5th Order linear Laguerre Filter with Input $SNR = \infty$ dB and different sampling rate T_s .

6.5.4 Experimental Setup: Antagonistic Actuator

Introduction: The phase transition encountered in SMA materials under proper stress and temperature condition provides large strains which make SMA material an attractive solution for actuation system. However, as already mentioned, it introduces a significant hysteresis which cannot be ignored when considering actuators for positioning applications. Moreover, despite possessing interesting properties such as large force to mass ratio, the SMA actuators have limited applications due to their large time constant. To address this issue, some authors recommend a bias spring which assists the recovering phase, allowing a faster actuation since complete cooling is not further needed for the SMA wire to recover the initial strain. Another configuration that can be considered is a two SMA wires antagonistic actuator in which one SMA wire is heated while the other wire is naturally cooled. In such a setup the two wires are generally pre-strained by the same amount. Heating of one wire causes it to recover its initial pre-strain while increasing the strain in the other which can be later actuated in the same way. It can be used to perform linear actuation. Fig. 6.26 illustrates such a structure which has been implemented. In the bias-spring/SMA actuator, there is no active control of movement when the actuator is naturally cooled as opposed to the antagonistic structure, where the time response depends theoretically on the thermal power that is put in the heated wire. Therefore the antagonistic configuration is expected to achieve better controllability and dynamic properties compared to a bias type

Chapter 6. Modelling

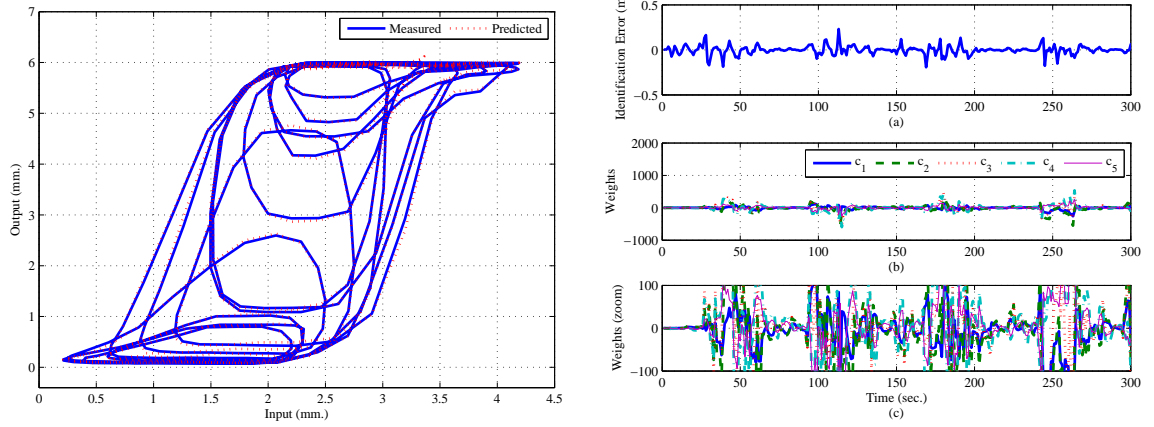


Figure 6.24: 5th order linear Laguerre filter with input $SNR = 45$ dB, $\lambda = 0.9$ and $T_s = 1$ sec.. Left: Hysteresis measured and Predicted, Right:(a)Identification Error (b) Filter Weights.

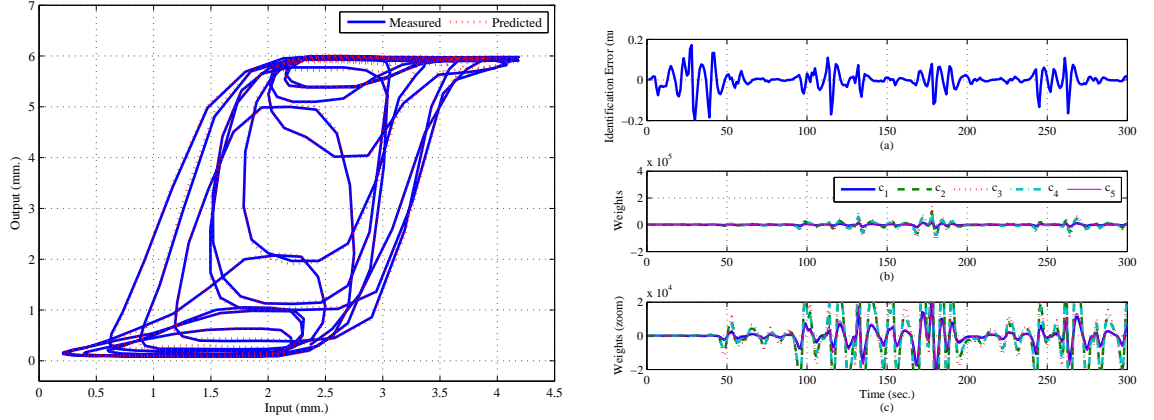


Figure 6.25: 5th order linear Laguerre filter with input $SNR = \infty$ dB, $\lambda = 0.9$ and $T_s = 1$ sec.. Left: Hysteresis measured and Predicted, Right:(a)Identification Error (b) Filter Weights.

SMA actuator.

Material preparation: Although the above advantages are interesting the antagonistic actuator has other problems. The repeated cyclic loading of SMA antagonistic wires results in the accumulation of plastic strain in the actuators which can diminish their actuation stroke. In [Sofla et al. \(2008b,a\)](#) it was showed that shape recovery is reduced by the repetitive actuation. However it was found that the degradation was stabilized after a relatively small number of cycles. The effect of shape memory pre-strain on the degradation was also investigated and a thermomechanical treatment was suggested that reduces the degradation in the antagonistic actuator. For the development of the antagonistic actuator in this thesis a relatively similar approach was followed. The steps taken to develop the antagonistic actuation system are summarized below:

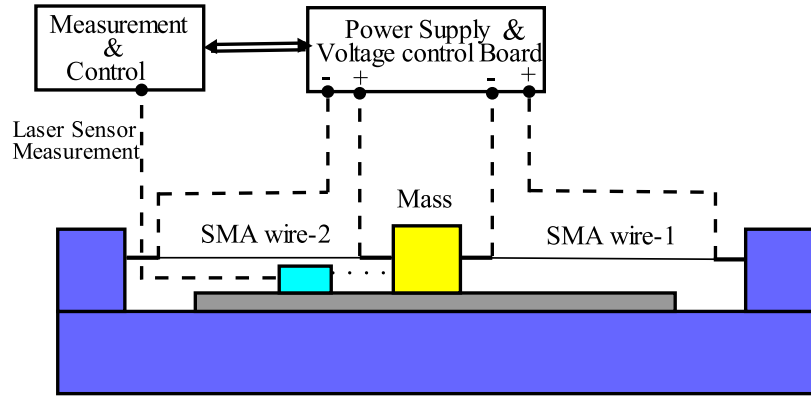


Figure 6.26: Sketch of the actuator

Step-1 A given length of Nitinol was chosen and cut into two halves.

Step-2 Each half was processed through the steps of thermomechanical treatment as that of a single wire which was discussed earlier.

Step-3 Both the wires were mounted onto the experimental setup as shown in Fig. 6.26 with one end of wire-1 fixed to the frame and the other end to the mass. One end of wire-2 was fixed to the opposite side of the mass and the other end of wire-2 is left free initially.

Step-4 Force is now applied to the free end of wire-2 such that a total strain of 4% is obtained and then the free end of wire-2 is also fixed to the frame of the setup. It is assumed that the strain is distributed as 2% + 2% in the two wires.

Step-5 Finally the antagonistic actuator was subjected to a cyclic input of symmetric sinusoidal signal.

After performing the above steps of thermomechanical treatment and the cyclic loading, degradation was initially visible. After approximately 50 cycles it was observed that the degradation had stopped (no precision measurement was made of the degradation). After 50 cycles it was noted from visual observation that the actuator had stabilized although with reduced actuation stroke and eventually introducing slack in the actuation system. Indeed the degradation in the antagonistic setup was also observed in Sofla *et al.* (2008b,a); Pathak (2010) and the problem is also discussed in Ditman *et al.* (1996). In the next paragraph the setup for modeling and control is discussed.

Setup for Modelling and control: The setup consists of two Nickel-Titanium wires of $200 \mu\text{m}$ diameter and 10 cm in length. The Austenite start temperature is 65°C and Austenite finish temperature is 93°C . The measured resistance was roughly 3Ω including contact resistance. The measurements available are displacement, thanks to a Waycon LAS-TM-10 ($5 \Omega\text{ m}$, sampling period 1 ms), and voltage across the wire. The temperatures were not measured. Two linear power supply using standard automotive

operational amplifiers were specially developed for the application, delivering 0 to 8V up to 3 A with a 5 kHz bandwidth. To protect the wire from overheating the applied voltages are limited to 3 V and 0.5 A. Each one is dedicated to the heating of one of the wire, and the signal is “routed” to one of the amplifier according to the direction of the demanded displacement simply by testing the sign of the reference signal. Other hardware solutions can be implemented using diodes (Moallem & Tabrizi, 2009), which requires only one power supply. However this solution was not initially adopted to avoid the deadband near zero volts induced by the diode’s threshold voltage.

Antagonistic Actuator: Open loop Identification

Tab. 6.17 and Tab. 6.18 sum up the mean error, mean square error, best fit (BFT) and variance accounted for (VAF) of the Laguerre model for various forgetting factor and sampling rate. The analysis is performed here in the same manner as it has been done in the case of the single wire actuator in the previous sections. As it had been understood before to be able to identify the nonlinearity, only the latest measurements should be taken into account, but too small a forgetting factor will cause sensitivity to noise. Thus this factor is predominant in the tuning of the identification and should be chosen carefully. In Fig. 6.27 and Fig. 6.28 we can see the actual measurement and the a priori prediction. It illustrates the influence of λ and of the Laguerre model’s truncation. Clearly, a second order filter and a forgetting factor of 0.9 gives excellent results compared with the same filter with $\lambda = 1$. However, in the context of the identification in closed loop, because the control signal might not be persistently exciting, robustness also comes into consideration. Similarly in order to test the robustness of the identification algorithm to sampling rate the experiments were conducted by reducing the sampling rate from 0.01 sec to 0.1 sec and 1 sec by fixing the forgetting factor $\lambda = 0.99$. The results in Tab. 6.18 show that the identification has not deteriorated vastly by reducing to 0.1 sec but further reduction increases the MSE drastically. The combination of Laguerre Filter and the RLS algorithm, although simple, can be shown to be similar to instrumental variable identification technique (Zervos *et al.*, 1988) which are usually robust.

Remark 6.5.1. *As observed from the material preparation of the antagonistic actuator, the repeated cyclic actuation had deformed the SMA wire which in turn introduced slacking or an inactive displacement range. Since the displacement is usually measured on the mass interconnecting the two SMA wires, this inactive displacement range is like a dead-zone and the mass does not displace to a smaller input reference voltage specially in open loop. Hence while performing open loop identification only the major loops of the hysteresis curve were simulated by activating the actuator to the maximum stroke.*

6.6 Conclusion

In this chapter recursive identification has been verified for a hysteretic system like SMA using an orthogonal filter like Laguerre. The resulting identified model can be considered as a projection of the actual system on to the Laguerre basis, by identifying a local linearized model of the nonlinear system at each instant. Further when Laguerre functions are used to approximate the Volterra kernels, it reduces the order

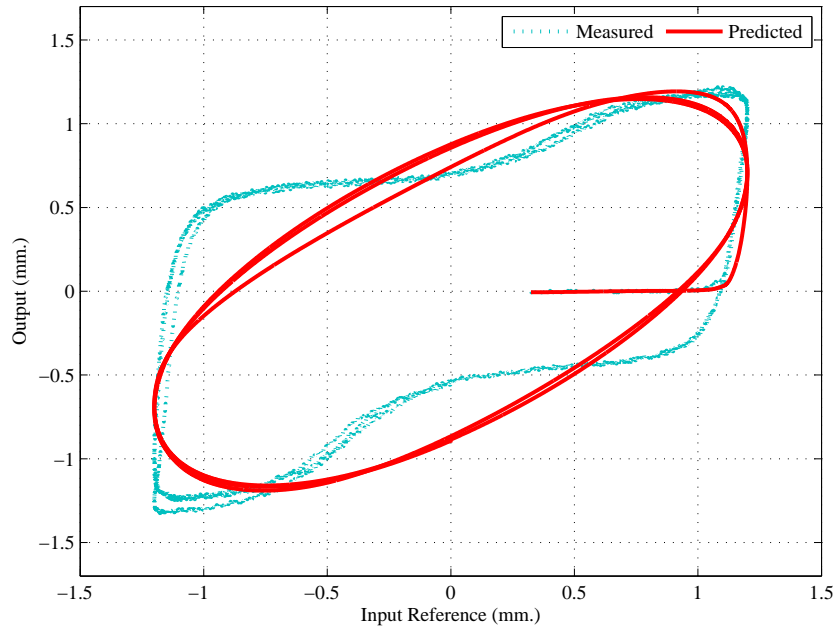


Figure 6.27: Identification of the output of the actuator with $\lambda = 1$ using a 2nd order filter.

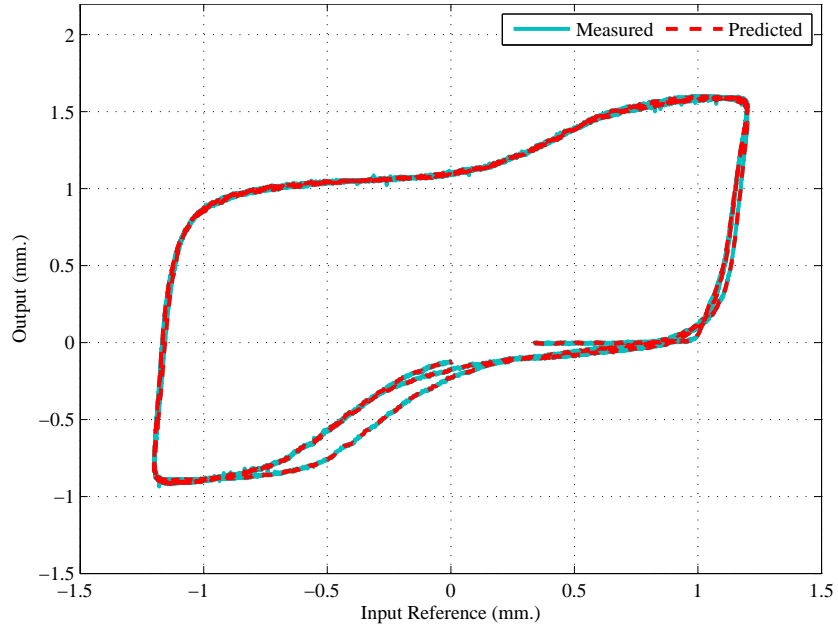


Figure 6.28: Identification of the output of the actuator with $\lambda = 0.9$ using a 2nd order filter.

Chapter 6. Modelling

| λ | MSE (mm^2) | BFT (%) | VAF (%) | Mean Error (mm) |
|-----------|------------------------|---------|---------|------------------------|
| 1 | 0.072 | 68.593 | 90.529 | 0.056 |
| 0.99 | 3.395×10^{-4} | 97.924 | 99.957 | 0.001 |
| 0.9 | 1.144×10^{-5} | 99.619 | 99.998 | 1.257×10^{-6} |
| 0.5 | 3.559×10^{-7} | 99.932 | 100 | 5.517×10^{-8} |

Table 6.17: Antagonistic:2nd Order linear Laguerre Filter with Input $SNR = \infty$ dB and different Forgetting factor λ .

| T_s sec | MSE (mm^2) | BFT (%) | VAF (%) | Mean Error (mm) |
|-----------|------------------------|---------|---------|-----------------|
| 0.01 | 3.395×10^{-4} | 97.924 | 99.957 | 0.001 |
| 0.1 | 1.950×10^{-4} | 98.372 | 99.973 | 0.001 |
| 1 | 0.033 | 78.690 | 96.661 | 0.095 |

Table 6.18: Antagonistic:2nd Order linear Laguerre Filter with Input $SNR = \infty$ dB and different sampling rate T_s .

of the identified model without considerable degradation in the identification. Different design parameters of the EF-RLS algorithm such as forgetting factor and sampling rate have been studied. Both parameters affect the identified linearized system since they define the number of data samples taken into account for identification. From observation it could be seen that with lower value of forgetting factor λ , the identified model is better with higher percentage of data fitted as expected but also identifies the input noise, which could be problematic for closed loop control. Therefore for control purposes λ might have to be increased. As far as the sampling rate is concerned the identification techniques perform well over a wide range of values but it degrades with slower sampling rates in the presence of noise. The observation of the experience using EF-RLS were also common to identification problem of Antagonistic actuator. During the extensive analysis of the EF-RLS method it was observed that the algorithm was suffering from the problem of covariance windup which eventually resulted in bursting of the parametric behaviour. This phenomenon would eventually be transmitted to the closed loop control and would create more problems to the actuator control. Eventually after extensive analysis of different RLS algorithms such as modified covariance RLS, variable λ RLS, it was concluded that the robust algorithm of directional forgetting RLS (DF-RLS) is the method which we need for adaptive modelling of the SMA actuator and finally be used in chapter-3 for classical Laguerre predictive control. It must also be mentioned that the analysis of EF-RLS was also essential in the development of a modified adaptive control which will be used in the chapter-3. Finally it has to be ascertained that the experiences gathered in the adaptive modelling in the current chapter is extensively helpful to develop and understand the adaptive control which will be the core area of the research handled in the following chapter.

Chapter 7

Adaptive Predictive Control

7.1 Introduction

The objective of this chapter is to develop and analyze an effective adaptive control strategy to tackle the hysteresis problem in the SMA actuator. In open-loop the hysteresis poses serious problem as can be seen in Figure 7.1(left), with the input reference and displacement response seen in Figure 7.1(right). The hysteresis behavior of the SMA actuator also changes over a period of time due to fatigue from cyclic thermal loading. For example compare the hysteresis in Figure 6.10 with Figure 7.1. The hysteresis in Figure 7.1 was measured after the SMA actuator had been subjected to a large number of cyclic thermal loading. These problems are very challenging from modeling and control point of view and hence adaptive modeling and control methods have been used here. An adaptive Laguerre predictive control method is preferred here due to the ease of modeling and implementation of adaptive control.

In the following section the closed loop identification methods are briefly explained. Then the basic idea of predictive control method is explained along with the discussion of suitable closed loop identification method for MPC. Further the predictive control method is dealt in detail which includes discussion on optimal input, prediction from state-space model and computing control signal from quadratic cost function. Broadly the results in this chapter can be classified into implementation of Classical Laguerre Predictive (CLaP) control and Modified Laguerre Predictive (MLaP)control. In the case of CLaP the problem of stability, robustness and parametric bursting is discussed in the context of control of single wire SMA actuator. In the case of MLaP the stability problem is also addressed and the experimental validation is performed on the single wire SMA actuator as well as a more complicated SMA actuator of the antagonistic type.

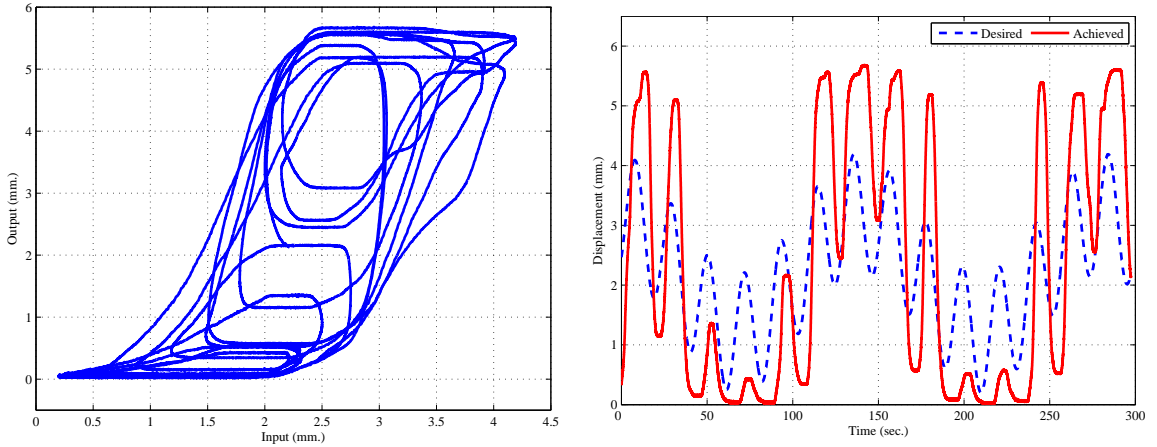


Figure 7.1: Left: Hysteresis measured in the single wire SMA actuator, Right: Input reference and the output displacement.

7.2 Closed Loop Identification (Offline/Non-Adaptive)

Closed loop identification is the process in which plant models are identified using data collected from closed loop experiments, where the process to be controlled is fully or partly under feedback as seen in Figure 7.2. The reference signal $r(t)$ is uncorrelated with the measurement noise $v(t)$. G and K are the plant and the controller respectively. The closed loop system equations are:

$$y(t) = GKSr(t) + Sv(t) \quad (7.1)$$

$$u(t) = SKr(t) - KSv(t) \quad (7.2)$$

where the sensitivity function is given by $S = (1 + KG)^{-1}$. Many open loop estimation methods fail when directly applied to closed loop data obtained from tests. The main reason for this is the correlation between the input reference and the unmeasurable noise. For example subspace approach and nonparametric methods would not work unless special measures are taken (Forssell & Ljung, 1999). The prediction error method is of the methods which work in the presence of input reference and noise correlation (Forssell & Ljung, 1999). Prediction error methods will consistently estimate if the data is informative and the model set contains the true system, irrespective of the closed loop feedback condition (Ljung, 1999). Next the closed loop estimation methods are briefly discussed which can be classified into direct, indirect and joint input-output methods which are discussed in brief here (Forssell & Ljung, 1999):

Direct method: In this approach the basic prediction error method is applied in a straightforward manner. The output $y(t)$ of the process and the input $u(t)$ are used in the same way as for the open loop identification ignoring any possible feedback and not using the reference signal $r(t)$ to estimate the model.

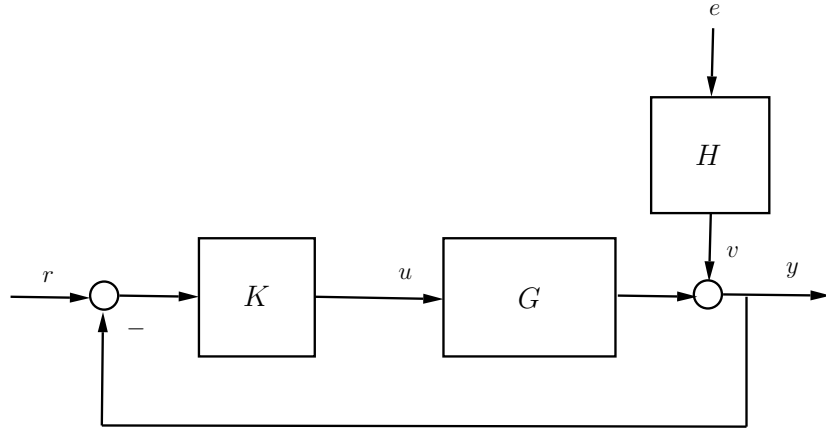


Figure 7.2: Closed loop system.

Indirect method: The closed loop system is identified from the reference input $r(t)$ to the output $y(t)$. From this identified closed loop system the open loop system is retrieved by precise knowledge of the controller.

Joint Input-Output method: The output $y(t)$ of the process and the input $u(t)$ of the plant are considered as outputs of a system driven by the reference input $r(t)$ and noise $v(t)$. Information about the plant and controller are retrieved from this joint model.

7.3 Introduction to Predictive control

Model Predictive control (MPC) refers to a family of controllers that use a distinctly identifiable model of the system to predict its future behaviour over an extended prediction horizon. A performance objective to be minimized is defined over the prediction horizon. This cost function is minimized by evaluating a profile of manipulated input moves to be implemented at successive instants over a control horizon. Closed loop optimal feedback is achieved by implementing only the first manipulated input move and repeating the complete sequence of steps at the subsequent sample time.

MPC depends on a model of the process to provide an optimal process input. The process model is usually obtained after conducting open loop tests on the process to be controlled. The performance of the model predictive control is closely related to the accuracy of the model employed: the performance usually degrades with poor model. Many types of predictive control methods have been developed to suit the necessity of different process. In all the different methods the closed loop performance is better if the model follows the process as closely as possible at all times during the operation. Therefore, the closed loop performance could deteriorate in operation over a period of time due to wearing and ageing of the subsystems. If the closed-loop performance of a given MPC deteriorates beyond a certain level, then re-identification of the process model in closed loop is needed in order to save time from performing open loop

identification (after dismantling the subsystems). Therefore development of closed loop identification techniques are necessary for MPC methods, specially in the presence of constraints ([Hjalmarsson *et al.*, 1996](#)).

7.3.1 Closed loop Identification (Non-Adaptive) for MPC

Normally in closed loop identification methods the controller is assumed to be linear and the process is single input single output. Practically the MPC controllers are not linear because of constraints which are often used on real systems. The plants are also multivariable making many closed loop identification methods not suitable for MPC applications. According to [Forssell & Ljung \(1999\)](#) the indirect and joint input-output approaches are typically used when the feedback law is linear, although they can also be used with nonlinear controllers. The MPC methods specially when using optimization with constraints makes the usage of the above two methods less attractive. Some extension such as the joint input-output approach using projection method works well with nonlinear controller. However they depend on derivation of non-causal finite impulse response (FIR) models which are non parametric methods. On the other hand, according to [Zhu & Butoyi \(2002\); Zhu \(1998\)](#) parametric models are better for usage in industrial process identification since these models are accurate and require short test time and can be more user friendly as compared to nonparametric models. Thus for many problems like industrial processes which are controlled by MPC, nonparametric models are not ideal which makes the projection method not ideal to be used.

The direct closed loop identification is thus the most preferable choice when MPC controllers are used ([Ljung, 1999](#)) due to the following advantages:

1. this method works regardless of the complexity of the controller,
2. no special algorithms and software are required,
3. consistency and optimal accuracy are obtained if the model set contains the true system and
4. unstable systems can be handled without problems, as long as the closed loop system is stable and the predictor is stable.

The only drawback with direct approach is that a good noise model is needed in order to prevent bias in the estimation of the plant model.

7.4 Predictive control as Receding Horizon Problem

The basic idea of receding horizon which is the core to the concept of Predictive control is discussed in this section. The system here is considered to be a single-input single-output (SISO) plant and a discrete time setting is assumed with the current time being defined as time step t . At current time the plant output is $y(t)$ and the history of the plant output trajectory can be seen in the Figure 7.3. The setpoint trajectory that the plant should follow can also be seen. The value of the setpoint trajectory at any time τ is denoted by $s(\tau)$. Distinct from setpoint trajectory is the reference trajectory. It starts at the current output $y(t)$ and defines an ideal trajectory that the plant should follow in order to reach the setpoint trajectory after, for instance, a

perturbation has occurred. The reference trajectory therefore defines the closed loop behaviour of the controlled plant. It is normally assumed that the reference trajectory approaches the setpoint exponentially from the current output value. Let us define the reference $r(t + j|t)$ which says that the reference trajectory depends on the conditions at time t .

Now coming back to the predictive controller, this method uses an internal model to predict the behaviour of the plant, starting at current time, over a future prediction horizon. This predicted behaviour depends on the assumed input trajectory $\hat{u}(t + j|t)$ where $\{j = 0, 1, \dots, H_p - 1\}$ which has to be applied over the prediction horizon, and the idea is to select the input which promises the best predicted behaviour. In our discussion it is assumed that the internal model is linear. Here it is assumed that the output measurement $y(t)$ is available when calculating the value of input $u(t)$ ¹. The internal model must therefore be strictly proper, that is $y(t)$ depends on the past inputs $u(t-1), u(t-2), \dots$, but not on the input $u(t)$.

A simple solution is that we choose the input trajectory such as to bring the plant output at the end of the prediction horizon (i.e., at time $(t + H_p)$), to the required reference value $r(t + H_p)$. In this case a terminology often used is that to have a single “coincidence point” at time $(t + H_p)$. There can be several input trajectories $\{\hat{u}(t|t), \hat{u}(t+1|t), \dots, \hat{u}(t+H_p-1|t)\}$ which could achieve this task, and a single input is chosen according to some criterion e.g. the smallest input energy. Generally, it is adequate and preferable to chose an input trajectory with simple structure and parametrized by a small number of variables. For example in Figure 7.3 the input is assumed to vary only over the first three steps of the prediction horizon and then remain constant from then onwards which is given as $\hat{u}(t+2|t) = \hat{u}(t+3|t) = \dots = \hat{u}(t+H_p-1|t)$, so that there are three parameters to choose such as $\{\hat{u}(t|t), \hat{u}(t+1|t), \hat{u}(t+2|t)\}$. Note that even more simple structure can be considered. In the development later presented (see section 7.4) the input will remain constant over the prediction horizon i.e.: $\hat{u}(t|t) = \hat{u}(t+1|t) = \dots = \hat{u}(t+H_p-1|t)$. In this case there is only one parameter such as $\hat{u}(t|t)$ since there is only one equation to be satisfied which can be given as $\hat{y}(t+H_p|t) = r(t+H_p|t)$.

After a future input trajectory is chosen, only the first element of that trajectory is applied as input signal to the plant. That is we set $u(t|t) = \hat{u}(t|t)$ where $u(t|t)$ denotes the actual control signal applied. Then the whole process of output measurement, prediction and input trajectory determination is because the prediction horizon remains of the same length, but moves along by one sampling interval at each step, this method of controlling a given process is a receding horizon control.

1. The notation $\hat{u}(t)$ as compared to $u(t)$ shows that at time t we only have a prediction of what the input at time $(t + j)$ may be. The actual input at that time $u(t + j)$ could probably be different from $\hat{u}(t + j|t)$.

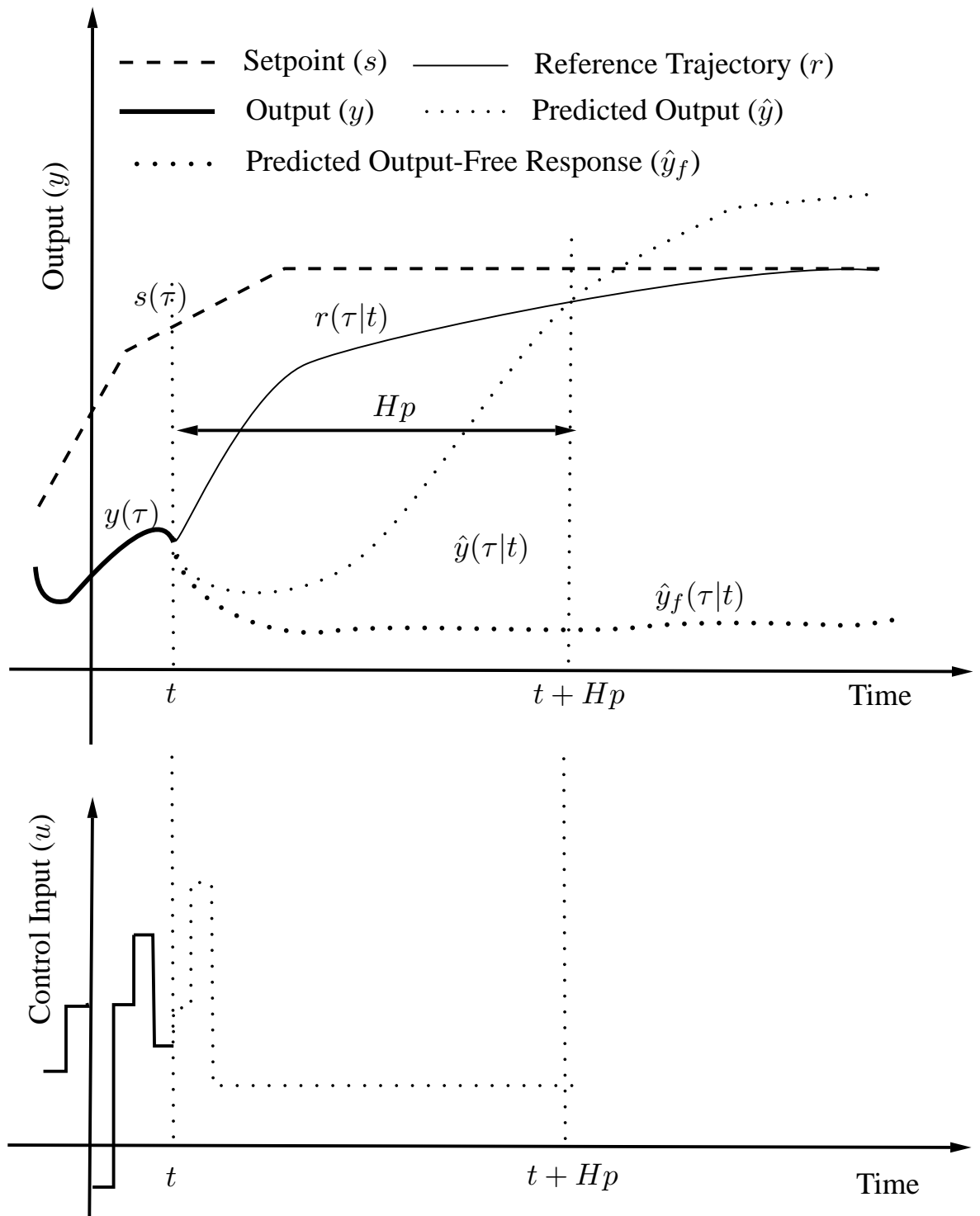


Figure 7.3: Predictive control: basic idea (Maciejowski, 2000)

Computing optimal inputs

For simplicity, the case with one coincidence point and only one parameter for future input trajectory is considered here. In such a case a unique solution is possible². For simplicity in notation, the dependence of the variables on time t is assumed: for instance $u(t|t)$ will be noted $u(t)$ and similarly for the other signals. The coincidence point occurs at time $(t + H_p)$ and one input parameter $\hat{u}(t)$ is to be defined. The internal model is first used to predict the free response $\hat{y}_f(t + H_p)$ of the plant, which is the response which will be obtained at the coincidence point if the future input trajectory remained at the latest value $u(t - 1)$. The method by which this can be obtained depends on the type of the model used due to the initial conditions it requires. If a step or pulse response is used as a model, then all the available past inputs are needed. For a transfer function or difference equation model, n past inputs and outputs are needed, where n is the order of the transfer function. For a state space model, the current state is needed, or an estimate of it. Now let $S(H_p)$ be the response of the model to a unit step input, H_p steps after the unit step is applied.

The predicted output at time $(t + H_p)$ is

$$\hat{y}(t + H_p) = \hat{y}_f(t + H_p) + S(H_p)\hat{u}(t) \quad (7.3)$$

Since the goal is to achieve:

$$\hat{y}(t + H_p) = r(t + H_p) \quad (7.4)$$

the optimal input can be given by:

$$\hat{u}(t) = \frac{r(t + H_p) - \hat{y}_f(t + H_p)}{S(H_p)} \quad (7.5)$$

Predictive control and Models

From a modeling point of view, predictive control methods can be classified into two main categories:

- methods that use a structured model representation, e.g. ARMAX or CARIMA models.
- methods that use an unstructured model representation, e.g. an impulse-response-based model or an orthonormal-series-based model.

In De Keyser & Van Cauwenbergh (1981), an ARMAX model is used to derive the extended-prediction self-adaptive controller (EPSAC). The EPSAC needs n self-tuning k -step-ahead predictors in parallel, where n is the model order. Here the

2. A more general approach consists in considering more coincidence points along with more input parameters. This results in a larger number of equations to be satisfied which is more difficult constraints to satisfy. That is, it is impossible to choose the future input trajectory such that the predicted output coincides with the reference inputs at all the coincidence points. Then a least square solution must be found that would satisfy a criterion such as the sum of squares of the errors $\sum_{j \in P} [r(t + j|t) - \hat{y}(t + j|t)]^2$ (where P is the set of time samples corresponding to the coincidence points). If the internal model used for the controller is linear then the least square problem can be solved easily.

Diophantine equation has to be solved for each predictor. In [Golden et al. \(1986\)](#) an ARMA model is used to derive the extended-horizon predictive control (EHC) using the receding horizon idea. In [Clarke et al. \(1987\)](#) a CARIMA model is used to derive the standard version of the GPC using a recursive solution of the Diophantine equation. In Model Algorithmic Control (MAC) the impulse response coefficients are used to model the plants ([Richalet et al., 1978](#)). In Dynamic Matrix Control (DMC) ([Cutler & Johnston, 1985](#)) the impulse response coefficients are used to derive the step response coefficients which are then used in the dynamic matrix. The use of impulse response coefficients is based on the assumption that the impulse response of the true plant converges to zero. This in turn means that the MAC and DMC are applicable only to stable systems. Furthermore, if the open loop system is poorly damped, the number of coefficients required to represent the system effectively increases.

Contrary to the above mentioned models there are many advantages in using Laguerre function-based models ([Elshafei et al., 1994](#)):

1. Any stable system can be modelled without the need for accurate information on the true plant order and time delay.
2. The Laguerre functions can represent signals which exhibit long time delays because of their similarity to Padé approximation.
3. Finally in the presence of unmodelled dynamics and noise in the system, contrary to ARMAX model using a Laguerre function based model results in an unbiased estimate of the nominal plant.

Remark 7.4.1. *Both structured and unstructured models in state-space form can be used to derive predictive control schemes. Most importantly, Laguerre function will be used here in the state-space form for the implementation of the predictive control strategy. Hence in the following section prediction models are developed in the state-space form.*

Prediction with state-space models

Although predictions can be made from other type of models such as transfer function, only state-space models will be dealt here. Consider the state space model which gives the one step prediction:

$$\begin{aligned} l(t+1) &= Al(t) + Bu(t) \\ y(t+1) &= Cl(t+1) \end{aligned} \tag{7.6}$$

The above equation can be used recursively to find predictions at other instances for example write (7.6) at time $(t+2)$

$$\begin{aligned} l(t+2) &= Al(t+1) + Bu(t+1) \\ y(t+2) &= Cl(t+2) \end{aligned} \tag{7.7}$$

now substitute (7.6) into (7.7) and to eliminate $l(t+1)$

$$\begin{aligned} l(t+2) &= A^2l(t) + ABu(t) + Bu(t+1) \\ y(t+2) &= Cl(t+2) \end{aligned} \quad (7.8)$$

The recursion can be reiterated to get a H_p -step ahead prediction that writes:

$$l(t+H_p) = A^{H_p} + A^{H_p-1}Bu(t) + A^{H_p-2}Bu(t+1) \cdots + Bu(t+H_p-1) \quad (7.9)$$

$$y(t+H_p) = C [A^{H_p}l(t) + A^{H_p-1}Bu(t) + A^{H_p-2}Bu(t+1) \cdots + Bu(t+H_p-1)] \quad (7.10)$$

Hence the above prediction equations can collected in the form of matrix and written as follows

$$\underbrace{\begin{bmatrix} l(t+1) \\ l(t+2) \\ l(t+3) \\ \vdots \\ l(t+H_p) \end{bmatrix}}_{\overrightarrow{l}} = \underbrace{\begin{bmatrix} A \\ A^2 \\ A^3 \\ \vdots \\ A^{H_p} \end{bmatrix}}_{K_A} l(t) + \underbrace{\begin{bmatrix} B & 0 & 0 & \dots \\ AB & B & 0 & \dots \\ A^2B & AB & B & \dots \\ \vdots & \vdots & \vdots & \vdots \\ A^{H_p-1}B & A^{H_p-2}B & A^{H_p-3}B & \dots \end{bmatrix}}_{K_{AB}} \underbrace{\begin{bmatrix} u(t) \\ u(t+1) \\ u(t+2) \\ \vdots \\ u(t+H_p-1) \end{bmatrix}}_{\overrightarrow{u}(t-1)} \quad (7.11)$$

and

$$\underbrace{\begin{bmatrix} y(t+1) \\ y(t+2) \\ y(t+3) \\ \vdots \\ y(t+H_p) \end{bmatrix}}_{\overrightarrow{y}} = \underbrace{\begin{bmatrix} CA \\ CA^2 \\ CA^3 \\ \vdots \\ CA^{H_p} \end{bmatrix}}_{K_{CA}} l(t) + \underbrace{\begin{bmatrix} CB & 0 & 0 & \dots \\ CAB & CB & 0 & \dots \\ CA^2B & CAB & CB & \dots \\ \vdots & \vdots & \vdots & \vdots \\ CA^{H_p-1}B & CA^{H_p-2}B & CA^{H_p-3}B & \dots \end{bmatrix}}_{K_{CAB}} \underbrace{\begin{bmatrix} u(t) \\ u(t+1) \\ u(t+2) \\ \vdots \\ u(t+H_p-1) \end{bmatrix}}_{\overrightarrow{u}(t-1)} \quad (7.12)$$

The above equations can be written in a more compact form as:

$$\underbrace{l}_{\overrightarrow{l}}(t) = K_A l(t) + K_{AB} \underbrace{u}_{\overrightarrow{u}}(t-1) \quad (7.13)$$

$$\underbrace{y}_{\overrightarrow{y}}(t) = K_{CA} l(t) + K_{CAB} \underbrace{u}_{\overrightarrow{u}}(t-1) \quad (7.14)$$

where K_A, K_{AB}, K_{CA} and K_{CAB} are the respective matrices defined in the above equations.

Remark 7.4.2. In the above section we have derived the state-space prediction equation. In the following sections the notation $\hat{y}(\cdot)$ will be the predicted output which is distinct from the true output $y(\cdot)$ of the system.

Optimal input from quadratic cost

The objective of the predictive control is to find a control law that minimizes the error between the predicted plant output $\hat{y}(t + j)$ and the future trajectory of the reference $y_r(t + j)$ given at instant $(t + j)$ with $0 < j \leq H_p$. Now define a cost function

$$J = \sum_{j=1}^{H_p} q(j) (y_r(t + j) - \hat{y}(t + j))^2 + r(j) u(t + j - 1)^2 \quad (7.15)$$

where $q(j)$ and $r(j)$ are tracking error and control effort weights used in order to add more flexibility in the controller design.

The minimization of this index calculated by:

$$\{u(t), \dots, u(t + H_p - 1)\} = \arg \min_{u(t), \dots, u(t + H_p - 1)} J \quad (7.16)$$

gives a sequence of future controls $\{u(t), \dots, u(t + H_p - 1)\}$ with H_p being the prediction horizon. It should be duly noted that the minimization is a quadratic programming problem and can be solved using standard optimization algorithms. But in the absence of constraints the minimization problem can be considered as a least square problem. The analytic solution ([Ikonen & Najim, 2002](#)) to the minimization problem can be give by

$$u(t) = \frac{\left[\underline{y}_r(t) - K_{CA} l(t) \right] Q K_{CAB}^T}{K_{CAB}^T Q K_{CAB} + R} \quad (7.17)$$

where the K_{CA}, K_{CAB} is obtained from (7.14) and the reference signal vector $\underline{y}_r(t)$ is given as below

$$\underline{y}_r(t) = [y_r(t) \ \cdots \ y_r(t + H_p)]^T \quad (7.18)$$

and the matrices are

$$Q = \text{diag}[q(1) \cdots q(H_p)], \quad R = \text{diag}[r(1) \cdots r(H_p)] \quad (7.19)$$

Consider the modified prediction equation with feedback rectification e , with prediction at $t = H_p$ given as

$$\hat{y}(t + H_p) = \hat{C}^T l(t + H_p) + e \quad (7.20)$$

where $e = y(t) - \hat{y}(t)$. The feedback rectification term is added to the prediction equation in order to take into consideration the errors due to identification and \hat{C} is the identified Laguerre filter weights. Now substituting $\hat{y}(t) = \hat{C}^T l(t)$ and further manipulating

$$\hat{y}(t + H_p) = y(t) + \hat{C}^T [l(t + H_p) - l(t)] \quad (7.21)$$

Now the objective is to obtain $y_r(t + H_p) = \hat{y}(t + H_p)$. Further substitute the prediction for $l(t + H_p)$ into Eq. (7.21) and use the cost function in Eq. (7.15) and set $y_r(t + H_p)$ to the the desired system output w which is also dependent on time t . Further suppose that $u(t) = u(t+1) = \dots = u(t+H_p-1)$, and that the weighting $q(j) = q$ and $r(j) = r$ for all j , an optimal solution can be given by:

$$u(t) = \frac{\left[w - y(t) - \hat{\Psi}^T(t)l(t) \right] Q\hat{\Phi}(t)}{\hat{\Phi}^T(t)Q\hat{\Phi}(t) + R} \quad (7.22)$$

where:

$$\hat{\Phi}(t) = \hat{C}^T(t) \sum_{j=1}^{H_p} A^{H_p-j} B \quad (7.23)$$

is a scalar gain involving the first H_p Markov parameters of the system and:

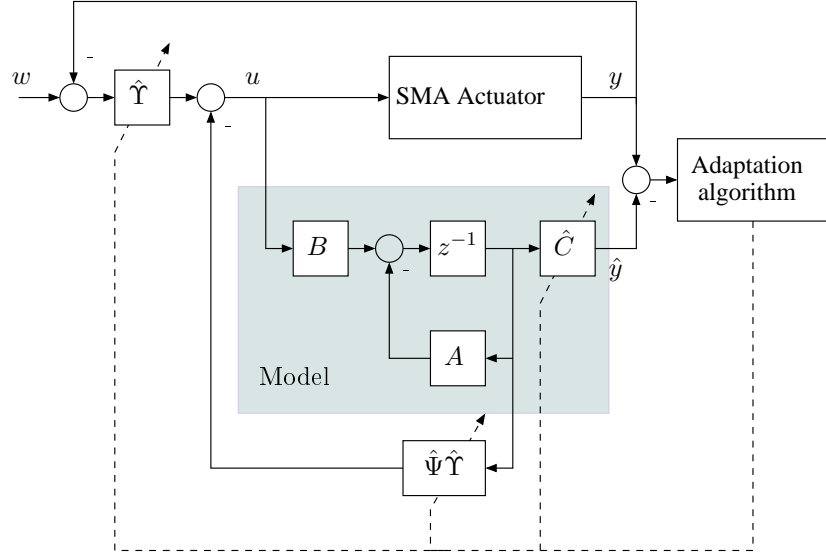
$$\hat{\Psi}^T(t) = \hat{C}^T(t)(A^{H_p} - \mathbb{I}) \quad (7.24)$$

where \mathbb{I} is the identity matrix and the weightings matrices are replaced by scalar ($Q = q$ and $R = r$) to ponderate the tracking error and the control effort respectively. Increasing or decreasing of the values of Q and R would effect the penalization of the tracking error and control signal used to control the system. The prediction horizon H_p is another important tuning factor as it indirectly influence the transient in that the controller is meant to reach the reference in a given time span. The tuning of the prediction horizon is very crucial. The value of prediction horizon H_p should be larger than the time delay in the system (if it exists) such that $\hat{\Phi} \neq 0$ and in general the criteria to satisfied while choosing H_p is that (Huzmezan *et al.*, 2002)

$$\hat{\Phi}(t)\text{sign}(\hat{C}^T(t)(I - A)^{-1}B) \geq 0.5|C^T(I - A)^{-1}B| \quad (7.25)$$

The CLaP method can be implemented using the schematic shown in Fig. 7.4. In Fig. 7.4 we can see that the $\{A, B, \hat{C}(t)\}$ matrices constitute the Laguerre approximation of the system to be controlled and are directly used in the predictive controller based on certainty equivalence principle. The matrices A and B are precalculated by the choice of the Laguerre pole a and the vector \hat{C} is identified in realtime. The controller is implemented using Eq. (7.22) where seen in Fig. 7.4, $\hat{\Psi} = Q\hat{\Phi}(t)(\hat{\Phi}^T(t)Q\hat{\Phi}(t) + R)^{-1}$ and as given earlier $\hat{\Psi}(t) = C^T(t)(A^{H_p} - I)$. The controller is time varying since $\hat{C}^T(t)$ is identified at each instant using the RLS algorithm which has been discussed earlier. Since model used in the given predictive control is identified explicitly in realtime, the discussed method is considered as Indirect Adaptive Predictive Control (Huzmezan *et al.*, 2002).

The advantage of using Laguerre model can be seen here as by choice of Laguerre pole we can precalculate the controller partially. Although nonlinear versions of the


 Figure 7.4: Classical Laguerre Predictive control (Zervos *et al.*, 1988)

Laguerre model exist (Dumont & Fu, 1993b) using Volterra Laguerre functions, linear models could also be used to control nonlinear system using an assumption that the sampling rate of implementation of the linear controller is faster than the rate of change of the nonlinear system (Huzmezan *et al.*, 2002).

7.5 Stability and Robustness

In this section we will consider the closed loop system and analyse the stability behavior. Consider the controller (7.22) and for simplicity let $R = 0$, then we have

$$u(t) = \frac{[w - y(t) - \hat{\Psi}^T(t)l(t)]}{\hat{\Phi}(t)} \quad (7.26)$$

Further substituting the above equation in $l(t+1) = Al(t) + Bu(t)$ we have

$$l(t+1) = Al(t) + B\hat{\Phi}^{-1}(t)w - B\hat{\Phi}^{-1}(t)y(t) - B\hat{\Psi}^T(t)\hat{\Phi}^{-1}(t)l(t) \quad (7.27)$$

$$= Al(t) + B\hat{\Phi}^{-1}(t)w - B\Phi^{-1}(t)y(t) - B\hat{C}^T(t)(A^{H_p} - I)\hat{\Phi}^{-1}(t)l(t) \quad (7.28)$$

$$= Al(t) + B\hat{\Phi}^{-1}(t)w - B\hat{\Phi}^{-1}(t)y(t) - B\hat{C}^T(t)A^{H_p}\hat{\Phi}^{-1}(t)l(t) + B\hat{\Phi}^{-1}(t)\hat{y}(t) \quad (7.29)$$

$$= [A - BC^TA^{H_p}\hat{\Phi}^{-1}(t)]l(t) + B\hat{\Phi}^{-1}(t)[w + \hat{y}(t) - y(t)] \quad (7.30)$$

Stability

In-order to study the stability of the above system the following lemma which can be found in (Landau *et al.*, 1998):

Lemma 1. Consider the system:

$$l(t+1) = \mathcal{A}(t)l(t) + v(t) \quad (7.31)$$

1. $\mathcal{A}(t)$ has finite coefficients for all t
2. The eigenvalues of $\mathcal{A}(t)$ are inside the unit circle for all t
3. $\|\mathcal{A}(t) - \mathcal{A}(t-1)\| \rightarrow 0$ for $t \rightarrow \infty$

Then there exists a time t such that

$$\|l(t+1)\|^2 \leq C_1 + C_2 \max_{0 \leq \tau \leq t} \|v(\tau)\|^2; \quad 0 \leq C_1, C_2 < \infty \quad (7.32)$$

By examination of (7.30) and (7.31), we identify the following correspondences:

$$\left[A - BC^T A^{H_p} \hat{\Phi}^{-1}(t) \right] = \mathcal{A}(t) \quad (7.33)$$

and:

$$B\hat{\Phi}^{-1}(t) [w + \hat{y}(t) - y(t)] = \mathbf{v}(t). \quad (7.34)$$

Proposition 1. If the parameter vector \hat{C}^T is not orthogonal to the input vector B , and the excitation is persistently exciting the plant, then the gain $\hat{\Phi}(t)$ defined by (7.23) is bounded so that the following relation holds:

$$0 < |\hat{\Phi}(t)| < \gamma \quad 0 < \gamma < \infty \quad (7.35)$$

Proof 1. We begin the proof by introducing a special induced norm proposed by (Tao, 2003). Since the matrix A has the eigenvalue a (with order of multiplicity N), there is a matrix P such that $P^{-1}AP = J_a$ where J_a is the $N \times N$ Jordan block with value a on its diagonal. Let D be the diagonal matrix $D = \text{diag}\{1, \epsilon, \dots, \epsilon^{N-1}\}$ and define $Q = PD$, then the matrix:

$$J_\epsilon = Q^{-1}AQ = \begin{bmatrix} a & \epsilon & 0 & \dots & 0 \\ 0 & \ddots & \ddots & \ddots & \\ & \ddots & \ddots & \ddots & 0 \\ 0 & \dots & 0 & a & \epsilon \\ 0 & \dots & 0 & a & \end{bmatrix} \quad (7.36)$$

Defining the induced norm as:

$$\|A\|_2 = \max_{\|\bar{x}\|=1} \|AQ\bar{x}\|_2 \quad (7.37)$$

the norm of A writes:

$$\|A\|_2^2 = [\lambda \bar{x}_1 + \epsilon \bar{x}_2 \quad \dots \quad \lambda \bar{x}_{n-1} + \epsilon \bar{x}_n \quad \lambda \bar{x}_n] \begin{bmatrix} \lambda \bar{x}_1 + \epsilon \bar{x}_2 \\ \vdots \\ \lambda \bar{x}_{n-1} + \epsilon \bar{x}_n \\ \lambda \bar{x}_n \end{bmatrix} \quad (7.38)$$

thus

$$\|A\|_2^2 \leq (\lambda + \epsilon)^2 \|\bar{x}\|_2^2 \quad (7.39)$$

Similarly, since:

$$A^n = P^{-1} \begin{bmatrix} \lambda^n & \binom{n}{1} \lambda^{n-1} & \binom{n}{2} \lambda^{n-2} & \dots \\ 0 & \lambda^n & \binom{n}{1} \lambda^{n-1} & \ddots \\ \ddots & & \ddots & \\ 0 & & & \lambda^n \end{bmatrix} P \quad (7.40)$$

and it can be derived following the previous lines that:

$$\|A^n\|_2 \leq (\lambda + \epsilon)^n \quad (7.41)$$

We first prove that the gain is bounded for a given bounded $\hat{C}^T(t)$. From (7.23), one can think of $\Phi(\hat{H}_p, t)$ as a sequence depending on H_p . Therefore, using the norm discussed, we form the absolute increment of the sequence:

$$\|\hat{\Phi}(H_p + 1, t) - \hat{\Phi}(H_p, t)\| \leq \|\hat{C}^T(t)\| \|B\| (a + \epsilon)^{H_p} \quad (7.42)$$

choosing ϵ such that $|\epsilon| < 1 - |a|$, the limit of the increment when increasing the prediction horizon is:

$$\lim_{H_p \rightarrow \infty} \|\hat{\Phi}(H_p + 1, t) - \hat{\Phi}(H_p, t)\| = 0 \quad (7.43)$$

Thus the gain is increasing monotonically toward a limit. Furthermore, we can evaluate an upper bound. To do so recall the property:

$$\lambda[\mathcal{P}(A)] = \mathcal{P}(\lambda[A]) \quad (7.44)$$

where the shorthand notation $\lambda[A]$ means “the eigenvalues of A ”, and \mathcal{P} is a polynomial. Since A has one eigenvalue a with multiplicity N , it can be concluded that $\sum_{i=0}^{H_p} A^{H_p-i}$ has one eigenvalue of multiplicity N which writes:

$$\lambda \left[\sum_{i=0}^{H_p} A^{H_p-i} \right] = \sum_{i=0}^{H_p} a^{H_p-i} = \frac{(a)^{H_p} - 1}{a - 1} \quad (7.45)$$

Thus the limit of the norm of the gain can be bounded:

$$\lim_{H_p \rightarrow \infty} \|\hat{\Phi}(H_p + 1, t)\| \leq \lim_{H_p \rightarrow \infty} \frac{(a + \epsilon)^{H_p} - 1}{(a + \epsilon) - 1} \|\hat{C}^T(t)\| \|B\| \quad (7.46)$$

and, it comes finally:

$$\lim_{H_p \rightarrow \infty} \|\hat{\Phi}(H_p + 1, t)\| \leq \frac{1}{1 - (a + \epsilon)} \|\hat{C}^T(t)\| \|B\| \quad (7.47)$$

Therefore, it can be concluded that:

$$\|\hat{C}^T(t)B\| \leq \Phi(H_p, t) \leq \frac{1}{1 - (a + \epsilon)} \|\hat{C}^T(t)\| \|B\|$$

Now if the PE is respected, the parameter vector $\hat{C}(t)$ is bounded, hence $\|\hat{C}(t)\|^2 < \kappa^2$ where $0 < \kappa^2 < \infty$, and we can conclude that, under the assumption that $\hat{C}^T(t)B \neq 0$:

$$\|\hat{C}^T(t)B\| \leq \|\hat{\Phi}(t)\| \leq \frac{(a + \epsilon)^{H_p} - 1}{(a + \epsilon) - 1} \|\hat{C}^T(t)\| \|B\| \leq \frac{1}{(a + \epsilon) - 1} \kappa \|B\| = \gamma$$

which completes the proof.

Proposition 2. If the PE condition is respected, then $\hat{\Phi}(t + 1) - \hat{\Phi}(t)$ belong to \mathcal{L}_2 .

Proof 2. We have:

$$\|\hat{\Phi}(H_p, t + 1) - \hat{\Phi}(H_p, t)\| \leq \|\hat{C}^T(t + 1) - \hat{C}^T(t)\| \|B\| \frac{(a + \epsilon)^{H_p} - 1}{(a + \epsilon) - 1} \quad (7.48)$$

and since that, due to the PE condition, $\|\hat{C}^T(t + 1) - \hat{C}^T(t)\|$ belong to \mathcal{L}_2 , it follows that $\|\hat{\Phi}(H_p, t + 1) - \hat{\Phi}(H_p, t)\|$ also belongs to \mathcal{L}_2 .

In order to apply Lemma 1, we must now verify that $\mathcal{A}(t)$ has all eigenvalues less than one.

Proposition 3. Assuming that the PE condition holds, there exists a prediction horizon H_p such that the matrix $\mathcal{A}(t)$ defined by (7.33) is stable i.e. it has all its eigenvalues in the unit circle.

Proof 3. We derive the inequality:

$$\begin{aligned} \|\mathcal{A}\|^2 &\leq \|A\|^2 + |\Phi(t)|^{-2} \|B\hat{C}^T(t)\|^2 \|A^{H_p}\|^2 \\ &\leq \|A\|^2 + |\hat{C}(t)^T B|^{-2} \|B\hat{C}^T(t)\|^2 \|A^{H_p}\|^2 \end{aligned} \quad (7.49)$$

using the previously defined induced norm. Now consider the matrix $B\hat{C}^T$. Its rank is one, its column space is supported by the vector B and the corresponding eigenvalue is $\hat{C}^T(t)B$. We consider the case where $\hat{C}^T(t)B \neq 0$. Then, there exist a change of

basis matrix $M(t) = [B|C_1(t)^\perp|\dots|C_{N-1}(t)^\perp]$ ($C_i(t)^\perp$ are the column vectors forming a basis spanning the subspace orthogonal to \hat{C}). $M(t)$ is full rank, thus it is invertible and $B\hat{C}(t)^T = M(t)Z(t)M^{-1}(t)$. $Z(t)$ is a matrix for which entries are all nil except for the first one which is equal to $\hat{C}^T(t)B$. It follows that $z = \frac{1}{\hat{C}^T(t)B}Z(t)$ is a constant matrix with the first entry equals to one the others being nil. Thus, an upper bound for $\|\mathcal{A}(t)\|^2$ is:

$$\|\mathcal{A}(t)\|^2 \leq |a + \xi| + \|M(t)zM(t)^{-1}\||a + \xi|^{H_p} \quad (7.50)$$

Since $\|M(t)zM(t)^{-1}\|$ is finite and choosing $|\xi| < 1 - |a|$, it can then be concluded that there exists a value H_p such that the expression at the right hand side of the inequality is less than one.

With these results we can state that provided that the PE condition is verified and that $\hat{C}(t)B \neq 0$:

1. The coefficient of $\mathcal{A}(t)$ are bounded, which follows from the fact that the norm calculated previously is bounded (note that this is independent on H_p but necessitate the condition $\hat{C}(t)B \neq 0$);
2. The eigenvalues can be confined within the unit circle for an adequate choice of H_p ;
3. Due to the property of the identification algorithm which under the PE condition guarantees that $\lim_{t \rightarrow \infty} \|\hat{C}(t) - \hat{C}(t-1)\| = 0$ thus there exists a matrix M_∞ such that $\lim_{t \rightarrow \infty} = M_\infty$. Moreover we found that the gain $\hat{\Phi}(t)$ has a limit $\hat{\Phi}_\infty$ therefore $\lim_{t \rightarrow \infty} \|\mathcal{A}(t)\| = |a + \epsilon| - \hat{\Phi}_\infty \|M_\infty z M_\infty^{-1}\| |a + \epsilon|^{H_p}$

therefore the three requirements of the lemma are fulfilled.

Since $\mathcal{A}(t+1)$ has bounded coefficients $l(t)$ can become unbounded if $v(t)$ becomes unbounded. However, since w is bounded and due to the properties of DFRLS that ensures that $\lim_{t \rightarrow \infty} |\hat{y}(t) - y(t)| < \infty$, it follows that $v(t) < \infty$. Owing to the lemma, we can conclude that $l(t)$ is bounded.

Define the state error:

$$\varsigma(t) = l_s(t) - l(t) \quad (7.51)$$

Both the system and the model are subject to the state equations:

$$l_s(t+1) = Al_s(t) + Bu(t) \quad l(t+1) = Al(t) + Bu(t) \quad (7.52)$$

Substracting one gets the equation for the state error:

$$\varsigma(t+1) = A\varsigma(t) \quad (7.53)$$

which means that the state error vanishes to zero whatever the initial error is. Hence the closed loop system is stable.

Robustness to Nonlinear systems (Elshhafei et al., 1994)

Consider discrete-time non-linear dynamic system

$$l(t+1) = Al(t) + bu(t) \quad (7.54)$$

$$y(t) = cl(t) \quad (7.55)$$

where, A, b and c are nonlinear operators. Assume that the nominal plant (linearized model) is represented by

$$l(t+1) = \hat{A}l(t) + \hat{B}u(t) \quad (7.56)$$

$$y(t) = \hat{C}l(t) \quad (7.57)$$

Now assume that the feedback rectification $e = 0$ in Eq. (7.20) and for simplicity $w = 0$ the controller Eq. (7.26) can be given as

$$u = -\hat{C}^T \hat{A}^{H_p} \hat{\Phi}^{-1} l(t) \quad (7.58)$$

$$= -K^T l(t) \quad (7.59)$$

Before going into the stability study an important definition is necessary:

Definition 7.5.1 (Graph). (*Safonov, 1980*) If \mathbf{G} is the mapping of points $x \in \mathcal{X}$ into points $\mathbf{G}x \in \mathcal{Y}$, then the graph of \mathbf{G} is the relation

$$\text{Graph } (\mathbf{G}) \triangleq \{(x, y) \in \mathcal{X} \times \mathcal{Y} | x \in \mathcal{X} \text{ and } y = \mathbf{G}x\}. \quad (7.60)$$

The stability of the closed loop system is studied by the following lemma (*Safonov, 1980; Elshhafei et al., 1994*)

Lemma 2. Let the constant matrices $P \in \mathbb{R}^{n \times n}$ and $S \in \mathbb{R}^{n \times n}$ be symmetric positive definite solutions of the discrete Lyapunov equation

$$P = (A - \hat{B}K^T)P(A - \hat{B}K^T) + S \quad (7.61)$$

If uniformly for all $(l(t), u(t))$

$$\text{Graph} \left(P^{1/2} \left[A - \hat{B}K^T + \Delta A + \Delta B(-K^T) \right] \right) \quad (7.62)$$

is strictly inside $(0, P^{1/2})$ where $\Delta A = A - \hat{A}$ and $\Delta B = b - \hat{B}$, then the system described by equation (7.54) and with state feedback given by equation (7.59) is closed loop stable

The above lemma gives a sufficient stability condition for the actual nonlinear state feedback system. Here K^T is chosen such that the linearized system (7.56) is stable, *not the true plant*. It has been shown that there always exists a prediction horizon H_p such that the control law given by (7.59) stabilizes the model given by (7.56). So equation (7.61) can always be satisfied. The above Lemma is satisfied if the deviation of the

model $(\Delta A, \Delta B)$ from the true plant is sufficiently small. Since the Laguerre functions form a complete orthonormal set, $(\Delta A, \Delta B)$ can be made arbitrarily small so that the stability of the closed loop system is always maintained.

Remark 7.5.1 (General strategy for Implementing Indirect Adaptive CLaP). *Here the general strategy to choose the tuning parameters is discussed globally. The given indirect adaptive control method has two parts comprising of online identification and predictive control. It can be seen that although we start the control with minimum information about the system model, we do need a model to calculate the control signal. So the idea is to choose optimal sampling rate T_s and Laguerre pole a depending on the facts ascertained in the chapter-2 and follow the steps*

Step-1 Choose forgetting factor $\lambda < 1$ and $P(0)$ large such that $|y(t) - \hat{y}(t)| \rightarrow 0$.

Step-2 Then start tuning the controller parameters (H_p, Q, R) such that $|w - y(t)| \rightarrow 0$.

Remark 7.5.2. *In the above indirect adaptive control strategy (Remark 7.5.1) the choice of forgetting $\lambda < 1$ and initialization $P(0)$ depends entirely on the type of RLS used. For example in EF-RLS which has exponential forgetting $\lambda \ll 1$ would make RLS algorithm very unstable due to exponential blow-up of the covariance matrix P . Where as in DF-RLS this can be prevented thanks to the choice of the threshold value ϵ (see section 7.7.1 for further details).*

7.6 Control of SMA using Classical Laguerre Predictive (CLaP) Control: Experimental Results

The classical Laguerre Predictive control is tested here on the basic experimental setup discussed earlier. The control law of Eq. (7.22) is used for the tests in this case. The controller with weighting variable is used which can be shown to be helpful by increasing the degree of freedom for tuning parameters. For purpose of realtime identification of the SMA actuator the actual input voltage across the SMA wire was measured and fed into the RLS algorithm for implementing the CLaP control method. Although it is a know fact that the SMA actuator is nonlinear, a controller based on linear model was used. It has been ascertained that in a RLS algorithm with exponential forgetting, when $\lambda < 1$ the identification algorithm converges exponentially fast (Bittanti *et al.*, 1990) making it suitable to be applicable to control nonlinear systems. Linear laguerre models of 2nd order and 5th order are tested using the CLaP controller working at a sampling rate of $T_s = 0.01$ sec under the assumption that the sampling rate at which the adaptive controller works is faster than the rate at which the nonlinear systems changes or in other words the linear model identified locally should have converged at least locally to the actual nonlinear system and should remain controllable and observable. So under these conditions the CLaP method with 2nd and 5th order model are tested.

7.6.1 Position Control using 2nd order linear Laguerre model with CLaP method

The controller in Eq. (7.22) is used with the following initial basic parameters given below:

- Sampling rate $T_s = 0.01$
- Laguerre pole $a = 0.9$,
- Covariance initialization $P(0) = 10^2 \mathbb{I}$
- Forgetting factor $\lambda = 0.8$

In general to analyze the performance the choice of Q and R is fixed or in particular the R/Q ratio (Shahian & Hassul, 1993) is fixed to be analyzed from the set of values $R/Q = \{1, 10^{-2}, 10^{-3}, 10^{-4}\}$. Preliminary tests showed that choosing the $R/Q = 10^{-2}$ or above resulted an attenuated control signal until complete cancellation for $R/Q = 1$. Reducing the R/Q ratio equal and below 10^{-4} introduces oscillations for all the steady state references values. Hence the response plots for $R/Q = 10^{-3}$ are considered in the discussion. The experimental results for displacement tracking of a mixed square signal can be seen in Figure 7.5 with $H_p = 30$, $R/Q = 10^{-3}$ along with the above mentioned initial basic parameters. From the displacement response it can be seen that the overshoot is maximum (126%) at step reference equal to 2.3 mm. Note that all the step references have produced similar transient with overshoot of almost equal magnitude. The steady state error (Fig. 7.6-i) is higher for reference close to zero with the maximum being 45% but again is common to all steady states. The closed loop identification error (Fig. 7.7-i) is almost white noise with a forgetting factor $\lambda = 0.8$ making the update of the weights faster (Fig. 7.7-ii) which also reflects in the control signal being reactive even when $H_p = 30$ as seen in Figure 7.6-i. The reference signal as shown in Figure 7.5 is used to analyze the influence of the prediction horizon for values $H_p = \{5, 20\}$. The test results of only 115 seconds was considered for detailed analysis (the plots have been omitted here). In general the observation is common for further longer periods of input reference. Reducing the prediction horizon $H_p = 20$ has a similar pattern of overshoot and steady state error as for $H_p = 30$ but has introduced oscillations for reference values which are away from zero value with oscillations ranging from approximately 5% and higher. Further reducing the prediction horizon to $H_p = 5$, reduces the overshoot at the cost of increasing oscillations above 5% for large demand of the reference signal.

After careful study of the implementation of the CLaP method using the 2nd order model it is clearly evident that the controller given by Eq. (7.22) is able to control the nonlinear hysteretic system but gives rather poor results regarding transient and steady states. In order to further evaluate the considered strategy a straightforward aspect is to increase the order of the linear model. Indeed, it is a well known fact that a non optimal Laguerre pole would influence the order of the Laguerre linear model used for predicting the system (Fu & Dumont, 1993), the problem might be caused by the fluctuation of the apparent time constant due to the non-linearity. Hence, in the proceeding section the same controller (Eq. (7.22)) was used to control the SMA actuator using a 5th order model (this choice is considered for the sake of comparison

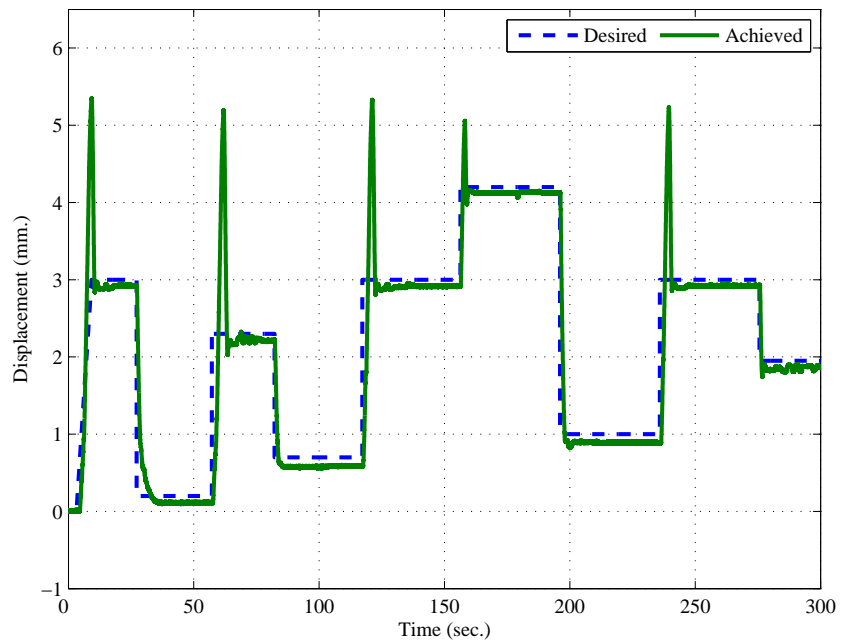


Figure 7.5: Tracking using CLaP method with 2nd order model, ($a = 0.9, H_p = 30, \lambda = 0.8, R/Q = 10^{-3}$).

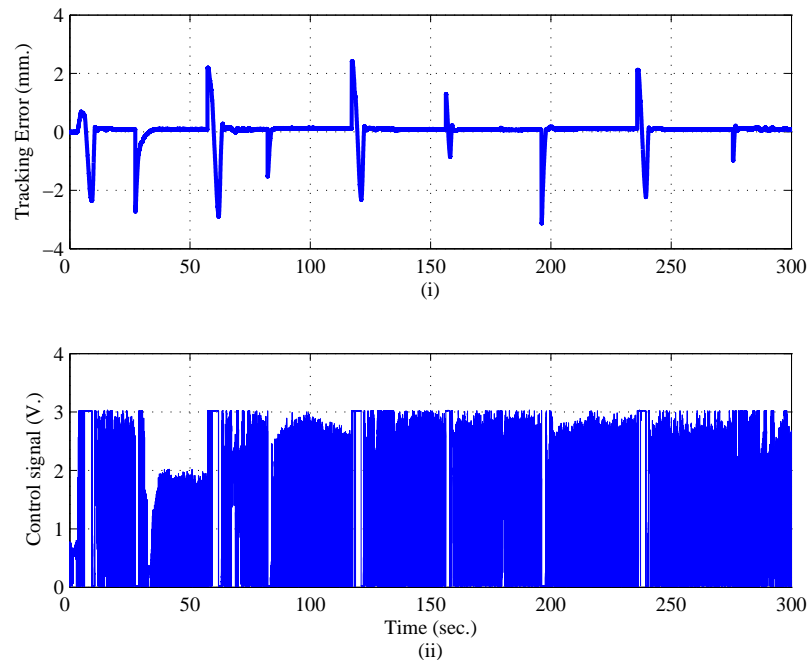


Figure 7.6: (i) Tracking error and (ii) Control signal using CLaP method with 2nd order model, ($a = 0.9, H_p = 30, \lambda = 0.8, R/Q = 10^{-3}$).

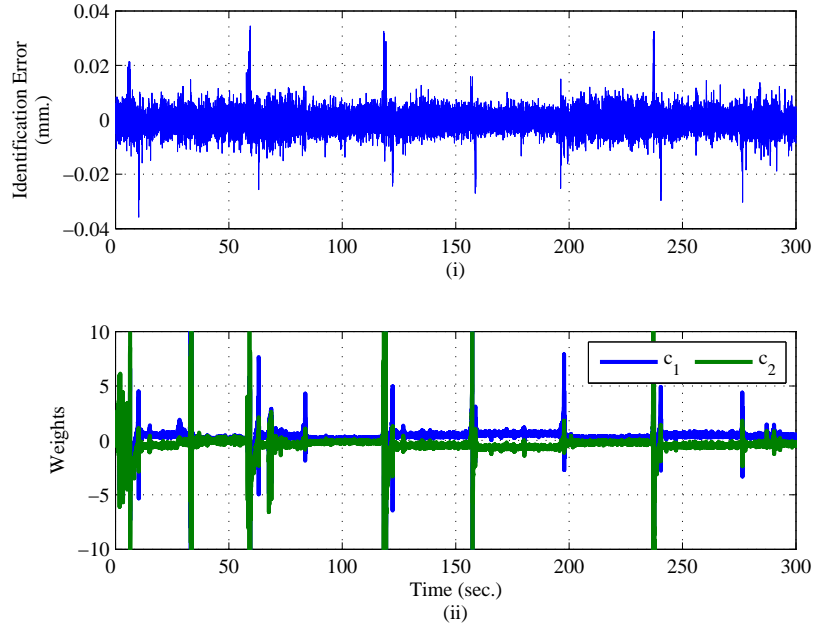


Figure 7.7: (i) Identification error and (ii) Laguerre filter weights using CLaP method with 2nd order model, ($a = 0.9, H_p = 30, \lambda = 0.8, R/Q = 10^{-3}$).

with the proposed control method (MLaP) implemented and discussed later).

7.6.2 Position Control using 5th order linear Laguerre model with CLaP method

The initial basic parameters considered for the 5th order model are $T_s = 0.01$, $a = 0.9$ and the forgetting factor used in the parameter update is at a much slower rate at $\lambda = 0.99$ compared to the 2nd order model. The reason for this choice is that for a 5th order model $\lambda = 0.99$ was sufficient to give a good identification error as compared to the 2nd order model. The ratio $R/Q = 10^{-3}$ is chosen with $Q = 1$ and $R = 10^{-3}$ in the controller Eq. (7.22) for the same reason as detailed in the previous case. The various values of prediction horizon chosen here are $H_p = \{5, 20, 30\}$. The experimental results for displacement tracking of a mixed square signal can be seen in Figure 7.8 with $H_p = 30$. When compared to the 2nd order model, the overshoots have disappeared, but unsteadiness causing inaccuracies (reaching up to 55% of reference value close to zero) now take place. Although the identification has been near white noise (Fig. 7.10-ii) the reactive nature of the control signal (Fig. 7.9-i) is evident from the plots of the weights (Fig. 7.9-ii). Reducing the value of the prediction horizon H_p to 20 and 5 the oscillations had increased further with $H_p = 5$ giving a maximum oscillation of 87% at reference value closer to zero.

Comments on Adaptive Classical Laguerre method using classical RLS

Considering the nonlinear system as a slowly time varying system (relative to sampling rate) dictate the choice of an adaptive predictive control based on linear model using RLS with exponential forgetting (EF) factor (Kulhavý, 1987; Bittanti *et al.*, 1990).

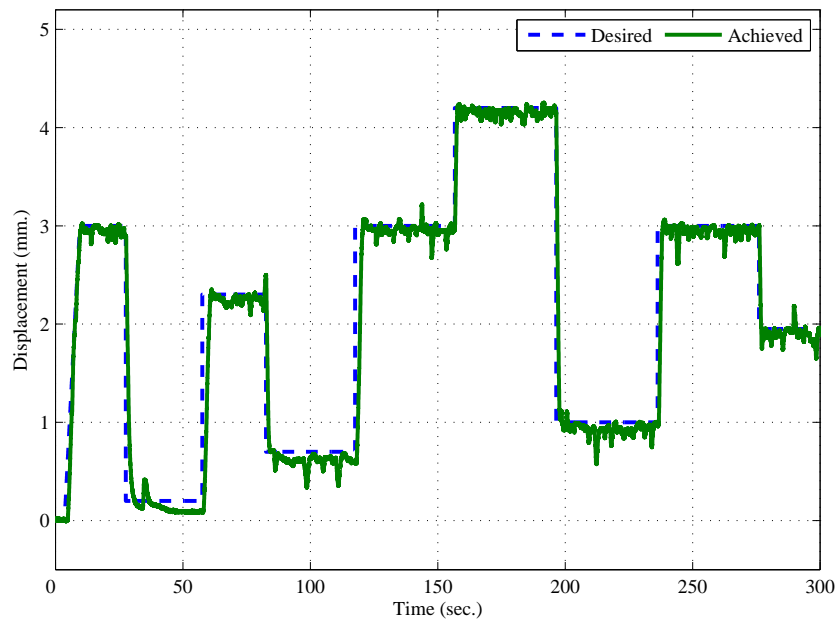


Figure 7.8: Tracking using CLaP method with 5th order model, ($a = 0.9, H_p = 30, \lambda = 0.99, R/Q = 10^{-3}$).

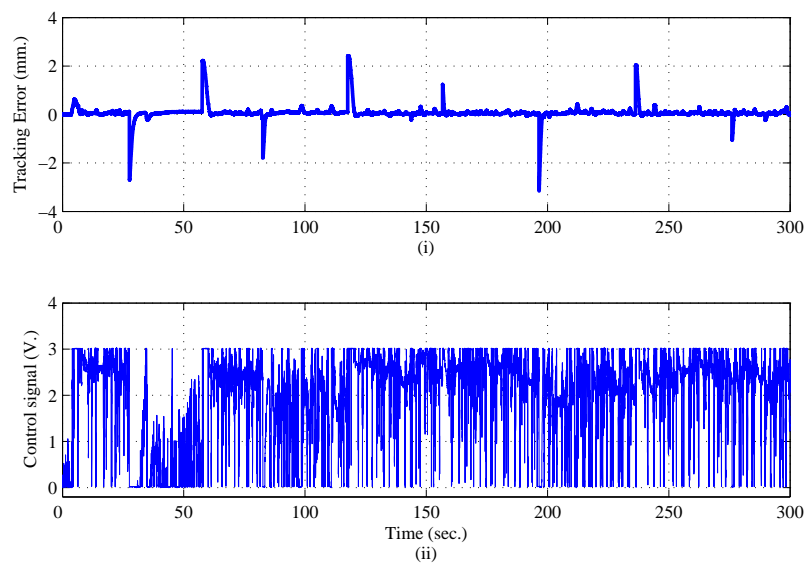


Figure 7.9: (i) Tracking error and (ii) Control signal using CLaP method with 5th order model, ($a = 0.9, H_p = 30, \lambda = 0.99, R/Q = 10^{-3}$).

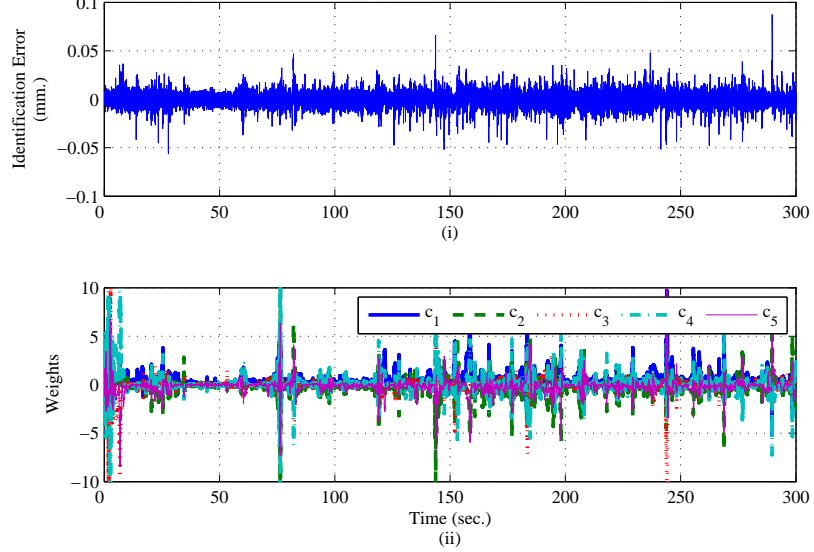


Figure 7.10: (i)Identification error and (ii) Laguerre filter weights using CLaP method with 5th order model,($a = 0.9, H_p = 30, \lambda = 0.99, R/Q = 10^{-3}$).

This identification algorithm guarantees boundedness of the parameters when the data sequence $\{l(t)\}$ is persistently exciting, that is it contains sufficient information about the system dynamic. If such a condition is not met, it results in loss of information about the system without any replacement with newer informations about the system ultimately resulting in exponential increase of estimator gain. The blow-up of the estimator gain makes the estimation of the RLS very sensitive to small perturbations in the information vector, for example a small amount of measurement noise, a setpoint change or some other disturbance. It can cause large changes in the estimated parameters and in the systems performance. This condition often arises using RLS with EF and also in closed loop control which is our case and is referred to as “bursting”. The estimator windup may then cause a burst in the output of the process. The adaptive control bursting may cause loss of equilibrium and parameter drift, leading to unstable control action. The current phenomenon is very common in adaptive control and is also very evident in our case from the observation of the control signals of control using 2nd order model (Fig.7.6-ii) and 5th order model (Fig.7.9-ii) and their respective time response of the filter weights in Figure 7.7-ii and Figure 7.10-ii respectively.

The RLS algorithm tend to minimize the ouput error:

$$e(t) = y(t) - \hat{y}(t) \quad (7.63)$$

which in the case of a Laguerre model is written:

$$e(t) = [C - \hat{C}(t)]l(t) \quad (7.64)$$

once the state of the model has converged to the state of the linearized state of the system. Hence, as long as $C - \hat{C}(t)$ remains orthogonal to $l(t)$, $e(t) = 0$ although $C \neq \hat{C}(t)$. Therefore the DC gain of the model $\hat{C}(t)(I - \hat{A})^{-1}\hat{B}$ can differ from the actual DC

gain of the plant $C(I - A)^{-1}B$ even though the output error remains nil due to the drift of the identified parameters. This occurs randomly in the cases when the PE condition is violated resulting in bursting phenomenon (Anderson, 1985) with intermittent phases of control signal resulting from intermittent behavior of the parameters.

Remark 7.6.1. *The bursting phenomenon occurs in adaptive control using RLS with EF and with gradient methods. For further details refer to Anderson (1985). Numerous techniques have been developed to avoid the estimation windup that frequently occur in practical applications of RLS. Some of these techniques include normalization of the regressor vector (Adel et al., 1999), directional forgetting factor (Bittanti et al., 1990; Cao & Schwartz, 2000) etc.,*

7.7 CLaP method using RLS estimation with Directional Forgetting factor

7.7.1 Directionnal Forgetting Factor Recursive Least Squares

The Directionnal Forgetting Factor Recursive Least Squares (DFRLS) has been proposed to circumvent the problems of bad conditionning of the correlation matrix which occurs when the information available in the excitation does not satisfy the PE condition. The idea is to take into account measurements only if they contribute to enhance the information stored in the correlation matrix. In this paradigm, the regressor is seen as a vector that should be stored only in some specified direction. To do so, the information matrix $R(t)$ ($R(t) = P^{-1}(t)$ with $P(t)$ the correlation matrix) is split into two part, R_1 and R_2 the forgetting being applied to the latest while the matrix R_1 is required to be orthogonal to the fresh regressor vector. Imposing the supplementary requirement that rank of R_2 is one³, a unique solution can be found. The algorithm used is the DFRLS version proposed by Cao & Schwartz (2000), which in addition to address the covariance matrix condition also guarantees that the eigenvalues of the information remain bounded, thus preserving the adaptation capability of the algorithm in all direction. The equation are summed up below directly using the regressor vector $\mathbf{l}(t)$, the state of the Laguerre filter:

$$\hat{\mathbf{C}}(t) = \hat{\mathbf{C}}(t-1) + \mathbf{P}(t)\mathbf{l}(t) \left[y(t) - \mathbf{l}(t)^T \hat{\mathbf{C}}(t-1) \right] \quad (7.65)$$

where $\mathbf{P}(t)$ is the covariance matrix and $y(t)$ is the measured output at time step t . The covariance matrix $\mathbf{P}(t)$ is updated based on the following rule:

$$\mathbf{P}(t) = \bar{\mathbf{P}}(t-1) - \frac{\bar{\mathbf{P}}(t-1)\mathbf{l}(t)\mathbf{l}^T(t)\bar{\mathbf{P}}(t-1)}{1 + \mathbf{l}^T(t)\bar{\mathbf{P}}(t-1)\mathbf{l}(t)} \quad (7.66)$$

3. which is consistent with the fact that the updating is using the matrix $\mathbf{l}^T\mathbf{l}$ (\mathbf{l} being the regressor) which has also rank one

$\bar{\mathbf{P}}(t-1)$ is the modified covariance matrix which is given by the following equations

$$\bar{\mathbf{P}}(t-1) = \begin{cases} \mathbf{P}(t-1) + \frac{1-\lambda}{\lambda} \frac{\mathbf{l}(t)\mathbf{l}^T(t)}{\mathbf{l}^T(t)\mathbf{P}^{-1}(t-1)\mathbf{l}(t)} & \text{if } \|\mathbf{l}(t)\| \geq \epsilon \\ \mathbf{P}(t-1) & \text{if } \|\mathbf{l}(t)\| < \epsilon \end{cases} \quad (7.67)$$

The inverse of the correlation matrix is also obtained in a recursive manner. As $R(t-1) = \mathbf{P}^{-1}(t-1)$, the updating law of the information matrix is:

$$\begin{aligned} R(t) &= [\mathbb{I} - M(t)]R(t-1) + \mathbf{l}(t)\mathbf{l}^T(t) \\ M(t) &= (1 - \lambda) \frac{R(t-1)\mathbf{l}(t)\mathbf{l}^T(t)}{\mathbf{l}^T(t)R(t-1)\mathbf{l}(t)} \end{aligned} \quad (7.68)$$

7.7.2 Methodology

The rest of section focuses on the CLaP method using DFRLS for identification. First the position control problem is dealt using the 5th order model, and the influence of tuning parameters (H_p, Q, R) is discussed. The effect of model order is also discussed by testing a 2nd order model. Then a 5th order model is used to analyze the influence of thermal disturbance and ambient temperature.

Remark 7.7.1 (General strategy for implementing CLaP-DFRLS). *The general strategy to implement the CLaP-DFRLS is similar to that of the one given in remark 7.5.1. The values of the parameters in the identification ($a, P(0), \epsilon, \lambda$) are first chosen such that $|y(t) - \hat{y}(t)| \rightarrow 0$ and then the parameters of the predictive control law (H_p, Q, R) are chosen.*

Remark 7.7.2. *As remarked earlier in Remark 7.5.1 it should be noted that the choice of forgetting factor λ and initialization $P(0)$ here can be different from the values chosen for CLaP-EFRLS as the RLS algorithm consists of an additional tuning variable such as the threshold value ϵ .*

A variable step signal was defined and applied during all tests in order to replicate the major and minor loops of the hysteresis curve and perform analysis on the displacement tracking results by studying the overshoot (%), settling time (s), steady state error (%) and oscillations (%) which occur at every step change in the reference signal. Further since the performance of the output changed for the different step changes mean of a given performance criterion (e.g overshoot, settling time etc.,) were calculated from the datas. The different mean performance index are:

- Mean Overshoot (MO) %;
- Mean Settling Time (MST) s;
- Mean Steady State Error (MSSE) %;
- Mean Oscillations (MOS) %.

7.7.3 Position Control using 5th order linear Laguerre model with CLaP-DFRLS method

The Laguerre predictive control is initially studied for displacement tracking considering the basic identification and controller settings as given below:

- Laguerre pole $a = 0.9$
- Covariance initialization $P(0) = 10^5 \mathbb{I}$
- Threshold value $\epsilon = 10^{-3}$
- Forgetting Factor $\lambda = 0.5$
- Prediction Horizon $H_p = 3$
- Controller weights: $R = 0, Q = 1$

With this parameters set, the result are (corresponding to the Tab. 7.1):

- Mean Overshoot (MO) = 0.71 %;
- Mean Settling Time (MST)= 5.3 s;
- Mean Steady State Error (MSSE)= 0 %;
- Mean Oscillations (MOS)= 0.47 %.

The experimental results for displacement tracking is seen in Figure 7.11, tracking error and control signal can be seen in Figure 7.12. Finally, the identification error and the identified Laguerre filter weights can be seen in Figure 7.13. The control signal seen in Figure 7.12 has large fluctuations which is due to the fact that the covariance matrix of the DFRLS was initialized at $P(0) = 10^5 \mathbb{I}$ by using $\delta = 10^{-5}$. But the choice of a very high $P(0)$ along with small threshold value ($\epsilon = 10^{-3}$) the identification algorithm is more responsive and sensitive to the changes in the measured output. This can also be seen in Figure 7.13 where the closed loop identification error is close to white noise. From the observation of the identified weights in closed loop we can see that the dominant behavior of the SMA actuator is close to a first order system. This inference is due to the fact that except the first weight of the Laguerre model all the other weights are close to zero (see Fig.7.13-ii).

In the next section the tuning factors that are involved in the control design such as tracking error weight (Q) and control signal weight (R) and choice of prediction horizon H_p are discussed.

7.7.4 Influence of Prediction Horizon (H_p) and Control weights (Q, R)

The influence of prediction horizon (H_p) and control weights (Q, R) is studied using the same reference signal. Considering the control weights most notably the performance is influenced by the ratio R/Q . The respective effects of the balance between the different choices of R and Q are discussed in [Shahian & Hassul \(1993\)](#). When the ratio $Q/R \rightarrow 0$ the method is known as a minimum energy control and $R/Q \rightarrow 0$ the method is called as cheap control. In the current control problem the minimum energy method was not suitable as when $Q/R \rightarrow 0$ increases the penalty on the control signal considerably affects the response. Since the current control method is an indirect adaptive control method the absence of sufficient input excitation does not facilitate the proper functioning of the closed loop identification algorithm. Hence only the cheap

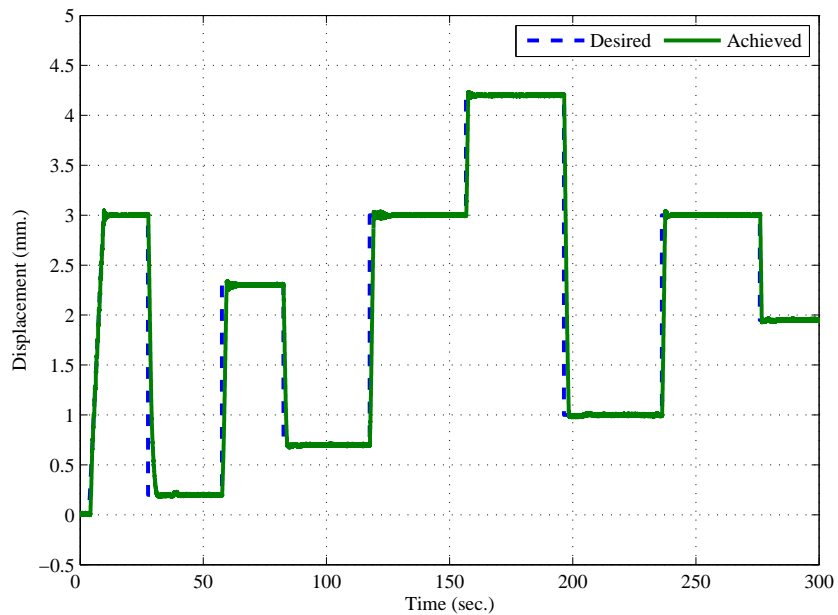


Figure 7.11: Tracking using CLaP-DFRLS method with 5th order model, ($a = 0.9, H_p = 3, \lambda = 0.5, \epsilon = 10^{-3}, Q = 1, R = 0$).

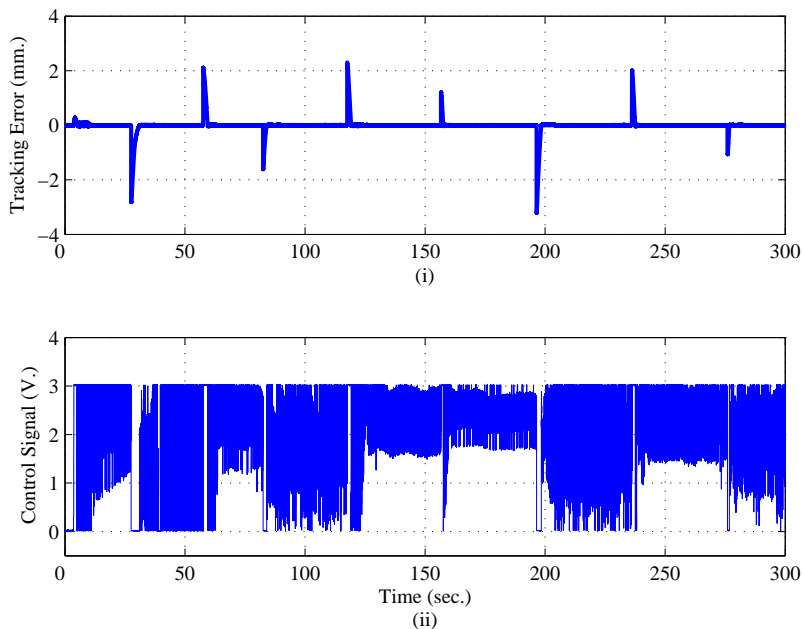


Figure 7.12: (i) Tracking error and (ii) Control signal using CLaP-DFRLS method with 5th order model, ($a = 0.9, H_p = 3, \lambda = 0.5, \epsilon = 10^{-3}, Q = 1, R = 0$).

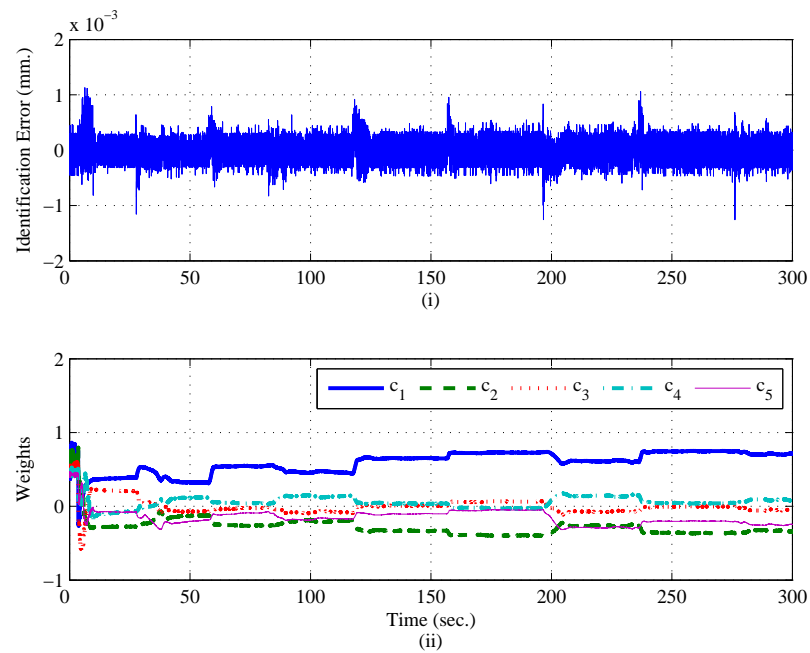


Figure 7.13: (i)Identification error and (ii) Laguerre filter weights using CLaP-DFRLS method with 5th order model,($a = 0.9$, $H_p = 3$, $\lambda = 0.5$, $\epsilon = 10^{-3}$, $Q = 1$, $R = 0$).

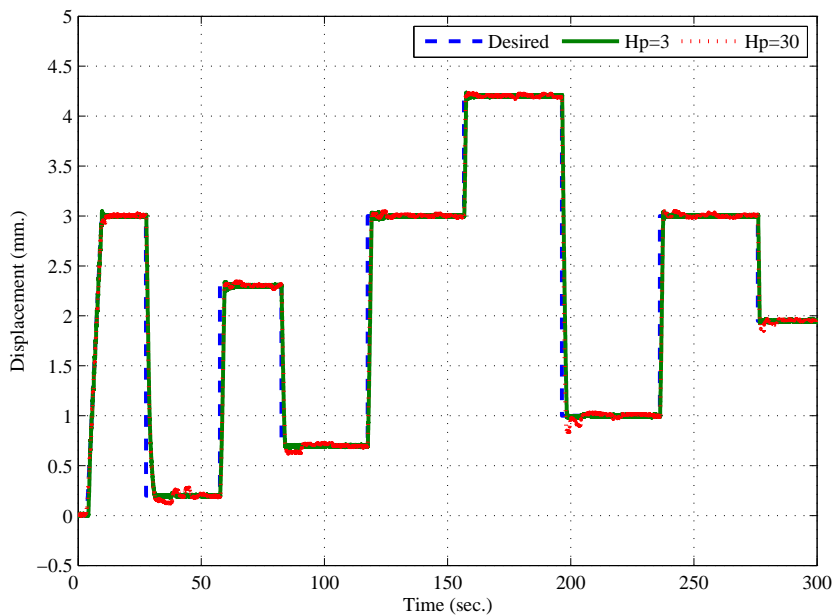


Figure 7.14: Tracking using CLaP-DFRLS method with 5th order model,($a = 0.9$, $H_p = 3, 30$, $\lambda = 0.5$, $\epsilon = 10^{-3}$, $Q = 1$, $R = 0$).

| H_p | Criteria | $r = 10^{-2}$ | $r = 10^{-4}$ | $r = 0$ |
|-------|----------|---------------|---------------|---------|
| 30 | MO | 0.8 | 15.0 | 14.2 |
| | MST | 12.8 | 16.0 | 22.5 |
| | MSSE | 34.2 | 11.7 | 0.0 |
| | MOS | 1.4 | 14.6 | 14.4 |
| 15 | MO | | 7.6 | 4.7 |
| | MST | n.a | 12.7 | 11.0 |
| | MSSE | | 0.0 | 0.0 |
| | MOS | | 5.9 | 8.7 |
| 3 | MO | | 3.7 | 0.7 |
| | MST | n.a | 8.3 | 5.3 |
| | MSSE | | 6.8 | 0.0 |
| | MOS | | 0.0 | 0.5 |

Table 7.1: Evaluation criteria for the adaptive predictive control. The entries resulting in instability are signaled by the “n.a” abbreviation

control (R/Q) strategy was tested here. The performance of the adaptive controller is charted in Table 7.1 with different R/Q ratio and H_p . The R/Q ratio takes the values $R/Q \in \{0, 10^{-4}, 10^{-2}\}$ and the prediction horizon $H_p \in \{30, 15, 3\}$ in order to look at a broader spectrum of performance variables. The performance is documented as mentioned earlier in terms of MO(%), MST (s), MSSE (%), and MOS (%). The data set considered to calculate the values in the table was limited to 100 s as it was sufficient to understand the behavior of the various choices of parameters with the help of variable step response. Going from right to left the R/Q ratio is decreased by fixing $Q = 1\mathbb{I}$ and changing $R = 10^{-2}\mathbb{I}$ and $Q = 10^{-4}\mathbb{I}$ while $R/Q = 0$ is achieved by choosing $R = 0, Q = 1\mathbb{I}$. For $R/Q = 0$ when the prediction horizon H_p is reduced from 30 to 3 the MO reduces by 94.52 %, MST reduces by 76.70 % and MOS reduces by 96.24 % while MSSE is equal to zero throughout. A superposition of displacement tracking for $H_p = \{3, 30\}$ can be seen in Figure 7.14 and their respective tracking tracking error and control signals can be seen in Figure 7.15. It is important to note that for $H_p = 30$ the control effort is considerably less compared to $H_p = 3$, at the cost of higher overshoot, settling time and oscillations.

For $R/Q = 10^{-4}$ the behavior of the closed loop system seems to be slightly different. The MO reduces by 74.14 %, MST reduces by 47.97 %, MOS is reduced by 100 %, but the MSSE reduces to 0 % at $H_p = 15$ and further increases to 6.7972% for $H_p = 3$ at the cost of decrease in the oscillations. Using $R/Q = 10^{-2}$ the controller works for $H_p = 30$ with very poor performance with respect to all the indexes and further reduction in the H_p makes the control signal reduce to zero due to insufficient excitation leading to the inability of the DFRLS to function properly.

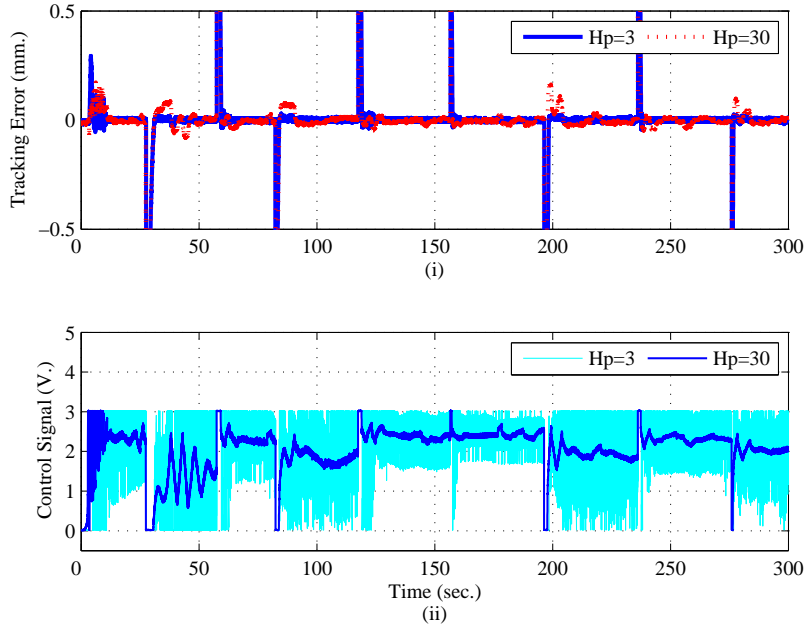


Figure 7.15: (i) Tracking error and (ii) Control signal using CLaP-DFRLS method with 5th order model, ($a = 0.9, H_p = 3, 30, \lambda = 0.5, \epsilon = 10^{-3}, Q = 1, R = 0$).

7.7.5 ClAP-DFRLS using 2nd order

The classical Laguerre predictive control is implemented here using a 2nd order model in order to study the influence of the model order on the control objective. The identification and controller parameters are taken as the same ones as used previously in the 5th order model that is $a = 0.9, H_p = 3, 30, \lambda = 0.5, \epsilon = 10^{-3}$, and a simpler control law is used with $Q = 1, R = 0$. The prediction horizon was chosen as $H_p = 3$ since this gave the best performance in the previous tests. The experimental results for displacement tracking can be seen in Figure 7.16. The displacement tracking error can be seen in Figure 7.17 with the identification error and model filter weights in Figure 7.18. The analysis was performed on the displacement results by considering a 300sec data set. the indexes values are

- MO= 3.9 %;
- MST= 20.5 s;
- MSSE= 0 %;
- MOS= 3.1 %.

Basically all the transient indexes are considerably higher than in the case of the 5th order model previously tested. The mean settling time is increased due to the presence of oscillations at the steady state with the maximum being 17.7% at reference signals close to zero (representing 30μm around the 0.2 mm reference). The presence of oscillations in the displacement is linked to the instantaneous spikes in the control signal seen in Figure 7.17. It is also correlated to the oscillatory behavior of the identified weights seen in the Figure 7.18. One of the reasons of the oscillatory behavior identified weights could be attributed to the choice of larger value initialization of the covariance matrix $P(0) = 10^5$ which was necessary to make the identification algorithm be very alert and

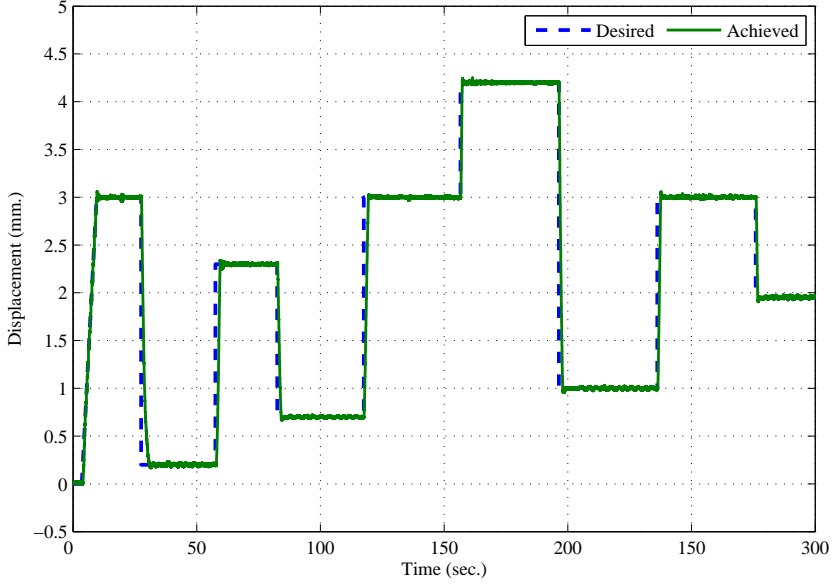


Figure 7.16: Tracking using CLaP-DFRLS method with 2nd order model, ($a = 0.9, H_p = 3, \lambda = 0.5, \epsilon = 10^{-3}, Q = 1, R = 0$).

also gives the closed loop identification error close to white noise as seen in Figure 7.18.

7.7.6 Influence of Thermal Disturbance and Ambient Temperature

In the current section, the behavior of the system in the presence of thermal disturbance is studied. For this purpose a 5th order model was used as it presented the best performances. The tuning parameters used for the test are Laguerre pole $a = 0.9$, forgetting factor $\lambda = 0.5$, covariance initialization $P(0) = 10^5 \mathbb{I}$, threshold value $\epsilon = 10^{-3}$, prediction horizon $H_p = 3$, and control weighting parameters $Q = 1, R = 0$. To produce the thermal disturbance, an instantaneous burst of air was blown toward the SMA wire. This introduces an unknown disturbance resulting from the change of the convection conditions which is modified from natural to forced convection. In Figure 7.19 we can see the displacement tracking response and in Figure 7.20 the respective controller signal is presented. The resulting perturbation affects the displacement which derives 12 % beneath the reference. During this period in-order to fight the cooling effect the control signal saturates to the highest values available from the power supply. It is important to note that in the presence of large perturbation there is a possibility of oscillations occurring later after recovering from the perturbation. In the current case, they appear at time $t=143$ s representing a deviation of 1.2 %. It is clear from the control signal that the output saturation of the power supply of 3 volts is responsible for this behavior (Fig. 7.20). The oscillations usually occur when the reference or the power needed to compensate a saturation becomes unfeasible due to the saturation. This can occur due to numerous number of reasons, most notably the ambient temperature. Since it is not controlled in this experiment, oscillations have also been observed occasionally.

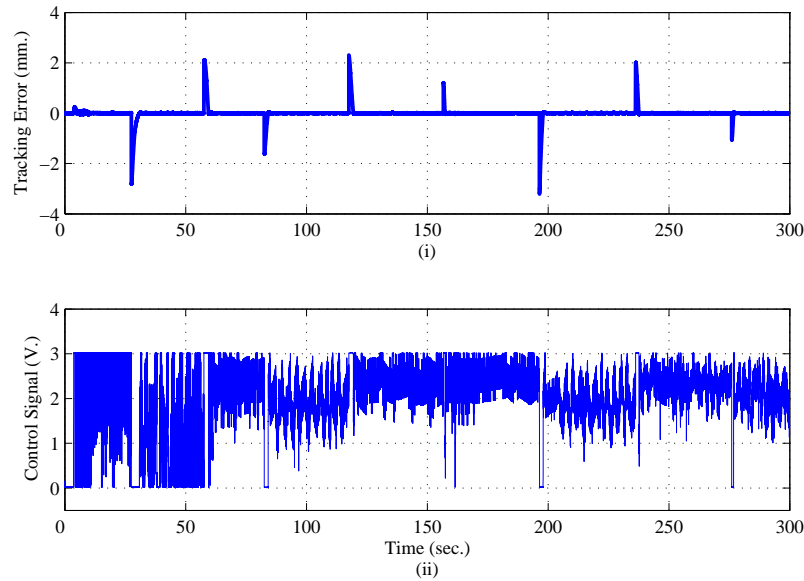


Figure 7.17: (i) Tracking error and (ii) Control signal using CLaP-DFRLS method with 2nd order model, ($a = 0.9, H_p = 3, \lambda = 0.5, \epsilon = 10^{-3}, Q = 1, R = 0$).

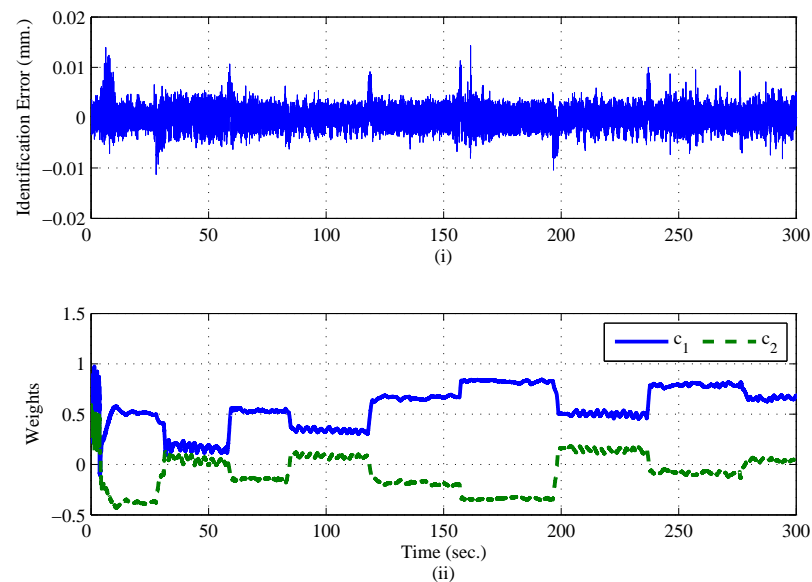


Figure 7.18: (i) Identification error and (ii) Laguerre filter weights using CLaP-DFRLS method with 2nd order model, ($a = 0.9, H_p = 3, \lambda = 0.5, \epsilon = 10^{-3}, Q = 1, R = 0$).

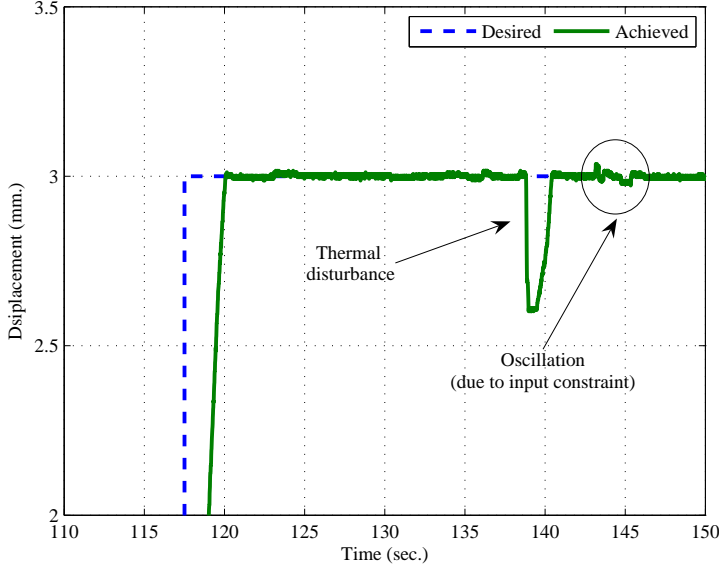


Figure 7.19: Perturbation Rejection:Tracking using CLaP-DFRLS method with 5th order model,($a = 0.9, H_p = 3, \lambda = 0.5, \epsilon = 10^{-3}, Q = 1, R = 0$).

One of the design aspect that is available is to augment the R/Q ratio to 10^{-4} . By this method the control objective can still be obtained as is the case seen in Figure 7.21. The control signal (Fig. 7.22) does not hit the upper saturation unless the tracking error is large and also prevents the output displacement from oscillatory behavior by keeping the control signal well below the saturation limits. But under this condition since less control effort is applied to achieve the target, the SMA wire might be more vulnerable to thermal disturbance which can be seen that the output displacement is perturbed to a greater amount of 18.9%.

7.8 Conclusion and Perspective on CLaP-DFRLS

An Indirect Adaptive Predictive control using Laguerre model and a RLS with Directional Forgetting was successfully tested on the SMA actuator experimental setup. The controller has been analyzed in the context of displacement tracking using a 5th order model initially. Design parameters involved in the closed loop Identification have been chosen appropriately to address stability of the RLS in closed loop. The controller using 5th order model was further analyzed for different control design parameters such as control weights and prediction horizon. The controller using 5th order model was further tested for robustness to thermal disturbance and strategy using cheap control i.e $R/Q = 0$ had shown intermittent phenomenon at certain instances after the thermal disturbance was introduced. This was due to the fact that for $R/Q = 0$ the control signal performed closer to the upper input constraint limit i.e 3 Volts and had introduced instability in the control signal. This phenomenon was absent by increasing the R/Q ratio to 10^{-4} . The influence of model order on the control strategy was also studied using the 2nd order model and $R/Q = 0$. The controller using 2nd order model performed

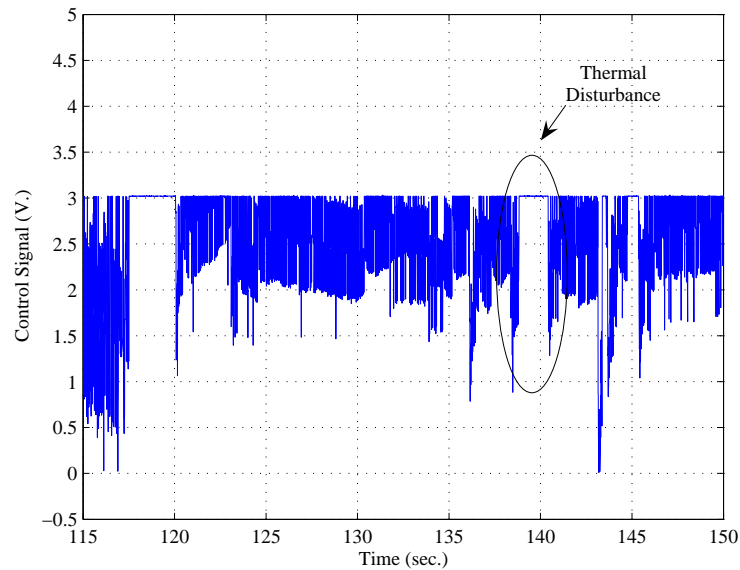


Figure 7.20: Perturbation Rejection:Control signal using CLaP-DFRLS method with 5th order model,($a = 0.9, H_p = 3, \lambda = 0.5, \epsilon = 10^{-3}, Q = 1, R = 0$).

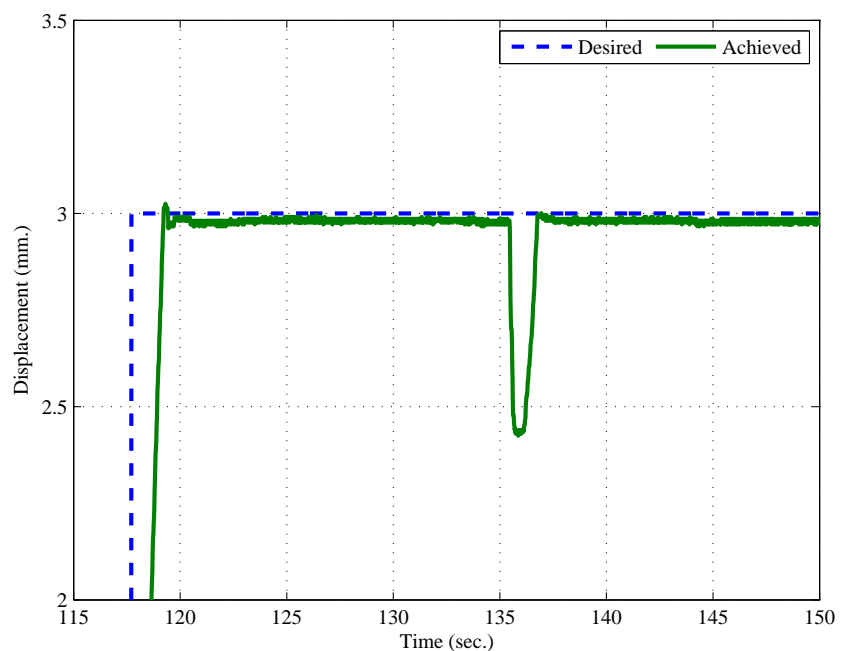


Figure 7.21: Perturbation Rejection:Tracking using CLaP-DFRLS method with 5th order model,($a = 0.9, H_p = 3, \lambda = 0.5, \epsilon = 10^{-3}, Q = 1, R = 10^{-4}$).

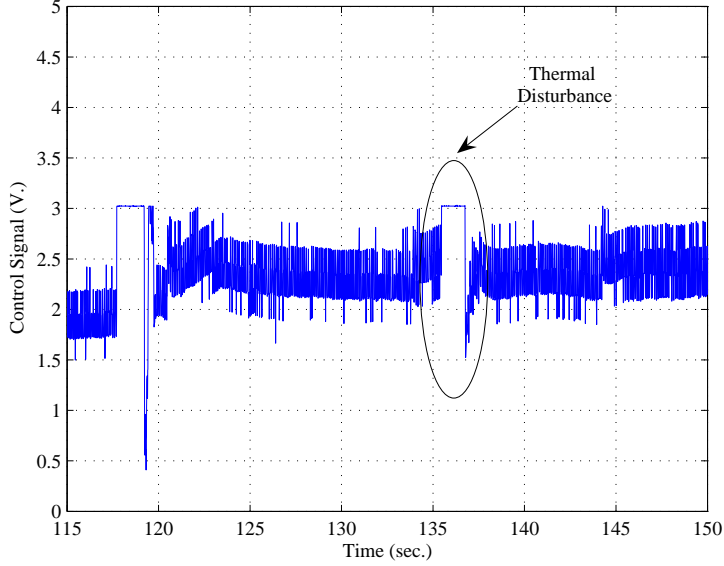


Figure 7.22: Perturbation Rejection:Control signal using CLaP-DFRLS method with 5th order model,($a = 0.9, H_p = 3, \lambda = 0.5, \epsilon = 10^{-3}, Q = 1, R = 10^{-4}$).

with equal satisfaction in terms of tracking error as compared to 5th order model. But reduction in the model order had introduced minor oscillations in the steady state tracking. The reasons for the presence of oscillations in the control using 2nd order model was the choice of very high initialization value of $P(0) = 10^5 \mathbb{I}$. Reduction in the value of $P(0)$ could mitigate this behavior. One of the important aspect that could be noted was the amount of chatter persisting in almost all the control experiments. Based on the observation the existing chattering behavior could be attributed to the input constraint which had to be introduced in the control design in order to assure the safety of the experimental setup. An important direction that could be pursued in the improvement of the control would be to investigate the influence of the input constraint and study further control methods using constraint handling.

7.9 Modified Adaptive Predictive Control

In this section an alternative adaptive predictive control method is proposed. It has been shown theoretically that the stability of the CLaP method relies essentially on the stability of the identification scheme. The main difficulty is that the PE condition is difficult to guarantee in closed loop, especially when the controller bandwidth is low. Unfortunately, this is the case when the prediction horizon is increased, which is also one of the condition to be respected according to our theoretical developments. The use of the DFRLS has proved to be fairly efficient and the condition on the prediction horizon is not so constraining when considering the experimental results. However, stability is *not* guaranteed unless the PE excitation is respected under all circumstances. Therefore, the next adaptive controller is based on an different identification paradigm: rather than identifying the plant in the closed loop, the complete closed loop will be

identified. In this case, the input of the identification algorithm consisting in the reference, is uncorrelated with the output of the plant, and the richness of the input signal is completely under control and an Exponential Forgetting RLS algorithm for estimation will therefore be used. In the following subsections the main results with proposition, description of the scheme and stability results are presented.

7.9.1 Main Results

The important result of the current chapter is the following proposition given by the schematic in Figure 7.23. The current method presented here is structurally comparable with Series-Parallel Model Reference Adaptive System which has been studied in Landau (1979). Let us consider the true system to be controlled be given as

$$\begin{aligned} x(t+1) &= Ax(t) + Bu(t) \\ y(t) &= C^T x(t) \end{aligned} \quad (7.69)$$

If the controller used to control the given system be given as

$$u(t) = \frac{w - y(t) - \hat{\Psi}^T l(t)}{\hat{\Phi}} \quad (7.70)$$

where $\hat{\Psi} = \hat{C}^T(\hat{A}^{H_p} - I)$, $\hat{\Phi} = \hat{C}_l^T \hat{S} \hat{B}$ with $\hat{S} = (\hat{A}^{H_p-1} + \dots + I)$. Suppose the closed loop system formed by the controller and the true system is approximated by a parallel Laguerre system given by

$$\begin{aligned} l(t+1) &= \hat{A}l(t) + \hat{B}w \\ \hat{y}(t) &= \hat{C}^T(t)l(t) \end{aligned} \quad (7.71)$$

which will be the model information used in the predictive control law. Substituting (7.70) in to equation (7.69) and substituting $y(t) = C^T x(t)$, the closed loop system can be given by

$$x(t+1) = [A - BC^T \hat{\Phi}^{-1}]x(t) - B\hat{\Psi}^T \hat{\Phi}^{-1}l(t) + Bw\hat{\Phi}^{-1} \quad (7.72)$$

Now collecting the state equation of the above closed system and the parallel Laguerre system (7.71)

$$\begin{bmatrix} x(t+1) \\ l(t+1) \end{bmatrix} = \begin{bmatrix} [A - BC^T \hat{\Phi}^{-1}] & -B\hat{\Psi}^T \hat{\Phi}^{-1} \\ 0 & \hat{A} \end{bmatrix} \begin{bmatrix} x(t) \\ l(t) \end{bmatrix} + \begin{bmatrix} B\hat{\Phi}^{-1} \\ \hat{B} \end{bmatrix} w \quad (7.73)$$

7.9.2 Stability analysis

Consider the equation (7.72), it can be rewritten as:

$$x(t+1) = Ax(t) - B\hat{\Phi}^{-1}C^T x(t) - \hat{C}^T B \hat{A}_l^{H_p} \hat{\Phi}^{-1} l(t) + B\hat{\Phi}^{-1} \hat{C}^T l(t) + B\hat{\Phi}^{-1} w \quad (7.74)$$

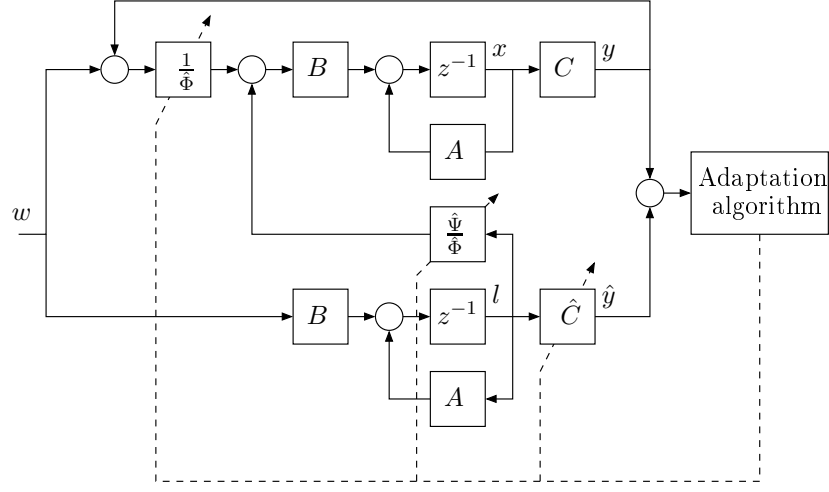


Figure 7.23: Modified Laguerre Predictive (MLaP) Control scheme.

Now consider the above equation and substitute $C^T x(t) = y(t)$ and $C_l^T l(t) = \hat{y}(t)$ and further by trivial algebraic manipulation we get:

$$\begin{bmatrix} x(t+1) \\ l(t+1) \end{bmatrix} = \left[\begin{array}{c|c} A & -\hat{C}^T B \hat{A}_l^{H_p} \hat{\Phi}^{-1} \\ \hline 0 & \hat{A}_l \end{array} \right] \begin{bmatrix} x(t) \\ l(t) \end{bmatrix} + \begin{bmatrix} B \hat{\Phi}^{-1} \\ \hat{B}_l \end{bmatrix} w \quad (7.75)$$

$$+ \begin{bmatrix} B \hat{\Phi}^{-1} \\ 0 \end{bmatrix} (\hat{y}(t) - y(t))$$

Proposition 4. Consider K is a predictive controller which uses the model $w(t)$ (reference signal) to $y(t)$ (plant output) instead of the model $u(t)$ (plant input) to $y(t)$ (plant output) to calculate the gain using adaptive Laguerre predictor, then the closed loop system is stable if:

- the signal $w(t)$ is persistently exciting;
- the condition $\hat{C}^T(t)B \neq 0$ holds.

Proof 4. Remark that the above equation can be given as time varying difference equation as:

$$\mathbf{x}(t+1) = \mathbf{F}(t)\mathbf{x}(t) + \mathbf{v}(t) \quad (7.76)$$

where $\mathbf{F}(t)$ is the state matrix of the closed loop system in Eq. (7.73) for any arbitrary sequences $\{v_1(t), v_2(t)\}$, the sequence $\mathbf{v}(t)$ is given as

$$\mathbf{v}(t) \doteq \begin{bmatrix} v_1(t) \\ v_2(t) \end{bmatrix} = \begin{bmatrix} B \hat{\Phi}^{-1} \\ \hat{B}_l \end{bmatrix} w + \begin{bmatrix} B \hat{\Phi}^{-1} \\ 0 \end{bmatrix} (\hat{y}(t) - y(t)) \quad (7.77)$$

1. Due to the boundedness of the gain $\hat{\Phi}(t)$ already studied in proposition 1, the matrix $\mathbf{F}(t)$ has finite coefficients;
2. $\mathbf{F}(t)$ is block triangular, therefore its eigenvalues are $\lambda\{\mathbf{F}(t)\} = \lambda\{A\} \cup \lambda\{\hat{A}_l\}$. Now since we choose the Laguerre pole $a < 1$ then $\lambda\{\hat{A}_l\} < 1$, and from our

assumption the original system is stable, that is $\lambda\{A\} < 1$, so $\lambda\{\mathbf{F}(t)\} < 1$.

3. under the PE assumption, there is a bounded value for the parameter vector $\lim_{t \rightarrow \infty} \hat{C}(t) = \hat{C}_\infty$ and the gain $\lim_{t \rightarrow \infty} \hat{\Phi}(t) = \hat{\Phi}_\infty$ hence $\lim_{t \rightarrow \infty} F(t+1) - F(t) = 0$

Hence the closed loop system can only be unstable if the sequence $\{\mathbf{v}(t)\}$ is unbounded. Here we can see that the sequence $\mathbf{v}(t)$ depends on the input reference sequence $\{w\}$ which is bounded and the identification error sequence $\{\hat{y}(t) - y(t)\}$. Since the identification error sequence remains bounded and converges provided that the RLS algorithm converges, $\lim_{t \rightarrow \infty} |\hat{y}(t) - y(t)|$ is bounded and so is $\hat{\Phi}(t)$. Moreover, we have $l(t+1) = A_l l(t) + B_l w(t)$ which is stable, thus for a bounded input signal $w(t)$, $l(t)$ is bounded. Therefore, $v_2(t)$ is bounded, and since $|v_1(t)| \leq \|B\hat{\Phi}^{-1}\| (|w(t)| + |\hat{y}(t) - y(t)|)$ then it follows that $|v_1(t)|$ is bounded and hence $\|\mathbf{v}(t)\| \leq |v_1(t)| + |v_2(t)|$ is also bounded. All the conditions of lemma 1 are verified and this proves the stability of the proposed control.

7.10 Control of SMA using Modified Laguerre Predictive (MLaP) Control: Experimental Results

The proposed adaptive control method given by Eq. (7.70) and described by the schematic in Figure 7.23 is implemented on the same experimental setup as described earlier. In order to analyze the performance the proposed method is first tested with 5th order and 2nd order model. Since the original system is nonlinear the order of the linear model used to predict the nonlinear system becomes crucial at least locally. Hence study of the controller for model with different order proves reasonable to understand and interpret the control.

The tuning steps are as follows:

Step-1 Choose forgetting factor $\lambda \approx 1$ and $P(0)$ large such that $|y(t) - \hat{y}(t)| \rightarrow 0$.

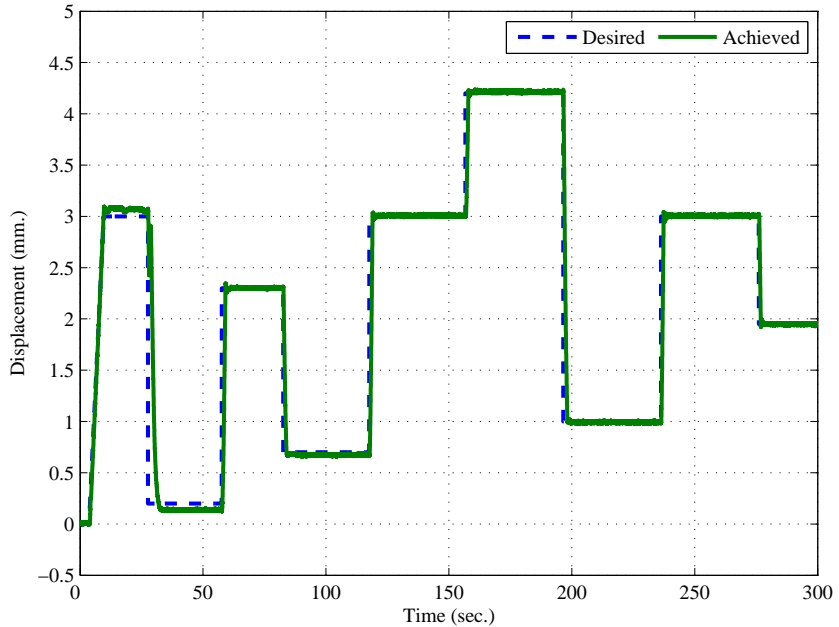
Step-2 Then start tuning the controller parameter (H_p) such that $|w - y(t)| \rightarrow 0$.

7.10.1 Position Control using 5th order linear Laguerre model with MLaP method

The same reference signal as the one applied to test the CLAP control, was used to evaluate the developed control strategy. The tuning parameters which influence the performance of the control algorithm for example sampling rate T_s , Laguerre pole a , forgetting factor λ in the recursive Identification routine and the most crucial in calculating the controller gain is the prediction horizon H_p . To begin with, the following initial parameters have been used:

- Sampling Rate $T_s = 0.01$ sec.
- Laguerre pole $a = 0.9$
- Covariance initialization $P(0) = 10^2 \mathbb{I}$
- Forgetting Factor $\lambda = 1$
- Prediction Horizon $H_p = 3$
- Controller weights: $R = 0, Q = 1$

| H_p | MO (%) | MST(sec) | MSSE (%) | MOS (%) |
|-------|--------|----------|----------|---------|
| 3 | 1.0 | 6.3 | 4.3 | 0 |
| 30 | 0.6 | 9.6 | 8.2 | 0.1 |

 Table 7.2: MLaP: 5th order model performance indexes.

 Figure 7.24: Tracking using MLaP method with 5th order model, ($a = 0.9, H_p = 3, \lambda = 1$).

In Figure 7.24 we can see from the experimental results that the controller is able to track a given reference with variable amplitudes and the static error has been reduced as can be seen in Figure 7.25. The control signal generated by the controller can be seen in Figure 7.25. One of the most important aspect of the current adaptive control is the recursive identification algorithm and the closed loop identification error and evolution of weights can be seen in Figure 7.26.

From the displacement response and the tracking error we can see that initially the error is high which is due to the fact that the Laguerre model weights are still in the tuning process and have not converged yet, which is also the conclusion from the closed loop identification error which converges to zero gradually. As described earlier the different mean performance variables such as Mean Overshoot, Mean Settling Time, Mean Steady State Error and Mean Oscillations for prediction error $H_p = 3$ can be seen in Table 7.2. The steady state error is minimum at zero for most of the different step references except for the case when the reference is close to zero the steady state error is 32.3%, which has ultimately lead to an average of 4.25% MSSE. From the controller action we can see that the tracking response has performed well even with input constraints of 0 – 3 V.

For the closed loop identification a forgetting factor of $\lambda = 1$ was used which ascertains

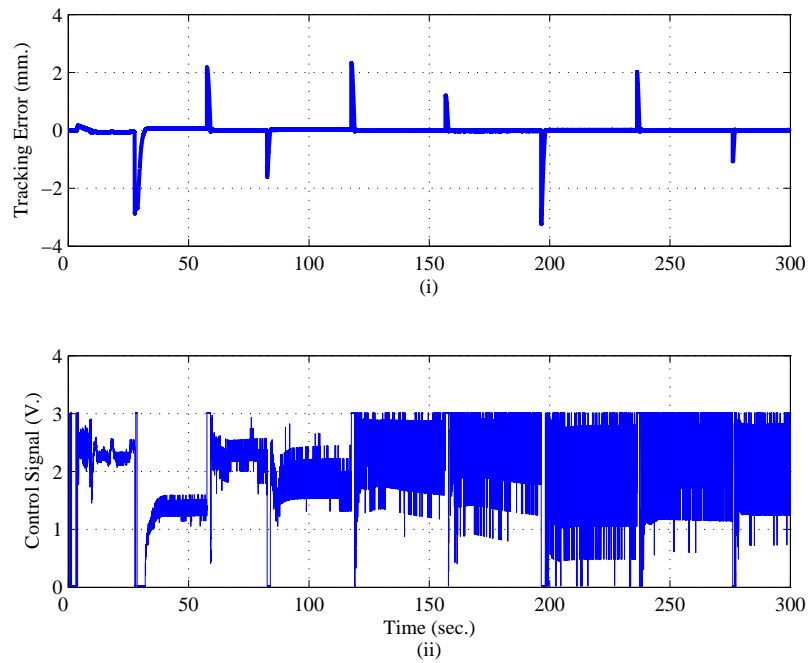


Figure 7.25: (i) Tracking error and (ii) Control signal using MLAP method with 5th order model, ($a = 0.9$, $H_p = 3$, $\lambda = 1$).

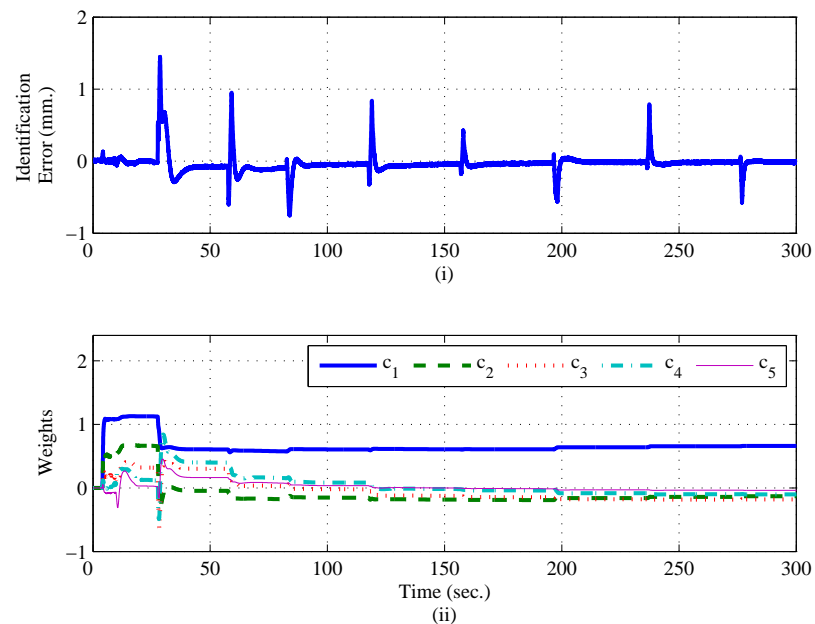


Figure 7.26: (i) Identification error and (ii) Laguerre filter weights using MLAP method with 5th order model, ($a = 0.9$, $H_p = 3$, $\lambda = 1$).

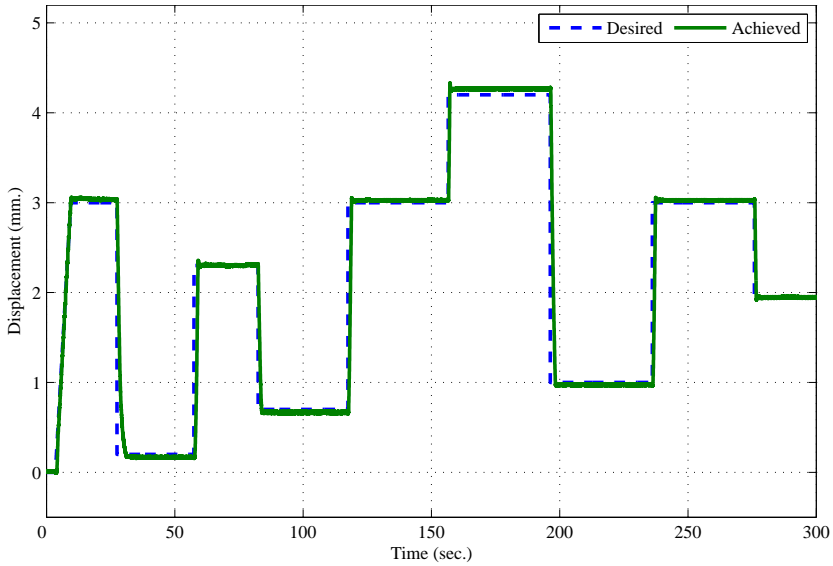


Figure 7.27: Tracking using MLAP method with 2nd order model, ($a = 0.9, H_p = 3, \lambda = 1$).

| H_p | MO (%) | MST(sec) | MSSE (%) | MOS (%) |
|-------|--------|----------|----------|---------|
| 3 | 1.03 | 5.96 | 2.70 | 0.10 |

Table 7.3: MLAP 2nd order model.

that the model has full memory of all the past data points of the closed loop response. The identification error becomes progressively similar to the tracking error, and the weights other than first weight vanish to zero. In the meantime, the closed loop error being zero we can conclude that thanks to the controller the nonlinear system is similar to a first order linear system in closed loop.

7.10.2 Position Control using 2nd order linear Laguerre model with MLAP method

To implement the MLAP method using 2nd order model the same controller is used as above with the following initial parameters: $T_s = 0.01$ sec, $a = 0.9, \lambda = 1$, and $H_p = 3$. The experimental results for displacement tracking of a mixed square signal can be seen in Figure 7.27. The displacement tracking error and control signal can be seen in Figure 7.28. The closed loop identification error and Laguerre filter weights can be seen in Figure 7.29.

The different mean performance variables can be seen in Table 7.3. From the displacement response and the tracking error we can see that the second order model is still able to handle the nonlinear hysteretic system. The steady state error at maximum displacement position is higher at 1.8% for 2nd order model controller compared to the 5th order model controller which was 0.4%. This is due to the fact that the prediction at the saturation level of the actuator using the 2nd order model is not as good as the 5th

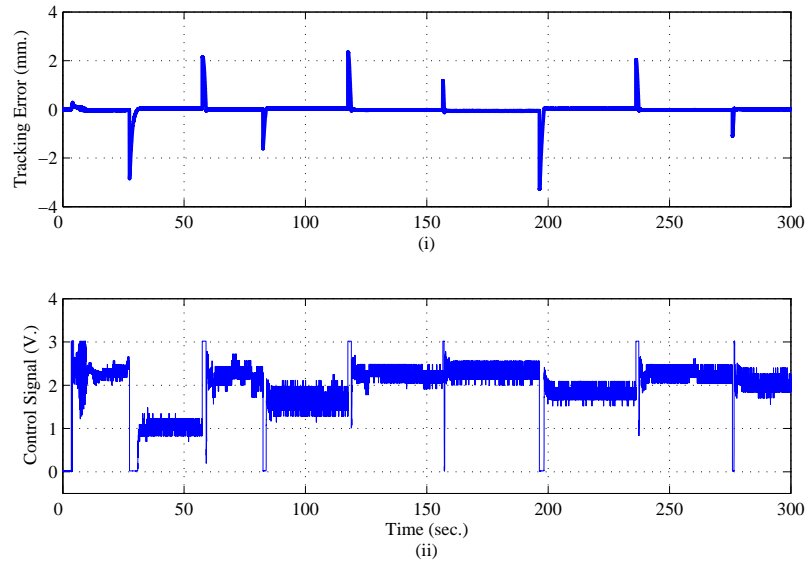


Figure 7.28: (i) Tracking error and (ii) Control signal using MLAP method with 2nd order model, ($a = 0.9, H_p = 3, \lambda = 1$).

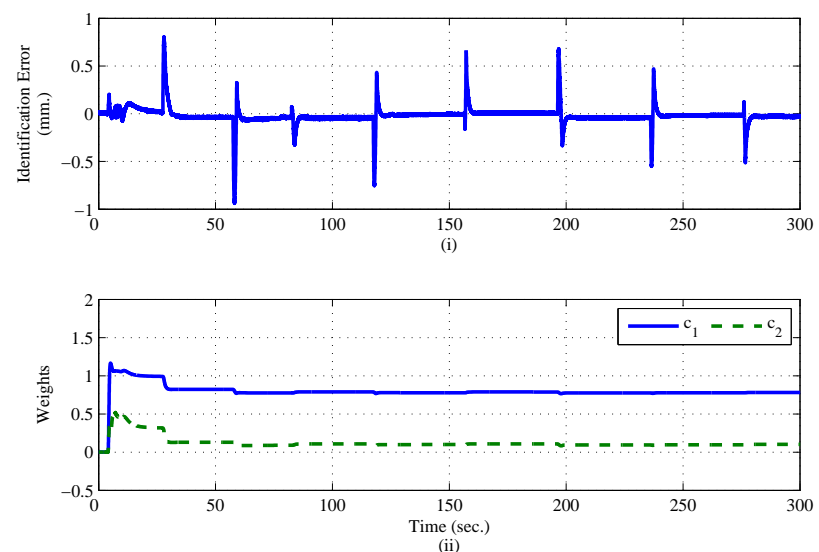


Figure 7.29: (i) Identification error and (ii) Laguerre filter weights using MLAP method with 2nd order model, ($a = 0.9, H_p = 3, \lambda = 1$).

order model which is also evident from the closed loop identification error. But steady state error close to the zero reference value was relatively less at 11.5% using 2nd order model as compared to 5th order model. Hence the mean steady state error was 2.70%. Considering the control signal, controller action using the 2nd order model controller is less reactive and well within the input constraints compared to the 5th order model controller for the same value of prediction horizon $H_p = 3$. The general behavior of the closed loop identification error and the trajectory of the model parameters is analogous to that of the 5th order model behavior and also shows the closed loop system is finally a first order system.

7.11 Discussions

In this section the MLaP method using the 5th order model is discussed considering the influence of the choice of the prediction horizon H_p , and the rejection of thermal disturbance is examined.

7.11.1 Influence of prediction horizon

The prediction horizon H_p is a very crucial tuning element in the design of the predictive control law. To conduct the experiment the following tuning parameters were used: $a = 0.9$, $\lambda = 1$, $H_p = \{3, 30\}$. From Figure 7.30 and Figure 7.31 it can be observed that the tracking error improves with a smaller prediction horizon and is better for $H_p = 3$ as compared to $H_p = 30$. The mean performance variables can be seen in Table 7.2. By increasing the prediction horizon to $H_p = 30$ the mean overshoot reduces by 35%, the mean settling time and mean steady state error increases by 52% and 92% respectively. The mean oscillation is only marginally increased. When a smaller prediction horizon is used the controller actually predicts a shorter period into the future and is recalculated at the end of each period. Hence shorter period means more number of recalculations of gain. For a system like SMA which has switching properties a faster rate of recalculation of gain is advantageous.

7.11.2 Perturbation Rejection

In order to test the robustness of the proposed control algorithm, experiments were conducted in the presence of thermal disturbance to track a given reference signal. The parameters used for this experimental test are $a = 0.9$, $H_p = 3$, $\lambda = 1$. The SMA wire is submitted to an instantaneous burst of air around 125 seconds which modifies the cooling conditions of wire. From the Figure 7.32 it can be seen that the controller adapts to disturbances but introduces oscillation of 8.6% for a brief period of time which can be seen from the control signal in Figure 7.33.

7.12 Antagonistic Actuator control

This section is dedicated to the control problem of antagonistic SMA actuator. The antagonistic actuator setup was modeled and studied in chapter-2.

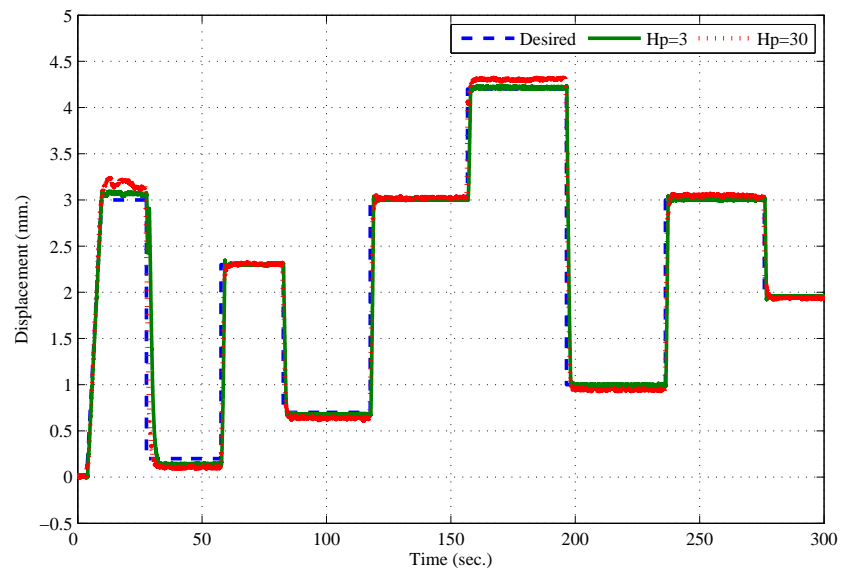


Figure 7.30: Tracking using MLaP method with 5th order model, ($a = 0.9, H_p = 3, 30, \lambda = 1$).

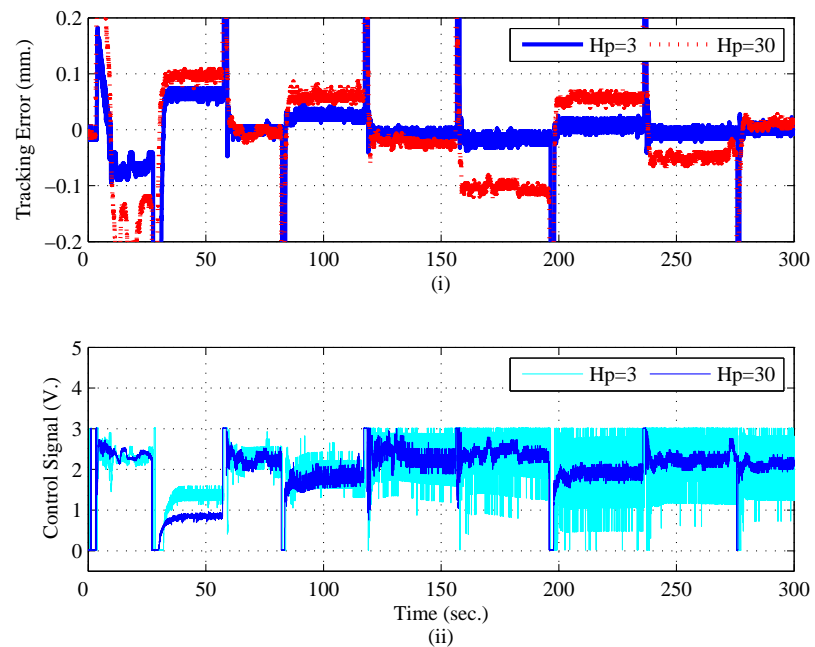


Figure 7.31: (i) Tracking error and (ii) Control signal using MLaP method with 5th order model, ($a = 0.9, H_p = 3, 30, \lambda = 1$).

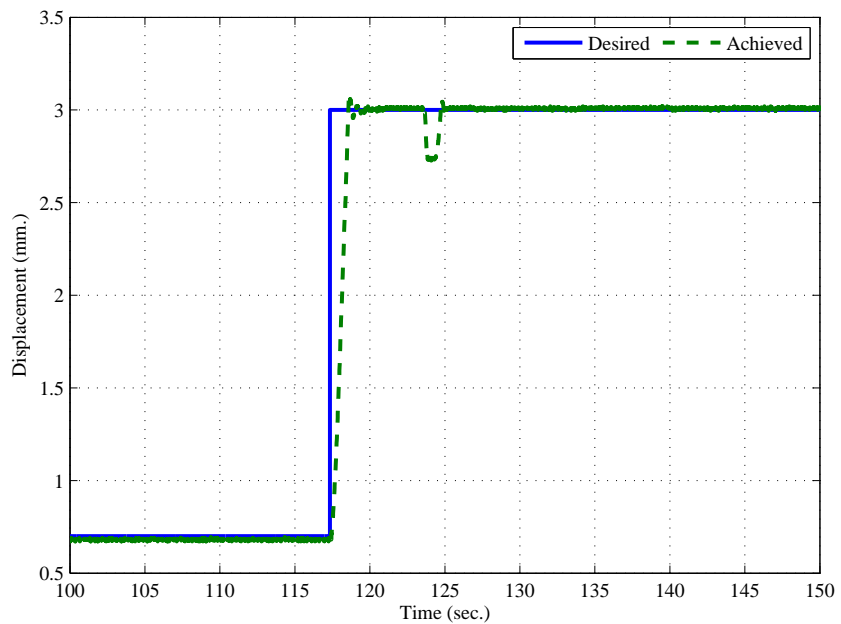


Figure 7.32: Perturbation Rejection: Tracking using MLaP method with 5th order model, ($a = 0.9$, $H_p = 3$, $\lambda = 1$).

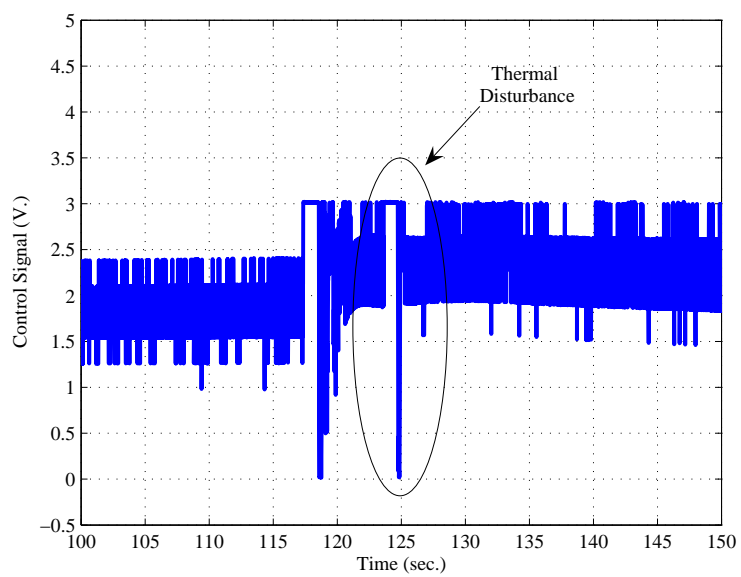


Figure 7.33: Perturbation Rejection: Control signal using MLaP method with 5th order model, ($a = 0.9$, $H_p = 3$, $\lambda = 1$).

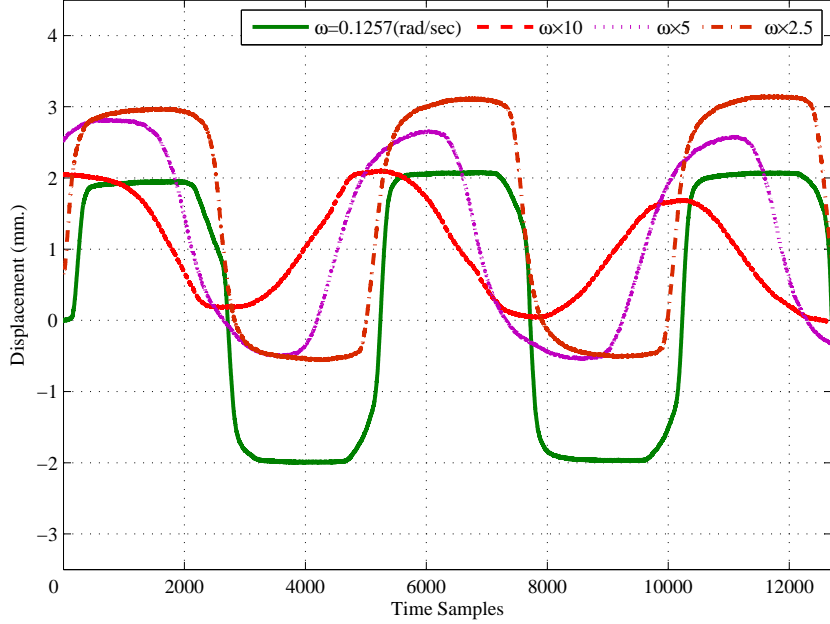


Figure 7.34: Displacement vs normalized time for different frequencies for a sinusoidal voltage (3 V amplitude).

7.12.1 Open loop characteristics

Before proceeding to the design of control, the setup was tested to evaluate the actual performances. As seen in Figure 7.34, the actuator was used in open loop and was fed with an alternative sinusoidal voltage (3 Volts amplitude) of different frequencies and the displacement was measured. In Figure 7.35 these measurements are presented for different frequencies evenly chosen on a logarithmic scale. Clearly, the displacement range is reduced over 0.7 rad.s^{-1} , which is consistent with an estimation of the thermal time constant of a wire (0.6 rad.s^{-1}). Also the shape is very distorted for low frequencies because of the hysteresis major loop, as opposed to high frequencies where the wire cannot be fully cooled hence only minor loop are covered (see Fig. 7.36 and Fig. 7.37). Another less expected phenomenon is a bias which seems dependent on the frequency. Dissymmetry of the setup can not solely explain this, and this trend may be linked to the modification of the hysteresis as the stress build up in the case of incomplete cooling of the wires. From the point of view of the identification and control, this actuator exhibits quite a challenging open-loop behavior. Indeed the bias raises reachability problems since the symmetry in actuation can be lost.

7.13 Experimental results and discussion

7.13.1 Position Control

The first test in closed loop consisted of following a step reference with different amplitude as shown in Figure 7.38. The criterion for the profile was that it should not be symmetric to explore the minor loops of the hysteresis and present some similar values to ensure that the performance were repeatable. Because of the limitation explained

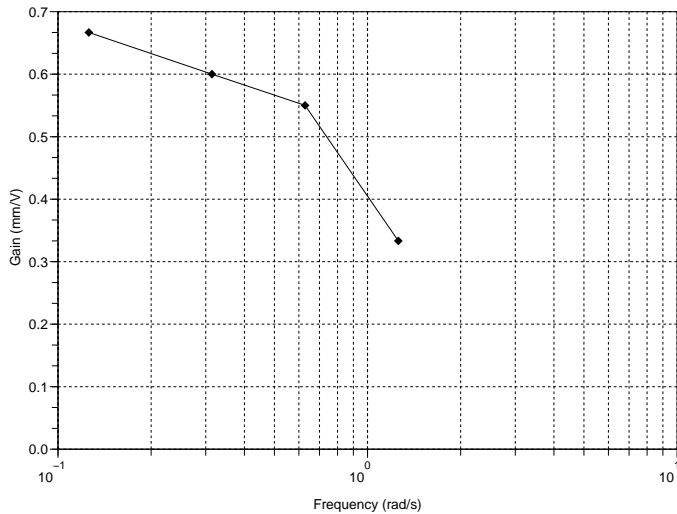


Figure 7.35: For different frequencies semilog plot of gain (mm/V) for a sinusoidal voltage (3 V amplitude).

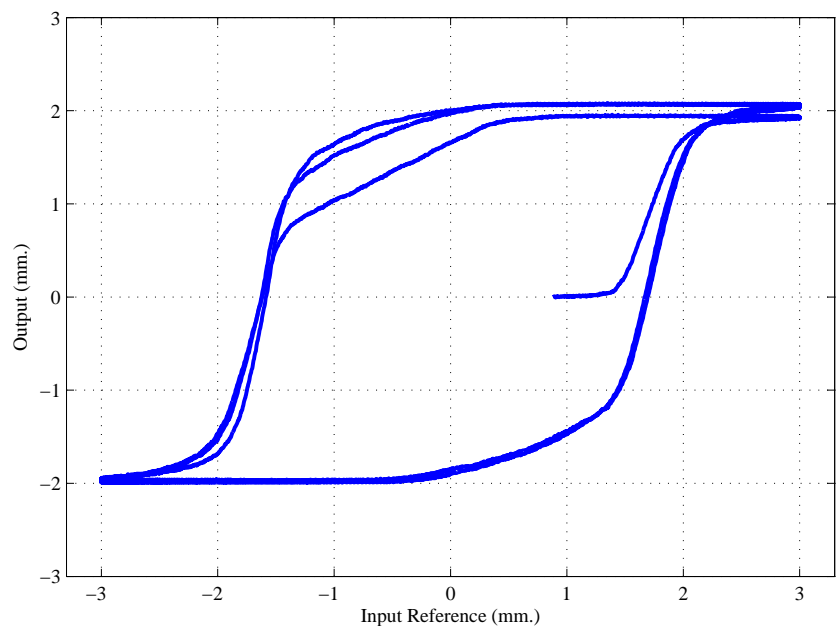


Figure 7.36: Hysteresis for input frequencies $\omega=0.12 \text{ rad.s}^{-1}$.

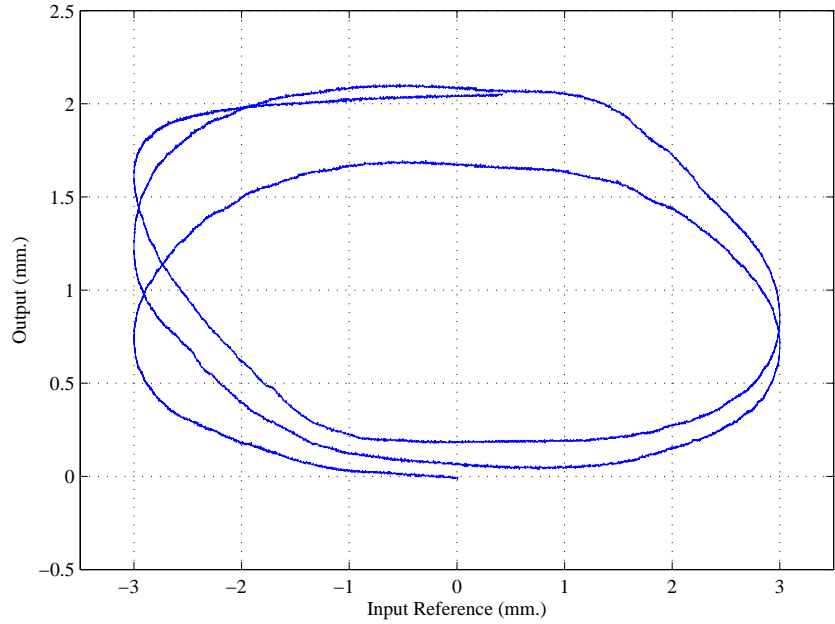


Figure 7.37: Hysteresis for input frequencies $\omega=1.2 \text{ rad.s}^{-1}$.

in Section 7.12.1 the overall range for the reference is kept around 2 mm. Some larger values were also tested without noticeable change in performance. Before each test initial bias position has to be measured in order to reset the zero position. The reference was scaled time wise in order to verify that at faster pace the thermal drift in the wires do not destabilize the controller. Even in the case where the plateau in the reference were less than the time constant of the wire, the performances were similar to the one of Figure 7.38. Every set of tests were repeated at least five times and the parameters of the controller were :

- Number of filters : $N = 2$
- Forgetting factor : $\lambda = 1$
- Prediction horizon : $H_p = 3$

The settling time is 0.8 s for almost every step except when the reference is around zero where it reduces to 0.4 s. The steady state error is always less than 3% in almost every case. However for a reference around zero it reaches 20%. On the Figure 7.39 the input voltage is shown. This figure was realized by adding the voltages of the two power supply in order to have a synthetic curve of the voltage applied to the wires. The limitation between -3V and 3V appears clearly during the transient but they are well supported by the controller and the identification. It can also be noted that the actual range of the voltage applied is relatively narrow in steady state indicating that the voltage must reach a threshold in order to trigger the phase transformation. In Figure 7.40 one can see the identification of the weights of the Laguerre filter. First, the small value for the coefficient c_2 indicate that the pole of the filter was correctly chosen, that is near the actual time constant of the system. Second, they change according to the working point, and since their evolution are similar it can be deduced that the gain of the system mainly changes, as opposed to the time constant which remains roughly

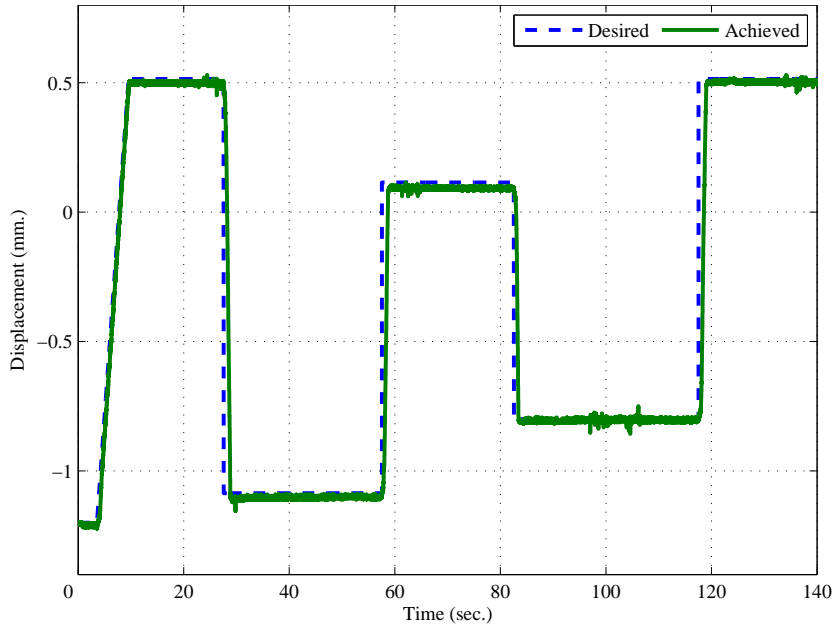


Figure 7.38: Displacement response for tracking a mixed square wave.

constant. Finally the identification error (Fig. 7.41) remains around zero, except for the transient during which it is rapidly corrected. Another test consisting in the following of a sine reference (frequency : 0.02 Hz) can be found in Figure 7.42 and Figure 7.43 where the open loop and closed loop hysteresis are shown respectively. This test is interesting because this signal is particularly severe on the identification point of view as is it not persistently exciting, still the controller and the identification performed well. It follows that the hysteresis is fairly compensated, and that it is near to a line with unitary slope. A problem remains for small displacements, as it was already mentioned in the case of the preceding test. This test was performed with a higher initial stress which explains the modification of the hysteresis shape.

Perturbation Rejection

In order to evaluate the ability of the controller to reject a thermal perturbation, a change of the thermal exchange was applied by blowing air toward the wire during the steady state. The perturbation is very well and rapidly rejected as Figure 7.44 shows. The respective control signal can be seen in Figure 7.45.

7.13.2 Influence of Prediction Horizon

In order to control the performance of the controller, the designer can only act on the prediction horizon. Since this fixes in how many samples the system should reach the specified reference, a smaller prediction horizon will result in a higher gain. In Figure 7.46, this effect is illustrated through two experiments with different prediction horizons $H_p = 3$ and $H_p = 30$. In the case of small values of H_p , the steady state error is small and the voltage activity is larger when compared to the one applied for $H_p = 30$ as seen in Figure 7.47. It is also worth noticing that the actual difference

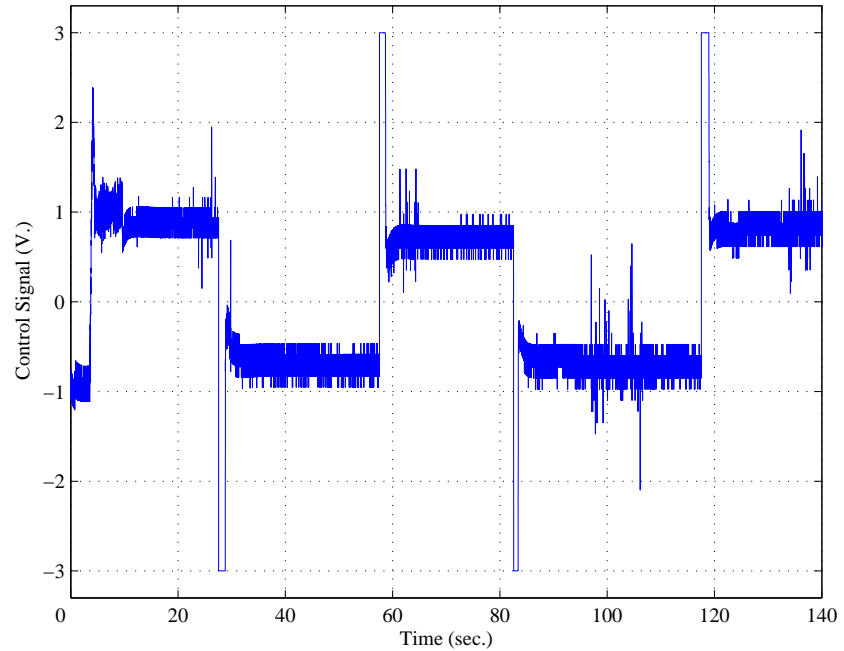


Figure 7.39: Control signal for tracking a mixed square wave.

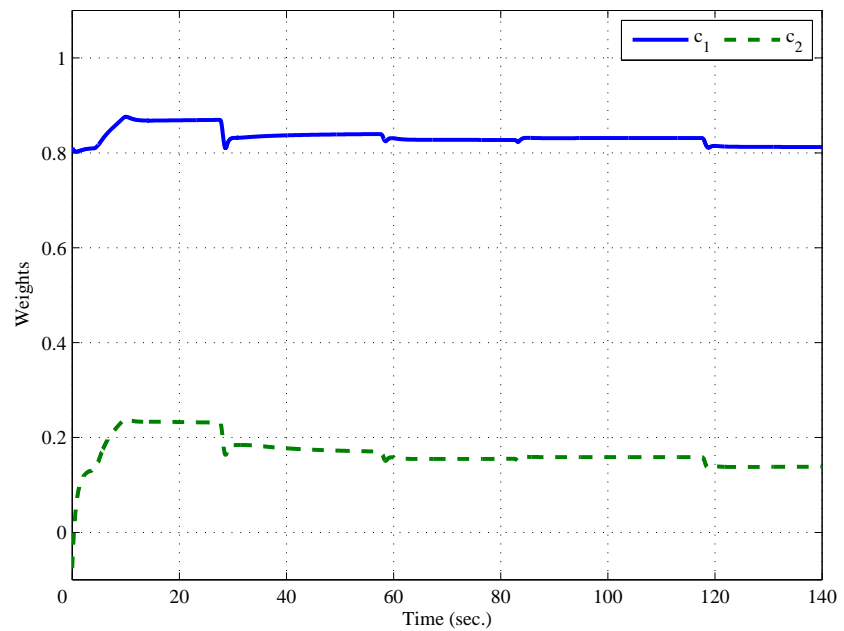


Figure 7.40: Identified Laguerre weights for tracking a mixed square wave.

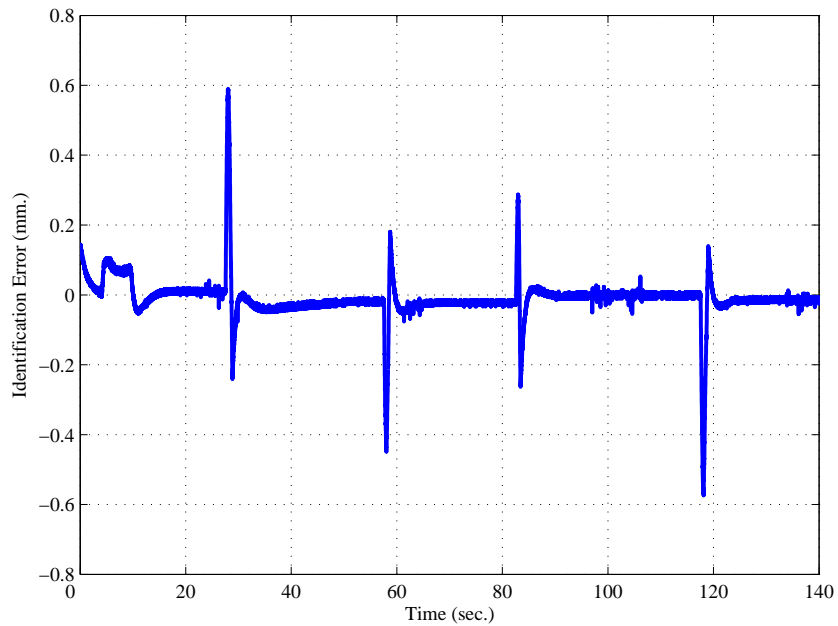


Figure 7.41: Closed loop Identification Error for tracking a mixed square wave.

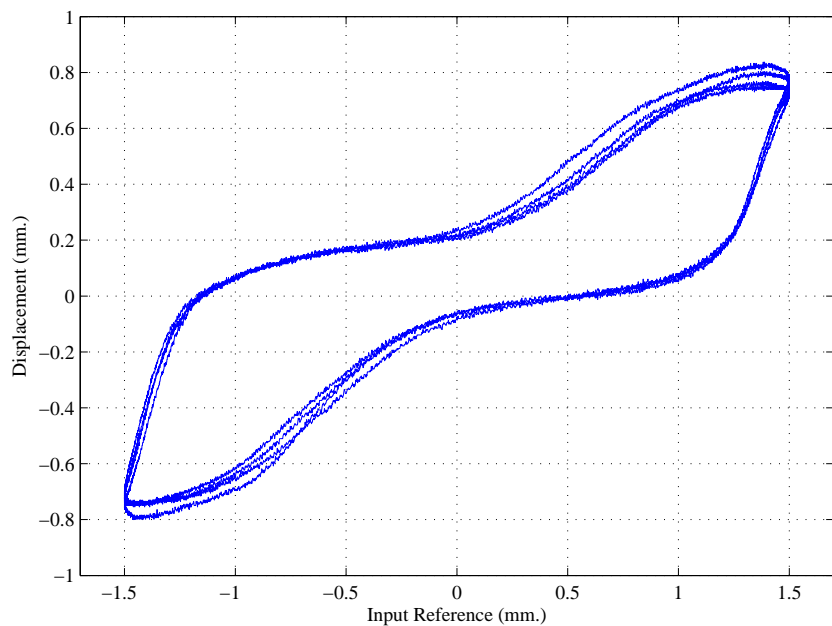


Figure 7.42: Hysteresis in open loop antagonistic system.

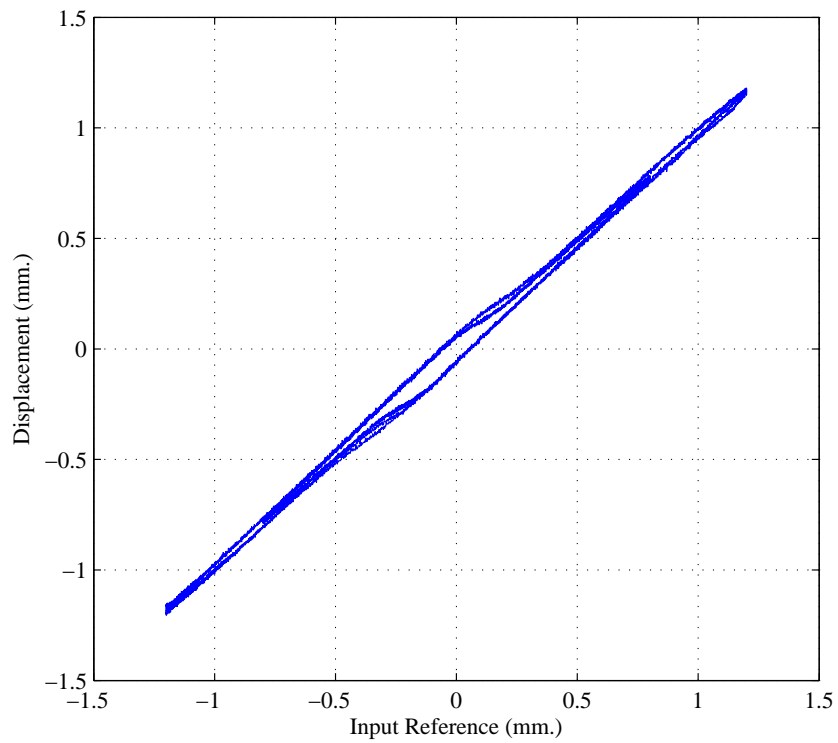


Figure 7.43: Hysteresis in closed loop controlled system.

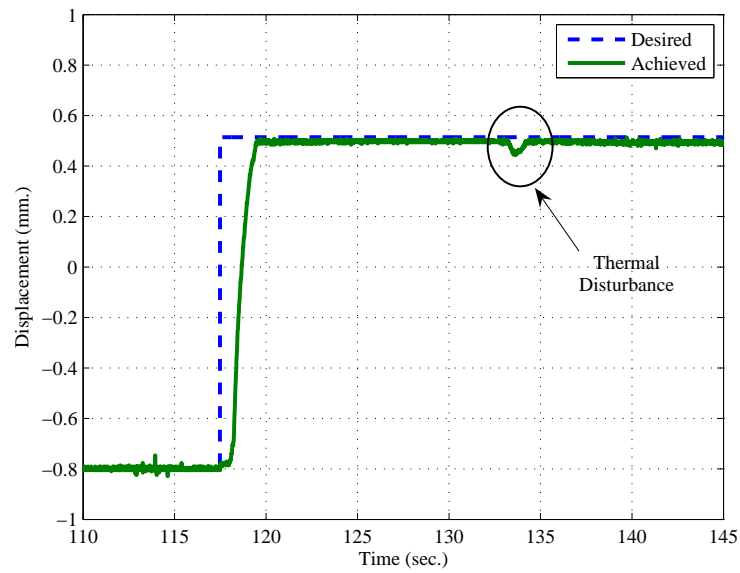


Figure 7.44: Output of the actuator under a thermal perturbation.

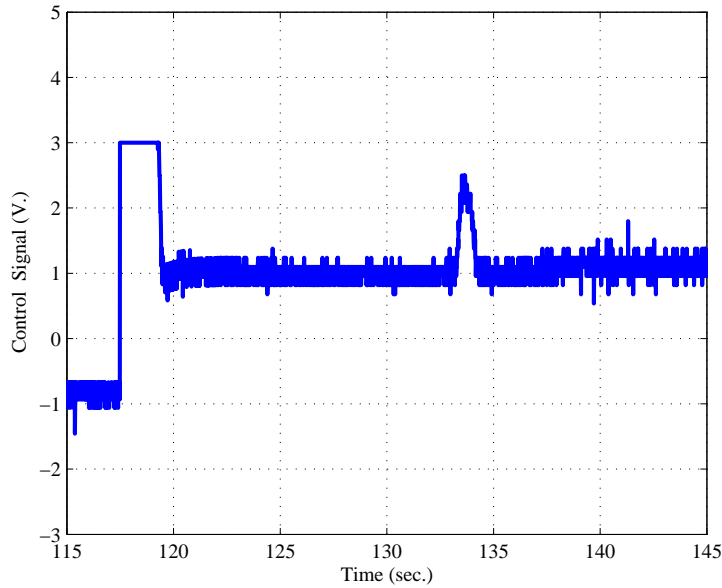


Figure 7.45: Applied voltage under a thermal perturbation.

between the voltage applied as seen in Figure 7.48 in both case is small due to the steep slope encountered in the hysteresis. In the case of a one step ahead prediction the behavior of the controller tends towards sliding mode control due to the limitation of the voltage, but still the control was ensured. Since this behavior is not a proper way to use the linear voltage supply the value $H_p = 3$ was adopted.

7.14 Antagonistic setup: Discussion

An adaptive predictive control developed to control a SMA wire under constant stress has been successfully applied to the problem of the control of antagonistic actuator. The open loop test of this later actuator was found to be more complex than the single wire especially because of the variable bias that was encountered. Nonetheless, only with a minor change in the filter configuration (two filters where used instead of five for the single SMA actuator), the controller was able to perform tracking of complex input with good performance. The originality of the control is that the only measurement needed is the displacement of the actuator, and that the model directly maps the voltage to this measurement. Both tracking capabilities and perturbation rejection were tested with satisfactory results. The core of the control is the identification scheme. Here a standard RLS algorithm was tested with success.

At this point linear voltage supplies were used. From the experiments realized with prediction horizon $H_p = 1$, which result in a controller signal similar to a sliding control, a promising way to improve the system is to replace those linear power supplies by a switched power supply and replace the proposed controller by a variable structure controller. This will probably improve robustness and simplicity of the hardware. The remaining weakness of the proposed controller remains the poor performances for

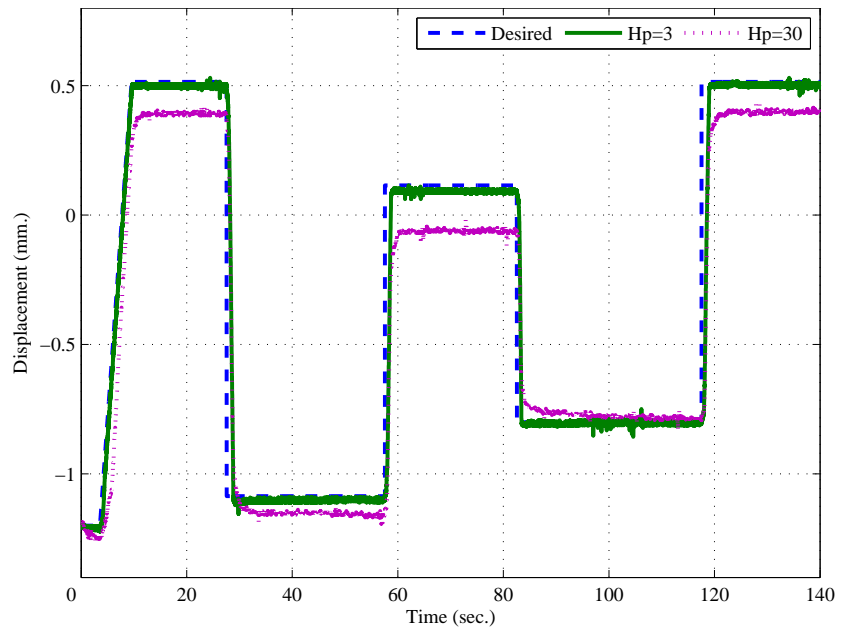


Figure 7.46: Actuator output for prediction horizons $H_p = 3$ and $H_p = 30$.

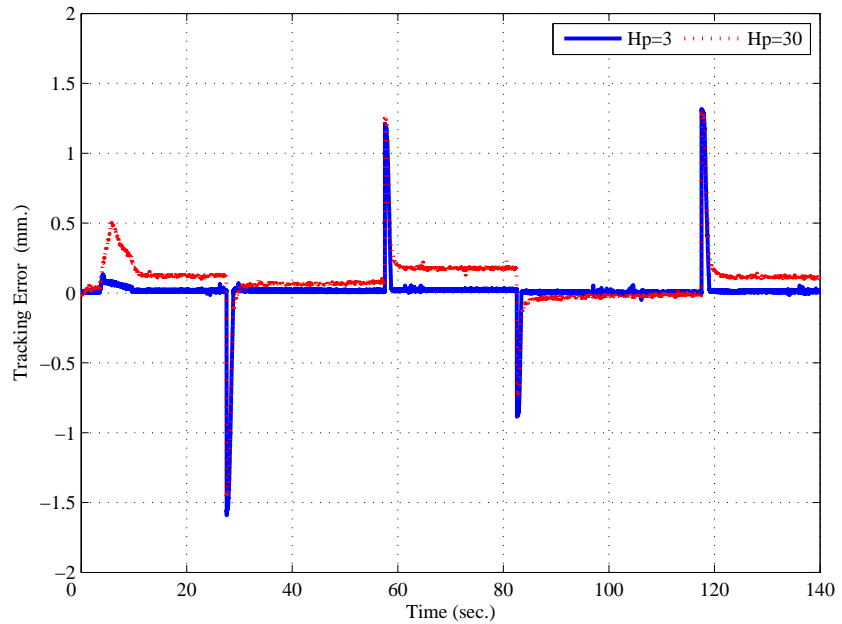


Figure 7.47: Antagonistic setup: Tracking error for prediction horizons $H_p = 3$ and $H_p = 30$.

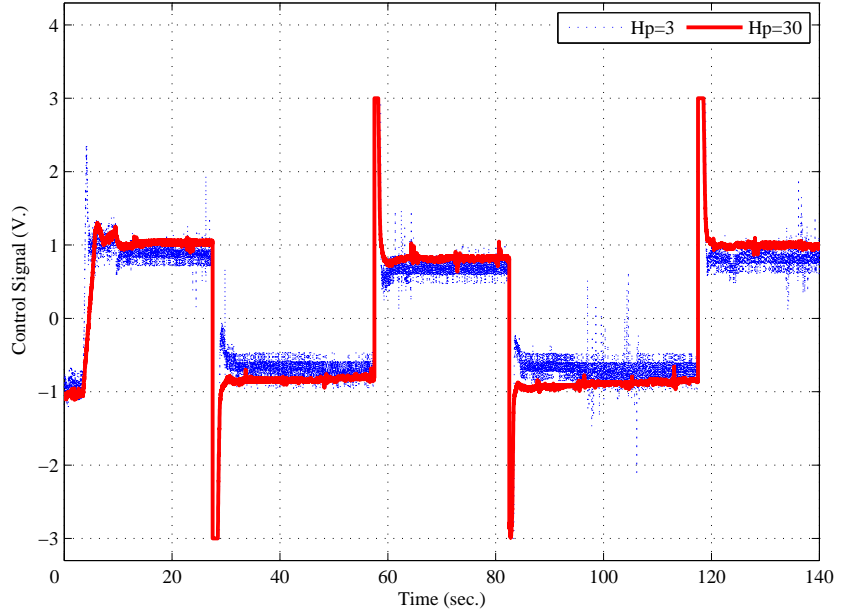


Figure 7.48: Antagonistic setup: control signals for prediction horizons $H_p = 3$ and $H_p = 30$.

reference values near zero. However, the controller proposed so far is essentially a proportional controller. A way to improve it would be to include an integrator in the control loop to handle the steady state error. Due to saturation an anti wind-up integrator will be implemented in the future. Although the dynamic model proposed involves no knowledge of the underlying physics of the system controlled, it was clearly demonstrated through the open loop test that one should not ignore the intrinsic limitations of the actuator. In this study the voltages applied were limited to 3 volts, an arbitrary value which in some case was not enough, and a supplementary protection was to limit the current which in some case were activated. Although the controller showed no stability problems in those situations, this should be directly handled by estimating the range of the actuator, a goal that involves some knowledge of the material state.

7.15 Conclusion

In the current chapter the problem of SMA control was handled using an adaptive predictive control. Initially, the closed loop identification strategy was introduced followed with the fundamental idea of the Model Predictive control. Optimal control input was also analytically developed. First the simple SMA actuator was studied for control purpose with predictive control using classical RLS with exponential forgetting (EF-RLS). Drawbacks in the Adaptive Predictive control using EF-RLS was investigated resulting in the analysis of bursting phenomenon in adaptive control. The bursting phenomenon was successfully solved using an advanced RLS algorithm using Directional Forgetting (DF-RLS). The second part of the chapter consist of development of a proposition for a Modified Laguerre Predictive (MLaP)control which solves the problems in CLaP-EFRLS by using a modified predictor based on closed loop behavior of

Chapter 7. Adaptive Predictive Control

the system. The proposed MLaP was also validated on a more complicated antagonistic SMA actuator. Further stability and convergence results for the modified method were also discussed.

Chapter 8

Conclusion

8.1 Summary of this work

Originally, the scope of thesis was the control of SMA actuators. This work rapidly focused on the two key problems encountered usually in the literature, namely the modeling and the control.

A model is an approximation of a real system, and the simplifications done should capture the features needed for a given application. In the context of control, the main points are:

- describe the dynamic of the system;
- easily identifiable
- mathematically simple, in order to make the design of the control tractable;

In the case at hand, the model should also be general enough to address as many SMA based actuator architecture as possible. Unfortunately, the SMA are hindered with a hysteresis which is difficult to handle with classical linear control design. For instance the saturation would destabilise a proportional integral, and even though one might argue that a fine tuning of such a controller is possible, the drift of the material due to thermal fatigue occurring with multiple cycling would degrade the performance of the controller.

On the other hand, non linear approaches can be found in literature. Often the non-linearity is modeled using hysteresis approximation such as Preisach and so forth, then inversed and used as a forward compensation. This approach suffers two main drawbacks:

- the identification on-line can only be approximate or is computationally intensive;
- this approach, which is fairly successful in the case of a Hammerstein non linearity¹, is more questionable in the case of a Wiener non-linearity particularly for tracking.

Non-linear control based on physical modeling were successfully applied to control SMA actuators. However, these models are very demanding on the apriori knowledge in the

1. such as the one encountered in piezoelectric or magnetostrictive devices control

form of physical parameter that must be identified off-line.

Therefore, in this thesis, we adopted an alternative viewpoint, that could be considered as a trade-off between the two extremes evocated before. The core idea is to use a linear model for simplicity and to take advantage of the well-established design techniques. To handle the intrinsic non-linear nature of SMA, a constantly adapting model was used. This paradigm supposes that the non-linearity can be assimilated to a “slow time variation” of the parameters of the linear model. The problem of linear approximation of non-linear system is still an open subject which received a lot of attention during the last years especially for separable nonlinearities. Results of this research is however at the moment addressing mostly the off-line identification using random multisine signals. Due to the lack of results concerning online identification and control, an experimental validation was presented. The generality of the approach was tested by directly transferring the identification and control methodology to the more complicated antagonistic actuator.

8.2 Contributions

8.2.1 Modeling for Control

Concerning the modeling the contribution of this work was to:

- propose the use of the orthogonal functions
- study the case of three models. Two of them consisting in linear Laguerre filters of different orders to address the problem of precision, and a non-linear Volterra-Laguerre model to evaluate its capacity to better approximate the hysteresis non-linearity.
- compare different recursive least squares algorithm
- study the influence of their main tuning.

The use of Orthogonal functions simplifies the modeling because the order of the filter is not directly linked to the actual order but to the precision of the approximation of the frequency response. With the sole knowledge of the dominant time constant, they allow to approximate a system with a limited number of functions, thus a limited number of parameters, even if the sampling is fast.

This was clearly demonstrated through the experiments consisting in identifying the SMA actuator response using signals hardly verifying the PEC. Indeed, it was possible to fit a fifth order filter with a signal for which content was limited to two frequencies. The Volterra Laguerre Model achieve similar results as a fifth order Laguerre filter, while its requirement in terms of excitation are comparable to the second order filter. Although the identification is satisfactory when a standard exponential forgetting RLS algorithm is used, it presented too large variation of the weights in some cases. As a solution, the directional forgetting RLS were proposed and successfully cancel the unwanted bursting phenomena observed.

Finally, the influence of the forgetting factor and of the sampling rate lead to the conclusion that:

- setting $\lambda = 0.99$ gives in almost all cases excellent model;
- the modeling is not too sensitive to the sampling time.

8.2.2 Adaptive control of SMA actuator

The first attempt to apply a predictive control based on the Laguerre model of the SMA actuator was hindered by strong overshoots during transients or bursting in steady state. Overshoot can be attenuated or even cancelled by choosing a small prediction horizon. However, the bursting being always present, this would cause chattering around the steady state. So indirectly, there is a kind of trade-off between prediction horizon and forgetting factor. Interestingly enough, there is no destabilization because sudden bursts generate enough information for the RLS to converge back to the weights value.

This phenomenon being unacceptable, the RLS algorithm was improved by introducing directional forgetting in the RLS. This allows to select the measurements incoming before introducing them in the covariance matrix. This allows to prevent the sensitivity to noise during phases where the excitation is too poor, typically in steady state. Moreover, it is very simple as far as the implementation is concerned. Adopting this, the bursting was totally eradicated. It is also worth noticing that the order of the filter needed can be kept small since results of the 2nd order are very similar to the 5th order. In addition to the previous structure, we proposed a modification of the controller that uses an identification of the closed loop system. This choice was initially dictated by the sensor used which gave a lot of noise on the measurements. By doing so the problems usually encountered with the previous controller (bursting) were eliminated since the inputs and the outputs used for the identification were no longer correlated. Basically, the identification is done using the input as an instrumental variable. More importantly, the strategy is departing from the initial adaptive predictive control framework and has more resemblance in structure to model reference adaptive control. Indeed, the RLS algorithm used successfully had no adaptation capability since $\lambda = 1$. Since the tracking error still remains close to zero, this means that the closed loop system is actually adapting to the model. This inference is confirmed by the fact that the weights rapidly vanishes to zero for order bigger than one. Owing to the relation:

$$c_n = \sum_{i=1}^n B_i \frac{\sqrt{1-a^2}}{1-az_i} \left(\frac{z_i - a}{1-az_i} \right)^i$$

where z_i are the pole of the system, and B_i the gain associated to its rational decomposition, it is clear that the Laguerre developmental weight of the system will decrease exponentially, if the two following conditions are verified:

1. the system is a first order
2. the Laguerre pole is close to the pole of the system

in this case the weights are decreasing with the geometric progression:

$$\frac{c_n + 1}{c_n} = \frac{z_i - a}{1-az_i}$$

Hence, when considering Fig. 7.26 or Fig. 7.29, it appears that the system in closed loop has a pole close to the pole of the Laguerre filters. In other words, the Laguerre pole has been imposed to the closed loop in implicit way.

8.3 Unsolved problems and Future Directions

The research conducted in this thesis had a major focus on the modeling and control of SMA actuators. While these two aforementioned aspects have been extensively studied, there still remains many problems that should be addressed.

8.3.1 Optimal Actuator design

In this thesis, the research was started with the assumption that the SMA actuator systems studied were optimal in design and the control development was to be performed thereafter with the belief that any further problems could be solved as a control problem. But this strategy was not entirely appropriate as it was brought to our notice while handling the electrical constraints problem. Further we can study in detail the problems faced in the single wire and antagonistic actuator individually.

Single wire SMA actuator

Although the adaptive methods in this thesis help us to cope with the changes in the material properties over a longer period of time, one has to keep in mind the span of time after which the material has to be replaced. Indeed, we have completely neglected the true physics of the SMA material, and the approach followed here does not give us any idea about life span or cyclic loading limits. To progress toward a proper mechatronic design, these important aspects should be specified to the control engineer.

To illustrate this, we found out in the early stage of the experimental work that constraints should be applied to the current through the SMA wire. Not doing so lead rapidly to incremental permanent deformations, until no actuation was possible any-more. Hence, it was necessary to choose a limit in the practical strain allowed that would preserve the lifetime of the actuator. This directly impacted the maximum achievable strain (approximately limited to 4 %) that was used in the controller design and validation. This resulted in a stroke of 4.2 mm, the total length of SMA wire being 200 mm. Now the real question is: Is the current limit of the SMA chosen an optimal choice ?

Studies have been performed by Teh & Featherstone (2004) to relate the current constraint to the measured resistance of the SMA wire used. The relation between the electric current limit and the resistance is nonlinear and, in order to simplify the strategy, a switched electric current limit was used in Teh & Featherstone (2004). In this thesis this aspect has not been studied, and after extensive experimentation the importance of this aspect is ascertained here.

In our case, since the current was not directly controlled, it was decided to limit the control signal voltage within 0 to 3 V. On top of this, to avoid break-down of the power supply maximum current was limited to 0.4 A. This choice was sufficient to reach the maximal stroke. However, these limits, which proved to be acceptable when the process of control design started, were found to be less than optimal later. Indeed, the

current obtained at 3 V was not sufficient any-more. This reveal that the resistance had increased with ageing or cycling loading occurring during the tests. This in return had a negative influence on the controller. Due to the higher resistance, the controller was often pushed in the voltage saturation limit and unable to achieve the maximum stroke initially chosen. This resulted for instance in chattering.

The purpose of this discussion was to stress the following facts:

1. To increase lifetime, the stroke has to be limited to avoid permanent strains and rapid degradation of the actuation capability of the wire;
2. For similar reasons, the current should be limited well below the safety current limit. This value can be estimated around 0.7 A (this value is extrapolated from the recommendation given for a 100 μm Flexinol wire);
3. To exploit the range offered by this limit, the voltage limits should be adapted to the resistance value of the wire which is not only changing between phase transformation, but also with age.

Antagonistic SMA wire

The material preparation that was applied to the SMA wires of the antagonistic actuator was discussed in section 6.5.4. Unfortunately, experimental observations have shown that this preparation process leads to a large inactive zone in the antagonistic actuator. The presence of this deadband, actually reduces the actuator stroke. We extended our bibliographic research to more material science oriented article and found out that this problem is being addressed in some recent publications. We sum up an alternative preparation of the antagonistic actuator setup suggested in [Sofla et al. \(2008b,a\)](#) here:

Step-1 Pre-strain the SMA wire-1 to 4% and fix it to the mass.

Step-2 Take the SMA wire-2 equal to the length of the pre-strained wire-1 and fix it to the other end of the mass.

Step-3 Start the thermal cyclic loading by applying 1 A current to the wire-1 and then to wire-2 and vice-versa for a given number of cycles.

The prestrain is thus applied non-symmetrically as opposed to the ones used in our tests. A comparison of the relative degradations measured on different prestressed configuration are presented on Fig. 8.3.1 where the arrows materialize the inactive strain (which corresponds to the dead band in the actuation). According to the authors this tends to show a relative improvement in using a unilateral initial prestrain over a symmetrical one² and a clear improvement over no treatment at all. It appears that this degradation stabilizes with cycling and remains unchanged after one hundred cycles, a result confirmed by our observations. More importantly, it appears that the apparition of a dead band is not avoidable and that the stabilized value of the degradation in the available stroke will increase with the initial strain. This later effect is however

2. although it can be noticed on Fig. 8.3.1 that the initial prestrains are different in both cases. Thus in our opinion some more investigations are needed.

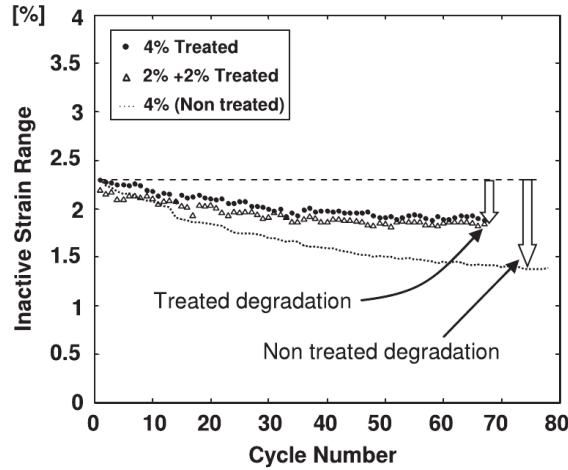


Figure 8.1: Effects of thermomechanical treatment on the achievable strain of the actuators in the case of equal initial prestrain of the wires (“2%+2%” treated), unilateral prestrain (“4%” treated) and untreated wires. The arrows shows the amount of degradation in the obtainable strain of the actuator (source [Sofla et al. \(2008b\)](#))

compensated so as the actual stroke is still greater for large initial prestrain, hence this choice is rather ruled by fatigue considerations.

Now considering the main motivation for using antagonistic actuators, namely improving the bandwidth of the actuation, some caution should be taken both on the design and the control and, to our knowledge, are still poorly documented. To illustrate the point discussed here, let us consider the evolution of the antagonistic actuator in a schematic where the temperature/stress state of the wires constituting the actuator are tracked as represented on Fig. 8.2). On this figure, one recognizes the transformation frontier in dash-dotted lines. For the sake of simplicity, they are supposed to be straight lines, although it is not the case in reality, this approximation suffices to demonstrate the intrinsic limitation on the actuation. Considering the initial state A where both wires are at ambient temperature, the stresses in both wires are the same assuming that the section are equal. Since only the case with no external load is considered, the stresses will remain equal throughout the whole evolution. Heating the wire “SMA-1” will cause the strain in it to reduce, while the strain in “SMA-2” will increase. In the process, the stress in it increases owing to the relationship between stress and strain. Thus, the evolutions of “SMA-1” and “SMA-2” are represented by the segments AB_1 and AB_2 respectively. In order to work at high frequency, the heating of “SMA-2” starts immediately when the heating of “SMA-1” stops. If enough power is available, heating can be made arbitrarily short and it is considered that the cooling of “SMA-1” is negligible³. At the intersection point C, which corresponds to temperature T_1 it can be seen that the transformation is not complete, thus the stroke would be less than the previous one. This is consistent with the fact that the temperature range where no activation

3. a more realistic cycle would include an inclined segment from B_1 to C_1 rather than a vertical one, but this does not modify the point we want to make here.

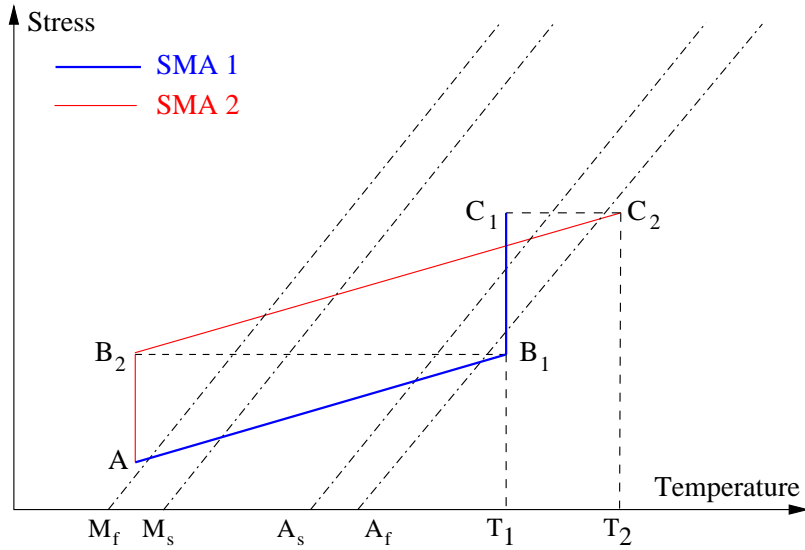


Figure 8.2: Schematic illustration of the building up of stress and temperature during actuation.

is obtained becomes larger. As a conclusion, it is necessary to reach temperature T_2 in order to achieve the same stroke during the “return” phase of the cycle corresponding to the points C_1 and C_2 . Note at this point that:

- the stress builds up
- temperature at which actuation occurs increase
- the cycle is not completed since the point C_1 is not brought back to the left of the M_f frontier

from this latest remark, it appears that rather than increasing the bandwidth, the antagonist actuator enables to reduce the actuation time over a displacement cycle. However, this is not a cycle as far as the phase fraction ratio is concerned, and for instance, there is no actuation possible from point C_1 unless the temperature T_2 is highly increased, or inversely, no current is applied and the system cools down to its initial state.

As said before, this problem should be addressed:

- by the design: the choice and the conditioning of the material is relevant for the deadband and the temperature/stress build-up during actuation
- by the control: security mechanism have to be implemented to conditionally allow actuation.

8.3.2 Modeling Problem

In the modeling aspect of the SMA we had chosen a given Laguerre pole a , and the influence of the linear Laguerre model order and was studied from the tests. The process of choosing optimal pole and model order can be done systematically using the Akaike Information Criteria (AIC) and Percentage Prediction Error (PPE) defined by (Saha *et al.*, 1998; Ljung, 1999):

$$AIC = N_s \ln \left[\frac{1}{N_s} \sum_{t=1}^{N_s} \varepsilon(t)^2 \right] + 2d_m \quad (8.1)$$

where d_m is the number of terms included in the model and $\varepsilon(t) = y(t) - \hat{y}(t)$ is the prediction error at time t .

$$PPE = \frac{\sum_{t=1}^{N_s} [y(t) - \bar{y}(t)]^2}{\sum_{t=1}^{N_s} [y(t) - \hat{y}(t)]^2} \times 100\% \quad (8.2)$$

where \bar{y} is the mean value of the plant output data. Now an optimal model can be obtained if we choose pole a and order d_m such that AIC and PPE are minimized.

8.3.3 Control Problem

The most important issue that has to be addressed in our control proposition is the problem of chattering in the control signal. The problem of chattering in the Laguerre Predictive control method is due the absence of integrator in the closed loop. In our proposed control design the integrator can be systematically added by the use of an incremental Laguerre Model. However, introducing an integrator in closed loop in the presence of saturation constraint can cause other problems which has to be addressed systematically using an anti windup for instance.

8.4 Future Applications of the contribution

In this thesis, the modeling and control problem have been treated on basic SMA actuator setups using SMA in the wire form. The method used being based on an input-output model of the dynamic of the actuator, it provides a general controller that does not depend on the knowledge of the physics of the actuator. This was demonstrated by the fact that the same control could be applied on two actuators (single SMA wire and antagonist actuators) with similar results without any modifications or specific tweaking. Thus it is expected that the controller could be used for other types of SMA actuators with different architecture or form such as spring based SMA actuator (Gédouin *et al.*, 2011), rotary SMA actuator (Elahinia & Ashrafiun, 2002) (wire and rotary setup)and bundle actuator (Mavroidis, 2002). Further, it can be seen that these SMA actuators (antagonistic or single wire) are the principal forms of SMA used in applications such as robotic arm (Cocaud *et al.*, 2006; Ishii & Ting, 2004; Lan & Fan, 2010), medical applications like endoscopy (Sars *et al.*, 2010), smart structure applications like SAR antenna (Synthetic Aperture Radar) , flexible beam (Khidir *et al.*, 2007; Da Silva, 2007; Peng *et al.*, 2008) and embedded SMA actuation like automotive SMA mirror (Williams *et al.*, 2010; Suleman & Crawford, 2008). Therefore, since the basic problem of control has been solved, it can be applied in these structures either directly if considered as a single input single output system, or included in a more complicated controller if several SMA actuators are used. But it is imperative to note that the application of the given control method is questionable to SMA foil types actuator and further investigation has to be made in this direction. On the modeling, the use

of Volterra-Laguerre basis had been addressed and tested with good results. Their approximation capabilities were comparable to that of higher order linear Laguerre filters. On the control, their potential has not been explored further, due to lack of time and because some difficulties are introduced in the design due to their non linearities.

Chapter 8. Conclusion

Bibliography

- ABADIE, J., CHAILLET, N. & LEXCELLENT, C. (2002). An integrated shape memory alloy micro-actuator controlled by thermoelectric effect. *Sensors and Actuators A: Physical*, **99**, 297–303.
- ADEL, M.E., M.MAKOUDI & RADOUANE, L. (1999). Decentralized adaptive control of linear interconnected systems based on Laguerre series representation. *Automatica*, **35**, 1873–1881.
- AHN, K.K. & KHA, N.B. (2007). Internal model control for shape memory alloy actuators using fuzzy based Preisach model. *Sensors and Actuators A*, **136**, 730–741.
- AHN, K.K. & KHA, N.B. (2008). Modeling and control of shape memory alloy actuator using Preisach model, genetic algorithm and fuzzy logic. *Mechatronics*, **18**, 141–152.
- ANDERSON, B.D.O. (1985). Adaptive systems, lack of persistent excitation and bursting phenomena. *Automatica*, **21**, 247–258.
- ASUA, A., ETXEBARRIA, V. & GARCIA-ARRIBAS, A. (2008). Neural network based micropositioning control of smart shape memory alloy actuator. *Engineering applications of Artificial Intelligence*, **21**, 796–804.
- BELT, H. (1997). *Orthonormal Basis for Adaptive Filtering*. Ph.D. thesis, Technische Universiteit Heindoven.
- BENZAQUI, H., CHAILLET, N., LEXCELLENT, C. & BOURJAULT, A. (1999). Nonlinear motion and shape control of Shape Memory Alloy. *Proc. of SPIE Sym. on Smart Structures and Materials*, 337–348.
- BHATTACHARYYA, A., LAGODAS, D.C., WANG, Y.C. & KINRA, V.K. (1995). On the role of thermoelectric heat transfer in the design of SMA actuators: theoretical modeling and experiment. *Smart Materials and Structures*, **4**, 252–263.
- BITTANTI, S., BOLZERN, P. & CAMPI, M. (1990). Convergence and exponential convergence of identification algorithms with directional forgetting factor. *Automatica*, **26**, 929–932.
- BOSSAVIT, A., EMSON, C. & MAYERGOYZ, I. (1991). *Méthodes Numériques en Electromagnétisme*. Edition Eyrolles, Paris.

Bibliography

- CAMPELLO, R., DO AMARAL, W. & FAVIER, G. (2006). A note on the optimal expansion of Volterra models using Laguerre functions. *Automatica*, **42**, 689–693.
- CAO, L. & SCHWARTZ, H. (2000). A directional forgetting factor based on decomposition of information matrix. *Automatica*, **36**, 1725–1731.
- CHASE, J.G., BEGOC, V. & BORROSE, L.R. (2005). Efficient structural health monitoring for a benchmark structure using adaptive RLS filters. *Computers and Structures*, **83**, 639–647.
- CHEN, X., HISAYAMA, T. & SU, C.Y. (2009). Pseudo-inverse-based adaptive control for uncertain discrete time systems preceded by hysteresis. *Automatica*, **45**, 469–476.
- CHOI, S.B. (2001). Force tracking control of a flexible gripper featuring shape memory alloy actuators. *Mechatronics*, **11**, 677–690.
- CLARKE, D., MOHTADI, C. & TUFFS, P. (1987). Generalized predictive control-part i. the basic algorithm. *Automatica*, **23**, 137–148.
- COCAUD, C., PRICE, A., JNIFENE, A. & NAGUIB, H. (2006). Position control of an experimental robotic arm driven by artificial muscles based on shape memory alloys. *International Journal of Mechanical Material Design*, **3**, 223–236.
- CUTLER, C.R. & JOHNSTON, C.R. (1985). Comparison of quality criterion for PID and predictive controllers. In *Proceedings of American control conference*, 214–219.
- DA SILVA, E.P. (2007). Beam shape feedback control by means of a shape memory actuator. *Materials & Design*, **28**, 1592–1596.
- DE KEYSER, R. & VAN CAUWENBERGHE, A. (1981). A self-tuning multistep predictor application. *Automatica*, **17**, 167–174.
- DITMAN, J.B., BERGMAN, L.A. & TSAO, T.C. (1996). The design of extended bandwidth shape memory alloy actuators. *Journal of Intelligent Material Systems and Structures*, **7**, 635–645.
- DUMONT, G.A. & FU, Y. (1993a). Non-linear adaptive control via Laguerre expansion of Volterra kernels. *International journal of adaptive control and signal processing*, **7**, 367–382.
- DUMONT, G.A. & FU, Y. (1993b). Non-linear adaptive control via Laguerre expansion of Volterra kernels. *Int. J. Adapt Control and Signal Processing*, **7**, 367–382.
- DUMONT, G.A., ZERVOS, C.C. & PAGEAU, G.L. (1990). Laguerre-based adaptive control of pH in an industrial bleach plant extraction stage. *Automatica*, **26**, 781–787.
- DUMONT, G.A., FU, Y. & LU, G. (1994). Nonlinear adaptive generalized predictive control and applications. In D. Clarke, ed., *Advances in Model Based Predictive Control*, 498–515, Oxford Science, Great Britain.

- ELAHINIA, M.H. & AHMEDIAN, M. (2006). Application of extended Kalman filter to control of a shape memory alloy arm. *Journal of Smart Materials and Structures.*, **15**, 1370–1384.
- ELAHINIA, M.H. & ASHRAFIUON, H. (2002). Nonlinear control shape memory alloy actuated manipulator. *Transactions of ASME*, **124**, 566–575.
- ELSHHAFEI, A.L., DUMONT, G.A. & ELNAGGAR, A. (1994). Adaptive GPC based on Laguerre filter modelling. *Automatica.*, **30**, 1913–1920.
- FORSSELL, U. & LJUNG, L. (1999). Closed loop identification revisited. *Automatica.*, **35**, 1215–1241.
- FU, Y. & DUMONT, G. (1993). An optimum time scale for discrete Laguerre network. *IEEE Transactions on Automatic Control*, **38**, 934–938.
- FURST, S.J. & SEELECKE, S. (2011). Experimental validation of different methods for controlling a flexible nozzle using embedded SMA wires as both positioning actuator and sensor. In *Proceedings of SPIE, Behavior and Mechanics of Multifunctional Materials and Composites 2011.*, USA.
- GÉDOUIN, P.A., DELALEAU, E., BOURGEOT, J.M., JOIN, C., ARBAB CHIRANI, S. & CALLOCH, S. (2011). Experimental comparison of classical PID and model-free control: Position control of a shape memory alloy active spring. *Control Engineering Practice*, **19**, 433–441.
- GOLDEN, M.P., LIU, L.K. & YDSTIE, B.E. (1986). Multivariable control using extended prediction horizons. In *Proceedings of American control conference.*, 1550–1551.
- GRANT, D. & HAYWARD, V. (1997). Variable structure control of shape memory alloy actuators. *IEEE Control system Magazine*, **17**, 80–88.
- HANGEKAR, R., FURST, S. & SEELECKE, S. (2010). Development of a 6-channel power controller for simultaneous actuation and resistance measurement of SMA wires. In *Proceedings of ASME, Smart Materials, Adaptive Structures and Intelligent Systems 2011.*, Philadelphia, USA.
- HJALMARSSON, H., GEVERS, M. & F.DE BRUYNE (1996). For model-based control design, closed-loop identification gives better performance. *Automatica*, **32**, 1659–1673.
- HUZMEZAN, M., GOUGH, W.A., DUMONT, G. & KOVAC, S. (2002). Time delay integrating systems: A challenge for process control industries.a practical solution. *Control Engineering Practice*, **10**, 1153–1161.
- IKONEN, E. & NAJIM, K. (2002). *Advanced Process Identification and Control.*. Marcel Dekker, New York.

Bibliography

- ISHII, H. & TING, K. (2004). SMA actuated compliant bistable mechanisms. *Mechtronics*, **14**, 421–437.
- IYER, R.V., TAN, X. & KRISHNAPRASAD, P.S. (2005). Approximate inversion of the Preisach hysteresis operator with application to control of smart actuators. *IEEE Transactions on Automatic Control*, **50**, 798–810.
- JANAIDEH, M.A., RAKHEJA, S. & SU, C.Y. (2010). An analytical generalized Prandtl-Ishlinskii model inversion for hysteresis compensation in micropositioning control.(accepted). *IEEE/ASME Transactions on Mechatronics*.
- JANOCHA, H. & KUHNEN, K. (2000). Realtime compensation of Hysteresis and Creep in Piezoelectric Actuators. *Sensors and Actuators*, **79**, 83–89.
- JAYENDRAN, J., PATEL, R.V., NIKUMB, S. & OSTOJIC, M. (2008). Modeling and control of shape memory alloy actuators. *IEEE Transactions on Control Systems Technology*, **16**, 279–287.
- JOHNSTONE, R.M., JOHNSON, JR, C.R., BITMEAD, R.R. & ANDERSON, B.D.O. (1982). Exponential convergence of recursive least squares with exponential forgetting factor. *Systems and Control Letters*, **2**, 77–82.
- JOSTROM, M.S. & VISONE, C. (2006). “Moving” Prandtl-Ishlinskii operators with compensators in a closed form. *Physica B*, **372**, 97–100.
- KHIDIR, E.A., MOHAMED, N.A., NOR, M.J.M. & MUSTAFA, M.M. (2007). A new concept of a linear smart actuator. *Sensors and Actuators A*, **135**, 244–249.
- KIM, B., LEE, M.G., LEE, Y.P., KIM, Y. & LEE, G. (2006). An earthworm-like micro robot using shape memory alloy actuator. *Sensors and Actuators A*, **125**, 429–437.
- KLOUCEKA, P., REYNOLDS, D.R. & SEIDMAN, T.I. (2003). On thermodynamic active control of shape memory alloy wires. *Systems & Control Letters*, **48**, 211–219.
- KUHNEN, K. (2003). Modeling ,identification and compensation of complex hysteretic nonlinearities. a modified Prandtl-Ishlinskii approach. *European Journal of Control*, **9**, 407–418.
- KULHAVÝ, R. (1987). Restricted exponential forgetting in real time identification. *Automatica*, **23**, 589–600.
- KUMAGAI, A., LUI, T.I. & HOZIAN, P. (2006). Control of shape memory alloy actuators with neuro-fuzzy feedforward model element. *Journal of Intelligent Manufacturing*, **17**, 45–56.
- LAGOUDAS, D.C., BO, Z. & QIDWAI, M.A. (1996). A unified thermodynamic constitutive model for SMA and finite element analysis of active matrix composites. *Mechanics of Composite Materials and Structures*, **4**, 153–179.

Bibliography

- LAN, C.C. & FAN, C.H. (2010). An accurate self-sensing method for the control of shape memory alloy actuated flexures. *Sensors and Actuators A.*, **163**, 323–332.
- LANDAU, I.D., LOZANO, R. & SAAD, M. (1998). *Adaptive Control..* Springer.
- LANDAU, Y.D. (1979). *Adaptive Control: Model Reference Approach..* Marcel Dekker, New York.
- LEARY, M., SCHIAVONE, F. & SUBIC, A. (2010). Lagging for control of shape memory alloy actuator response time. *Materials and Design*, **31**, 2124–2128.
- LECLERCQ, S. & LEXCELLENT, C. (1996). A general macroscopic description of the thermomechanical behavior of shape memory alloys. *Journal of Mechanics and Physics of solids*, **44**, 953–980.
- LIANG, C. & ROGERS, C.A. (1992). Design of shape memory alloy actuator. *ASME Journal of Mechanical Design*, **114**, 223–230.
- LIU, S.H. & YEN, T.S.H.J.Y. (2010). Tracking control of shape memory alloy actuators based on self-sensing feedback and inverse hysteresis compensation. *Sensors*, **10**, 112–127.
- LJUNG, L. (1999). *System Identification: Theory for the user.* Prentice Hall.
- LJUNG, L. (2006). *System Identification Toolbox, for use with Matlab..* The Mathworks Inc.
- MA, N. & SONG, G. (2003). Control of shape memory alloy using pulse width modulation. *Smart Materials and Structure*, **12**, 712–719.
- MA, N., SONG, G. & LEE, H. (2004). Position control of shape memory alloy actuators with internal electrical resistance feedback using neural network. *Smart Materials and Structure*, **13**, 777–783.
- MACIEJOWSKI, J.M. (2000). *Predictive control with constraints..* Prentice Hall.
- MAJIMA, S., KODAMA, K. & HASEGAWA, T. (2001). Modeling of shape memory alloy actuator and tracking control system with the model. *IEEE Transaction on Control System Technology*, **9**, 54–59.
- MAVRIDIS, C. (2002). Development of advanced actuators using shape memory alloys and electrorheological fluids. *Research in Nondestructive Evaluation*, **14**, 1–32.
- MAVRIDIS, C., PFEIFFER, C. & MOSLEY, M. (2000). *Automation, Miniature Robotics and sensors for Non-destructive Testing and Evaluation..* chap. Conventional actuators, shape memory alloys and electrorheological., 189–214. The American Society for Nondestructive Testing.
- MOALLEM, M. & JUN, L. (2005). Application of shape memory alloy for flexure control: theory and experiments. *IEEE/ASME Transactions on Mechatronics*, **10**, 495–501.

Bibliography

- MOALLEM, M. & TABRIZI, V.A. (2009). Tracking control of an antagonistic shape memory alloy actuator pair. *IEEE Trans. on Control Systems Technology*, **17**, 184–190.
- MOSLEY, M.J. & MAVROIDIS, C. (2001). Experimental nonlinear dynamics of a shape memory alloy bundle actuator. *Journal of Dynamic Systems, Measurement and Control*, **123**, 103–112.
- NGUYEN, B.K. & AHN, K.K. (2009). Feedforward control of shape memory alloy actuators using fuzzy-based inverse Preisach model. *IEEE Transactions on Control Systems Technology*, **17**, 434–441.
- PAJUNEN, G. (1992). Adaptive control of Weiner type nonlinear systems. *Automatica*, **28**, 781–785.
- PATHAK, A. (2010). *The Development of an Antagonistic SMA Actuation Technology for the Active Cancellation of Human Tremor*. Ph.D. thesis, University of Michigan.
- PENG, F., JIANG, X.X., HU, Y.R. & NG, A. (2008). Actuation precision control of SMA actuators used for shape control of inflatable SAR antenna. *Acta Astronautica*, **63**, 578–585.
- PICCIRILLO, V., BALTHAZAR, J.M., PONTES JR, B.R. & FELIX, J.L.P. (1996). Chaos control of a nonlinear oscillator with shape memory alloy using an optimal linear control: Part i: Idea energy source. *Mechanics of Composite Materials and Structures*, **4**, 153–179.
- PRICE, A.D., JNIFENE, A. & NAGUIB, H.E. (2007). Design and control of a shape memory alloy based dexterous robot hand. *Smart Materials and Structures*, **16**, 1401–1414.
- REYNAERTS, D. & VAN BRUSSEL, H. (1998). Design aspects of shape memory actuators. *Mechatronics*, **8**, 635–656.
- RICHALET, J., RAULT, A., TESTUD, J. & PAPON, J. (1978). Model predictive heuristic control: applications to industrial processes. *Automatica*, **14**, 413–428.
- RICHARD, J. (2001). *Algèbre et analyse pour l'automatique*. Hermès Science.
- ROMANO, R. & TANNURI, E.A. (2009). Modeling, control and experimental validation of a novel actuator based on shape memory alloy. *Mechatronics*, **19**, 1169–1177.
- SAFONOV, M. (1980). *Stability and Robustness of Multivariable Feedback Systems*. MIT Press, Cambridge, MA.
- SAHA, P., KRISHNAN, S.H., RAO, V.S.R.O. & PATWARDHAN, S.C. (1998). Modeling and predictive control of MIMO nonlinear systems using Weiner-Laguerre models. *Chemical Engineering Communication*, **191**, 1083–1119.

- SARS, V.D., HALIYO, S. & SZEWCZYK, J. (2010). A practical approach to the design and control of active endoscopes. *Mechatronics*, **20**, 251–264.
- SASTRY, S. (1999). *Nonlinear Systems: Analysis, Stability and Control*. Springer.
- SHAHIAN, B. & HASSUL, M. (1993). *Control system design using Matlab*. Prentice Hall, New Jersey.
- SHAMELI, E., ALASTY, A. & SALAARIEH, H. (2005). Stability analysis and nonlinear control of a miniature shape memory alloy. *Mechatronics*, **15**, 471–486.
- SOFLA, A.Y.N., ELZEY, D.M. & WADLEY, H. (2008a). Two-way antagonistic shape actuation based on the one-way shape memory effect. *Journal of Intelligent Material Systems and Structures*, **19**, 1017–1027.
- SOFLA, A.Y.N., ELZEY, D.M. & WADLEY, H.N.G. (2008b). Cyclic degradation of antagonistic shape memory actuated structures. *Smart Materials and Structures*, **17**.
- SONG, G. (2003). A neural network inverse model for a shape memory alloy wire actuator. *Journal of Intelligent Material Systems and Structures*, **14**, 371–377.
- SONG, G. & MA, N. (2007). Robust control of a shape memory alloy wire actuated flap. *Smart Materials and Structures*, **16**, N51–N57.
- SREEKUMAR, M., SINGAPERUMAL, M., NAGARAJAN, T., ZOPPI, M. & MOLFINA, R. (2007). Recent advances in nonlinear control technologies for shape memory alloy actuators. *Journal of Zhejiang University SCIENCE A*, **8**, 818–829.
- SULEMAN, A. & CRAWFORD, C. (2008). Design and testing of biomimetic tuna using shape memory alloy induced propulsion. *Computers & Structures*, **86**, 491–499.
- TAN, X. & BARAS, J. (2005). Adaptive identification and control of hysteresis in smart materials. *IEEE Transactions on Automatic Control*, **50**, 827–839.
- TAN, X. & BARAS, J.S. (2004). Modeling and control of hysteresis in magnetostrictive actuators. *Automatica*, **40**, 1469–1480.
- TAN, X., BARAS, J.S. & KRISHNAPRASAD, P.S. (2005). Control of hysteresis in smart actuators with application to micro-positioning. *Systems and Control Letters*, **54**, 483–492.
- TAO, G. (2003). *Adaptive control design and analysis*, vol. 37. Wiley-IEEE Press.
- TEH, Y.H. & FEATHERSTONE, R. (2004). A new control system for fast motion control of sma actuator wires. In *Proceedings of Shape Memory And Related Technologies (SMART 2004)*, 24–26, Singapore.
- TÓTH, R. (2008). *Modeling and Identification of Linear Parameter Varying Systems: An Orthonormal Basis function approach*. Ph.D. thesis, Tech. Uni. Delft.

Bibliography

- TÓTH, R. (2010). *Modeling and identification of linear parameter-varying systems*, vol. 403 of *Lecture Notes in Control and Information Sciences*. Springer Verlag, springer edn.
- VAN HUMBEECK, J. (2001). Shape memory alloys: A material and a technology. *Advanced Engineering Materials*, **3**, 837–849.
- VERDULT, V. & VERHAEGEN, M. (2002). Subspace identification of multivariable linear parameter-varying system. *Automatica*, **38**, 805–814.
- VISINTIN, A. (1994). *Differential Models of Hysteresis..* Springer Verlag, New-York.
- WAHLBERG, B. (1991). System Identification using Laguerre Models. *IEEE Transactions on Automatic Control*, **36**, 551–562.
- WEBB, G.V., LAGOUDAS, D.C. & KURDILA, A.J. (1998). Hysteresis modeling of SMA actuators for control applications. *Journal of Intelligent Materials, Systems and Structures*, **9**, 432–448.
- WILLIAMS, E.A., SHAW, G. & ELAHINIA, M. (2010). Control of an automotive shape memory alloy mirror actuators. *Mechatronics*, **20**, 527–534.
- ZEHETNER, J., REGER, J. & HORN, M. (2007). A derivative estimation toolbox based on algebraic methods-theory and practice. In *Proceedings of IEEE 2007 Multi-Conference on Systems and Control (MSC)*, Singapore.
- ZERVOS, C., BÉLANGER, P.R. & DUMONT, G.A. (1988). On PID controller tuning using orthonormal series identification. *Automatica*, **24**, 165–175.
- ZHU, Y. (1998). Multivariable process identification for MPC: Asymptotic methods and its application. *Journal of Process Control.*, **8**, 101–115.
- ZHU, Y. & BUTOYI, F. (2002). Case studies on closed loop identification for MPC. *Control Engineering Practice.*, **10**, 403–417.

MODELISATION ET COMMANDE D'ACTIONNEUR À ALLIAGE À MEMOIRE DE FORME

RÉSUMÉ : Dans cette thèse, une approche boîte noire pour la modélisation et le contrôle d'actionneurs à AMF est étudiée en tant qu'alternative aux commandes utilisant des modèles phénoménologiques ou physiques classiques. Des modèles utilisant des fonctions de Laguerre ont été utilisés ici en raison de leur simplicité, des bonnes propriétés de convergence de ces modèles et du peu d'informations nécessaires a priori. De plus, des généralisations au cas non-linéaire par le biais de série de Volterra sont possibles. Dans tous les cas les modèles sont linéairement paramétrés ce qui permet une identification en ligne par moindres carrés récursifs. Après avoir démontré expérimentalement la capacité de plusieurs modèles linéaires et non-linéaires à prédire le comportement de deux structures d'actionneurs à AMF, la thèse s'attache à définir des lois de commandes. Une première commande classique utilisant un prédicteur simple a été testé. Les conditions de stabilité ont été précisées et fournissent un critère conservatif pour le choix de l'horizon de prédiction. Une validation expérimentale a mis en évidence des problèmes relatifs à l'identification en boucle fermée, et l'algorithme d'identification a été amélioré pour pallier au manque d'excitation des signaux utilisés. Une seconde stratégie de commande originale est ensuite proposée consistant en une identification globale. Cette approche est comparable à l'utilisation de variables instrumentales et évite la corrélation des signaux utilisés pour l'identification. L'étude démontre la stabilité du schéma de commande qui n'est plus dépendante de l'horizon de prédiction. Une validation expérimentale a démontré les bonnes performances de cette solutions et mis en évidence des parallèles avec la commande adaptative avec modèle de référence.

Mots clés : Actionneur à Alliage Mémoire de Forme (AMF), fonction de Laguerre, Commande Adaptative, Commande Prédictive.

MODELING AND CONTROL OF SHAPE MEMORY ALLOY (SMA) ACTUATOR

ABSTRACT: This thesis propose a black box approach for the modeling and the control of SMA actuators, as an alternative to the usual phenomenological and physic models. Models using Laguerre functions are used due to their simplicity of implementation, their good convergence properties and the small amount of a prior knowledge needed. Moreover, using Volterra series, nonlinear models can be developed. All these models being linear in the parameters, they can be identified on-line using classical exponential forgetting recursive least squares algorithms. An experimental study demonstrates the ability of these models to predict the output of two different setups using SMA actuators. The second part of the thesis addresses the control problem. First adaptive predictive controller using Laguerre predictor is selected and the stability conditions are carefully studied showing conditional stability based on prediction horizon. Experimental results demonstrate the limitation due to the lack of excitation and a directional forgetting RLS algorithm is successfully tested. To address the problem of closed loop identification, a second controller structure is proposed that uses a global Laguerre model of the closed loop system. By doing so, the reference is used as an instrumental variable and solves the problem of stability of the identification, thus a simple RLS algorithm is used. The stability of the controller is proved and does not depend on the prediction horizon. Experimental assessment on the two actuators gives good results; moreover it reveals some parallel with model reference adaptive control.

Keywords : Shape Memory Alloy (SMA) Actuator, Laguerre functions, Adaptive control, Laguerre Predictive control, Modified Laguerre Predictive control.

